



The
University
Of
Sheffield.

**Formalisation and experimental validation of a novel
design methodology to estimate finite lifetime under
fretting fatigue loading**

Thesis submitted in partial fulfilment of the requirements for the degree of Doctor of Philosophy

by

Cedric Vary Teuchou kouanga

The University of Sheffield

Faculty of Engineering

Department of Civil and Structural Engineering

Supervisors:

Prof. Luca Susmel

Prof. Rob Dwyer-Joyce

Prof. David Nowell

Submission Date

January 2023

This page is left intentionally blank

Abstract

Fretting fatigue is a damage phenomenon which occurs at the contact interface of two mechanical components subjected to both contact and fatigue loading. One of the most challenging tasks of structural engineer is to predict the number of cycles to failure of operational life components subjected to fretting fatigue damage. The aim of this thesis is to formulate and validate with experimental data a novel design methodology suitable for predicting finite lifetime of mechanical components subjected to both constant and variable amplitude fretting fatigue loading. The material to be assessed under fretting fatigue damage is cast iron cut from engine block and engine liner.

In the first part of the thesis, the proposed design method which is based on the use of the Modified Wöhler Curve Method (MWCM) applied in conjunction with both the Theory of Critical Distance (TCD) and the Shear Stress-Maximum Variance Method (τ -MVM) is formalised. The TCD, applied in the form of the Point Method (PM), takes into account the damaging effect of the multiaxial stress in the vicinity of the contact region. The τ -MVM is used to calculate the material critical plane and its relative stress quantities. The stress quantities relative to the critical plane are post-processed according to the MWCM which is capable of modelling the presence of non-zero mean stresses, the degree of multiaxiality and the non-proportionality of the investigated load history.

In the second part of the thesis, tensile tests, uniaxial and torsional fatigue tests are carried out in order to calibrate the MWCM's and the critical distance, L_M equations.

In the third part of the thesis, fretting fatigue experiments under constant and variable amplitude loading are carried out. In all tests, the fretting specimens are made from cast iron and fretting pads machined either from steel or cast iron. For the constant amplitude (CA) regime, a constant or CA cyclic load is applied to the pads and a CA fatigue load applied to the specimen. To run the variable amplitude (VA) fretting tests, a constant

load is applied to the pads and a VA fatigue load applied to the specimen. After each CA and VA fretting fatigue test, the number of cycles to failure is recorded.

In the final part of this thesis, the fretting fatigue tests are modelled and simulated using ANSYS Workbench. The time variable linear-elastic stress field in the vicinity of the contact (pads/specimen) obtained from the simulation are post-processed using the proposed design method. The predicted number of cycles to failure, $N_{f,e}$ obtained from the post-processing of the stress field is quantitatively compared to the experimental number of cycles to failure, N_f .

It is concluded that, the estimated fretting fatigue lifetime falls within a scattered band error of 2. The good agreement between the experimental number of cycles to failure and the predicated cycles demonstrates that the proposed design methodology is highly accurate in predicting finite lifetime of cast iron subjected to CA and VA fretting fatigue loading.

Acknowledgements

Firstly, I would like to express my profound gratitude to my supervisors Professor Luca Susmel, Professor Rob Dwyer-Joyce and Professor David Nowell for their continuous support, guidance and encouragement throughout the course of this research. Without their suggestions and advice, the results obtained in this work would not have been possible. I also would like to thank the lab technicians Paul Blackburn, Richard Kay and Chris Todd who supported my experimental work in the Lea Lab at the University of Sheffield.

I would like to express my special gratitude to Cummins Inc. and the Engineering and Physical Sciences Research Council (EPSRC) for financing this work. I would also like to thank Jeffrey Jones, Andrew Wormald and Iain Revill at Cummins Inc. for their relevant technical input and constant advices.

Finally, I would like to take this opportunity to thank my wife Nerissa Musi for her unconditional support and encouragement during the course of this research. I also thank my elder brother Gaethan Donlap who has always been very impactful in my life.

Contents

Abstract.....	i
Acknowledgement.....	iii
Contents.....	iv
List of figures.....	viii
List of Tables.....	xiv
1 Introduction.....	1
1.1 Background.....	1
1.2 Research aims and objectives.....	1
1.3 Publications.....	3
2 literature review.....	4
2.1 Overview of fretting fatigue.....	4
2.2 Review of contact mechanics.....	10
2.2.1 Different types of contact.....	10
2.2.2 Mechanics of fretting fatigue.....	11
2.3 Review of stress quantities used in fatigue assessment.....	16
2.3.1 Multiaxial stress state.....	16
2.3.2 Critical Plane concept.....	17
2.3.3 Stress quantities used in fatigue assessment.....	18
2.3.4 Stress concentration factor.....	19
2.4 Review of fundamental concepts in fatigue assessment.....	21
2.4.1 Crack initiation and growth in metallic materials.....	21
2.4.2 The Wöhler curves.....	22
2.4.3 Statistical determination of fatigue curve.....	24
2.4.4 Effect of notch in fatigue assessment.....	26
2.4.5 Maximum Variance Method and the critical plane stress components ...	27
2.4.6 Theory of Critical Distance.....	33

2.4.7	The Modified Wöhler Curve Method (MWCM).....	36
2.4.8	The mean stress sensitivity index	38
2.4.9	Palmgren-Miner Rule	39
3	Proposed design methodology	42
3.1	Overview.....	42
3.2	Finite lifetime of materials under constant amplitude fretting fatigue loading.....	42
3.3	Finite lifetime of materials under variable amplitude fretting fatigue loading.....	45
4	Characterisation of fatigue properties of cast iron	51
4.1	Material description	51
4.2	Determination of the ultimate tensile strength of the assessed materials.....	51
4.3	Calibration of the critical distance L_M	52
4.3.1	Calculation of constants A and B associated to material 40054.....	53
4.3.1.1	Fatigue experiments of plain and notched specimens	53
4.3.1.2	Calculation of the gross nominal stress and the stress damaging the plain specimen at a given cycle	58
4.3.1.3	Numerical analysis of the notched specimen	60
4.3.1.4	Calculation of constants A and B in the L_M vs N_f equation.....	63
4.3.2	Calculation of constants A and B associated to material 40060	65
4.3.2.1	Fatigue experiments of plain and notched specimens	65
4.3.2.2	Calculation of the gross nominal stress and the stress damaging the plain specimen at a given cycle	69
4.3.2.3	Numerical analysis of the notched specimen 40060	70
4.3.2.4	Calculation of constants A and B in the L_M vs N_f equation.....	72
4.4	Calibration of the MWCM's governing equations.....	74
4.4.1	Endurance limit and negative inverse slope under fully- reversed uniaxial fatigue loading	75
4.4.2	Endurance limit and the negative inversed slope under fully-reversed torsional fatigue loading.....	75
4.4.2.1	Experimental procedure under torsional fatigue loading.....	75
4.4.2.2	Post-processing of the experimental results	79

4.4.2.3	S-N curve, endurance limit and negative inverse slope under fully-reversed torsional loading.....	81
4.5	Calculation of the mean stress sensitivity index	83
4.5.1	The endurance limit under fully reversed uniaxial fatigue loading.....	83
4.5.2	The endurance limit under fully reversed torsional fatigue loading	83
4.5.3	The endurance limit under uniaxial fatigue loading with load ratio equal to 0.1.....	84
4.5.4	Calculation of the mean stress sensitivity index.....	88
4.6	Summary of the material properties used to calibrate the proposed design methodology	88
5	Fretting fatigue experiments.....	89
5.1	Calibration of the fretting fatigue machine.....	89
5.1.1	First calibration test (P CA-cyclic and F VA-cyclic)	91
5.1.2	Second calibration test (P constant and F VA-cyclic).....	92
5.1.3	Third calibration test (P CA-cyclic and F CA-cyclic)	92
5.1.4	Fourth calibration test (P constant and F CA-cyclic)	93
5.1.5	Post-processing and interpretation of the calibration tests	93
5.2	Fretting fatigue experiments under constant amplitude loading	96
5.3	Fretting fatigue experiments under variable amplitude loading	102
6	Validation of the design methodology	108
6.1	Finite element (FE) analysis of the fretting fatigue experiments	108
6.2	Prediction of the fretting fatigue lives.....	123
6.3	Results and discussion	127
7	Conclusion and recommendation for future work	130
7.1	Conclusion.....	130
7.2	Recommendation for future work.....	132
8	Bibliography.....	133
Appendix A: Results of the ultimate tensile experiments.....		137
Appendix B: Uniaxial fatigue experiment: dimensions of all the tested specimens.....		139

Appendix C: Use of the online tool e-fatigue to calculate the stress concentration factor.....	142
Appendix D: Torsional fatigue experiments: dimensions of all the tested specimens...	143
Appendix E: Stiffness behaviour of specimens during the fatigue test under torsion....	145
Appendix F: Calibration results of the fretting fatigue machine.....	155
Appendix G: Damage material 40054 under constant amplitude fretting fatigue loading.....	160
Appendix H: Damage material 40054 under variable amplitude fretting fatigue loading.....	164
Appendix I: Damage material 40060 under constant amplitude fretting fatigue loading.....	169
Appendix J: Damage material 40060 under variable amplitude fretting fatigue loading.....	174

List of Figures

Figure 2-1 Estimated vs observed fretting fatigue lifetime with and without wear damage [23].	7
Figure 2-2 Fretting fatigue life prediction of material Al7050-T7451 [27]	8
Figure 2-3 Characterisation of contacts; (a) Incomplete and non-conformal, (b) Complete, (c) Flat and round punch [1].....	11
Figure 2-4 Schematic of Hertzian contact [1].....	12
Figure 2-5 Hertzian contact stress distribution.	13
Figure 2-6 Schematisation of fretting fatigue.	14
Figure 2-7 Schematic of the stick and slip regions in partial slip.....	15
Figure 2-8 Cylindrical specimen subjected to combined sinusoidal tension and torsion [17].	17
Figure 2-9 Definition of stresses used to predict fatigue damage under uniaxial loading.	19
Figure 2-10 Definition of: (a) net and gross nominal stress and (b) linear elastic peak stress at the tip of a notch	20
Figure 2-11 Definition of loading mode.....	22
Figure 2-12 (a) Wöhler curve of ferrous material. (b) and (c) Wöhler curves of non-ferrous material [17].	23
Figure 2-13 Wöhler diagram showing fatigue curves calculated for different probabilities of survival [17].	24
Figure 2-14 Definition of the fatigue strength reduction factor, K_f	27
Figure 2-15 Definition of a generic material plane [40].....	28
Figure 2-16 In-field procedure to determine the critical distance L_M , in the medium-cycle fatigue regime by using two calibration curves.....	35
Figure 2-17 Modified Wöhler diagram.	36
Figure 2-18 Palmgren and Miner rule.....	41

Figure 3-1 Design methodology to estimate the finite lifetime under CA fretting fatigue.	44
Figure 3-2 Multiaxial stress field along the focus path of a mechanical assembly subjected to VA fretting fatigue loading.	45
Figure 3-3 Use of the τ -MVM to calculate the critical plane along the focus path of a mechanical assembly subjected to VA fretting fatigue loading.	46
Figure 3-4 Calculation of the MWCM functions at a given location r_i	47
Figure 3-5 Shear stress spectrum associated to $\tau_{MV(t)}$ at a given location r_i	48
Figure 3-6 Use of the MWCM with the PM to estimate the finite lifetime of mechanical assembly under VA fretting fatigue loading.....	49
Figure 3-7 Design methodology to predict the finite lifetime under VA fretting fatigue	50
Figure 4-1 Example of plain specimen used for the static and fatigue test.	52
Figure 4-2 Uniaxial fatigue test of the plain specimen.....	54
Figure 4-3 Uniaxial fatigue test of the notched specimen.....	54
Figure 4-4 Example of the notched specimen used for fatigue test.	54
Figure 4-5 S-N Curve of plain material 40054 under fully reversed uniaxial loading.	57
Figure 4-6 S-N Curve of notched material 40054 under fully reversed uniaxial loading.	57
Figure 4-7 Comparison of the S-N Curves of plain and notched material 40054 under fully reversed uniaxial loading.	58
Figure 4-8 Definition of the focus path.	61
Figure 4-9 Geometry, boundary condition and mesh profile used to model the notched specimen 40054.	62
Figure 4-10 Linear elastic maximum principal stress along the focus path of the notched specimen 40054 when $\sigma_{g,nom,a} = 1 MPa$	63
Figure 4-11 Critical distance vs. the number of cycles to failure relationship according to PM, for cast iron 40054.	65

Figure 4-12 S-N Curve of plain material 40060 under fully reversed uniaxial loading.	67
Figure 4-13 S-N Curve of notched material 40060 under fully reversed uniaxial loading.	68
Figure 4-14 Comparison of the S-N Curves of plain and notched material 40060 under fully reversed uniaxial loading.....	69
Figure 4-15 Linear elastic maximum principal stress along the focus path when $\sigma_{g_nom,a} = 1$	72
Figure 4-16 Critical distance vs. the number of cycles to failure relationship according to PM, for the cast iron 40060.....	74
Figure 4-17 Fully-reversed torsion fatigue experiment rig.	76
Figure 4-18 Example of the specimen used for the torsion experiments.	76
Figure 4-19 Crack propagation during the torsion test.....	77
Figure 4-20 Stiffness behaviour of specimen L6 during the fully-reversed torsional fatigue experiment.	80
Figure 4-21 Stiffness behaviour of specimen B8 during the fully-reversed torsional fatigue experiment.	80
Figure 4-22 S-N Curve of material 40054 under fully-reversed torsional fatigue loading.....	82
Figure 4-23 S-N Curve of material 40060 under fully-reversed torsional fatigue loading.....	82
Figure 4-24 S-N curve of plain material 40054 under uniaxial fatigue loading with $R =$ 0.1.....	86
Figure 4-25 S-N curve of plain material 40060 under uniaxial loading with $R = 0.1$	87
Figure 5-1 Hydraulic fretting fatigue test rig.....	90
Figure 5-2 Calibration set-up test.....	91
Figure 5-3 First calibration test: VA fatigue load spectrum.....	92

Figure 5-4 First calibration test (Test N° 1): Comparison between the load feedback from actuator 4 and the load obtained from the strain gauge signal attached to the specimen.	94
Figure 5-5 First calibration test (Test N° 1): Comparison between the load feedback from actuator 1 and the load obtained from the strain gauge attached to the pads.	95
Figure 5-6 Third calibration test (Test N° 1): Comparison between the load feedback from.....	95
Figure 5-7 Third calibration test (Test N° 1): Comparison between the load feedback from.....	95
Figure 5-8 Geometry of the specimens used to assess the fretting fatigue damage of materials 40054 and 40060.	97
Figure 5-9 Damaged fretting specimen of test N°1 in Table 6-1.....	99
Figure 5-10 Variable amplitude fatigue load spectrum with a load ratio $R = -1$ used to assess material 40054 under fretting fatigue.	102
Figure 5-11 Variable amplitude fatigue load spectrum with a load ratio $R \geq 0$ used to assess the material 40054 under fretting fatigue.	103
Figure 5-12 Variable amplitude load spectrum used to assess the cast iron 40060 under fretting fatigue.....	103
Figure 5-13 Damaged fretting specimen of test N° 12 in Table 6-11.	105
Figure 6-1 Schematic of the fretting fatigue experiment under constant and variable amplitude loading.	108
Figure 6-2 Model 1: Fretting fatigue experiment with a pad radius of 100 mm.	109
Figure 6-3 Model 2: Fretting fatigue experiment with a pad radius of 20 mm.	109
Figure 6-4 Model 3: Fretting fatigue experiment with a pad radius of 75 mm.....	109
Figure 6-5 Boundary condition assigned to model 1.....	110
Figure 6-6 Boundary condition assigned to model 2.	110
Figure 6-7 Boundary condition assigned to model 3.....	111
Figure 6-8 Loads applied on model 1.	112

Figure 6-9 Loads applied on model 2.....	112
Figure 6-10 Loads applied on model 3.....	112
Figure 6-11 Stress σ_{xx} along the contact surface of model 1.....	113
Figure 6-12 Stress σ_{yy} along the contact surface of model 1.....	113
Figure 6-13 Shear stress τ_{xy} along the contact surface of model 1.....	114
Figure 6-14 Stress σ_{xx} along the contact surface of model 2.....	114
Figure 6-15 Stress σ_{yy} along the contact surface of model 2.....	115
Figure 6-16 Shear stress τ_{xy} along the contact surface of model 2.....	115
Figure 6-17 Stress σ_{xx} along the contact surface of model 3.....	116
Figure 6-18 Stress σ_{yy} along the contact surface of model 3.....	116
Figure 6-19 Stress τ_{xy} along the contact surface of model 3.....	117
Figure 6-20 Mesh profile used in model 1.....	117
Figure 6-21 Mesh profile used in model 2.....	118
Figure 6-22 Mesh profile used in model 3.....	118
Figure 6-23 Stress contours at the contact zone of model 1.....	119
Figure 6-24 Stress contours at the contact zone of model 2.....	120
Figure 6-25 Stress contours at the contact zone of model 3.....	121
Figure 6-26 Comparison between the FEA and the Hertzian solution of model 1.....	121
Figure 6-27 Comparison between the FEA and the Hertzian solution of model 2.....	122
Figure 6-28 Comparison between the FEA and the Hertzian solution of model 3.....	122
Figure 6-29 Stress components of test N ^o 1 in Table 5-6.....	123
Figure 6-30 Accuracy of the MWCM applied in conjunction with the PM and τ -MVM in estimating the lifetime of material 40054 subjected to constant amplitude fretting fatigue loading.....	128
Figure 6-31 Accuracy of MWCM applied in conjunction TCD and τ -MVM in estimating the lifetime of the material 40060 subjected to constant amplitude fretting fatigue loading.....	128

Figure 6-32 Accuracy of the MWCM applied in conjunction with the TCD and τ -MVM in estimating the lifetime of material 40054 subjected to variable amplitude fretting fatigue loading.....	129
Figure 6-33 Accuracy of MWCM applied in conjunction TCD and τ -MVM in estimating the lifetime of the material 40060 subjected to variable amplitude fretting fatigue loading.....	129
Figure 7-1 Summary of all the fretting fatigue results under CA and VA loading of material	131
Figure 7-2 Summary of all the fretting fatigue results under CA and VA loading of cast iron 40054.....	131

List of Tables

Table 2-1 Index q with different probabilities of survival, PS and a 95% confidence level [17].	26
Table 4-1 Chemical composition of materials 40054 and 40060.	51
Table 4-2 Static test results of material 40054.....	52
Table 4-3 Static test results of material 40060.	52
Table 4-4 Summary of the uniaxial fatigue results generated by testing the plain material 40054 under $R=-1$	55
Table 4-5 Summary of the uniaxial fatigue test results generated by testing the notched material 40054 under $R=-1$	55
Table 4-6 Fully reversed uniaxial fatigue properties of the plain and notched material 40054.	58
Table 4-7 Stress damaging the plain specimen 40054 and the corresponding gross nominal stress at a given Nf	60
Table 4-8 Dimensions of the notched specimen 40054 used in the FE analysis.	62
Table 4-9 Critical distances, L corresponding to a given number of cycles to failure, Nf for the material 40054.	64
Table 4-10 Constant A and B governing the relationship LM vs Nf for material 40054.	65
Table 4-11 Summary of the uniaxial fatigue results generated by testing the plain material 40060 under $R=-1$	66
Table 4-12 Summary of the uniaxial fatigue test results generated by testing the notched material 40060 under $R=-1$	66
Table 4-13 Fully reversed uniaxial fatigue properties of the plain and notched material 40060.....	68
Table 4-14 Stress damaging the plain specimen 40060 and the corresponding gross nominal stress at a given Nf	70

Table 4-15 Dimensions of the notched specimen 40060 used in the FE analysis.	71
Table 4-16 Critical distances, LM corresponding to a given number of cycles to failure, Nf for the material 40060.	73
Table 4-17 Constant A and B governing the relationship LM vs Nf for material 40060.	74
Table 4-18 σA and k values used in the MWCM's governing equations for the assessed materials.....	75
Table 4-19 Fully-reversed torsion test input parameters for material 40054.....	78
Table 4-20 Fully-reversed torsion test input parameters for material 40060.....	78
Table 4-21 Summary of the torsional fatigue test results generated by testing material 40054 under fully-reversed loading.	81
Table 4-22 Summary of the torsional fatigue test results generated by testing material 40060 under fully-reversed loading.	81
Table 4-23 Torsion fatigue properties of materials 40054 and 40060.....	83
Table 4-24 Summary of the uniaxial fatigue results for plain material 40054 under $R = 0.1$	85
Table 4-25 Summary of the uniaxial fatigue results for plain material 40060 under $R=0.1$	85
Table 4-26 Endurance limit under uniaxial fatigue loading with $R = 0.1$	87
Table 4-27 Critical plane stress components under $R = 0.1$	87
Table 4-28 Mean stress sensitivity index values.	88
Table 4-29 Summary of the material properties to be used in the proposed design methodology.....	88
Table 5-1 First calibration test: Contact load.....	92
Table 5-2 First calibration test: Maximum amplitude applied to the fatigue load spectrum.....	92
Table 5-3 Third calibration test: Contact load inputs.....	93
Table 5-4 Third calibration test: Fatigue load inputs.	93

Table 5-5 Fourth calibration test: Fatigue load inputs.	93
Table 5-6 Fretting fatigue input loads used to test the material 40054. P is constant, F is CA and the pads are made from steel coated with zinc phosphate	97
Table 5-7 Fretting fatigue input loads used to test material 40060. P is constant, F is CA and the pads are made from material 40054.	98
Table 5-8 Fretting fatigue input loads used to test the material 40060. P is constant, F is CA and the pads are made from steel coated with zinc phosphate.	98
Table 5-9 Fretting fatigue input loads to test the material 40060. P and F are CA and the pads made from material 40054.	98
Table 5-10 Fretting fatigue input loads to test the material 40060. P and F are CA load and the pads are made from steel coated with zinc phosphate.	98
Table 5-11 Summary of the fretting fatigue results of specimens 40054. P is constant, F is CA and the pads are made from steel coated with zinc phosphate	100
Table 5-12 Summary of the fretting fatigue results of material 40060. P is constant, F is CA and pads are made of material 40054	100
Table 5-13 Summary of the fretting fatigue results of material 40060. P is constant, F is CA and pads made from steel coated with zinc phosphate.....	101
Table 5-14 Summary of the fretting fatigue results of material 40060. P and F are both CA and pads made from material 40054.....	101
Table 5-15 Summary of the fretting fatigue results of material 40060. P and F are both CA and pads made from steel coated with zinc phosphate.....	101
Table 5-16 Fretting fatigue input loads used to test material 40054. P is constant, F is VA and pads made from steel coated with zinc phosphate.	104
Table 5-17 Fretting fatigue input loads used to test material 40060. P is static, F is VA and the pads made from material 40054.	104
Table 5-18 Fretting fatigue input loads used to test material 40060. P is static, F is VA and the pads made from steel coated with zinc phosphate.	105

Table 5-19 Summary of the fretting fatigue results of material 40054. P is constant, F is VA and pads made from steel coated with zinc phosphate.....	106
Table 5-20 Summary of the fretting fatigue results of material 40060. P is static, F is VA fatigue and pads made of material 40054.	106
Table 5-21 Summary of the fretting fatigue results of material 40060. P is static, F is VA fatigue and pads made from steel coated with zinc phosphate.	107
Table 6-1 Prediction of the fretting fatigue lifetime of experiments summarised in Table 5-11. Specimens made from material 40054 and pads from steel, coated with zinc phosphate. P is constant and F is CA.	124
Table 6-2 Prediction of the fretting fatigue lifetime of experiments summarised in Table 5-12. Specimens made from material 40060 and pads from material 40054. P is static and F is CA.	124
Table 6-3 Prediction of the fretting fatigue lifetime of experiments summarised in Table 5-13. Specimens made from material 40060 and pads from steel coated with zinc phosphate. P is static and F is CA.	125
Table 6-4 Prediction of the fretting fatigue lifetime of experiments summarised in Table 5-14. Specimens made from material 40060 and pads from material 40054. P and F are CA.	125
Table 6-5 Prediction of the fretting fatigue lifetime of experiments summarised in Table 5-15. Specimens made from material 40060 and pads made from steel coated with zinc phosphate.....	125
Table 6-6 Prediction of the fretting fatigue lifetime of experiments summarised in Table 5-19. Specimens made from material 40054 and pads from steel coated with zinc phosphate. P is constant and F is VA.....	126
Table 6-7 Prediction of the fretting fatigue lifetime of experiments summarised in Table 5-20. Specimens made from material 40060 and pads from material 40054. P is static and F is VA.	126

Table 6-8 Prediction of the fretting fatigue lifetime of experiments summarised in Table 5-21. Specimens made from material 40060 and pads from steel coated with zinc phosphate. P is static and F is VA. 127

Chapter 1

Introduction

1.1 Background

Fretting is a term used to describe the wear damage that occurs at the surface of two materials in contact subjected to small amplitude oscillatory movements. This is different to fatigue which is a damage mechanism of engineering materials subjected to cyclic loading. In situations where the material undergoes both fretting and fatigue, the wear damage from fretting becomes more detrimental, leading to an early failure called fretting fatigue. This damage mechanism is very complex and responsible for premature failure of engineering materials when they are in contact [1].

A classic example of fretting fatigue damage is found at the contact interface of disc to blade assemblies of aero-turbine engines. Fretting fatigue damage has also been seen on the cylinder block and gasket of internal combustion diesel engines. Therefore, the challenging task faced by engineers is to predict the operational life of components subjected to fretting fatigue loading. This research is intended to address this challenging problem by providing a suitable design approach that can be used.

1.2 Research aims and objectives

The aim of this research is to formalise and experimentally validate a novel design methodology which can predict the in-service lifetime of materials under fretting fatigue loading. In this research work, the material to be assessed under fretting fatigue damage is cast iron. The novelty characterising this work is the fact that the finite lifetime estimation of materials subjected to variable amplitude fretting fatigue loading has not been examined in detail. Hence, the proposed design methodology predicts the finite lifetime under constant amplitude and most importantly under variable amplitude fretting fatigue loading.

In order to design materials against fretting fatigue, the “notch analogue” concept introduced by Giannakopoulos et al. [2] is one of the most relevant breakthrough. This concept postulated that the cracking behaviour in the notched metallic materials subjected to fatigue loading are similar to those observed under fretting fatigue. This idea was used by Dini D et al. [3] to investigate fretting fatigue damage of metallic materials. It was concluded that the stress gradient of the fretted and notched components is similar. More fretting fatigue investigations using the “notch analogue” concept are summarised in chapter 2.1.

By taking advantage of existing similarities in terms of cracking behaviour between notch fatigue and fretting summarised in the previous paragraph, the proposed design methodology uses the Modified Wöhler Curve Method (MWCM). This is applied in conjunction with the Theory of Critical Distance (TCD) in the form of Point Method (PM) and the Shear Stress-Maximum Variance Method (τ -MVM). The objectives (OBJ) of this work are:

- OBJ 1: To review the work done on fretting fatigue.
- OBJ 2: To run fatigue tests under uniaxial and torsion in order to calibrate the MWCM's and the critical distance equations.
- OBJ 3: To formalise a design methodology that can estimate the finite lifetime of materials under constant and variable amplitude fretting fatigue loading.
- OBJ 4: To run the fretting fatigue experiments under constant and variable amplitude loading.
- OBJ 5: To use the fretting fatigue experimental results to validate the proposed design methodology.

1.3 Publications

The outcomes of the fretting fatigue investigations presented in this thesis were published in the International Journal of Fatigue as well as in the conference proceedings of the 7th and 9th International Conference on Fracture Fatigue and Wear.

Journal Papers:

- C.T. Kouanga, J.D. Jones, I. Revill, A. Wormald, D. Nowell, R.S. Dwyer-Joyce, J.A. Araújo, L. Susmel. On the estimation of finite lifetime under fretting fatigue loading. International Journal of Fatigue 2018; 112: 138-152.
<https://doi.org/10.1016/j.ijfatigue.2018.03.013>
- C.T. Kouanga, J.D. Jones, I. Revill, A. Wormald, D. Nowell, R.S. Dwyer-Joyce, L. Susmel. A variable amplitude fretting fatigue life estimation technique: Formulation and experimental validation. Tribology International 2023; Volume 178, Part A, 108055.
<https://doi.org/10.1016/j.triboint.2022.108055>

Conference Proceedings Paper:

- C. V. Teuchou Kouanga, J. D. Jones, I. Revill, A. Wormald, D. Nowell, R. S. DwyerJoyce, J. A. Araújo, L. Susmel. Finite Lifetime Estimation of Mechanical Assemblies Subjected to Fretting Fatigue Loading. In: Proceedings of the 7th International Conference on Fracture Fatigue and Wear. The 7th International Conference on Fracture Fatigue and Wear, 09-10 Jul 2018, Ghent University, Belgium. Lecture Notes in Mechanical Engineering. Springer Nature, pp. 345-358. <https://eprints.whiterose.ac.uk/133459/1/FAT%2031.pdf>
- Kouanga, C.V.T., Nowell, D., Joyce, R.S.D., Susmel, L. (2022). Critical Plane and Critical Distance Approaches to Assess Damage Under Variable Amplitude Fretting Fatigue Loading. In: Abdel Wahab, M. (eds) Proceedings of the 9th International Conference on Fracture, Fatigue and Wear. FFW 2021. Lecture Note in Mechanical Engineering. Springer, Singapore.
https://doi.org/10.1007/978-981-16-8810-2_13

Chapter 2

literature review

2.1 Overview of fretting fatigue

Fretting fatigue is a very complex phenomenon which is influenced by a number of physical, environmental and mechanical factors. These include: contact geometry, contact load, coefficient of friction, fatigue load, microstructure of the material, surface condition of materials in contact, material properties and temperature [4]. Fretting fatigue normally leads to the premature failure of mechanical assemblies. This premature failure results from the reduction of the fatigue limit of materials by up to 50% [5]. Therefore, the prediction of in-service lifetime of materials under fretting fatigue loading is of great interest in engineering. In this regard, multiaxial critical plane approaches and continuum damage mechanics have been used in the past to predict fretting fatigue life [6, 7]. However, multiaxial critical plane approaches are more popular for fretting fatigue life prediction. The review of some of the most used critical plane approaches is summarised in the next paragraphs.

One of the approaches is the Smith-Watson-Topper (SWT). The SWT criterion is a multiaxial strain energy parameter which states that crack initiates on the material plane maximising the product of the normal strain range and the maximum tensile stress during a loading cycle. It is expressed as [8, 9]:

$$SWT = \sigma_{max} \cdot \frac{\Delta \epsilon}{2} \quad 2-1$$

According to Manson-Coffin and Basquin's law [10], the SWT criterion can also be expressed as follows:

$$SWT = \frac{\sigma_f^2}{E} (2N_f)^{2b} + \sigma_f \epsilon_f (2N_f)^{b+c} \quad 2-2$$

Where, $\sigma_f, \varepsilon_f, b$ and c are material constants obtained from fatigue and static tests of plain specimens. The formulation in Eqs. 2-1 and 2-2 allows the estimation of the fatigue life.

Another approach is formalised by Fatemi and Socie (FS). The FS criterion is a strain base multiaxial approach which assumes that failure occurs on the material plane experiencing the maximum shear strain during a loading cycle. It is expressed as follows [11]:

$$FS = \frac{\Delta\gamma}{2} \left(1 + k \frac{\sigma_{n,max}}{\sigma_y} \right) = B \cdot N_f^c \quad 2-3$$

Where, $\Delta\gamma$ is the shear strain range and $\sigma_{n,max}$ is the maximum normal stress. These quantities are related to the plane experiencing the maximum shear strain amplitude. σ_y is the yield stress, k is a material parameter and N_f is the number of cycles to failure. B and C are material constants obtained from fatigue and static tests of plain specimens.

The Findley parameter (FP) is a multiaxial stress approach which defines the critical plane as the material plane experiencing the maximum combination of the shear stress amplitude and the maximum normal stress. This can be written as [12]:

$$FP = \tau_a + k\sigma_{n,max} = \tau_f' N_f^{b'} \quad 2-4$$

Where, k is the material crack growth sensitivity to normal stress, N_f is the number of cycles to failure, τ_f' and b' are the fatigue strength coefficients under shear and torsion respectively.

The Modified Wöhler Curve Method (MWCM) is another multiaxial stress based criterion which assumes that failure occurs on the material plane experiencing the maximum shear stress amplitude. The way the MWCM is used to estimate the number of cycles to failure of a material is reviewed in detail in chapter 2.4.7.

Over the past years, the above multiaxial critical plane criteria have been used to predict the lifetime of materials under fretting fatigue loading. For instance, Belloula et al. [13]

investigated the fretting fatigue behaviour of Al-Mg-Si alloy by running a CA fretting fatigue experiment. To estimate the finite lifetime, the multiaxial fatigue parameter SWT was used. This paper found out that the predicted fatigue life was in good agreement with the experimental results.

Following a different philosophy, Castro et al. [14, 15, 16] estimated the finite lifetime of Al4%Cu alloy subjected to CA fretting fatigue loading by using the MWCM in conjunction with the Theory of Critical Distance (TCD) [17, 18] and the Maximum Rectangular Hull [19, 20, 21, 22] concept. In their design approach, the Maximum Rectangular Hull approach was used to locate the critical plane. The TCD applied in the form of the Point Method (PM) was used in order to account for the damaging effect of the multiaxial stress gradients acting in the vicinity of the contact region. This is reviewed in chapter 2.4.6. In order to estimate the fretting fatigue life, the stress components relative to the critical plane were post-processed according to the MWCM. Again, the predicted lives were in agreement with the experimental results with an error factor of two.

In a series of investigations, Araújo et al [23] examined how fretting wear affected the estimation of fretting fatigue lifetime under CA loading. They also compared the level of accuracy of the three multiaxial fatigue criteria review above, i.e. SWT, FP and MWCM in the estimation of fretting fatigue life. The design method used to predict the fretting fatigue life was based on the TCD in conjunction with either SWT, FP or MWCM. The TCD was formalised in terms of point method (PM). The critical distance was calibrated experimentally [18, 23]. This is explained in chapter 2.4.6. The PM which accounted for the stress gradient at the contact, was used either with the SWT, FP or MWCM to calculate the fretting fatigue life. The wear damage was accounted for using the dissipated friction energy law [24, 25]. The proposed design method was validated with experimental data produced by Cardoso et al. [26], which involved a cylindrical pad on-plane contact configuration. In this experimental setting, the assessed material was Ti-6AL-4V and all tests were set under partial slip condition. The loading condition for each test involved a constant load normal to the pad as well as a CA fatigue load on the fretting

specimen. Figure 2-1 compares the level of accuracy of the three multiaxial fatigue criteria SWT, FP and MWCM.

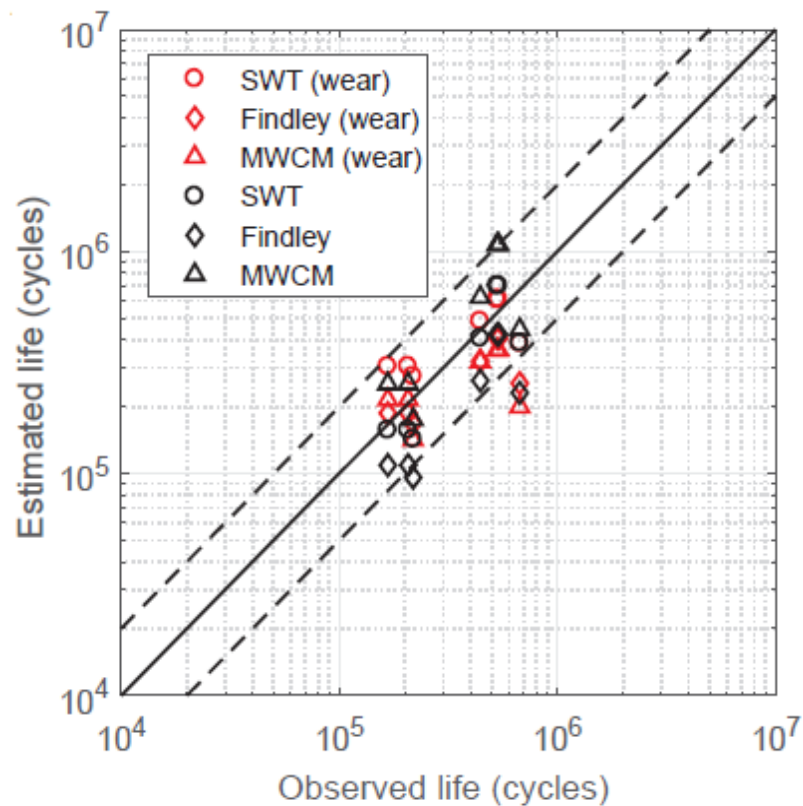


Figure 2-1 Estimated vs observed fretting fatigue lifetime with and without wear damage [23].

It was concluded that the use of PM in conjunction with either one of the multiaxial fatigue criteria, SWT, FP or MWCM gives good estimation within a scattered band of 2. Similarly, Gaillieue et al [27] assessed the accuracy of the multiaxial critical plane criteria, MWCM, SWT and FS in the prediction of the fretting fatigue life of Al7050-T7451 subjected to CA loading. In this case, the PM was used in conjunction with either the MWCM, SWT or FS. The MWCM, SWT and FS were calibrated using the uniaxial fatigue data. In order to validate the design methodology, several fretting fatigue tests using a cylindrical pad on a flat specimen configuration were carried out. In each tests, the contact load was constant, the tangential loads applied to the pad CA cyclic and the fatigue load applied to the specimen CA cyclic.

In order to predict the number of cycles to failure, the stress field at the trailing edge of the contact was post-processed using the PM in conjunction with either MWCM, SWT or

FS. Figure 2-2 below compares the experimental number of cycles to failure against the estimated number of cycles to failure for all the fretting fatigue tests.

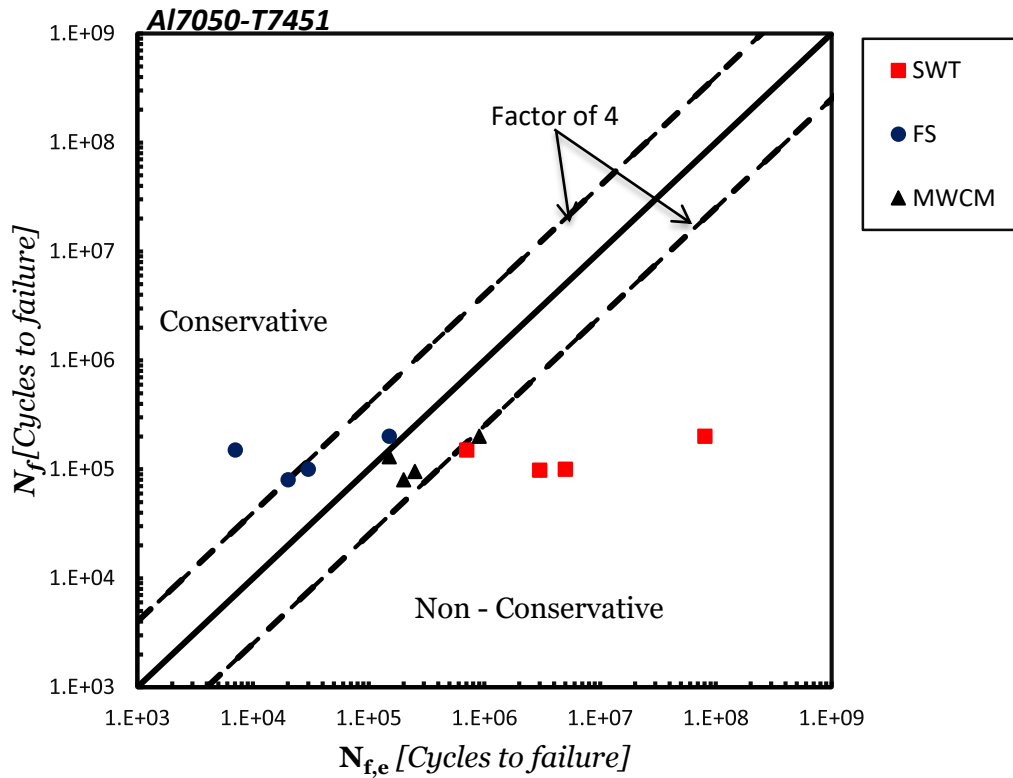


Figure 2-2 Fretting fatigue life prediction of material Al7050-T7451 [27]

Clearly, the results obtained with SWT were overestimated, meanwhile the results obtained with the MWCM and FS were in good agreement with the experimental results. Pinto et al. [28] carried out a numerical analysis to investigate the fretting fatigue damage under variable amplitude shear loading. The fretting fatigue configuration used for this purpose was a cylindrical pad on a flat specimen. Both pads and specimens were made of the Al-7075-7651. The pads were subjected to a constant normal load and a VA cyclic tangential force. Whereas, the fatigue load on the specimen was CA cyclic. Both the tangential and fatigue loads were in phase. To estimate the lifetime of the assessed material, they post-processed the stress field at the contact edge using the TCD in conjunction with the SWT and Palmgren-Miner law (this law is reviewed in chapter

2.4.9). In the proposed design methodology, the stress gradient at the contact was accounted using the TCD formalised in terms of the PM. The critical distance used in the PM was a constant calculated using Tanaka's relation (Eq.2-73). The Palmgren-Miner law was used to evaluate the cumulative damage of the applied load. Finally, the number of cycles to failure was calculated using the SWT. The proposed methodology was not validated because of the lack of variable amplitude fretting fatigue experimental data. This work is recommended to be used as a basis to generate experimental data of fretting fatigue under VA loading.

Dini et al. [3] used a short crack arrest criterion [29] in conjunction with the critical distance concept [30] to predict fretting fatigue thresholds. The aim of the short crack arrest was to assess fretting fatigue damage resulting from severe stress gradients along the contact of materials. To validate their predictions, fretting test results generated by Nowell [31] and the fretting fatigue experiments reported in [29] were used. It was concluded that the criteria provide good predictive capabilities. Fretting fatigue performance of blade-to-disc assemblies in aircraft gas turbines was also investigated by Nowell et al. [32]. To simulate the loading experienced by dovetail blade roots in turbines of aero-engines, a number of bespoke CA fretting fatigue experiments were carried out using blade-type specimens. In order to predict the fretting fatigue lives of the specimens, they used short crack arrest methods [29, 33] to post-process the stress fields located at the contact zone of the specimen.

The above studies show that several works have been carried out in predicting the lifetime of materials subjected to fretting fatigue loading. In most of the fretting fatigue experiments covered in the literature, the contact load applied to the pads was constant, while the tangential load at the contact interface and the fatigue load applied to the fretting specimen were both CA cyclic. This shows that very little work has been done in the prediction of material lifetime under VA fretting fatigue loading. Therefore, this research is intended to close this gap by initially running fretting fatigue experiments where the contact load is constant and the fatigue load is VA cyclic. The next steps will

involve investigating how multiaxial critical plane approach used in conjunction with the TCD can predict the lifetime of materials subjected to VA fretting fatigue loading. In order to achieve this goal, a review of the principles underlining contact mechanics used in assessing fretting fatigue damage of mechanical assemblies is summarised in the chapter 2.2.

2.2 Review of contact mechanics

Contact mechanics is the study of the deformation which arises as a result of two bodies being pressed against each other. This type of deformation occurs at the contact surface of mechanical components such as dovetail connection, riveted connection, gears and bearing. To predict the lifetime of mechanical assemblies under fretting fatigue loading, the linear elastic stress field at the contact region should be estimated and post-processed [15, 34]. Therefore, understanding the type of contact as well as the calculation of stresses around the contact zones are of significant importance in designing real components against fretting fatigue.

2.2.1 Different types of contact

Over the years, different approaches have been used to estimate the stress field at the contact area. These approaches depend on the type of contact used. The first classification of contact is non-conforming contact as shown in Figure 2-3a. For this type of contact, the contact area increases with applied load. The maximum contact pressure occurs at the centreline and not at the edges of the contact [1]. By contrast, Figure 2-3b shows complete contact. It consists of a rigid flat end punch pressed onto an elastic plane. In this configuration, the contact area changes with the geometry of the contacting body and most importantly, does not depend on the contact load [1].

In practice, some fretting damage may result from the combination of both complete and incomplete contact. This is the case of flat punch with round edge shown in Figure 2-3c. In this type of configuration, contact is said to be locally incomplete at the round edge

because at this location, the contact area changes slightly with the normal load. Away from the round edge, contact is considered as complete.

In this research, because of time constrain, only the contact configuration described in Figure 2-3a will be used throughout the fretting fatigue experiments.

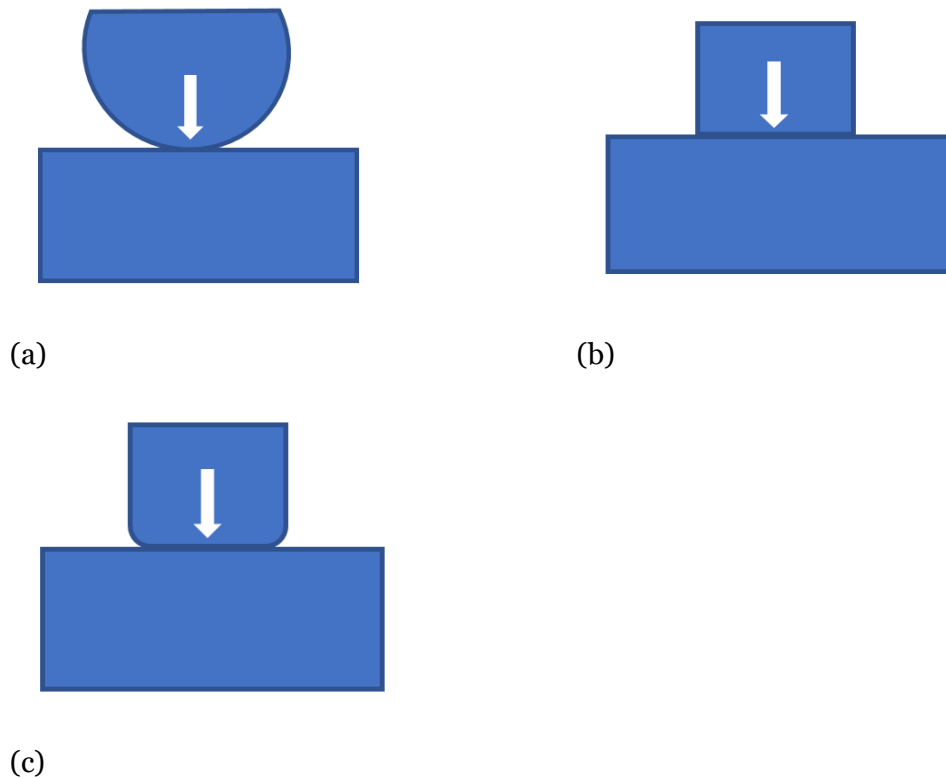


Figure 2-3 Characterisation of contacts; (a) Incomplete and non-conformal, (b) Complete, (c) Flat and round punch [1].

2.2.2 Mechanics of fretting fatigue

When two components are brought into contact, they initially make contact at a single point or along a line depending on the contact surface. Loads are often supported on a small surface area of the component, resulting in very high contact stress. For example, the size of the railway wheel is approximately 1 meter in diameter. However, the apparent contact area between the railway wheel and the track is very small and results in very high contact stress. This means that, metallic materials need to be designed to withstand high contact stress in order to prevent component failure.

In 1881, Heinrich Hertz developed an analytical method for estimating the contact area and stress for non-conforming contact. His model was based on the following assumptions [1]:

- Contact load is normal to the interface, which means negligible friction at the interface.
- The contacting materials are homogenous and the yield stress is not exceeded.
- The contacting bodies are at rest and in equilibrium.
- The effect of surface roughness is negligible.
- The size of the contact is small compared to the relevant dimensions of the bodies in contact.

Hertz analytical tools can be applied to two dimensional (2D) and three dimensional (3D) elastic contacts. In Figure 2-4, the 2D contact parameters essential to many engineering applications are evaluated.

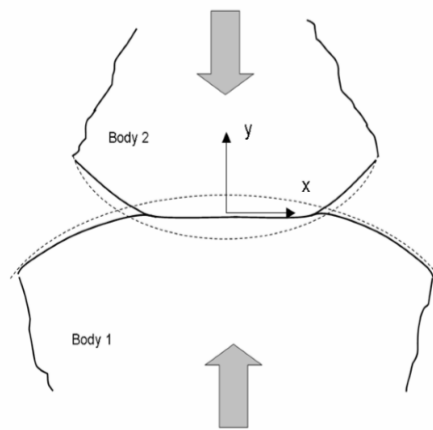


Figure 2-4 Schematic of Hertzian contact [1].

The elastic deformation within the contacting bodies in Figure 2-4 results in a contact half width, a , given as follows [1]:

$$a = \sqrt{\frac{4PR'}{\pi E^*}} \quad 2-5$$

Where, P , is the normal load per unit length, R' the reduced radius of curvature of the contact bodies and E^* the reduced elastic modulus. The reduced radius is defined by:

$$\frac{1}{R'} = \frac{1}{R_1} + \frac{1}{R_2} \quad 2-6$$

Where, R_1 and R_2 are the radii of curvature of the contacting bodies '1' and '2' respectively, while the reduced elastic modulus is given by:

$$\frac{1}{E^*} = \left(\frac{1 - \nu_1^2}{E_1} + \frac{1 - \nu_2^2}{E_2} \right) \quad 2-7$$

In the above definition, ν_1 and ν_2 are the Poisson's ratio of the contacting bodies '1' and '2', respectively. E_1 and E_2 are the elastic moduli associated to bodies '1' and '2'.

The Hertz stress distribution $P(x)$, within the contact area is governed by the following equation [1]:

$$P(x) = P_0 \sqrt{1 - \frac{x^2}{a^2}} \quad 2-8$$

Where, a is the contact half width, P_0 is the peak contact pressure and x is the horizontal distance along the contact. The peak contact pressure is given by:

$$P_0 = \frac{2P}{a\pi} \quad 2-9$$

The Hertzian stress distribution, $P(x)$, resulting from the contact between bodies '1' and '2' in Figure 2-4, has an elliptical form as shown in Figure 2-5. The peak contact stress occurs at the centreline and reduces gradually to zero at the edges of the contact.

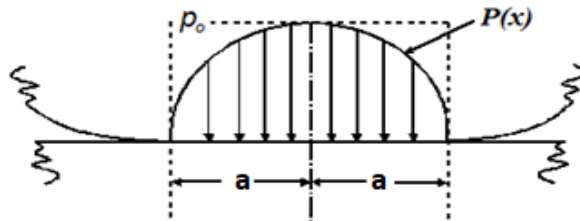


Figure 2-5 Hertzian contact stress distribution.

The above Hertz' theory was extended by Cattaneo and Mindlin [1] to cover the application of fretting shown in Figure 2-6.

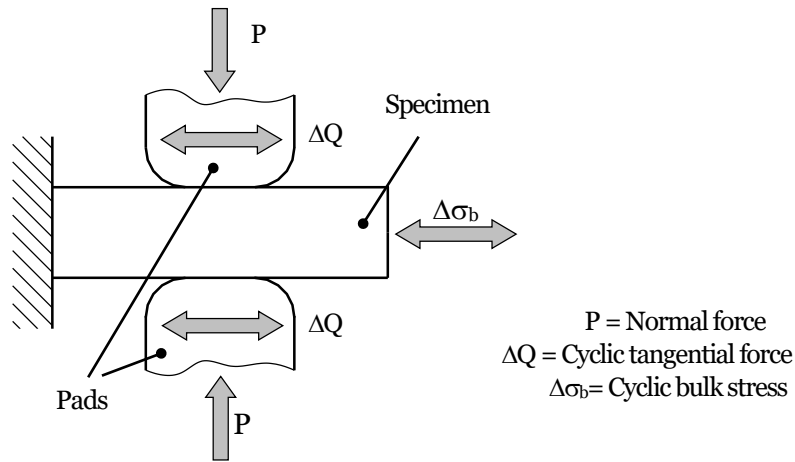


Figure 2-6 Schematisation of fretting fatigue.

The above figure shows one of a schematic of the fretting fatigue experimental set-up. In this schematisation, two cylindrical pads are pressed against a specimen by a normal load, P to form a Hertzian contact of half-width, a , and pressure distribution given by Eq.(2-8). Also, a cyclic tangential force, Q is applied to the pads such that the Coulomb limit is not exceeded, i.e.

$$Q < f * P \quad 2-10$$

Where, f represents the coefficient of friction.

The loading condition in definition (2-10) is the *so-called* partial slip. Under this condition, particles around the centre of the contact stick because there is a high normal pressure to sustain tangential load through the mechanism of friction, whereas near the edges of the contact the low contact pressure causes slip. Figure 2-7 shows the stick and slip regions in partial slip regime. The central stick zone corresponds to the region $-c < x < c$ and the slip zone to the region $-a < x \leq -c$ or $c \leq x < a$. The shear traction $q(x)$ across the contact which satisfies the slip and stick zones is given by the Cattaneo and Mindlin equations [1]:

$$q(x) = fp_0\sqrt{1 - (x/a)^2} + q'(x) \quad 2-11$$

Where $q'(x) = 0 \quad -a < x \leq -c \text{ or } c \leq x < a \quad 2-12$

and $q'(x) = -fp_0 (c/a)\sqrt{1 - (x/c)^2} \quad -c < x < c \quad 2-13$

c represents the size of the stick zone given by:

$$\frac{c}{a} = \sqrt{1 - \left| \frac{Q_{max}}{fP} \right|} \quad 2-14$$

Q_{max} is the amplitude of the tangential cyclic load.

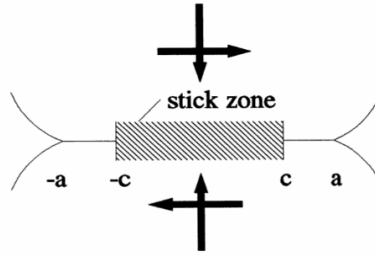


Figure 2-7 Schematic of the stick and slip regions in partial slip.

Fretting fatigue normally occurs in the presence of a remote cyclic bulk stress, $\Delta\sigma_b$ (Figure 2-6). This allowed Nowell et al [1] to extend the Cattaneo-Mindlin shear traction in Eq. (2-13) to account for damage caused by the remote bulk stress. In more detail, the presence of bulk stress in the fretting specimen creates an eccentricity to the Mindlin-Cattaneo shear traction distribution and shifts the location of the central stick zone by an amount, e . Therefore, the shear traction distribution, $q(x)$ along the contact region which satisfies the slip and stick zones is still defined by Eq. 2-11. In this equations, $q'(x) = 0$ in the slip zone and in the stick zone it becomes [1]:

$$q'(x) = -fp_0 \left(\frac{c}{a} \right) \sqrt{1 - ((x - e)/c)^2} \quad -c < x < c \quad 2-15$$

Where, e is the amount by which the central stick zone is shifted defined by:

$$e = \frac{a \cdot \sigma_{b,a}}{4fP_0} \quad 2-16$$

In Eq.(2-16), $\Delta\sigma_b$ is the amplitude of the remote bulk stress. For very large remote bulk stresses, the stick zone will approach the contact edge and invalidate the solution in Eq. (2-15). Therefore, this solution is only valid if [1]: $e + c \leq a$.

To estimate fretting fatigue lifetime under constant amplitude loading, the above analytical solution was used to estimate the stress field at the contact zone [35, 36]. Therefore, this analytical tool will be used in this research to validate the finite element analysis of the fretting fatigue experiments.

2.3 Review of stress quantities used in fatigue assessment

2.3.1 Multiaxial stress state

Consider a cylindrical specimen subjected to a sinusoidal constant amplitude loads in tension and torsion as shown in Figure 2-8, at any given time, the multiaxial stress state at a generic material point is defined by the following tensor:

$$[\sigma(t)] = \begin{bmatrix} \sigma_x(t) & \tau_{xy}(t) & \tau_{xz}(t) \\ \tau_{xy}(t) & \sigma_y(t) & \tau_{yz}(t) \\ \tau_{xz}(t) & \tau_{yz}(t) & \sigma_z(t) \end{bmatrix} \quad 2-17$$

Where, $\sigma_x(t)$, $\sigma_y(t)$ and $\sigma_z(t)$ are the normal stress components while $\tau_{xy}(t)$, $\tau_{xz}(t)$ and $\tau_{yz}(t)$, are the shear stress components.

In practice, when mechanical components are subjected to multiaxial loading, fatigue cracks occur mainly at the surface of the components [37]. Therefore the design is simplified by a biaxial stress state at the component surface. Such a biaxial stress is defined by the following tensor:

$$[\sigma(t)] = \begin{bmatrix} \sigma_x(t) & \tau_{xy}(t) & 0 \\ \tau_{xy}(t) & \sigma_y(t) & 0 \\ 0 & 0 & 0 \end{bmatrix} \quad 2-18$$

Where:

$$\sigma_x(t) = \sigma_{x,m} + \sigma_{x,a} \cdot \sin(w \cdot t - \delta_{xy,x}) \quad 2-19$$

$$\tau_{xy}(t) = \tau_{xy,m} + \tau_{xy,a} \cdot \sin(w \cdot t - \delta_{xy,x}) \quad 2-20$$

As can be seen in Figure 2-8 (b), $\sigma_{x,m}$ and $\tau_{xy,m}$ represent the mean normal and mean shear stress amplitude, respectively. Similarly, $\sigma_{x,a}$ is the normal amplitude, $\tau_{xy,a}$ is the shear stress amplitude and $\delta_{xy,x}$ is the so-called *out-of-phase angle*. According to [17], the out-of-phase angle and the presence of non-zero mean stresses can be beneficial, neutral or detrimental to the multiaxial fatigue lifetime of materials.

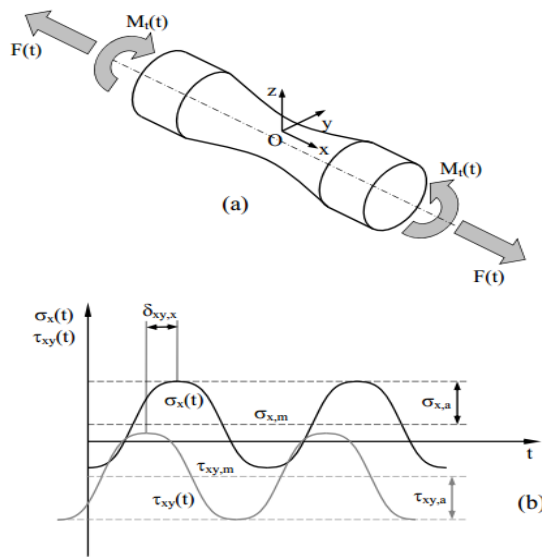


Figure 2-8 Cylindrical specimen subjected to combined sinusoidal tension and torsion [17].

2.3.2 Critical Plane concept

Metallic materials subjected to fatigue loading can experience crack initiation and propagation within the component or at the surface. If the crack is located at the surface of the material, Brown [38] suggested the use of the critical plane approach to predict fatigue lifetime. The critical plane approach here depends on the crack propagation mode. According to Brown [38] and Socie [39] if a Stage I crack is mainly Mode I governed, the critical plane is the region where the normal stress components reach their maximum values. However, if the Stage I crack is mode II governed, the critical plane is the plane experiencing the maximum shear stress amplitude. Most recently, Susmel [40]

has reformulated the Maximum Variance Method in order to calculate the orientation of the critical plane in multiaxial fatigue problems.

2.3.3 Stress quantities used in fatigue assessment

Let assume that the specimen in Figure 2-8 (a) is now subjected only to a time variable uniaxial tension. The uniaxial stress state at a point o is given by:

$$[\sigma(t)] = \begin{bmatrix} \sigma_x(t) & 0 & 0 \\ 0 & 0 & 0 \\ 0 & 0 & 0 \end{bmatrix} \quad 2-21$$

Where, $\sigma_x(t)$ is a sinusoidal time dependent stress quantity as defined in Eq. (2-19). This time variable stress is quantified by a minimum value $\sigma_{x,min}$, a maximum value $\sigma_{x,max}$, a mean value $\sigma_{x,m}$ and the stress amplitude $\sigma_{x,a}$.

The ratio of the minimum stress to the maximum stress is an impactful quantity in fatigue assessment known as the load ratio, R . This is defined as:

$$R = \frac{\sigma_{x,min}}{\sigma_{x,max}} \quad 2-22$$

The minimum and maximum stresses can be expressed in term of the mean stress and the stress amplitude. *i. e.*,

$$\sigma_{x,min} = \sigma_{x,m} - \sigma_{x,a} \quad 2-23$$

$$\sigma_{x,max} = \sigma_{x,m} + \sigma_{x,a} \quad 2-24$$

In fatigue assessments the load ratio can take on three range of values, $R > 0$, $R = 0$ and $R < 0$. This is illustrated in Figure 2-9. In particular, when $R = -1$, the load is said to be fully-reversed.

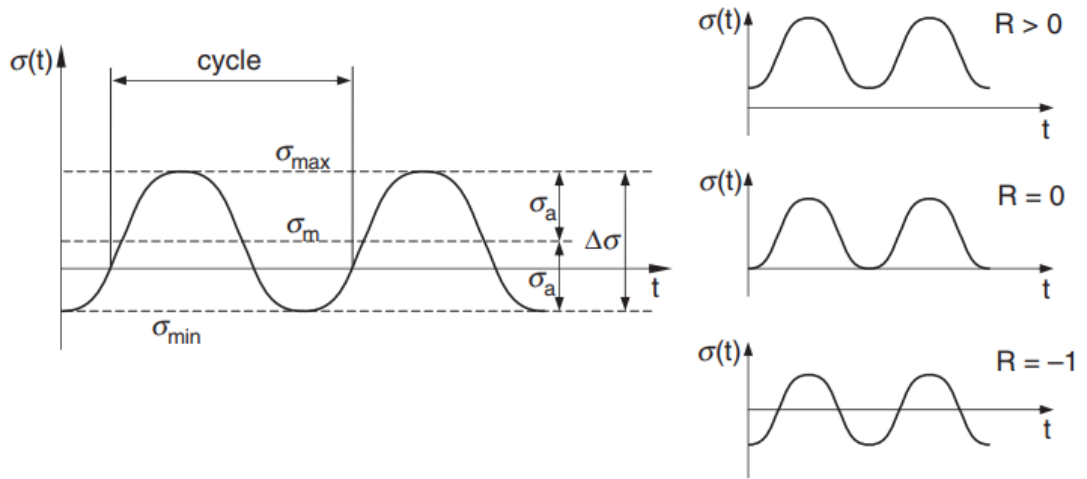


Figure 2-9 Definition of stresses used to predict fatigue damage under uniaxial loading.

The stress amplitude $\sigma_{x,a}$, the range $\Delta\sigma_a$, the mean stress, $\sigma_{x,m}$ and the maximum stress, $\sigma_{x,max}$ defined in Figure 2-9 are mathematically expressed as follows:

$$\sigma_{x,a} = \frac{\sigma_{x,max} - \sigma_{x,min}}{2} = \sigma_{x,max} - \sigma_{x,m} \quad 2-25$$

$$\Delta\sigma_a = \sigma_{x,max} - \sigma_{x,min} = 2\sigma_{x,a} \quad 2-26$$

$$\sigma_{x,m} = \frac{\sigma_{x,max} + \sigma_{x,min}}{2} \quad 2-27$$

$$\sigma_{x,max} = \frac{2\sigma_{x,a}}{1 - R} \quad 2-28$$

Due to limit number of materials, all fretting fatigue tests will be carried out under fatigue load ratio $R = -1$ and $R = 0.1$. Also, as summarised in chapter 2.1, this two load ratios are the most used in carrying out fretting fatigue experiments.

2.3.4 Stress concentration factor

In general, the change in the geometry of a material affects its stress distribution. Consequently, the material can experience extreme or less severe stress concentration, depending on the type of geometry. Extreme cases are mainly found in materials experiencing cracks whereas less severe stress concentration are associated to notched materials. Therefore, the detrimental effect of the stress concentration should be

accounted for during any fatigue assessment of metallic components. The extent to which the notch increases the local stress is explained in the next paragraph.

Consider for example, a notched plate subjected to a uniaxial tensile force as shown in Figure 2-10.

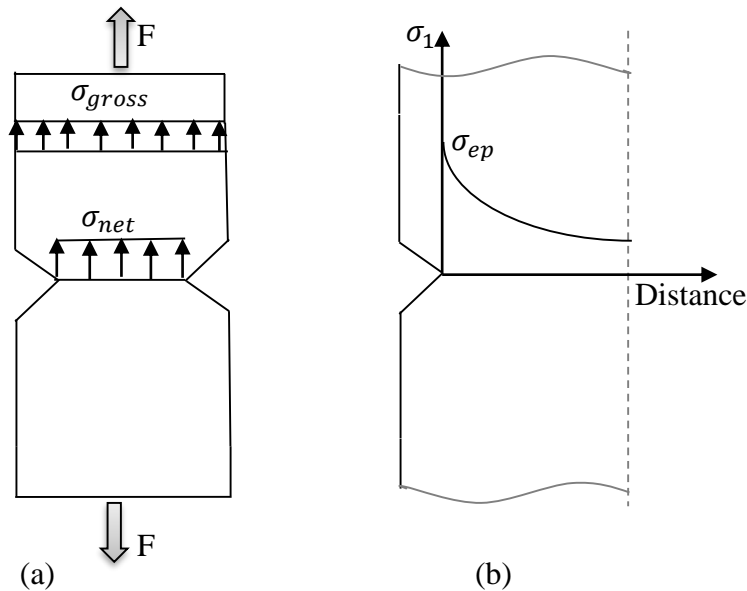


Figure 2-10 Definition of: (a) net and gross nominal stress and (b) linear elastic peak stress at the tip of a notch

The three types of stresses characterising the notched plate are σ_{ep} , σ_{gross} and σ_{net} . The stress quantity σ_{ep} is the maximum principal linear elastic stress resulting from uniaxial loading. The nominal gross stress, σ_{gross} is calculated from the maximum cross sectional area while the nominal net stress, σ_{net} is calculated from the minimum cross sectional area of the plate. At the tip of the notch, σ_{ep} is maximum and decreases further away from the notch tip. The extent to which the notch increases the local stress is quantified by the stress concentration factor, K_t as proposed by Peterson [17].

$$K_{t,net} = \frac{\sigma_{ep}}{\sigma_{net}} \quad 2-29$$

$$K_{t,gross} = \frac{\sigma_{ep}}{\sigma_{gross}} \quad 2-30$$

Similarly, in situations where the notched specimen is loaded in torsion, the stress concentration factor K_{ts} is expressed as:

$$K_{ts,net} = \frac{\tau_{ep}}{\tau_{net}} \quad 2-31$$

$$K_{ts,gross} = \frac{\tau_{ep}}{\tau_{gross}} \quad 2-32$$

Where, τ_{ep} is the linear elastic peak shear stress, τ_{net} is the nominal net and τ_{gross} is the gross shear stress.

2.4 Review of fundamental concepts in fatigue assessment

2.4.1 Crack initiation and growth in metallic materials

Metallic materials subjected to cyclic loading, experiences a fatigue damage after a certain number of cycles. During this regime, the material experiences a crack initiation and propagation phenomenon which can be summarised in the following stages [41].

- Stage I: In the first stage of the propagation phenomenon, micro cracks initiate and propagate along the plane of maximum shear stress reaching a length of few grains.
- Stage II: At the end of Stage I, cracks are orientated in a direction perpendicular to tensile stress on the material.

Each stage of the cracking propagation phenomenon is governed by the *so-called* cracking Mode. In most cases, Stage I is governed by Mode II while Stage II is governed by Mode I. The definition of the different cracking modes is summarised in Figure 2-11.

- **Mode I** refers to the opening mode resulting from a tensile force. In this mode, the crack surfaces are perpendicular to the tensile stress.
- **Mode II** refers to in-plane shear mode. In this mode, the crack surfaces are parallel to the acting shear stress.
- **Mode III** refers to the out-of-plane shear mode.

In this thesis, the proposed design approach to predict fretting fatigue lifetime assumed crack initiates on the plane experiencing the maximum shear stress. This correspond to Stage I crack initiation, governed by Mode II.

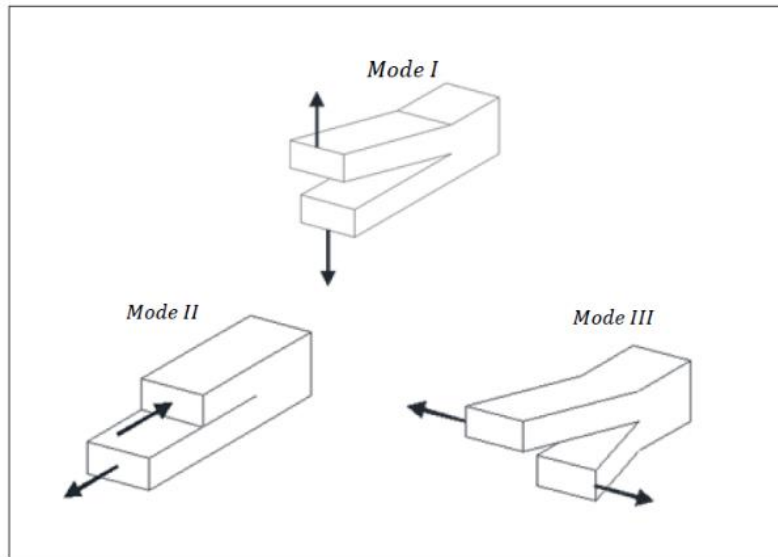


Figure 2-11 Definition of loading mode.

2.4.2 The Wöhler curves

In 1830, August Wöhler carried out an in situ fatigue assessment on a railway axle while the rail carriage was in service. He concluded that the stress amplitude and the mean stress had a detrimental effect on fatigue life [42]. Few years later, Wöhler's fatigue data were plotted in a log-log diagram which represented the foundation of the Wöhler curve used nowadays. The Wöhler curve (also referred to as the S-N curve) is a log-log graph of the applied stress amplitude against the number of cycles to failure, N_f . A typical fatigue behaviour of ferrous metallic materials is shown in Figure 2-12 (a). In this figure, σ_0 represents the fatigue limit stress and below this threshold value, fatigue failure will never occur. However, non-ferrous materials such as cast iron do not exhibit fatigue limit. Consequently, they must be designed for finite life. For this design purpose, a so called endurance limit σ_A is required. This is the stress amplitude extrapolated in a high cycle fatigue regime for which $N_A \approx 10^6 - 10^8$ cycles [17]. Therefore, the endurance limit

ensures that the assessed non-ferrous materials survives a number of cycles before failure. An example in this case is shown in Figure 2-12 (b and c). Furthermore, Figure 2-12 (c) shows that in some non-ferrous materials, the line representing the fatigue behaviour in the medium-cycle fatigue regime is steeper than that in the high cycle.

The Wöhler curve is characterised by the negative inverse slope, k and the reference stress amplitude σ_0 for ferrous materials and σ_A for non-ferrous materials both of which are extrapolated at a given number of cycles N_0 and N_A respectively. For any stress amplitude, $\sigma_{x,a}$ with a corresponding number of cycles to failure, N_f the Wöhler curve can be mathematically expressed as [17]:

$$\sigma_{x,a}^k \cdot N_f = \sigma_0^k \cdot N_0 = \sigma_A^k \cdot N_A = \text{constant} \quad 2-33$$

However, a non-ferrous material exhibiting a Wöhler curve similar to Figure 2-12 (c) is expressed mathematically as [17]:

$$\sigma_{x,a}^{k_1} \cdot N_f = \sigma_{kp}^{k_1} \cdot N_{kp} \quad \text{for } N_f \leq N_{kp} \quad 2-34$$

$$\sigma_{x,a}^{k_2} \cdot N_f = \sigma_{kp}^{k_2} \cdot N_{kp} \quad \text{for } N_f \geq N_{kp} \quad 2-35$$

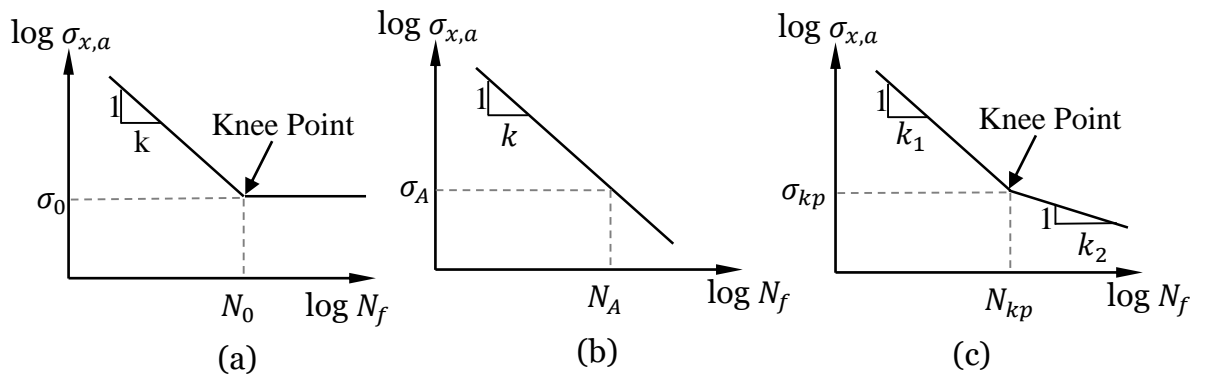


Figure 2-12 (a) Wöhler curve of ferrous material. (b) and (c) Wöhler curves of non-ferrous material [17].

In this research, the material to be investigate under fretting fatigue damage is cast iron which is a non-ferrous material. Therefore, it will be designed for finite life.

2.4.3 Statistical determination of fatigue curve

In order to determine the endurance limit, σ_A of a material, several fatigue tests at different stress levels are required. In each test, a stress level σ_i produces a corresponding number of cycles to failure, N_f . The total number of tests generate a set of fatigue data which is used to generate the Wöhler diagram. Figure 2-13 is an example of a Wöhler diagram generated from the fatigue data by post-processing the data using the least-square regression analysis approach [17, 43].

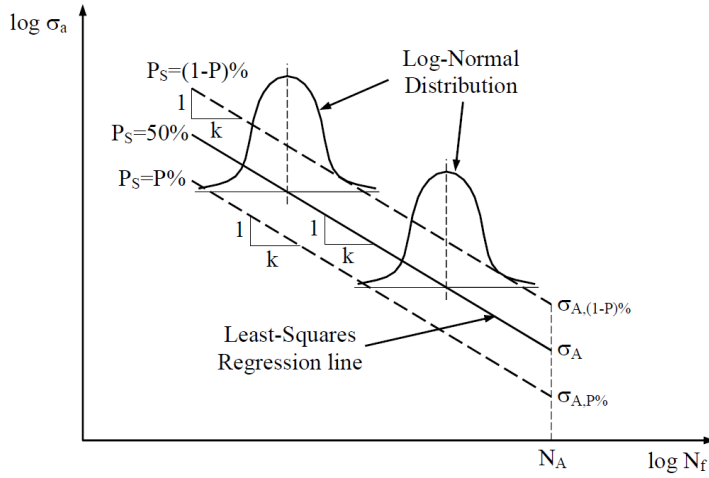


Figure 2-13 Wöhler diagram showing fatigue curves calculated for different probabilities of survival [17].

In order to explain the least-square regression approach, let us consider a set of fatigue experiments which consist of testing the i^{th} specimens ($i = 1, 2, \dots, n$) with different stress amplitude level $\sigma_{a,i}$ ($i = 1, 2, \dots, n$), the tested specimens fails at $N_{f,i}$ ($i = 1, 2, \dots, n$). The Wöhler curve having a probability of survival, P_S , equal to 50% as shown in Figure 2-13 is described by the following linear equation [17, 43]:

$$\log(N_{f,i}) = c_0 + c_1 \cdot \log(\sigma_{a,i}) \quad 2-36$$

Where c_0 and c_1 are constants which can be calculated as follows [43] :

$$c_1 = \frac{\sum_{i=1}^n (x_i - x_m) \cdot (y_i - y_m)}{\sum_{i=1}^n (x_i - x_m)^2} = \frac{\sum_{i=1}^n (\log \sigma_{a,i} - x_m) \cdot (\log N_{f,i} - y_m)}{\sum_{i=1}^n (\log \sigma_{a,i} - x_m)^2} \quad 2-37$$

$$c_0 = c_1 x_m - y_m \quad 2-38$$

where

$$x_m = \frac{\sum_{i=1}^n x_i}{n} = \frac{\sum_{i=1}^n \log \sigma_{a,i}}{n} \quad 2-39$$

$$y_m = \frac{\sum_{i=1}^n \log N_{f,i}}{n} \quad 2-40$$

From equation (2-36), the endurance limit, σ_A extrapolated at N_A and the negative inverse slope, k of the Wöhler curve having a probability of survival $P_S = 50\%$ take on the following values:

$$\sigma_A = \left(\frac{10^{c_0}}{N_A} \right)^{\frac{1}{k}} \quad 2-41$$

$$k = -c_1 \quad 2-42$$

Similarly, with a probability of survival $P\%$, the endurance limit $\sigma_{A,P\%}$ and $\sigma_{A,(1-P)\%}$ extrapolated at N_A can be expressed as follows [17, 43]:

$$\sigma_{A,P\%} = \sigma_A \left(\frac{N_A}{10^{\log(N_A)+q \cdot s}} \right)^{\frac{1}{k}} \quad 2-43$$

$$\sigma_{A,1-P\%} = \sigma_A \left(\frac{N_A}{10^{\log(N_A)-q \cdot s}} \right)^{\frac{1}{k}} \quad 2-44$$

where, s is the standard deviation and q is a statistical index which accounts for the confidence level corresponding to the number of tested samples [44]. Table 2-1 lists some values of q .

$$s = \sqrt{\frac{\sum_{i=1}^n \left\{ \log(N_{f,i}) - \log \left[\left(\frac{\sigma_A}{\sigma_{a,i}} \right)^k \right] \right\}^2}{n-1}} \quad 2-45$$

Finally, having calculated $\sigma_{A,P\%}$ and $\sigma_{A,(1-P)\%}$, the width of the scatter band, T_σ is defined as a ratio of $\sigma_{A,(1-P)\%}$ to $\sigma_{A,P\%}$.

Table 2-1 Index q with different probabilities of survival, P_s and a 95% confidence level [17].

n	q			
	$P_s=90\%$	$P_s=95\%$	$P_s=97.7\%$	$P_s=99\%$
3	6.158	7.655	9.445	10.552
4	4.163	5.145	6.317	7.042
5	3.407	4.202	5.152	5.741
6	3.006	3.707	4.544	5.062
7	2.755	3.399	4.167	4.641
8	2.582	3.188	3.907	4.353
9	2.454	3.031	3.719	4.143
10	2.355	2.911	3.573	3.981
15	2.068	2.566	3.155	3.52
20	1.926	2.396	2.951	3.295
25	1.838	2.292	2.828	3.158
30	1.778	2.22	2.742	3.064
35	1.732	2.166	2.678	2.994
40	1.697	2.126	2.630	2.941
45	1.669	2.092	2.589	2.897
50	1.646	2.065	2.559	2.863
55	1.626	2.042	2.531	2.833
60	1.609	2.022	2.507	2.807
65	1.594	2.005	2.487	2.785
70	1.581	1.990	2.471	2.765
75	1.570	1.976	2.453	2.748
80	1.559	1.964	2.439	2.733

The least-square regression analysis is used in this research to calculate the endurance limit, σ_A and the negative inverse slope, k (extrapolated at N_A) of the investigated materials.

2.4.4 Effect of notch in fatigue assessment

According to [45, 46, 47], notches have a detrimental effect on the fatigue lifetime of materials under any loading conditions be it static or dynamic. Figure 2-14 shows the Wöhler fatigue curves for plain and notched specimens made of the same material. Both specimens are subjected to uniaxial tensile cyclic load. The detrimental effect of the considered notched specimen is quantified in terms of the fatigue strength reduction factor, K_f as shown in Figure 2-14. According to [48], the fatigue strength reduction factor is given by:

$$K_f = 1 + q(K_{t,net} - 1) \quad 2-46$$

Where, q ranges from 0 to 1 and $K_{t,net}$ as defined in Eq. 2-29. For a non-damaging notch, q equals zero whereas for a fully sensitive notch, q equals one. The fatigue strength reduction factor can also be calculated according to [49]:

$$K_f = 1 + \frac{K_t - 1}{1 + \sqrt{\frac{a_n}{r_n}}} \quad 2-47$$

Where, a_n and r_n are the critical distances calculated using the material's ultimate tensile strength and the notch root radius, respectively.

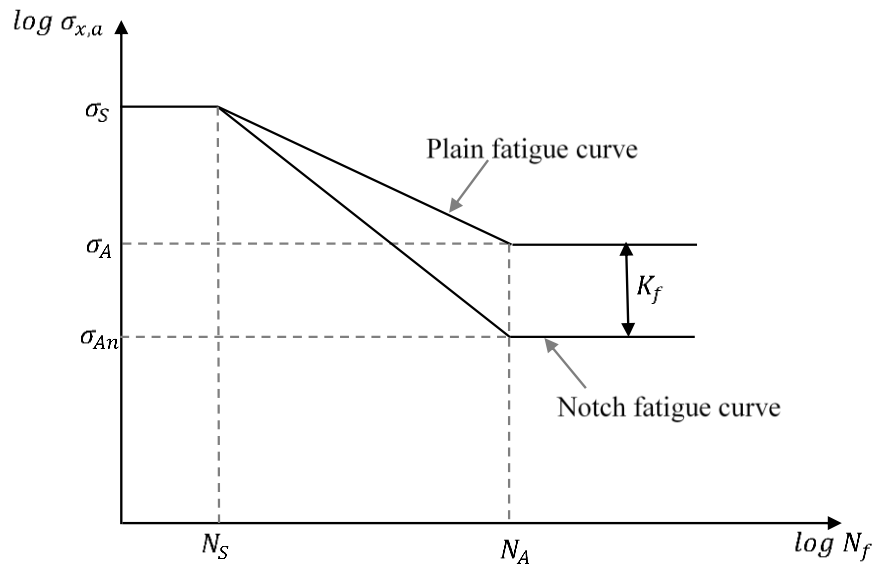


Figure 2-14 Definition of the fatigue strength reduction factor, K_f .

2.4.5 Maximum Variance Method and the critical plane stress components

In order to perform the fatigue assessment of mechanical assemblies, one of the trickiest task is to determine the orientation of the critical plane and its associated stress quantities. This task has led Susmel [40] to reformulate the maximum variance method (MVM) to efficiently determine the orientation of the critical plane in multiaxial fatigue problems. It suggested that the Shear Stress–Maximum Variance Method (τ -MVM) defines the critical plane as the material plane containing the direction experiencing the maximum variance of the resolved shear stress, $\tau_{MV}(t)$ [50, 51]. In situations where at

least two different directions experience the maximum variance of the resolved shear stress, the critical plane to be used for the fatigue assessment is the plane experiencing the largest value of the maximum normal stress. The full algorithm for the determination of the critical plane according to the τ -MVM can be found in [40] while its validation is found in [52].

In order to describe the τ -MVM in details, considered a body subjected to an external system of cyclic forces as shown in Figure 2-15 (a). Consider also the center of the body to be at point O, which coincides with the most critical location (where crack initiates).

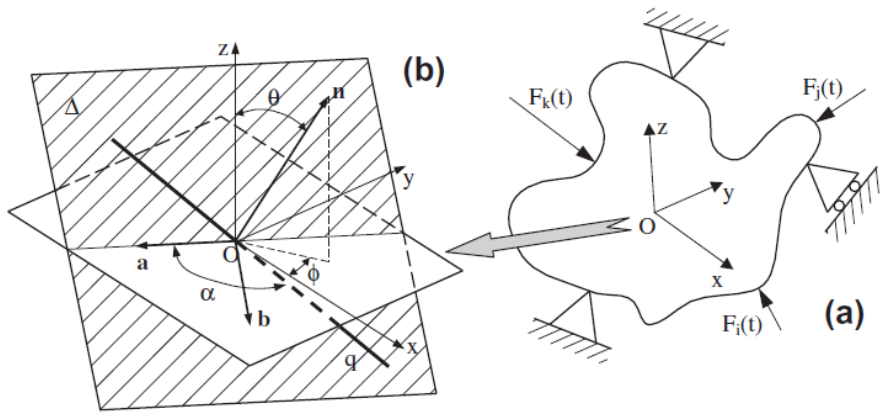


Figure 2-15 Definition of a generic material plane [40].

The stress state at this point is described by the stress tensor:

$$\sigma(t) = \begin{bmatrix} \sigma_x(t) & \sigma_{xy}(t) & \sigma_{xz}(t) \\ \sigma_{xy}(t) & \sigma_y(t) & \sigma_{yz}(t) \\ \sigma_{xz}(t) & \sigma_{yz}(t) & \sigma_z(t) \end{bmatrix} \quad 2-48$$

Where, $\sigma_x(t)$, $\sigma_y(t)$ and $\sigma_z(t)$ are the normal stress components while $\sigma_{xy}(t)$, $\sigma_{xz}(t)$ and $\sigma_{yz}(t)$ are the shear stress components. A generic plane, Δ is indicated by the hatch area having a unit vector \mathbf{n} and defined through angles ϕ and θ . The angle ϕ is the angle between the x-axis and the projection of the unit vector \mathbf{n} on the x-y plane while θ is the angle between the unit vector \mathbf{n} and the z-axis. To calculate the stress components relative to the plane under consideration, a new system of coordinates, onab is introduced and defined as follows [40]:

$$n = \begin{bmatrix} n_x \\ n_y \\ n_z \end{bmatrix} = \begin{bmatrix} \sin(\theta) \cos(\phi) \\ \sin(\theta) \sin(\phi) \\ \cos(\theta) \end{bmatrix} \quad 2-49$$

$$b = \begin{bmatrix} b_x \\ b_y \\ b_z \end{bmatrix} = \begin{bmatrix} \cos(\theta) \cos(\phi) \\ \cos(\theta) \sin(\phi) \\ -\sin(\theta) \end{bmatrix} \quad 2-50$$

$$a = \begin{bmatrix} a_x \\ a_y \\ a_z \end{bmatrix} = \begin{bmatrix} \sin(\phi) \\ -\cos(\theta) \\ 0 \end{bmatrix} \quad 2-51$$

Let us now consider a generic direction, q , passing through the point O and lying on the considered plane, Δ . The unit vector, q can be expressed as [40]:

$$q = \begin{bmatrix} q_x \\ q_y \\ q_z \end{bmatrix} = \begin{bmatrix} \cos(\alpha) \sin(\phi) + \sin(\alpha) \cos(\theta) \cos(\phi) \\ -\cos(\alpha) \cos(\phi) + \sin(\alpha) \cos(\theta) \sin(\phi) \\ -\sin(\alpha) \sin(\theta) \end{bmatrix} \quad 2-52$$

Where, α is the angle between the a -axis and the generic direction q .

According to the above definitions, the instantaneous values of the stress, $\sigma_n(t)$ normal to the plane, Δ and the shear stress, $\tau_q(t)$ relative to the generic direction, q can be calculated respectively as [40]:

$$\sigma_n(t) = [n_x \ n_y \ n_z] \begin{bmatrix} \sigma_x(t) & \sigma_{xy}(t) & \sigma_{xz}(t) \\ \sigma_{xy}(t) & \sigma_y(t) & \sigma_{yz}(t) \\ \sigma_{xz}(t) & \sigma_{yz}(t) & \sigma_z(t) \end{bmatrix} \begin{bmatrix} n_x \\ n_y \\ n_z \end{bmatrix} \quad 2-53$$

$$\tau_q(t) = [q_x \ q_y \ q_z] \begin{bmatrix} \sigma_x(t) & \sigma_{xy}(t) & \sigma_{xz}(t) \\ \sigma_{xy}(t) & \sigma_y(t) & \sigma_{yz}(t) \\ \sigma_{xz}(t) & \sigma_{yz}(t) & \sigma_z(t) \end{bmatrix} \begin{bmatrix} n_x \\ n_y \\ n_z \end{bmatrix} \quad 2-54$$

The shear stress, $\tau_q(t)$ relative to the generic direction, q can be simplified using the following scalar product:

$$\tau_q(t) = \mathbf{d} \cdot \mathbf{s}(t) \quad 2-55$$

Where \mathbf{d} is a vector of direction cosines and $\mathbf{s}(t)$ is a vector defined as:

$$\mathbf{d} = [n_x q_x \quad n_y q_y \quad n_z q_z \quad n_x q_y + n_y q_x \quad n_x q_z + n_z q_x \quad n_y q_z + n_z q_y] \quad 2-56$$

$$\mathbf{s}(t) = [\sigma_x(t) \quad \sigma_y(t) \quad \sigma_z(t) \quad \sigma_{xy}(t) \quad \sigma_{xz}(t) \quad \sigma_{yz}(t)] \quad 2-57$$

Therefore, according to these definitions, the variance of the shear stress $\tau_q(t)$ relative to the direction q can be calculated directly as:

$$Var[\tau_q(t)] = Var\left[\sum_k d_k s_k(t)\right] = \sum_i \sum_j d_i d_j Cov[s_i(t), s_j(t)] \quad 2-58$$

Eq.2-58 holds based on the fact that $Cov[s_i(t), s_j(t)] = Var[\sigma_i(t)]$ when $i = j$ and

$Cov[s_i(t), s_j(t)] = Cov[s_j(t), s_i(t)]$ when $i \neq j$. Therefore, Eq. (2-58) can be rewritten in the following simplified form:

$$Var[\tau_q(t)] = \mathbf{d}^T [C] \mathbf{d} \quad 2-59$$

[C] is a square matrix containing both the variance and covariance as defined in 2-60.

$$[C] = \begin{bmatrix} V_x & C_{x,y} & C_{x,z} & C_{x,xy} & C_{x,xz} & C_{x,yz} \\ C_{x,y} & V_y & C_{y,z} & C_{y,xy} & C_{y,xz} & C_{y,yz} \\ C_{x,z} & C_{y,z} & V_z & C_{z,xy} & C_{z,xz} & C_{z,yz} \\ C_{x,xy} & C_{y,xy} & C_{z,xy} & V_{xy} & C_{xy,xz} & C_{xy,yz} \\ C_{x,xz} & C_{y,xz} & C_{z,xz} & C_{xy,xz} & V_{xz} & C_{xz,yz} \\ C_{x,yz} & C_{y,yz} & C_{z,yz} & C_{xy,yz} & C_{xy,yz} & V_z \end{bmatrix} \quad 2-60$$

Where:

$$V_i = Var[\sigma_i(t)] \text{ for } i = x, y, z, xy, xz, yz \quad 2-61$$

$$C_{i,j} = Cov[\sigma_i(t), \sigma_j(t)] \text{ for } i = x, y, z, xy, xz, yz \quad 2-62$$

It can be seen from the terms defined from Eq. 2-60 to 2-62, that the variance of the resolved shear stress depends on the load history damaging the material but does not depend on the orientation of the considered material plane. Consequently, Eq. 2-59 represents the fundamental mathematical frame work of the τ -MVM.

In order to calculate the critical plane using conventional methods, the number of iterations required to post-process the load history are equals to the number of material

planes. Whereas, only two iterations of post-processing of the load history is required to determine the critical plane according to the τ -MVM [40]. The first iteration consists of the determination of the mean value of the time variable stress tensor. In the second iteration, the variance and the co-variance terms of the stress components are calculated. Therefore, as soon as the variance defined in Eq.2-61 and co-variance in Eq.2-62 are known, the computational time required to determine the critical plane becomes a conventional multi-variable optimisation problem. This does not depend on the length of the input load history itself. The full algorithm to determine the critical plane according to the τ -MVM is reported in [40].

In order to understand the application of the τ -MVM, consider the specimen in Figure 2-15 (a). It is subjected to a time variable constant amplitude (CA) stress state at the assumed critical location. Having determined the critical plane using τ -MVM, then the mean value, $\sigma_{n,m}$, and the amplitude, $\sigma_{n,a}$, of the stress normal to the critical plane, $\sigma_n(t)$ can be directly calculated in accordance to the following standard definitions [50]:

$$\sigma_{n,m} = \frac{1}{2}(\sigma_{n,max} + \sigma_{n,min}) \quad 2-63$$

$$\sigma_{n,a} = \frac{1}{2}(\sigma_{n,max} - \sigma_{n,min}) \quad 2-64$$

Where, $\sigma_{n,max}$ and $\sigma_{n,min}$ are the maximum and minimum values of $\sigma_n(t)$, respectively. Similarly, the mean value, τ_m , and the amplitude, τ_a , of the shear stress relative to the critical plane, $\tau_{MV}(t)$, take on the following values [50]:

$$\tau_m = \frac{1}{2}(\tau_{MV,max} + \tau_{MV,min}) \quad 2-65$$

$$\tau_a = \frac{1}{2}(\tau_{MV,max} - \tau_{MV,min}) \quad 2-66$$

Where, $\tau_{MV,max}$ and $\tau_{MV,min}$ are the maximum and minimum values of $\tau_{MV}(t)$, respectively.

Under variable amplitude (VA) loading, the mean value, $\sigma_{n,m}$, and the amplitude, $\sigma_{n,a}$, of the stress normal to the critical plane, $\sigma_n(t)$ can also be calculated using Eq.s 2-67 and 2-68 [50]:

$$\sigma_{n,m} = \frac{1}{T} \int_0^T \sigma_n(t) \cdot dt \quad 2-67$$

$$\sigma_{n,a} = \sqrt{2 \cdot Var[\sigma_n(t)]} \quad 2-68$$

Where, $Var[\sigma_n(t)]$ is the variance of the stress component $\sigma_n(t)$ given by:

$$Var[\sigma_n(t)] = \frac{1}{T} \int_0^T (\sigma_n(t) - \sigma_{n,m})^2 \cdot dt \quad 2-69$$

In the same way, the mean, τ_m and the amplitude value, τ_a of the shear stress relative to the critical plane, $\tau_{MV}(t)$ are given by the following equations [50]:

$$\tau_m = \frac{1}{T} \int_0^T \tau_{MV}(t) \cdot dt \quad 2-70$$

$$\tau_a = \sqrt{2 \cdot Var[\tau_{MV}(t)]} \quad 2-71$$

Where $Var[\tau_{MV}(t)]$ is the variance of the stress component $\tau_{MV}(t)$ given by:

$$Var[\tau_{MV}(t)] = \frac{1}{T} \int_0^T (\tau_{MV}(t) - \tau_m)^2 \cdot dt \quad 2-72$$

The τ -MVM has been used by Susmel et al. [46, 47, 53] to calculate the critical plane of plain and notched components subjected to CA and VA fatigue loading. These work concluded that, the τ -MVM is a powerful engineering tool suitable in locating the critical plane. Also, Kouanga et al. [35, 36] used the τ -MVM to calculate the orientation of the critical plane required to estimate the fretting fatigue lifetime under CA loading.

In this thesis, the τ -MVM will be used to determine the orientation of the critical plane and its associated stresses.

2.4.6 Theory of Critical Distance

In general, notched components are in fatigue limit condition when the applied stress is lower than or equal to the material plain fatigue limit, σ_A . The stress at which this condition hold is the *so-called* effective stress σ_{eff} , which can be calculated using the Theory of Critical Distance (TCD). The TCD was first formalised by Neuber [49]. In this formalisation, the effective stress was calculated by averaging the linear elastic maximum principal stress $\sigma_{1,a}$ in the vicinity of the notch tip [49]. This approach is known as the Line Method (LM). Neuber's idea was simplified by Peterson who suggested that the effective stress can be calculated at a given distance from the tip of the notch [48]. This method is now referred to as the Point Method (PM). Peterson's intuition was further developed by Taylor [30] and concluded that the reference stress could be obtained halfway the critical distance, L . Taylor went further and proposed a simpler way of calculating the critical distance by combining the threshold value of the stress intensity factor range with the plain fatigue limits as follows [18, 54]:

$$L = \frac{1}{\pi} \left(\frac{\Delta K_{th}}{\Delta \sigma_0} \right)^2 \quad 2-73$$

Where ΔK_{th} is the stress intensity factor threshold and $\Delta \sigma_0$ is the plain fatigue limit.

The TCD can also be used to perform static assessments of notched components. In this case the critical distance L_s , is calculated by using the material Ultimate Tensile Strength and the plain strain fracture toughness as expressed below [55]:

$$L_s = \frac{1}{\pi} \left(\frac{K_{Ic}}{\sigma_s} \right)^2 \quad 2-74$$

In Eq. 2-74, K_{Ic} is the plain material toughness and σ_s the ultimate tensile strength.

According to [56, 34, 17], in a medium-cycle fatigue regime, the critical distance L_M , increases as the number of cycles to failure N_f , decreases. This can be mathematically modelled by the L_M versus N_f relationship as:

$$L_M = A \cdot N_f^B$$

2-75

Where, A and B are material constants to be determined by post-processing simultaneously the plain and notched fatigue curves [46, 56]. The step by step procedure to determine the material constants A and B for any given material is as follow:

- **Step 1:** Plot the S-N curves of the plain and notched specimens subjected to a fully-reversed uniaxial load (Figure 2-16a).
- **Step 2:** Perform the finite element analysis (FE) of the notched specimen subjected to the nominal gross stress σ_{nom_g} (obtained at $N_f = N_{f,i}$ cycles). The linear elastic maximum principal stress around the notch of the specimens is plotted as shown in Figure 2-16b.
- **Step 3:** According to the PM, the notched material will fail if the amplitude of the linear elastic maximum principal stress at a distance $L_M/2$ from the notch tip is equal to the stress amplitude, $\sigma_{1i,a}$ damaging the plain material at $N_f = N_{f,i}$ cycles (Figure 2-16b).
- **Step 4:** Finally, by applying the strategy in Step 3, for any $N_f = N_{f,i}$ cycles the critical distance can be calculated. The least-squares method can then be used to estimate the values of A and B (Figure 2-16c).

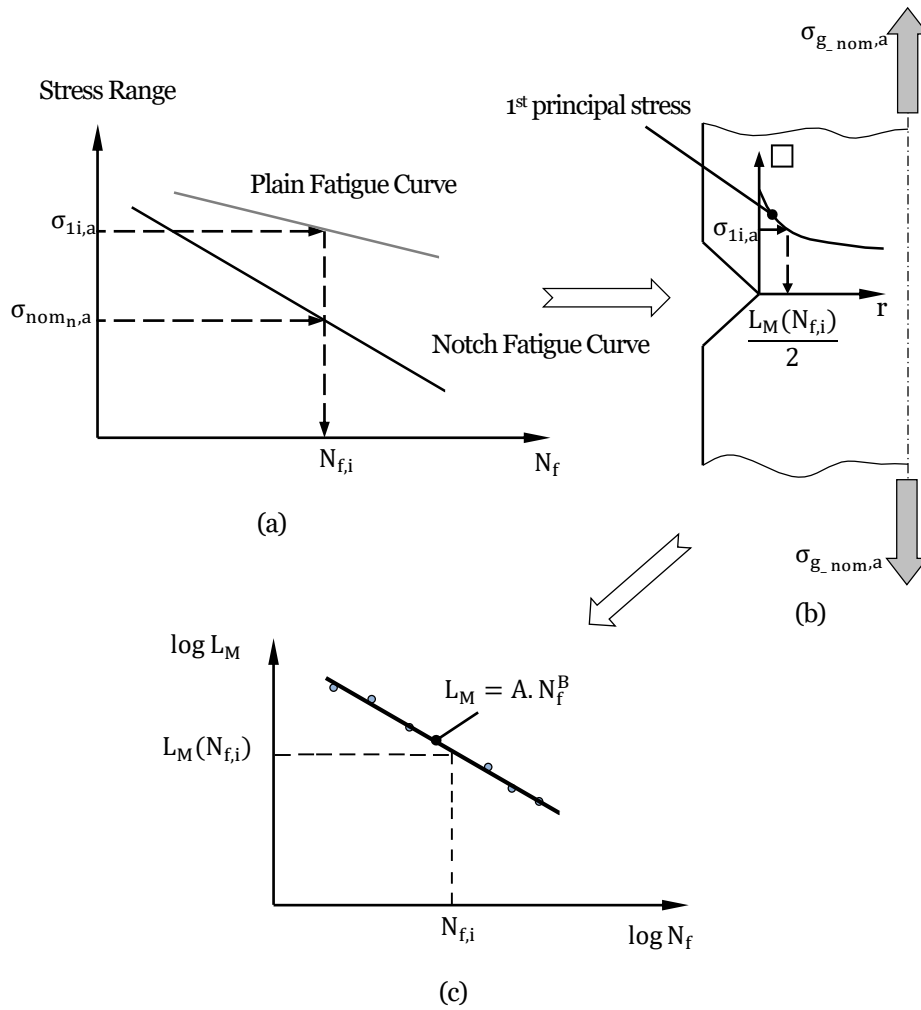


Figure 2-16 In-field procedure to determine the critical distance L_M , in the medium-cycle fatigue regime by using two calibration curves.

Susmel and Taylor [56] used the Wöhler relation (Eq. 2-33) in conjunction with the PM to predict fatigue life of notched specimens of low-carbon steel in medium-cycle fatigue regime. The idea was based on the fact that the critical distance L_M , decreases as the number of cycles to failure N_f , increases (Eq. 2-75). The critical distance was firstly calibrated using Eqs. 2-73 and 2-74. Then follow the calibration method summarised in Figure 2-16. It was found that the second calibration approach gave a higher accuracy of the prediction of the fatigue life. Therefore, because of its simplicity and accuracy, the PM is used in this research project and L_M vs N_f relationship defined in Eq. 2-75 is calibrated according to the experimental procedure summarised in Figure 2-16.

2.4.7 The Modified Wöhler Curve Method (MWCM)

The MWCM is a multiaxial fatigue criterion which assumes that the fatigue lifetime is predicted via the material plane experiencing the maximum shear stress amplitude [51, 57, 17]. Such a plane is the *so-called* critical plane. This assumption is supported by the experimental evidence provided by Miller et al. [58] and Socie [39]. Both showed that there is a very high probability for a crack to initiate on the material plane experiencing the maximum shear stress amplitude. The stress quantities relative to the critical plane are used to formalise the MWCM through the effective critical plane stress ratio, ρ_{eff} , as [59]:

$$\rho_{eff} = \rho_m + \rho_a = \frac{m \cdot \sigma_{n,m}}{\tau_a} + \frac{\sigma_{n,a}}{\tau_a} \quad 2-76$$

Where, $\sigma_{n,m}$ is the mean normal stress, $\sigma_{n,a}$ the normal stress amplitude, τ_a the maximum shear stress amplitude relative to the critical plane and m the mean stress sensitivity index [59]. In definition (2-76) the term, ρ_m considers the effect of the non-zero mean stresses while ρ_a accounts for the degree of non-proportionality and multiaxiality of the applied loading. [59, 17].

Schematically, the MWCM is illustrated by a log-log modified Wöhler diagram shown in Figure 2-17. It plots the shear stress amplitude relative to the critical plane, τ_A against the number of cycles to failure, N_f .

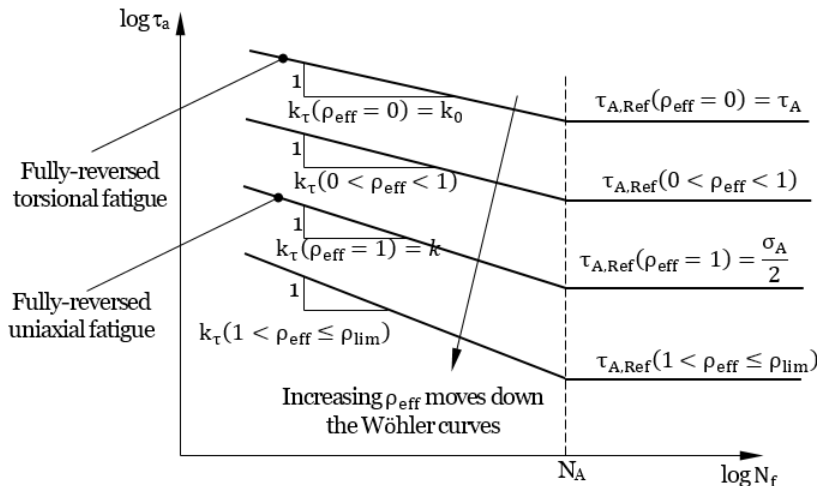


Figure 2-17 Modified Wöhler diagram.

As illustrated in Figure 2-17, the modified Wöhler curve is defined by its negative inverse slope, $K_\tau(\rho_{eff})$, and the reference shear stress amplitude, $\tau_{A,Ref}(\rho_{eff})$, calculated at a number of cycles N_A . In addition, under a fully-reversed uniaxial loading, ρ_{eff} takes the value of one whereas ρ_{eff} equals to zero for a fully-reversed torsional loading [17].

According to [46, 60], the MWCM functions $K_\tau(\rho_{eff})$ and $\tau_{A,Ref}(\rho_{eff})$ are expressed as:

$$k_\tau(\rho_{eff}) = (k - k_0) \cdot \rho_{eff} + k_0 \quad \text{for } \rho_{eff} \leq \rho_{lim} \quad 2-77$$

$$\tau_{A,Ref}(\rho_{eff}) = \left(\frac{\sigma_A}{2} - \tau_A \right) \cdot \rho_{eff} + \tau_A \quad \text{for } \rho_{eff} \leq \rho_{lim} \quad 2-78$$

Where, σ_A and k are the endurance limit and the negative inverse slope, respectively. They are both obtained from the fully-reversed uniaxial fatigue curve, whereas τ_A and k_0 are the corresponding quantities obtained from a torsional fatigue curve. In definitions (2-77) and (2-78), ρ_{lim} represents the material threshold limit as defined in Eq 2-81. It extends the use of the MWCM in situations where the critical plane experiences high values of ρ_{eff} . In more detail, for very high values of ρ_{eff} , Eq. 2-76 shows that the amplitude of the stress component perpendicular to the critical plane is much larger than the maximum shear stress amplitude. In this scenario, the mechanism leading to the final breakage is governed by Mode I instead of Mode II. Therefore, it is no longer justified to say that fatigue lifetime is predicted on the plane experiencing the maximum shear stress. However, by using the threshold limit ρ_{lim} , the MWCM as it stands can still be applied to situations of very high ratio, ρ_{eff} . In order to model situations involving large values of stress ratio ρ_{eff} , the negative inverse slope and the reference shear stress amplitude are calculated as [61]:

$$k_\tau(\rho_{eff}) = (k - k_0) \cdot \rho_{lim} + k_0 \quad \text{for } \rho_{eff} > \rho_{lim} \quad 2-79$$

$$\tau_{A,Ref}(\rho_{eff}) = \left(\frac{\sigma_A}{2} - \tau_A \right) \cdot \rho_{lim} + \tau_A \quad \text{for } \rho_{eff} > \rho_{lim} \quad 2-80$$

where:

$$\rho_{lim} = \frac{\tau_A}{2\tau_A - \sigma_A} \quad 2-81$$

Having estimated the required MWCM functions $K_\tau(\rho_{eff})$ and $\tau_{A,Ref}(\rho_{eff})$, the predicted number of cycles to failure is given by the following equation [17] :

$$N_{f,e} = N_A \cdot \left[\frac{\tau_{A,ref}(\rho_{eff})}{\tau_a} \right]^{k_\tau(\rho_{eff})} \quad 2-82$$

where, ρ_{eff} is the critical plane stress ratio and τ_a the maximum shear stress amplitude relative to the critical plane.

According to [46, 47, 61, 53], the MWCM in conjunction with the PM and the τ -MVM can be used to estimate the lifetime of notched components subjected to CA and VA loading. In this case, the τ -MVM is used to determine the critical plane and its relative stresses. The PM is used to account for the damaging effect of the multiaxial stress gradient in the vicinity of the notch while the MWCM is used to post-process the stress quantities relative to the critical plane and the calculation of the number of cycles to failure. The accuracy of this approach confirms with experimental results.

In conclusion, the use of the MWCM in conjunction with the PM and τ -MVM is a good tool in the prediction of finite lifetime of materials under fatigue loading. The MWCM is used in this research to post-process the stress quantities relative to the critical plane and also calculate the number of cycles to failure.

2.4.8 The mean stress sensitivity index

The mean stress sensitivity index m in Eq. 2-76 is a material property. It accounts for the portion of the mean stresses normal to the critical plane which effectively contributes to the opening of the micro cracks. In addition, m ranges between 0 and 1 [62]. The material is assumed to be insensitive to mean stresses when $m = 0$ while fully-sensitive when $m = 1$. [59, 17]. The mean stress sensitivity index is estimated as [46]:

$$m = \frac{\tau_a^*}{\sigma_{n,m}^*} \left(2 \frac{\tau_A - \tau_a^*}{2\tau_A - \sigma_A} - \frac{\sigma_{n,a}^*}{\tau_a^*} \right) \quad 2-83$$

Where, τ_a^* , $\sigma_{n,a}^*$ and $\sigma_{n,m}^*$ are the stress components relative to the critical plane generated by testing plain specimens under load ratio $R > 0$ and calculated at N_A cycles.

In order to determine m , the following experimental procedure can be executed [46]:

- **Step 1:** Estimate σ_A (extrapolated at N_A cycles) from a fully-reversed uniaxial fatigue curve.
- **Step 2:** Estimate τ_A (extrapolated at N_A cycles) from a fully-reversed torsional fatigue curve.
- **Step 3:** Estimate σ_a (extrapolated at N_a cycles) from a uniaxial fatigue curve generated with $R > 0$.

Having calculated σ_a in step 3, the stress components relative to the critical plane τ_a^* , $\sigma_{n,a}^*$ and $\sigma_{n,m}^*$ are defined as [17]:

$$\tau_a^* = \frac{\sigma_a}{2} \quad 2-84$$

$$\sigma_{n,a}^* = \frac{\sigma_a}{2} \quad 2-85$$

$$\sigma_{n,m}^* = \frac{\sigma_m}{2} \quad 2-86$$

$$\sigma_m = \sigma_{max} - \sigma_a \quad 2-87$$

$$\sigma_{max} = \frac{2\sigma_a}{1-R} \quad 2-88$$

The procedure described in the steps above will be used to determine the mean stress sensitivity index of the assessed materials in this study.

2.4.9 Palmgren-Miner Rule

The S-N curve described in Figure 2-17 is a tool widely used to predict the failure of materials under constant amplitude fatigue loading. However, during life service the fatigue loading may vary thereby making the direct use of an S-N curve under constant amplitude inapplicable [63, 64]. To overcome this, Palmgren-Miner proposed a linear-cumulative damage rule which allows the failure of materials under variable amplitude loading to be estimated using the standard constant amplitude S-N curves. What follows is the review of the Palmgren [63]-Miner [64] rule.

Figure 2-18a represents a notched material subjected to a variable amplitude loading, $\sigma(t)$. The applied load spectrum $\sigma(t)$ is made up of constant amplitude blocks k , with each block having stress amplitude σ_i and a number of cycles n_i (Figure 2-18b).

According to the Palmgren-Miner rule each block with stress amplitude σ_i , produces a small fraction of fatigue damage, D_i given by:

$$D_i = \frac{n_i}{N_{f,i}} \text{ for } i = 1, 2, \dots, k \quad 2-89$$

Where, $N_{f,i}$ is the number of cycles resulting to the breakage of the material if only the CA stress σ_i was present. $N_{f,i}$ is obtained from the S-N curve data (Figure 2-18c). By taking into account all the blocks of the loading spectrum, the resulting fatigue damage, D_{tot} (Figure 2-18d) is equal to:

$$D_{tot} = \sum_{i=1}^k \frac{n_i}{N_{f,i}} \quad 2-90$$

If failure is defined when $D_{tot} = D_{cr}$, then the number of blocks to failure, $N_{b,e}$ and cycles to failure, $N_{f,e}$ are given by:

$$N_{b,e} = \frac{D_{cr}}{D_{tot}} \quad 2-91$$

$$N_{f,e} = N_{b,e} \cdot \sum_{i=1}^k n_i \text{ for } i = 1, 2, \dots, k \quad 2-92$$

According to Palmgren-Miner rule, D_{cr} is the critical damage sum which takes the value of one. However, experiments conducted on mechanical components subjected to VA uniaxial fatigue loading have shown that D_{cr} can vary in the range 0.002 – 5 . In particular, the average D_{cr} for steel is equal to 0.27 and 0.37 for aluminium [65]. The limitation of Palmgren-Miner rule is the fact that it does not account for the sequence in which the constant amplitude loads occurs.

In this research, Palmgren-Miner rules is used to assess the cumulative damage associated to VA fretting fatigue loading.

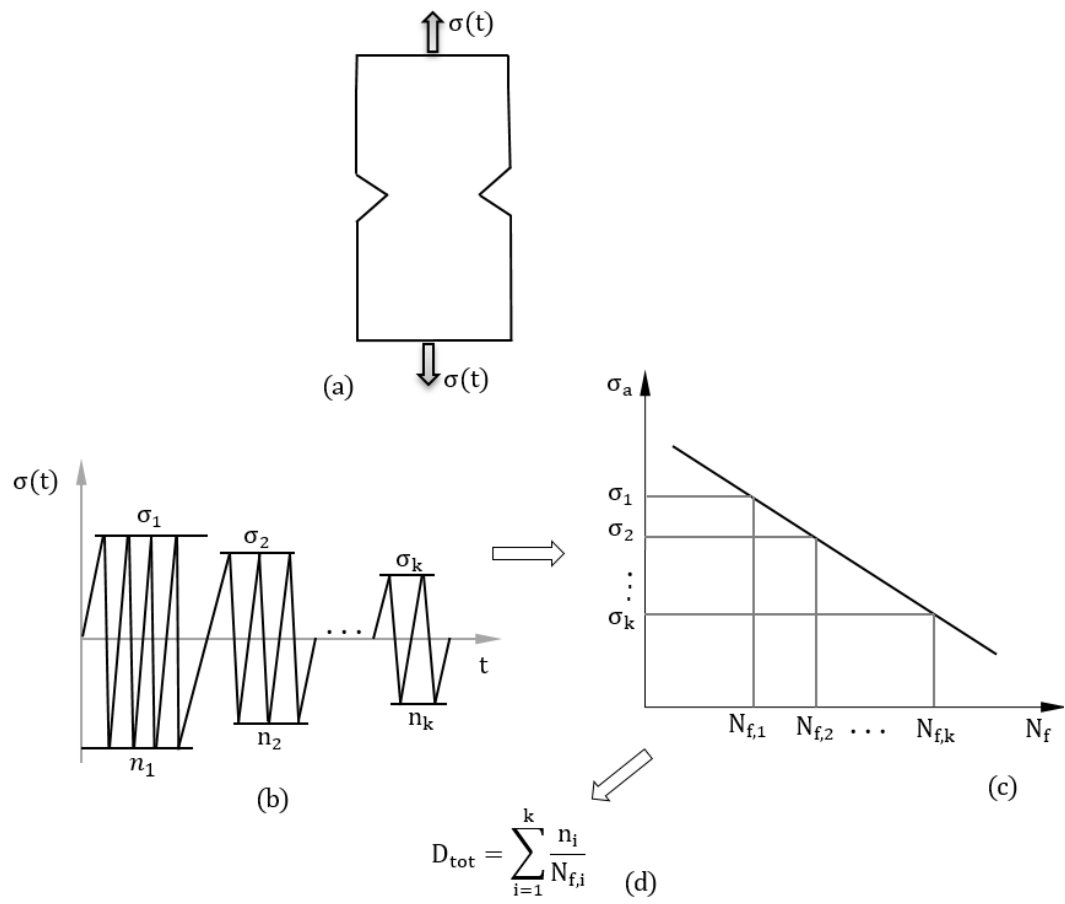


Figure 2-18 Palmgren and Miner rule

Chapter 3

Proposed design methodology

3.1 Overview

This chapter set out to describe the design methodology for predicting the finite lifetime of mechanical assemblies subjected to constant and variable amplitude fretting fatigue loading. As explained in chapter 1.2, the proposed methodology assumes that the cracking behaviour in metallic materials under fretting fatigue loading is similar to those observed in notched components subjected to fatigue loading [15]. The review of the literature have shown that when materials are subjected to fretting fatigue loading, crack initiates at the trailing edge of the contact [31, 15]. Therefore, finite lifetime under fretting fatigue loading is estimated in this research by post-processing the linear elastic multiaxial stress field damaging the material at the contact edge.

The proposed methodology to be used to post-process the linear elastic multiaxial stress field is based on the use of the modified Wöhler curve method (MWCM) applied in conjunction with the theory of critical distance (TCD) and the shear-stress maximum variance method (τ -MVM). In this methodology, the TCD is applied in the form of the point method (PM). It accounts for the effect of the multiaxial stress gradients damaging the material in the vicinity of the contact region. The τ -MVM is used to determine the orientation of the critical plane while the MWCM post-processes the time-variable linear-elastic stress quantities relative to the critical plane. The τ -MVM, the PM and the MWCM are outlined in chapters 2.4.5 , 2.4.6 and 2.4.7 , respectively.

3.2 Finite lifetime of materials under constant amplitude fretting fatigue loading

The proposed design methodology used in this research to predict the finite lifetime of mechanical assemblies subjected to constant amplitude (CA) fretting fatigue loading has been summarised in Figure 3-1. Before using this methodology in situation of practical

interest, the fatigue properties of the material have to be assessed. During the characterisation process, the constants governing the MWCM's functions $\tau_{A,Ref}(\rho_{eff})$ and $K_{\tau}(\rho_{eff})$ as defined in Eqs.(2-77)-(2-81) and the constants defining the critical distance criterion $L_M(N_f)$ in Eq.2-75 are estimated by experiments. The experimental procedures required to determine these constants are outlined in chapter 4. Having characterised the materials, the proposed methodology can now be used to predict the finite lifetime as illustrated in the next paragraph.

Let consider for example the mechanical assembly subjected to time-variable CA fretting fatigue loading as shown in Figure 3-1a. To predict its finite lifetime, the first step is the estimation of the time-variable CA multiaxial stress field along the focus path. In the fretting fatigue context, the focus path is a straight line emanating from the crack initiation location, A, and normal to the contact surface as shown in Figure 3-1b. The second step of the methodology consists of a recursive procedure which leads to the finite lifetime estimation. At the start of this recursive procedure, the τ -MVM reported in chapter 2.4.5 is used to post-process the time-variable CA stress tensor $\sigma_{r,i}(t)$ extracted at a distance r_i along the focus path (Figure 3-1c) in order to calculate the critical plane (Figure 3-1 d). The time variable CA stresses $\sigma_n(t)$ and $\tau_{MV}(t)$, normal and tangential to the calculated critical plane are then used to determine the stress quantities, τ_a , $\sigma_{n,a}$ and $\sigma_{n,m}$ (Figure 3-1e and f) according to Eqs. (2-63)-(2-66). Having determined the stress quantities relative to the critical plane i.e. τ_a , $\sigma_{n,a}$ and $\sigma_{n,m}$, the critical plane stress ratio, ρ_{eff} in Figure 3-1g is estimated using Eq.2-76. From the calculated ρ_{eff} , the corresponding MWCM's calibrating functions $\tau_{A,Ref}(\rho_{eff})$ and $K_{\tau}(\rho_{eff})$ in Figure 3-1h are then estimated according to Eqs.(2-77)-(2-81). Subsequently, the resulting number of cycles to failure, N_f in Figure 3-1i is calculated using Eq.2-82. Having estimated the N_f corresponding to the r_i value under investigation, the corresponding critical distance, $L_M(N_f)$ is calculated using Eq.2-75. Finally, according to the PM (chapter 2.4.6), the assessed material subjected to constant amplitude fretting fatigue loading is assumed to

fail at the number of cycles to failure, $N_{f,e}$, if the convergence in Figure 3-1j is reached.

i.e. $\frac{L_M(N_{f,e})}{2} = r_i$

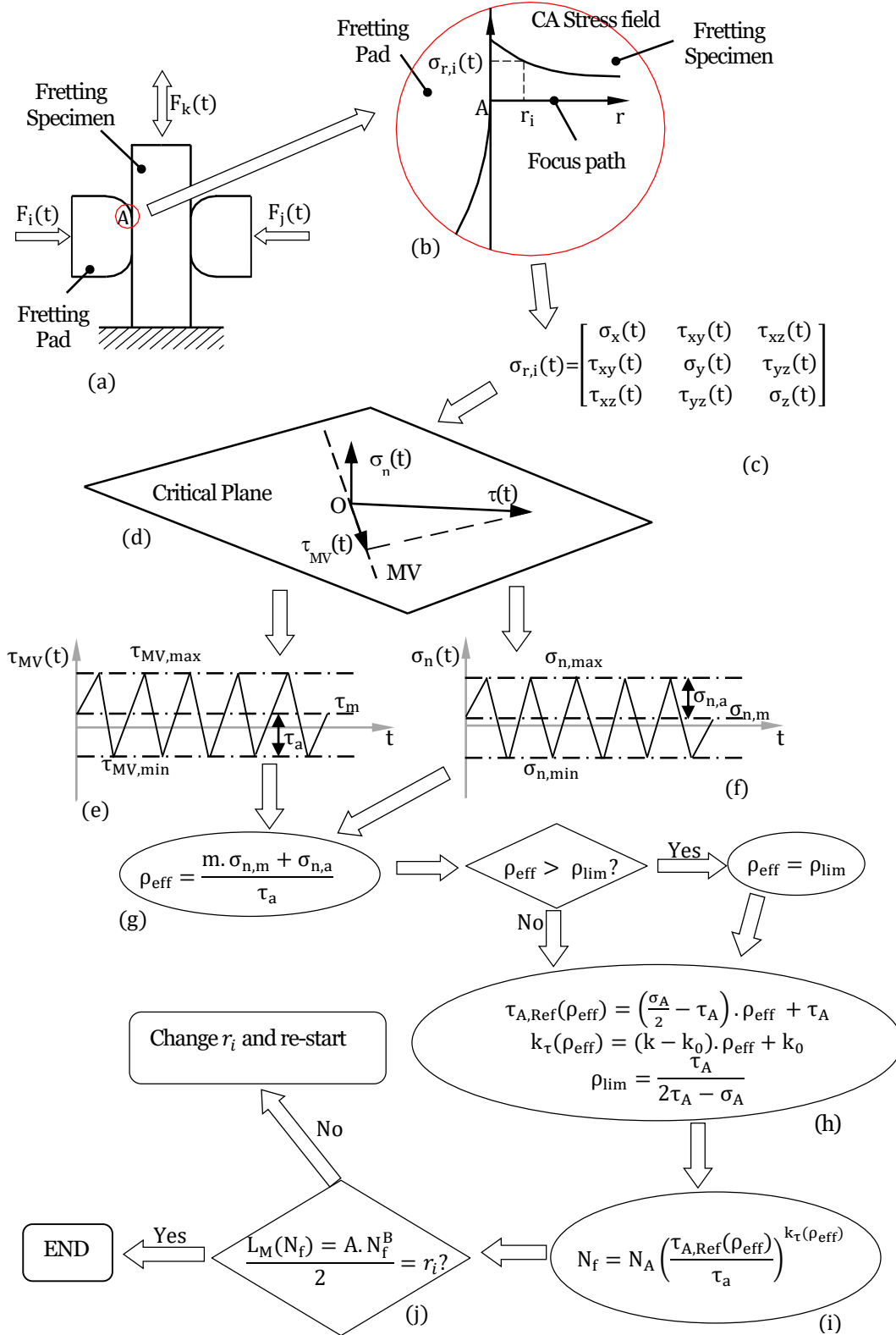


Figure 3-1 Design methodology to estimate the finite lifetime under CA fretting fatigue.

3.3 Finite lifetime of materials under variable amplitude fretting fatigue loading

In this section, the proposed design methodology to predict finite lifetime of mechanical assemblies subjected to variable amplitude (VA) fretting fatigue loading is discussed. Similar to the CA case described in chapter 3.2, the assessed material has to be characterised. In order to formalise the proposed design methodology, consider the mechanical assembly subjected to a complex system of time-variable VA fretting fatigue loading as shown in Figure 3-2a. To predict the finite lifetime of this mechanical assembly, the first step is to estimate the time-variable VA multiaxial stress field along the focus path as shown in Figure 3-2b.

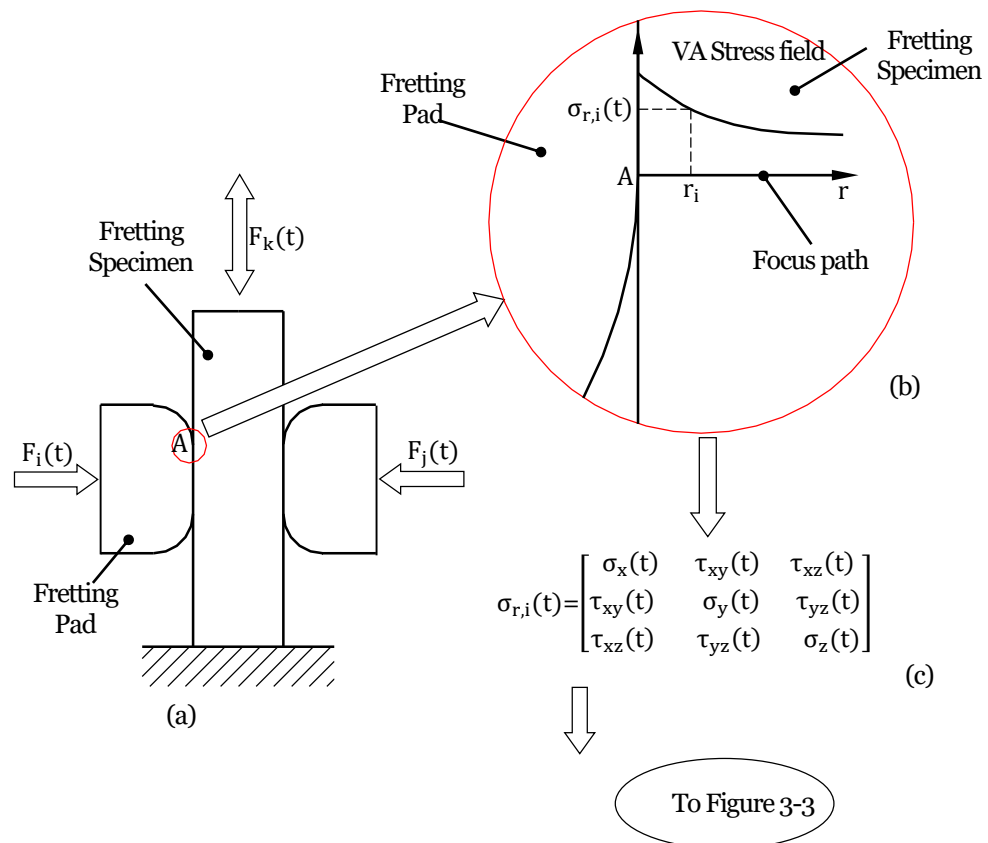


Figure 3-2 Multi-axial stress field along the focus path of a mechanical assembly subjected to VA fretting fatigue loading.

The second step of the methodology consists of a recursive procedure which leads to the finite lifetime estimation. The starting point of this procedure is to choose a point r_i along

the focus path shown in Figure 3-2b. At this location, the VA stress tensor $\sigma_{r,i}(t)$ is extracted (Figure 3-2b and Figure 3-2c). The τ -MVM reported in chapter 2.4.5 is then used to post-process the stress tensor $\sigma_{r,i}(t)$ so that the critical plane and its VA stress components $\sigma_n(t)$ and $\tau_{MV}(t)$ are calculated as shown in Figure 3-3. The stress components $\sigma_n(t)$ and $\tau_{MV}(t)$ are normal and tangential to the critical plane respectively.

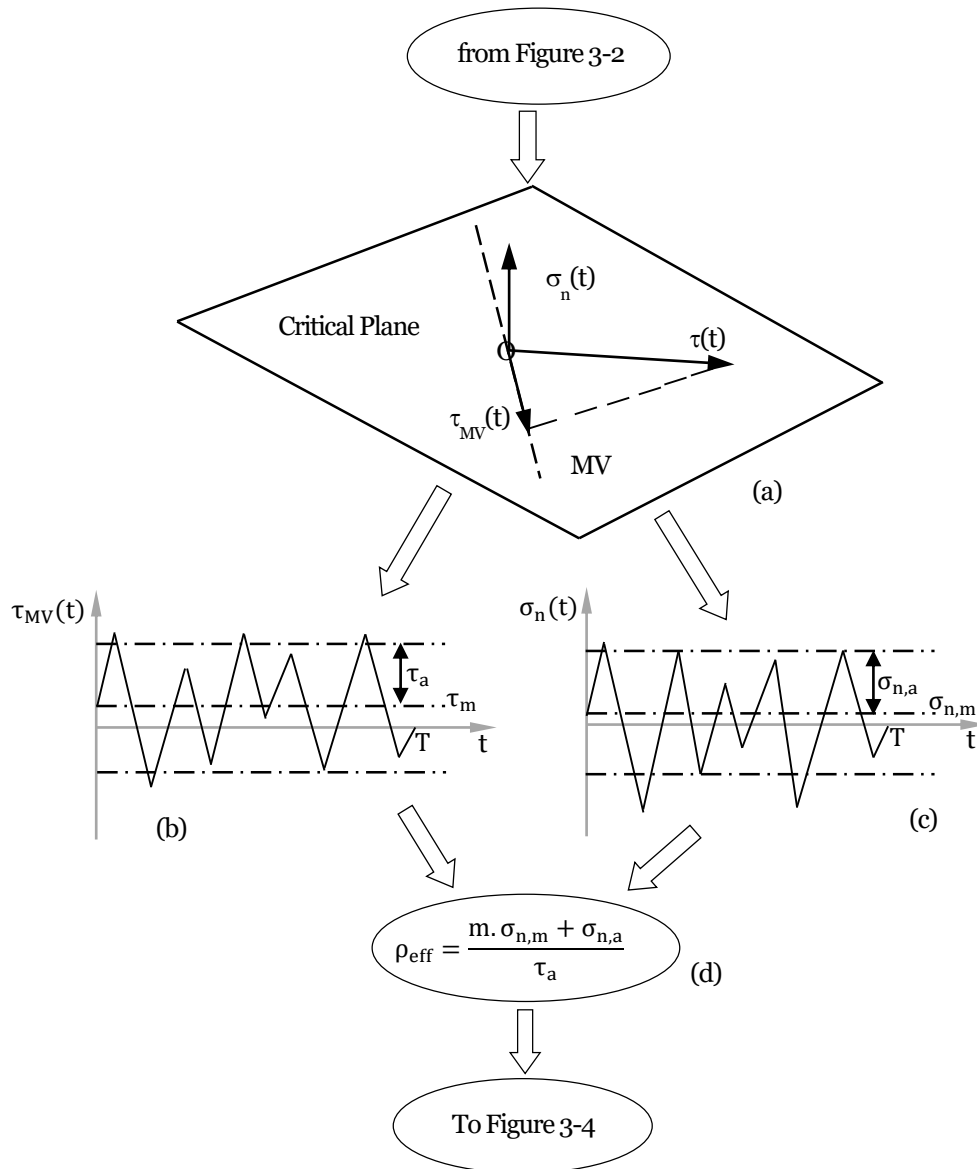


Figure 3-3 Use of the τ -MVM to calculate the critical plane along the focus path of a mechanical assembly subjected to VA fretting fatigue loading.

The calculated VA stress components, $\sigma_n(t)$ and $\tau_{MV}(t)$ in Figure 3-3b and Figure 3-3c are then used to calculate the critical plane stress quantities τ_a , $\sigma_{n,a}$ and $\sigma_{n,m}$ according

to Eqs.(2-67) – (2-72). Having calculated the stress quantities τ_a , $\sigma_{n,a}$ and $\sigma_{n,m}$, the critical plane stress ratio, ρ_{eff} (Figure 3-3d) can be obtained according to Eq.2-76. The critical plane stress ratio, ρ_{eff} is then used to calculate the corresponding MWCM's calibrated functions, $\tau_{A,Ref}(\rho_{eff})$ and $K_\tau(\rho_{eff})$ in Figure 3-4a. Furthermore, in order to account correctly for the damaging effect causes by low cycles fatigue loading, Haibach [66] recommended to correct the negative inverse slope, $K_\tau(\rho_{eff})$ in the long-life regime with the slope $m_\tau(\rho_{eff})$ as shown in Figure 3-4a and b.

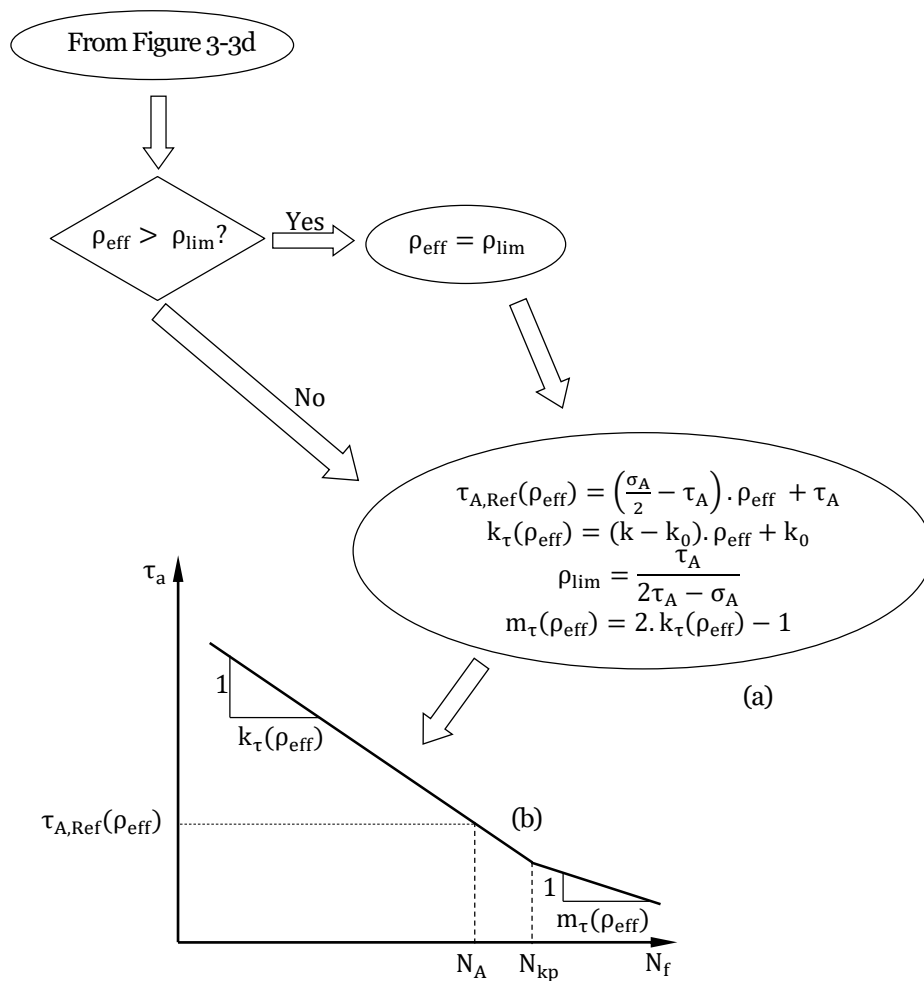


Figure 3-4 Calculation of the MWCM functions at a given location r_i .

After calculating the MWCM's functions in Figure 3-4, the next task is to use the classical Rain flow method [67] to convert the irregular shear stress history $\tau_{MV}(t)$ in Figure 3-3b to a shear stress spectrum shown in Figure 3-5b. The resulting shear stress spectrum is

made of a sequence of constant amplitude blocks having shear stress amplitude $\tau_{a,i}$ and number of cycles n_i . In this design approach, $\tau_{MV}(t)$ is chosen over $\sigma_n(t)$ to perform cycle counting because the MWCM reported in chapter 2.4.7 assumes that the crack initiation is shear stress governed.

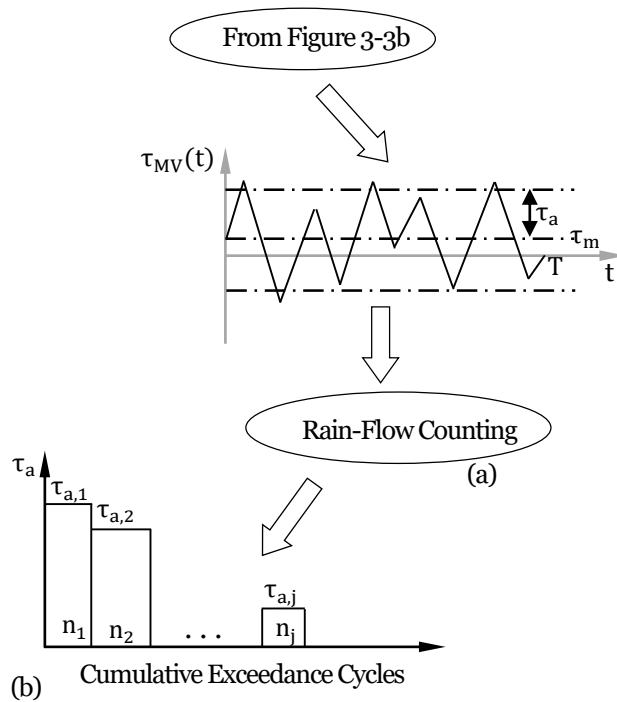


Figure 3-5 Shear stress spectrum associated to $\tau_{MV}(t)$ at a given location, r_i

The final step leading to the estimation of the finite lifetime is summarised in Figure 3-6. In this step, the shear stress spectrum in Figure 3-5b is used in conjunction with the modified Wöhler curve in Figure 3-4 to calculate the total fatigue damage content D_{tot} (Figure 3-6c) according to the Palmgren-Miner rule reported in chapter 2.4.9. This is then used to determine the equivalent number of cycles $N_{f,eq}$ (Figure 3-6d). Finally, by using the PM reported in chapter 2.4.6, the assessed mechanical component will fail at the number of cycles $N_{f,e}$ (Figure 3-6f), if the convergence in Figure 3-6e is reached.

$$\text{i.e. } \frac{LM(N_{f,eq})}{2} = r_i$$

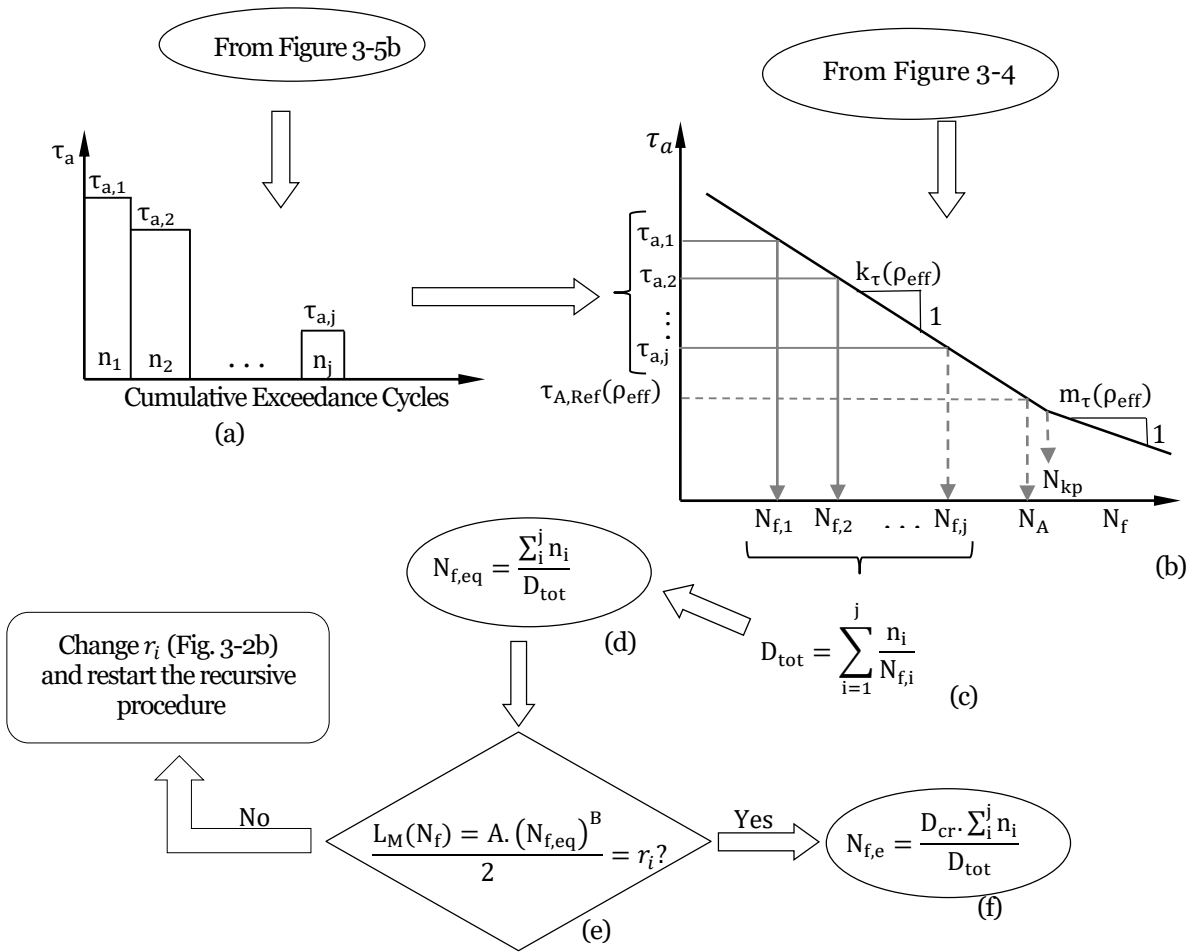


Figure 3-6 Use of the MWCM with the PM to estimate the finite lifetime of mechanical assembly under VA fretting fatigue loading.

For more clarification, all the steps from Figure 3-2 to Figure 3-6 leading to the estimation of the finite lifetime under VA fretting fatigue loading have been summarised in Figure 3-7.

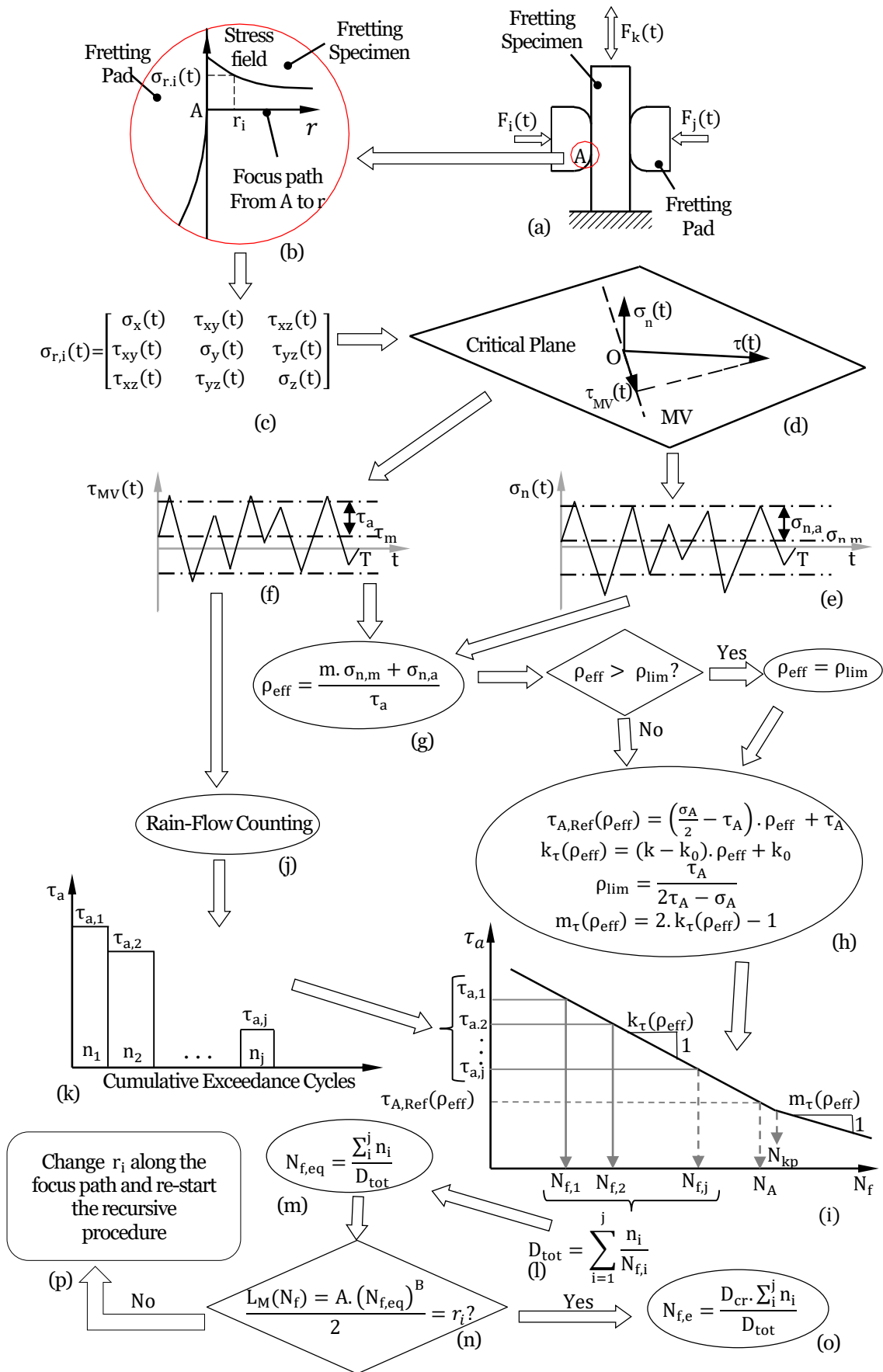


Figure 3-7 Design methodology to predict the finite lifetime under VA fretting fatigue loading.

Chapter 4

Characterisation of fatigue properties of cast iron

4.1 Material description

The materials chosen to investigate fretting fatigue damage were provided by Cummins Inc. These materials are cast iron 40054 and cast iron 40060. Both materials differ in their chemical composition and mechanical properties as summarised in Table 4-1.

Table 4-1 Chemical composition of materials 40054 and 40060.

Name: Iron, cast gray Engineering Standard Number: 40054		Name: Iron, cast gray (controlled carbon) Engineering Standard Number: 40060	
Element	Weight Percent	Element	Weight Percent
Total Carbon	2.80 - 3.40	Total Carbon	3.10 - 3.35
Silicon	1.90 - 2.50	Silicon	1.70 - 2.30
Manganese	0.50 - 0.80	Manganese	0.35 - 0.80
Phosphorus	0.25 Maximum	Phosphorus	0.08 maximum
Sulfur	0.12 maximum	Sulfur	0.05 - 0.15
Chromium	0.25 - 0.55	Chromium	0.20 - 0.40
Copper	0.60 - 1.20	Copper	0.60 - 0.90
Molybdenum	0.50 maximum	Molybdenum	0.15 maximum
Nickel	1.00 maximum	Nickel	N/A
Titanium	0.020 maximum	Titanium	N/A

4.2 Determination of the ultimate tensile strength of the assessed materials

To determine the ultimate tensile strength (UTS) of the materials 40054 and 40060, tensile tests were carried out using the Mayes 1 (± 100 KN, ± 50 mm) servo-hydraulic uniaxial device (Figure 4-2) located at the structure laboratory of the university of Sheffield . For each type of material, three tensile tests were carried out. Before the start of the tests, the specimen shown in Figure 4-1 was clamped between two grips of the Mayes 1 machine. During the tests, one end of the specimen was fixed while the other end was pulled at the displacement rate of 0.0333 m/s until failure. Also, the force and

the displacement were recorded at the sample rate of 50 Hz until failure. The force versus displacement graphs of all the tensile tests can be seen in Appendix A. The UTS was calculated by averaging the results of three tests. The UTS of the materials 40054 and 40060 were found to be equal to 354 MPa and 278 MPa, respectively. Table 4-2 and Table 4-3 summarise the static test results for both materials.



Figure 4-1 Example of plain specimen used for the static and fatigue test.

Table 4-2 Static test results of material 40054.

Tests Number	Specimens	Gross section			Net section			Static test results	
	Length (mm)	Width (mm)	Thickness (mm)	Area (mm ²)	Width (mm)	Thickness (mm)	Area (mm ²)	Force at failure (N)	UTS (MPa)
Test 1	120.01	25.72	6.12	157.36	9.97	6.08	60.64	21,350	352.09
Test 2	119.99	25.87	5.98	154.65	9.94	5.94	59.10	20,160	341.14
Test 3	120.00	25.72	6.06	155.83	9.95	6.03	60.05	22,130	368.52

Table 4-3 Static test results of material 40060.

Tests Number	Specimens	Gross section			Net section			Static test results	
	Length (mm)	Width (mm)	Thickness (mm)	Area (mm ²)	Width (mm)	Thickness (mm)	Area (mm ²)	Force at failure (N)	UTS (MPa)
Test 1	119.95	25.74	6.00	154.47	9.82	6.06	59.56	14,860	249.49
Test 2	119.98	25.71	6.15	157.99	9.89	6.09	60.21	17,330	287.83
Test 3	119.92	25.65	6.14	157.41	9.85	6.08	59.94	17,780	296.62

4.3 Calibration of the critical distance L_M

As explained in chapter 2.4.6, the Point Method (PM) is used in this research to calculate the reference stress, $\sigma_{eff,a}$. According to the PM, the $\sigma_{eff,a}$ is obtained at half the critical distance, L_M . This section describes the fatigue experiments needed to calculate the

material parameters A and B governing the L_M vs N_f relationship in Eq. 2-75 . This is done according to the procedure summarised in Figure 2-16.

4.3.1 Calculation of constants A and B associated to material 40054

4.3.1.1 Fatigue experiments of plain and notched specimens

In order to estimate the constant A and B, one of the requirement is to determine the S-N curves of both plain and notched materials. As described in 2.4.2, the S-N curve is a log-log graph of the stress amplitude versus the number of cycles to failure. To plot the S-N curve of the plain and notched materials, several uniaxial fatigue tests were carried out. These tests were performed on the Mayes 1 Moog Integrated test suite servo-hydraulic uniaxial machine (± 100 KN, ± 50 mm) under load control.

The fatigue tests consisted of clamping a plain or notched specimen between two grips of the Mayes 1 machine. One end of the specimen was fixed while the other was subjected to a sinusoidal constant amplitude load set at a frequency of 10Hz and load ratio $R = -1$. For both plain and notched specimens, unless failure occurred earlier, all fatigue tests were carried out up to 2 million cycles. This number of cycles were chosen because the knee point characterising the S-N curve of cast iron is estimated at 500,000 cycles [68]. The dimension of all the tested plain and notched specimens (including the radius of curvature) can be seen in Appendix B while the fatigue results are summarised in Table 4-4 and Table 4-5.

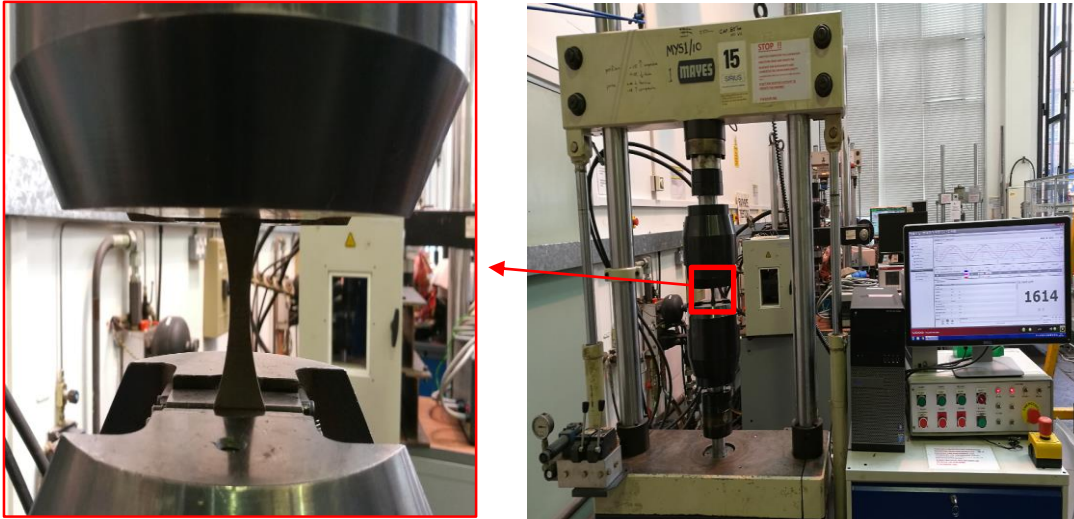


Figure 4-2 Uniaxial fatigue test of the plain specimen.

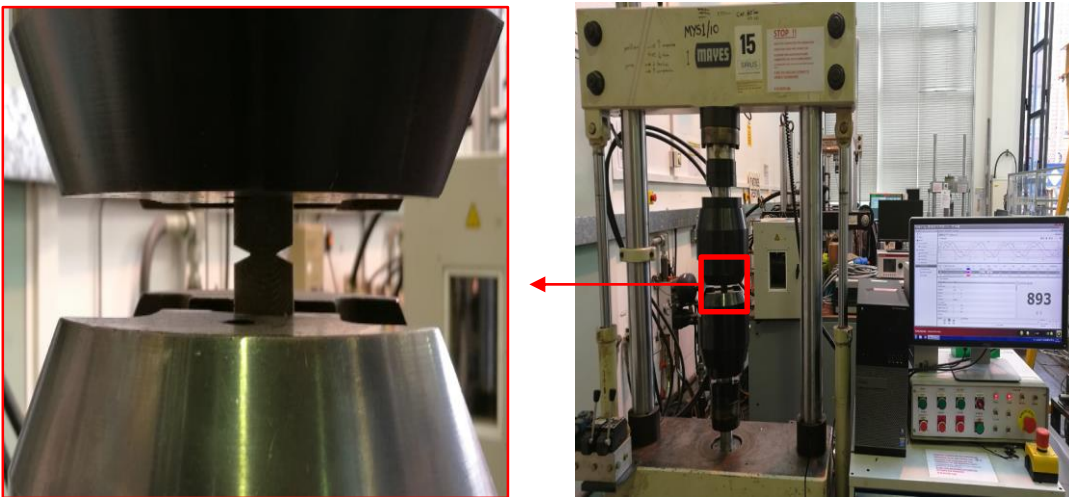


Figure 4-3 Uniaxial fatigue test of the notched specimen.



Figure 4-4 Example of the notched specimen used for fatigue test.

Table 4-4 Summary of the uniaxial fatigue results generated by testing the plain material 40054 under R=-1.

Specimens reference	Fatigue test results					
	R	$\Delta\sigma_{A,net}$ (MPa)	$\sigma_{A,net}$ (MPa)	F_{max} (KN)	F_{min} (KN)	N_f (Cycles)
P(R1)U1	-1	280	140	8.444	-8.444	45,984
P(R1)U2	-1	247	123.5	7.467	-7.467	Run-out
P(R1)U2*	-1	318	159	9.614	-9.614	24,461
P(R1)U3	-1	280	140	8.419	-8.419	39,016
P(R1)U4	-1	265	132.5	8.056	-8.056	99,285
P(R1)U5	-1	265	132.5	7.844	-7.844	70,480
P(R1)U6	-1	247	123.5	7.18	-7.18	83,843
P(R1)U7	-1	212	106	6.256	-6.256	Run-out
P(R1)U7**	-1	230	115	6.787	-6.787	Run-out
P(R1)U7***	-1	336	168	9.916	-9.916	13,893
P(R1)U8	-1	247	123.5	7.537	-7.537	243,372
P(R1)U9	-1	240	120	7.258	-7.258	247,646
P(R1)U10	-1	230	115	7.032	-7.032	Run-out
P(R1)U10****	-1	318	159	9.723	-9.723	29,350

- * Specimen P(R1)U2 re-tested at $\sigma_A = 159$ MPa after the run-out
 ** Specimen P(R1)U7 re-tested at $\sigma_A = 115$ MPa after the run-out
 *** Specimen P(R1)U7** re-tested at $\sigma_A = 168$ MPa after the run-out
 **** Specimen P(R1)U10 re-tested at $\sigma_A = 159$ MPa after the run-out

Table 4-5 Summary of the uniaxial fatigue test results generated by testing the notched material 40054 under R=-1.

Specimens reference	Fatigue Test					
	R	$\Delta\sigma_{A,net}$ (MPa)	$\sigma_{A,net}$	F_{max} (KN)	F_{min} (KN)	N_f (Cycles)
L1	-1	200	100.0	5.783	-5.783	40,912
L2	-1	160	80.0	4.727	-4.727	165,788
L3	-1	140	70.0	3.932	-3.932	185,329
L4	-1	115	57.5	3.440	-3.440	782,085
L5	-1	95	47.5	2.719	-2.719	Run-Out
L6	-1	250	125.0	6.990	-6.990	4,593
L7	-1	200	100.0	5.769	-5.769	11,291
L8	-1	140	70.0	3.969	-3.969	104,210
L9	-1	115	57.5	3.280	-3.280	Run-Out
L9*	-1	250	125.0	7.131	-7.131	2,731
L10	-1	160	80.0	4.720	-4.720	40,257

- *Specimen L9 re-tested at $\sigma_A = 125$ Mpa after a run-out

In TABLE 4-4 and Table 4-5, F_{max} and F_{min} are the amplitudes of the fully-reversed fatigue load. $\sigma_{A,net}$ is the corresponding stress damaging the net section of the specimen.

For a given $\sigma_{A,net}$ value, F_{max} and F_{min} are calculated using the following equations:

$$2\sigma_{A,net} = \sigma_{max} - R \cdot \sigma_{max} \quad 4-1$$

$$\sigma_{max} = \frac{2 \cdot \sigma_{A,net}}{1 - R} \quad 4-2$$

$$F_{max} = -F_{min} = \frac{2 \cdot \sigma_{A,net} \cdot A_{net}}{1 - R} \quad 4-3$$

where, A_{net} is the cross section area of the net section of the specimen.

The fatigue results in Table 4-4 and Table 4-5 were post-processed in order to plot the S-N curves associated with the plain and notched materials. All the experimental data excluding the run-outs were post-processed using the least-square analysis summarised in chapter 2.4.3. Figure 4-5 and Figure 4-6 show the S-N curves for the plain and notched material 40054 while Figure 4-7 compares both curves. It can also be observed that the endurance limit σ_A of the notched material 40054 is less than that of the plain material. This supports the idea that for a plain and notched specimen made of the same material, notches have a detrimental effect on the fatigue lifetime of material under cyclic loading [39, 40, 41]. The endurance limit extrapolated in a high cycle regime i.e. 10^6 cycles, the inverse slope k of the S-N curve and the scattered band index, T_σ of the plain and notched material are summarised in Table 4-6. The index, T_σ provides the width of the scattered band corresponding to the probability of survival P% and 1-P% (with 95% of confidence level).

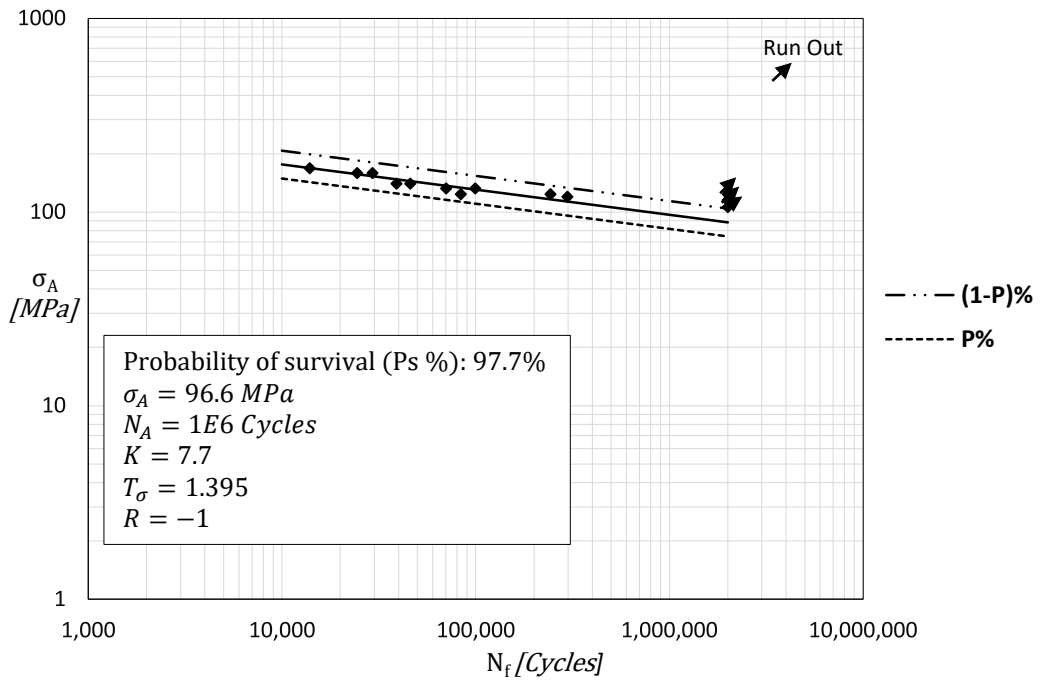


Figure 4-5 S-N Curve of plain material 40054 under fully reversed uniaxial loading.

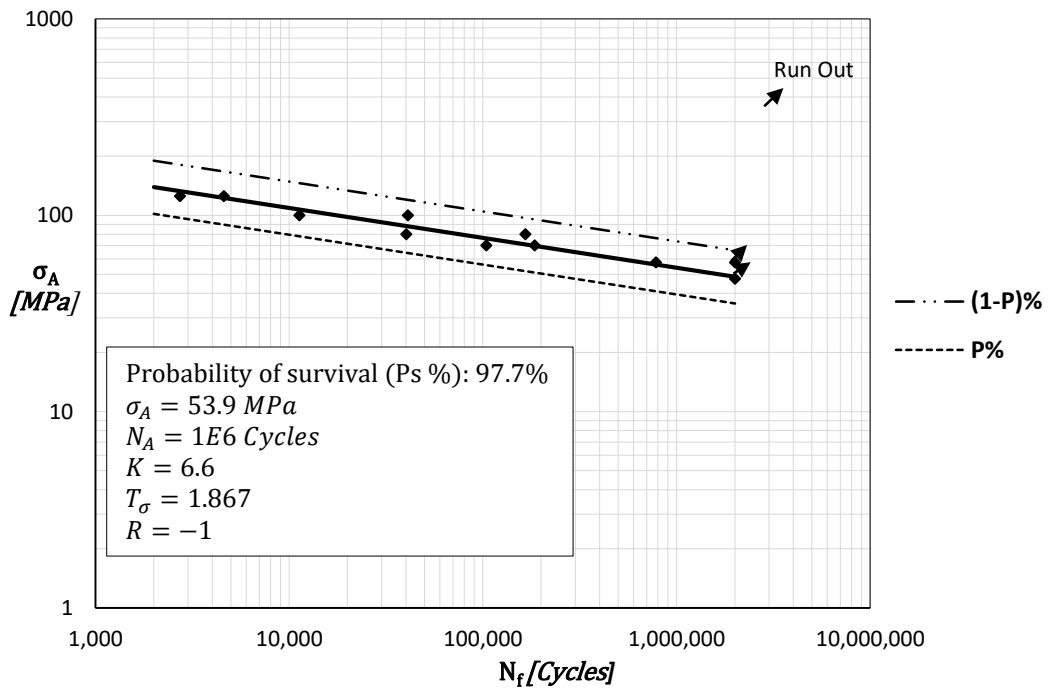


Figure 4-6 S-N Curve of notched material 40054 under fully reversed uniaxial loading.

Table 4-6 Fully reversed uniaxial fatigue properties of the plain and notched material 40054.

Material geometry	R	K	σ_A (MPa)	N_A (Cycles)	P %	T
Plain	-1	7.7	96.6	1E+06	97.7	1.395
Notched	-1	6.6	53.9	1E+06	97.7	1.867

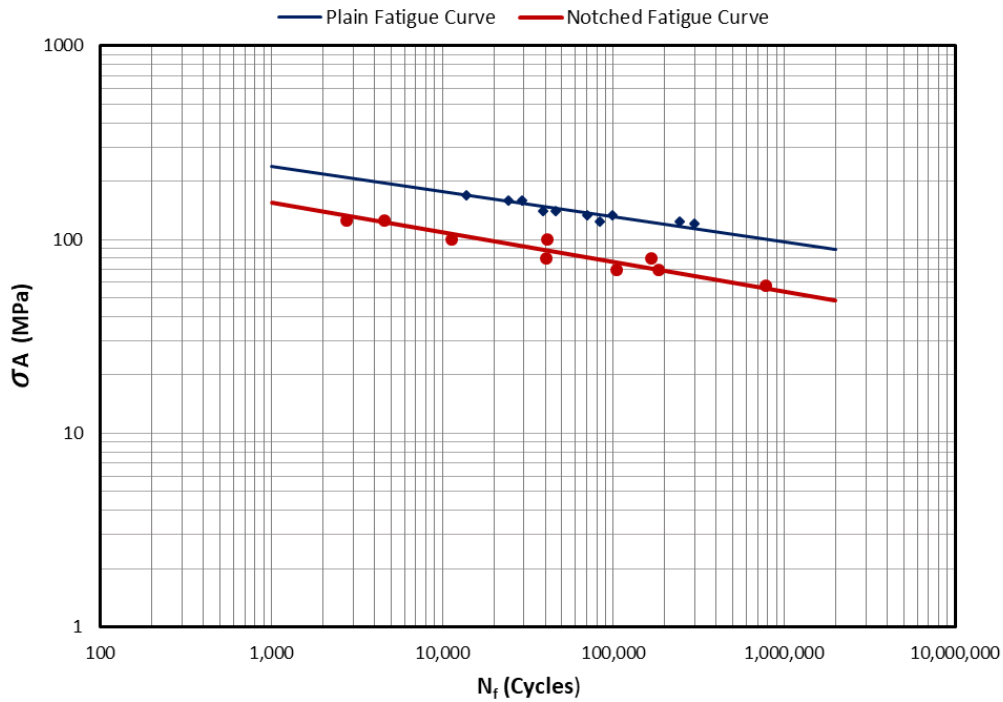


Figure 4-7 Comparison of the S-N Curves of plain and notched material 40054 under fully reversed uniaxial loading.

4.3.1.2 Calculation of the gross nominal stress and the stress damaging the plain specimen at a given cycle

To calculate the material properties A and B according to the procedure summarised in Figure 2-16, the gross nominal stress amplitude, ($\sigma_{g_nom,a}$) associated to the notched specimen and the stress amplitude damaging the plain specimen ($\sigma_{1,a}$) at a given cycle are required. These stress quantities are obtained from the S-N curve in Figure 4-7. For example, at 1,000,000 cycles, $\sigma_{1,a}$ is equal to 96.63 MPa and the net nominal stress amplitude, $\sigma_{net_nom,a}$ damaging the notched specimen is 53.95 MPa.

Having calculated $\sigma_{net_nom,a}$, the corresponding gross nominal stress amplitude of the notched specimen ($\sigma_{g_nom,a}$) at 1,000,000 cycles is obtained using the following equation

$$\sigma_{g_nom,a} = \sigma_{net_nom,a} \frac{w_{net}}{w_{gross}} \quad 4-4$$

Where w_{gross} and w_{net} are the width of the gross and net sections of the notch specimens, respectively (Figure 4-4). The value of w_{gross} and w_{net} equals to 25.7 mm and 9.96 mm , respectively.

By using the above strategy, $\sigma_{1,a}$ and $\sigma_{g_nom,a}$ can be calculated for any number of cycles in Figure 4-7. The different values of $\sigma_{1,a}$ and $\sigma_{g_nom,a}$ associated to the range of cycles 1,000 to 1,000,000 are summarised in Table 4-7.

Table 4-7 Stress damaging the plain specimen 40054 and the corresponding gross nominal stress at a given N_f .

Plain Specimen		Notch Specimen		
$\sigma_{1,a}$ (MPa)	N_f (Cycles)	$\sigma_{net,nom,a}$ (MPa)	$\sigma_{g,nom,a}$ (MPa)	N_f (Cycles)
96.63	1,000,000	53.95	20.91	1,000,000
97.97	900,000	54.83	21.25	900,000
99.48	800,000	55.82	21.63	800,000
101.22	700,000	56.96	22.08	700,000
103.27	600,000	58.32	22.60	600,000
105.75	500,000	59.96	23.24	500,000
108.86	400,000	62.03	24.04	400,000
113.01	300,000	64.80	25.11	300,000
119.13	200,000	68.93	26.71	200,000
130.37	100,000	76.59	29.68	100,000
132.17	90,000	77.83	30.16	90,000
134.21	80,000	79.24	30.71	80,000
136.56	70,000	80.87	31.34	70,000
139.32	60,000	82.79	32.08	60,000
142.67	50,000	85.12	32.99	50,000
146.87	40,000	88.06	34.13	40,000
152.47	30,000	92.00	35.65	30,000
160.72	20,000	97.85	37.92	20,000
175.88	10,000	108.74	42.14	10,000
192.47	5,000	120.83	46.83	5,000
198.14	4,000	125.01	48.45	4,000
205.69	3,000	130.60	50.61	3,000
216.83	2,000	138.91	53.84	2,000
237.29	1,000	154.37	59.82	1,000

4.3.1.3 Numerical analysis of the notched specimen

The calculation of the material constants A and B according to the protocol described in Figure 2-16, requires the estimation of the linear-elastic maximum principal stress, σ_{ep} along the focus path of the notched specimen subjected to $\sigma_{g,nom,a}$. The focus path here is a straight line from the notch tip and perpendicular to the free surface as shown in Figure 4-8.

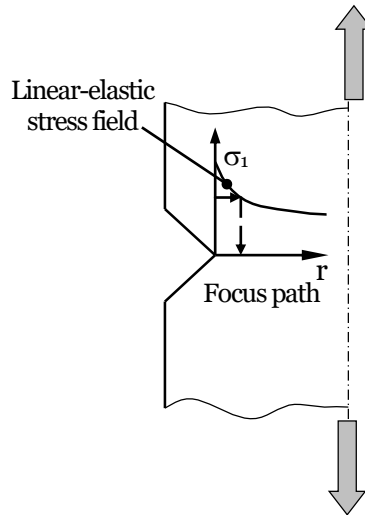


Figure 4-8 Definition of the focus path.

A two-dimensional finite element (FE) model of the notched specimen was created in ANSYS Mechanical APDL. The geometry of the finite element model was built using the average dimensions of all the notched specimens tested during the experiment. Table 4-8 shows the dimensions of the notched specimen used in FE modelling. By taking advantage of the symmetry of the model along its vertical axis, only half of the notched specimen was modelled. The geometry and the mesh used are illustrated in Figure 4-9. A two-dimensional plain strain 8-noded quadrilateral elements of size $h_e = 0.006 \text{ mm}$ are used near the notch tip and a coarse mesh away from the notch. A tensile stress, $\sigma_{g_nom,a} = 1 \text{ MPa}$ is applied to the gross section of the notched model. Finally, the stress field is obtained by refining the mesh in the vicinity of the notch until convergence. Figure 4-10 shows the linear elastic maximum principal stress along the focus path when $\sigma_{g_nom,a} = 1 \text{ MPa}$.

The validation of the model consists of comparing the numerical net stress concentration factor k_{t,net_num} against the analytical net stress concentration factor, k_{t,net_anal} calculated as follows:

$$k_{t,net_anal} = \frac{\sigma_{ep}}{\sigma_{net,a}} \quad 4-5$$

$$\sigma_{net,a} = \sigma_{g_nom,a} * \frac{W_{gross}}{W_{net}} \quad 4-6$$

Where σ_{ep} is the linear elastic maximum principal peak stress obtained from the FE analysis and $\sigma_{net,a}$ is the amplitude of the net nominal stress. k_{t,net_num} is calculated by using the online e-fatigue tools shown in Appendix C. k_{t,net_anal} and k_{t,net_num} are equal to 5.65 and 5.71, respectively. Therefore, this qualitative analysis confirms with the FE model.

Table 4-8 Dimensions of the notched specimen 40054 used in the FE analysis.

Sample	Gross section			Net section			
	Length (mm)	Width (mm)	Thickness (mm)	length (mm)	Width (mm)	Thickness (mm)	Root notch (mm)
101.00	25.67	5.90	48.38	9.96	5.90	0.22	29.87

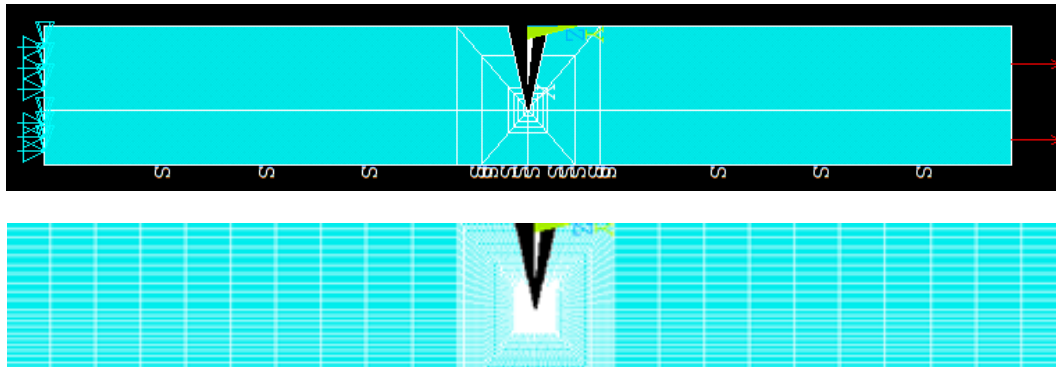


Figure 4-9 Geometry, boundary condition and mesh profile used to model the notched specimen 40054.

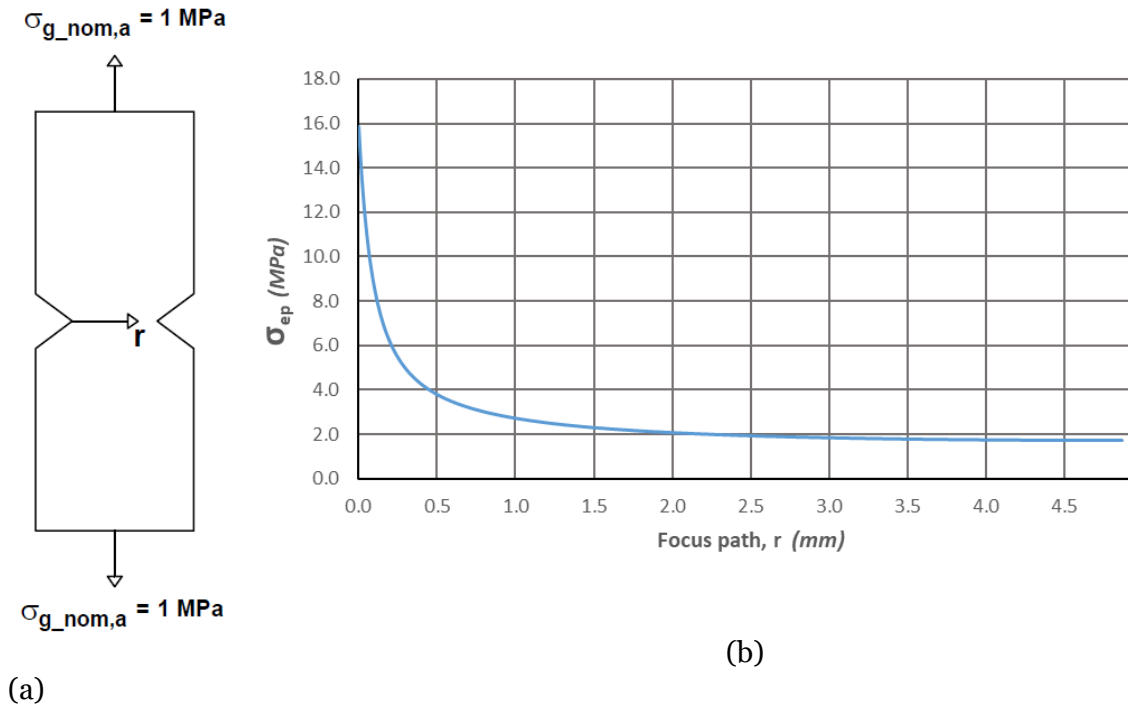


Figure 4-10 Linear elastic maximum principal stress along the focus path of the notched specimen 40054 when $\sigma_{g_nom,a} = 1MPa$.

4.3.1.4 Calculation of constants A and B in the L_M vs N_f equation

To calibrate L_M vs N_f according to the PM (Figure 2-16), the values of $\sigma_{1,a}$, $\sigma_{g_nom,a}$ and the linear elastic maximum principal stress, σ_{ep} along the focus path of the notched specimen subjected to $\sigma_{g_nom,a}$ are required. These stress quantities are calculated as follows:

For instance, when $N_f = 1,000,000$ cycles, $\sigma_{1,a} = 96.63$ MPa and $\sigma_{g_nom,a} = 20.91$ MPa (Table 4-7). The corresponding σ_{ep} along the focus path of the notched specimen is calculated by multiplying the maximum principal stress field in Figure 4-10 by $\sigma_{g_nom,a}$ (superposition theory). Finally, according to the PM, the position r along the focus path where the amplitude of the maximum principal stress, $\sigma_{ep,a}$ equal to the stress $\sigma_{1,a}$ damaging the plain specimen is half of the critical distance, L_M . In this example, at $N_f=1,000,000$ cycles, $\sigma_{1,a} = 96.63$ MPa, $\sigma_{g_nom,a} = 20.91$ MPa, $r= 0.3391$ mm and therefore $L_M= 0.6782$ mm.

By applying this strategy to any N_f , the corresponding $\sigma_{1,a}$, $\sigma_{g_nom,a}$ and critical distance, L_M can be calculated. The critical distance associated to any N_f between 1,000 and 1,000,000 cycles are summarised in Table 4-9.

Table 4-9 Critical distances, L_M corresponding to a given number of cycles to failure, N_f for the material 40054.

Plain Specimen		Notch Specimen		Critical distance	
$\sigma_{1,a}$ (MPa)	N_f (Cycles)	$\sigma_{g_nom,a}$ (MPa)	N_f (Cycles)	r (mm)	L_M (mm)
96.63	1,000,000	20.91	1,000,000	0.3391	0.6782
97.97	900,000	21.25	900,000	0.3413	0.6826
99.48	800,000	21.63	800,000	0.3433	0.6866
101.22	700,000	22.08	700,000	0.344	0.688
103.27	600,000	22.60	600,000	0.3463	0.6926
105.75	500,000	23.24	500,000	0.3491	0.6982
108.86	400,000	24.04	400,000	0.3528	0.7056
113.01	300,000	25.11	300,000	0.3542	0.7084
119.13	200,000	26.71	200,000	0.3652	0.7304
130.37	100,000	29.68	100,000	0.3744	0.7488
132.17	90,000	30.16	90,000	0.3757	0.7514
134.21	80,000	30.71	80,000	0.3771	0.7542
136.56	70,000	31.34	70,000	0.3791	0.7582
139.32	60,000	32.08	60,000	0.3822	0.7644
142.67	50,000	32.99	50,000	0.3849	0.7698
146.87	40,000	34.13	40,000	0.3867	0.7734
152.47	30,000	35.65	30,000	0.3947	0.7894
160.72	20,000	37.92	20,000	0.3999	0.7998
175.88	10,000	42.14	10,000	0.4112	0.8224
192.47	5,000	46.83	5,000	0.4237	0.8474
198.14	4,000	48.45	4,000	0.4292	0.8584
205.69	3,000	50.61	3,000	0.4337	0.8674
216.83	2,000	53.84	2,000	0.4408	0.8816
237.29	1,000	59.82	1,000	0.4564	0.9128

Finally, the results in Table 4-9 can be used to plot L_M vs N_f curve and the constant A and B deduced from this graph as shown in Figure 4-11.

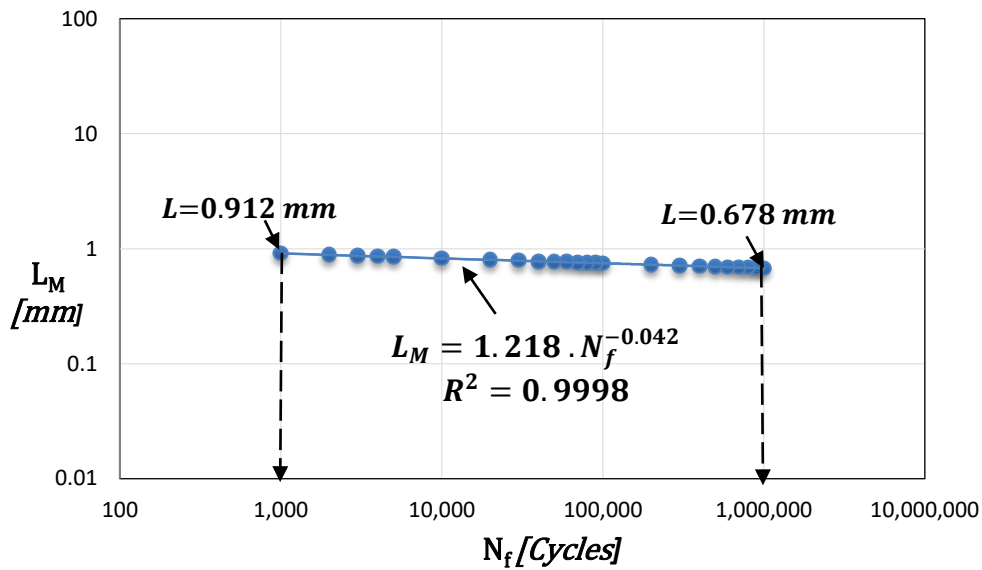


Figure 4-11 Critical distance vs. the number of cycles to failure relationship according to PM, for cast iron 40054.

To conclude, the value of A and B associated to the material 40054 are summarised in Table 4-10.

Table 4-10 Constant A and B governing the relationship L_M vs N_f for material 40054.

Material	A	B
40054	1.218	-0.042

4.3.2 Calculation of constants A and B associated to material 40060

4.3.2.1 Fatigue experiments of plain and notched specimens

To plot the S-N curve of plain and notched material 40060, the Mayes 1 Moog Integrated servo-hydraulic (Figure 4-2) was used to carry uniaxial fatigue tests. The shapes of the plain and notched specimens used during the tests are similar to the one in Figure 4-1 and Figure 4-4, respectively. All uniaxial fatigue tests were done according to the protocol described in chapter 4.3.1.1. The dimensions of all the tested plain and notched specimens can be seen in Appendix B while the fatigue tests results are summarised in Table 4-11 and Table 4-12.

Table 4-11 Summary of the uniaxial fatigue results generated by testing the plain material 40060 under R=-1.

Specimens reference	Fatigue Results					
	R	$\Delta\sigma_a$ (MPa)	σ_a (MPa)	F_{max} (KN)	F_{min} (KN)	N_f (Cycles)
B(R1)1	-1	222	111.0	6.718	-6.718	65,719
B(R1)3	-1	195	97.5	5.897	-5.897	133,874
B(R1)4	-1	153	76.5	4.626	-4.626	run-out
B(R1)4*	-1	250	125.0	7.558	-7.558	27,583
B(R1)5	-1	167	83.5	5.076	-5.076	run-out
B(R1)5**	-1	264	132.0	8.024	-8.024	12,977
B(R1)6	-1	181	90.5	5.454	-5.454	409,392
B(R1)7	-1	181	90.5	5.537	-5.537	120,689
B(R1)9	-1	175	87.5	5.345	-5.345	run-out
B(R1)9***	-1	200	100.0	6.108	-6.108	109,879
B(R1)10	-1	200	100.0	6.107	-6.107	56,773
B(R1)12	-1	167	83.5	5.114	-5.114	run-out
B(R1)12****	-1	264	132	8.085	-8.085	15,339

* Specimen B(R1)4 re-tested at $\sigma_A = 125$ MPa after the run-out

** Specimen B(R1)5 re-tested at $\sigma_A = 132$ MPa after the run-out

*** Specimen B(R1)9 re-tested at $\sigma_A = 100$ MPa after the run-out

**** Specimen B(R1)12 re-tested at $\sigma_A = 132$ MPa after the run-out

Table 4-12 Summary of the uniaxial fatigue test results generated by testing the notched material 40060 under R=-1.

Specimens reference	Fatigue Results					
	R	$\Delta\sigma_{A,net}$ (MPa)	$\sigma_{a,net}$ (MPa)	F_{max} (KN)	F_{min} (KN)	N_f (Cycles)
B1	-1.00	153.00	76.50	4.781	-4.781	131,993
B2	-1.00	125.00	62.50	3.983	-3.983	559,599
B3	-1.00	97.30	48.65	3.037	-3.037	run-out
B4	-1.00	194.60	97.30	6.087	-6.087	31,834
B5	-1.00	111.20	55.60	3.519	-3.519	442,270
B6	-1.00	166.80	83.40	5.213	-5.213	29,516
B7	-1.00	125.00	62.50	3.917	-3.917	331,405
B8	-1.00	153.00	76.50	4.760	-4.760	50,539
B9	-1.00	97.30	48.65	3.052	-3.052	run-out
B10	-1.00	194.60	97.30	5.996	-5.996	20,204
B11	-1.00	139.00	69.50	4.403	-4.403	190,081
B12	-1.00	139.00	69.50	4.434	-4.434	144,118
B13	-1.00	111.20	55.60	3.543	-3.543	755,908

* Specimen B3 re-tested at $\sigma_A = 111.2$ MPa after the run-out

** Specimen B9 re-tested at $\sigma_A = 111.2$ MPa after the run-out

In Table 4-11 and Table 4-12, F_{max} and F_{min} are calculated using to Eqs. 4-1 to 4-3. The fatigue tests results summarised in Table 4-11 and Table 4-12 were post-processed in order to plot the S-N curves associated to the plain and notched specimens. The procedure used here is similar to the one used to post-process the fatigue results of material 40054 (See chapter 4.3.1.1). The generated S-N curves for the plain and notched specimens of material 40060 are shown in Figure 4-12 and Figure 4-13 while Figure 4-14 compares both curves. The endurance limit, σ_A (extrapolated at 10^6 cycles), the inverse slope k and the scatter band index, T_σ are summarised in Table 4-13.

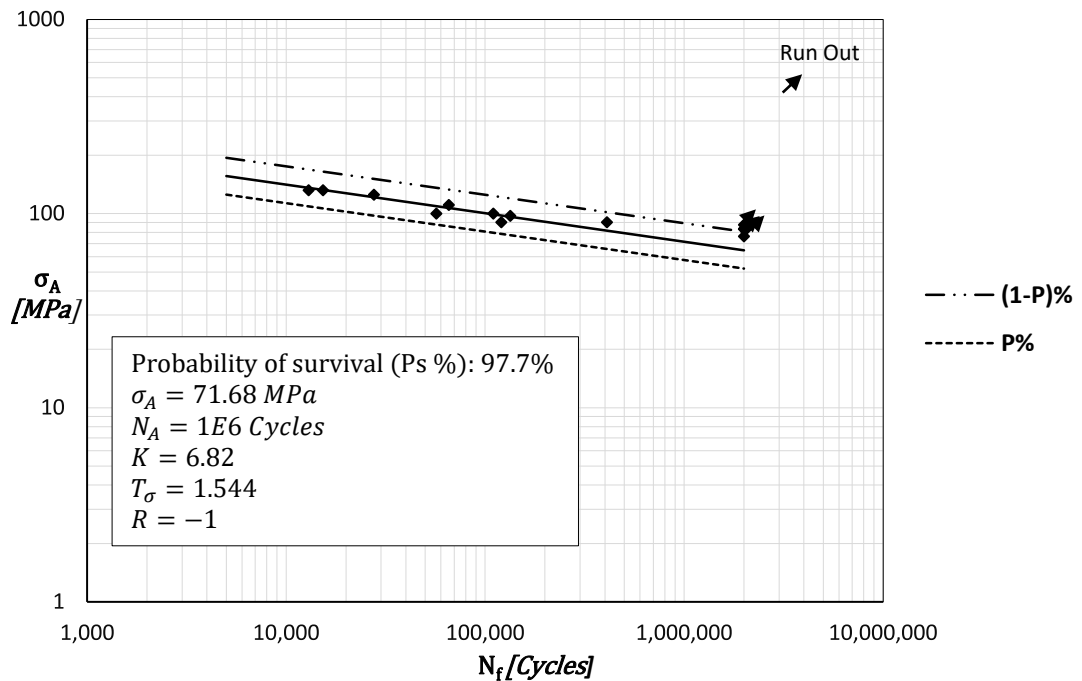


Figure 4-12 S-N Curve of plain material 40060 under fully reversed uniaxial loading.

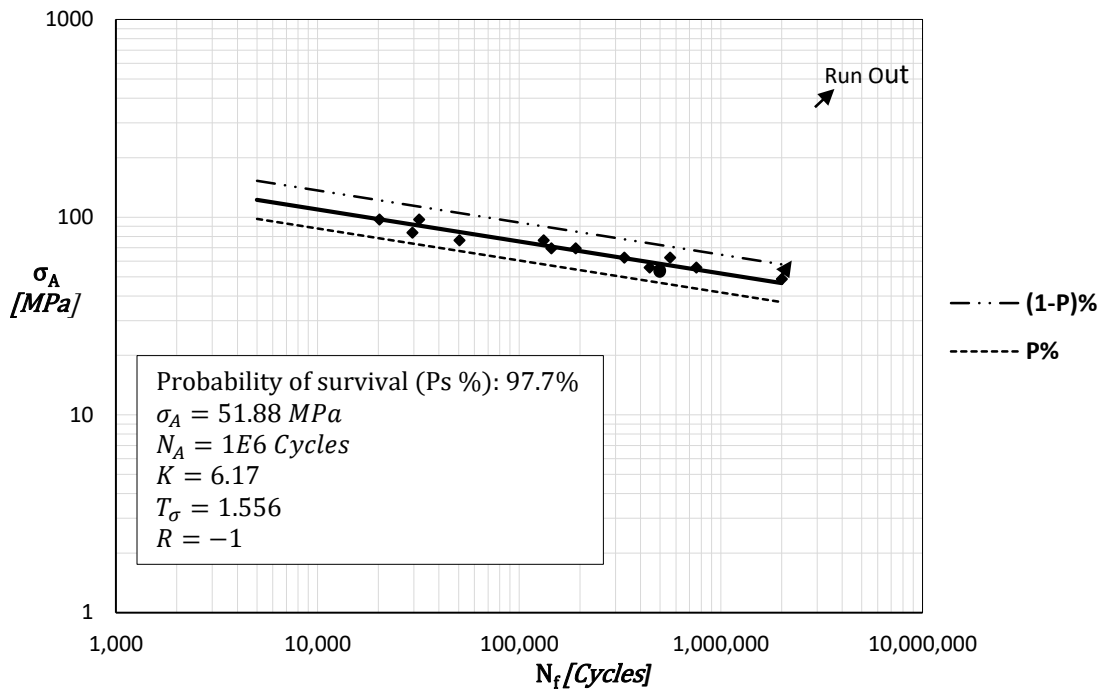


Figure 4-13 S-N Curve of notched material 40060 under fully reversed uniaxial loading.

Table 4-13 Fully reversed uniaxial fatigue properties of the plain and notched material 40060.

Material type	R	K	σ_A (MPa)	N_A (Cycles)	P %	T
Plain	-1	6.82	71.68	1E+06	97.7	1.544
Notched	-1	6.17	51.88	1E+06	97.7	1.556

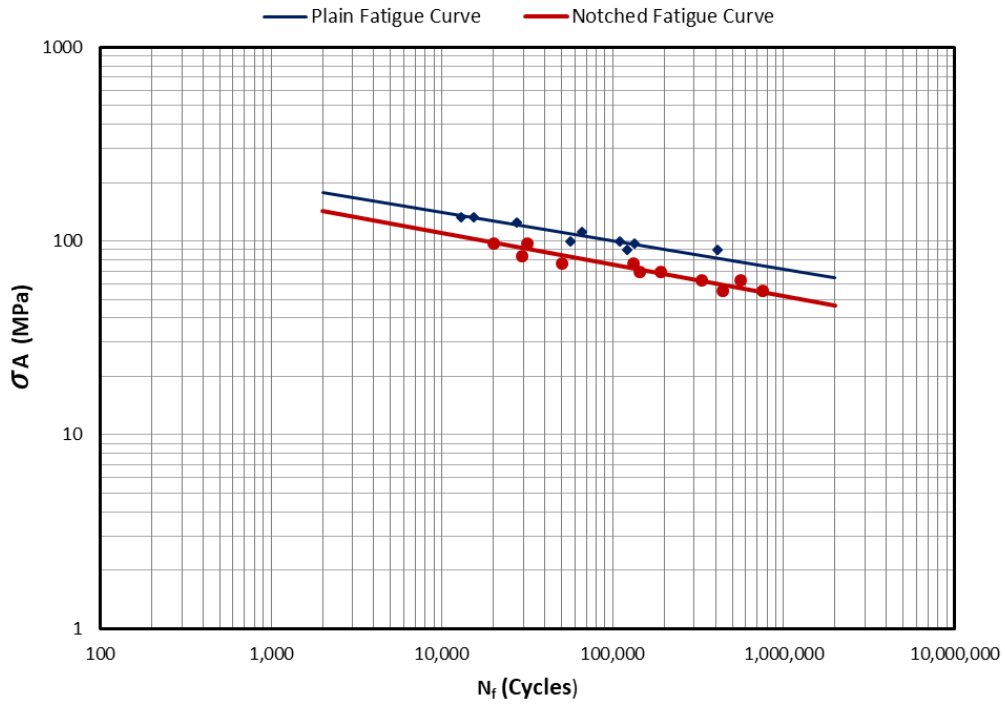


Figure 4-14 Comparison of the S-N Curves of plain and notched material 40060 under fully reversed uniaxial loading.

4.3.2.2 Calculation of the gross nominal stress and the stress damaging the plain specimen at a given cycle

The calibration of L_M vs N_f relationship according to the approach summarised in Figure 2-16 requires the calculation of the gross nominal stress amplitude ($\sigma_{g_nom,a}$) of the notched specimen and the stress damaging the plain specimen ($\sigma_{1,a}$) at any given cycle. These stress quantities are obtained by using the S-N curves shown in Figure 4-14 along with the procedure summarised in chapter 4.3.1.2. Table 4-14 shows the values of $\sigma_{1,a}$ and $\sigma_{g_nom,a}$ corresponding to the range of cycles 1,000 to 1,000,000.

Table 4-14 Stress damaging the plain specimen 40060 and the corresponding gross nominal stress at a given N_f .

Plain Specimen		Notched Specimen		
$\sigma_{1,a}$ (MPa)	N_f (Cycles)	$\sigma_{net,nom,a}$ (MPa)	$\sigma_{gnom,a}$ (MPa)	N_f (Cycles)
71.68	1,000,000	51.8772	19.9186	1,000,000
72.80	900,000	52.7701	20.2614	900,000
74.06	800,000	53.7865	20.6517	800,000
75.53	700,000	54.9625	21.1032	700,000
77.25	600,000	56.3521	21.6367	600,000
79.35	500,000	58.0410	22.2852	500,000
81.98	400,000	60.1772	23.1054	400,000
85.52	300,000	63.0476	24.2075	300,000
90.75	200,000	67.3272	25.8507	200,000
100.46	100,000	75.3267	28.9222	100,000
102.02	90,000	76.6233	29.4200	90,000
103.80	80,000	78.0991	29.9866	80,000
105.85	70,000	79.8067	30.6423	70,000
108.27	60,000	81.8244	31.4170	60,000
111.20	50,000	84.2768	32.3586	50,000
114.90	40,000	87.3785	33.5495	40,000
119.85	30,000	91.5464	35.1498	30,000
127.19	20,000	97.7605	37.5358	20,000
140.79	10,000	109.3760	41.9956	10,000
155.85	5,000	122.3716	46.9854	5,000
161.03	4,000	126.8754	48.7146	4,000
167.96	3,000	132.9273	51.0383	3,000
178.25	2,000	141.9503	54.5027	2,000
197.31	1,000	158.8163	60.9785	1,000

4.3.2.3 Numerical analysis of the notched specimen 40060

According to the procedure summarised in Figure 2-16, the calculation of A and B requires the linear-elastic maximum principal stress σ_{ep} , along the focus path of the notched specimen subjected to $\sigma_{g,nom,a}$ to be estimate. This was achieved by creating a two-dimensional finite element (FE) model of the notched specimen in ANSYS Mechanical APDL. Table 4-15 shows the dimensions of the notched specimen used in FE modelling.

Table 4-15 Dimensions of the notched specimen 40060 used in the FE analysis.

Sample	Gross Section			Net Section			
	Length (mm)	Width (mm)	Thickness (mm)	length (mm)	Width (mm)	Thickness (mm)	Root notch (mm)
101.00	25.68	6.06	48.40	9.86	6.12	0.16	29.03

Because of the symmetry, only half of the specimen is modelled. The mesh used here is similar to the one described in Figure 4-9. The uniaxial tensile stress, $\sigma_{g_{nom,a}} = 1$ MPa is applied to the gross section of the model and the stress field is obtained by refining the mesh in the vicinity of the notch until convergence. Figure 4-15 shows the linear elastic maximum principal stress along the focus path when $\sigma_{g_{nom,a}} = 1$ MPa.

The validation of the model consisted of comparing the numerical net stress concentration factor $k_{t,net,num}$ against the analytical net stress concentration factor, $k_{t,net,anal}$. The $k_{t,net,num}$ is calculated by using the online e-fatigue tools shown in Appendix C while $k_{t,net,anal}$ is calculated using Eqs.4-5 and 4-6. $k_{t,net,anal}$ and $k_{t,net,num}$ are found to be equal to 6.38 and 6.65, respectively. Hence, this validation confirms with the FE model.

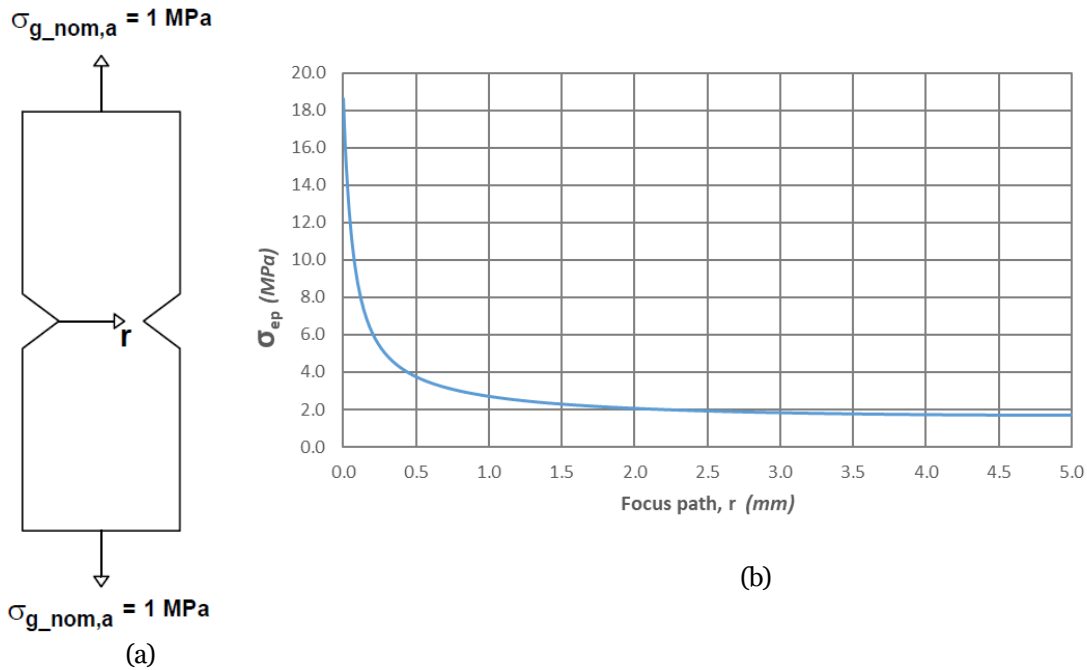


Figure 4-15 Linear elastic maximum principal stress along the focus path when $\sigma_{g_nom,a} = 1$ MPa.

4.3.2.4 Calculation of constants A and B in the L_M vs N_f equation

The calibration of L_M vs N_f according to the PM, requires the calculation of the critical distance, L_M associated to $\sigma_{1,a}$, $\sigma_{g_nom,a}$ and N_f . This is done in accordance with the protocol described in chapter 4.3.1.4. Table 4-16 summarises the critical distance associated to any N_f between 1,000 and 1,000,000 cycles.

Table 4-16 Critical distances, L_M corresponding to a given number of cycles to failure, N_f for the material 40060.

Plain Specimen		Notched Specimen		Critical distance	
$\sigma_{1,a}$ (MPa)	N_f (Cycles)	$\sigma_{gnom,a}$ (MPa)	N_f (Cycles)	r (mm)	L_M (mm)
64.76	2,000,000	17.8033	2,000,000	0.5267	1.0534
71.68	1,000,000	19.9186	1,000,000	0.5387	1.0774
72.80	900,000	20.2614	900,000	0.5406	1.0812
74.06	800,000	20.6517	800,000	0.5427	1.0854
75.53	700,000	21.1032	700,000	0.5451	1.0902
77.25	600,000	21.6367	600,000	0.5479	1.0958
79.35	500,000	22.2852	500,000	0.551	1.102
81.98	400,000	23.1054	400,000	0.5551	1.1102
85.52	300,000	24.2075	300,000	0.5603	1.1206
90.75	200,000	25.8507	200,000	0.5677	1.1354
100.46	100,000	28.9222	100,000	0.5803	1.1606
102.02	90,000	29.4200	90,000	0.5824	1.1648
103.80	80,000	29.9866	80,000	0.5844	1.1688
105.85	70,000	30.6423	70,000	0.5868	1.1736
108.27	60,000	31.4170	60,000	0.5898	1.1796
111.20	50,000	32.3586	50,000	0.5931	1.1862
114.90	40,000	33.5495	40,000	0.5974	1.1948
119.85	30,000	35.1498	30,000	0.6028	1.2056
127.19	20,000	37.5358	20,000	0.6106	1.2212
140.79	10,000	41.9956	10,000	0.6242	1.2484
155.85	5,000	46.9854	5,000	0.638	1.276
161.03	4,000	48.7146	4,000	0.6424	1.2848
167.96	3,000	51.0383	3,000	0.6482	1.2964
178.25	2,000	54.5027	2,000	0.6565	1.313
197.31	1,000	60.9785	1,000	0.6709	1.3418

Finally, by plotting L_M vs N_f , the constants A and B are estimated shown in Figure 2-16.

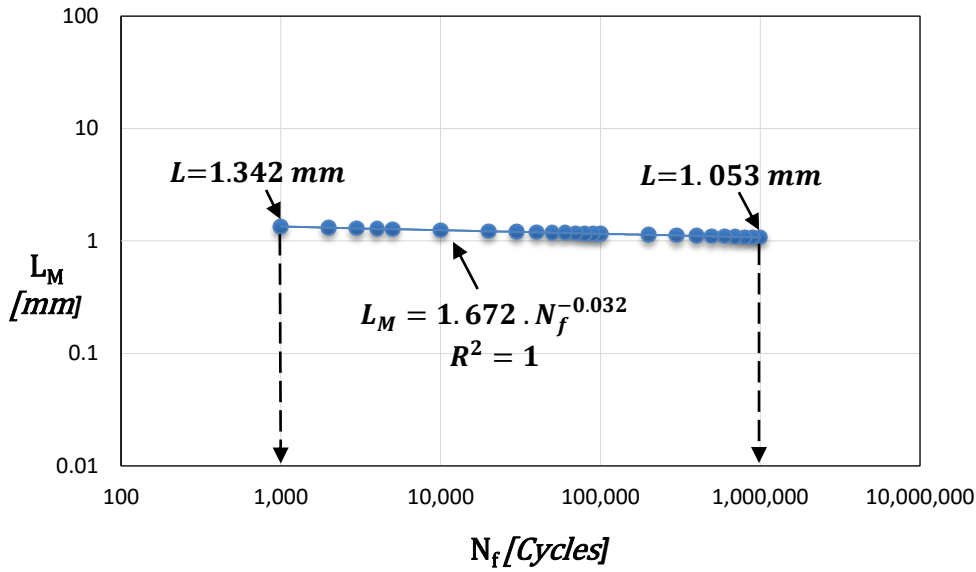


Figure 4-16 Critical distance vs. the number of cycles to failure relationship according to PM, for the cast iron 40060.

To conclude, the value of the material properties A and B associated to the cast iron 40060 are summarised in Table 4-17.

Table 4-17 Constant A and B governing the relationship L_M vs N_f for material 40060.

Material	A	B
40060	1.672	-0.032

4.4 Calibration of the MWCM's governing equations

As explained in chapter 2.4.7, the MWCM functions $K_\tau(\rho_{eff})$ and $\tau_{A,Ref}(\rho_{eff})$ are expressed using the following governing equations [40, 55]:

$$k_\tau(\rho_{eff}) = (k - k_0) \cdot \rho_{eff} + k_0 \quad 4-7$$

$$\tau_{A,Ref}(\rho_{eff}) = \left(\frac{\sigma_A}{2} - \tau_A \right) \cdot \rho_{eff} + \tau_A \quad 4-8$$

Where, σ_A and k are the endurance limit and the negative inverse slope (extrapolated at N_A cycles to failure) respectively. They are calculated using the experimental tests results of plain specimens under fully-reversed uniaxial fatigue loading. Similarly, τ_A and k_0 are

the endurance limit and the negative inverse slope obtained by testing round specimens under fully-reversed torsional fatigue loading. The next sections explain how σ_A , k , τ_A and k_0 have been calculated for both materials 40054 and 40060.

4.4.1 Endurance limit and negative inverse slope under fully-reversed uniaxial fatigue loading

To calculate the endurance limit, σ_A and the inverse slope, k (both extrapolated at N_A equal 1,000,000 cycles), the plain specimens were tested under fully-reversed uniaxial fatigue loading. The experimental fatigue results used to determine σ_A and k are detailed in chapters 4.3.1.1 and 4.3.2.1 for both materials. Table 4-18 summarises the calculated values of σ_A and k associated to both materials.

Table 4-18 σ_A and k values used in the MWCM's governing equations for the assessed materials.

Plain material type	Loading	R	K	σ_A (MPa)	N_A (Cycles)
40054	Axial	-1	7.69	96.63	1E+06
40060	Axial	-1	6.82	71.68	1E+06

4.4.2 Endurance limit and the negative inverted slope under fully-reversed torsional fatigue loading

The fully-reversed torsional fatigue experiments were carried out in order to determine the endurance limit τ_A and the inverse slope k_0 associated to both materials in the structure laboratory of the university of Sheffield. The sections that follow summarise the experimental procedure and the estimation of τ_A and k_0 associated to materials 40054 and 40060.

4.4.2.1 Experimental procedure under torsional fatigue loading

In order to estimate the material constants τ_A and k_0 , the SCHENCK machine (Figure 4-17) located in the structural laboratory of the university of Sheffield were used to run fatigue experiments under torsion. The machine is equipped with a hydraulic actuator

which is capable of loading the specimen in the axial direction (axial capacity of 250 KN) as well as twisting the specimen (torsion capacity of 2200 Nm).

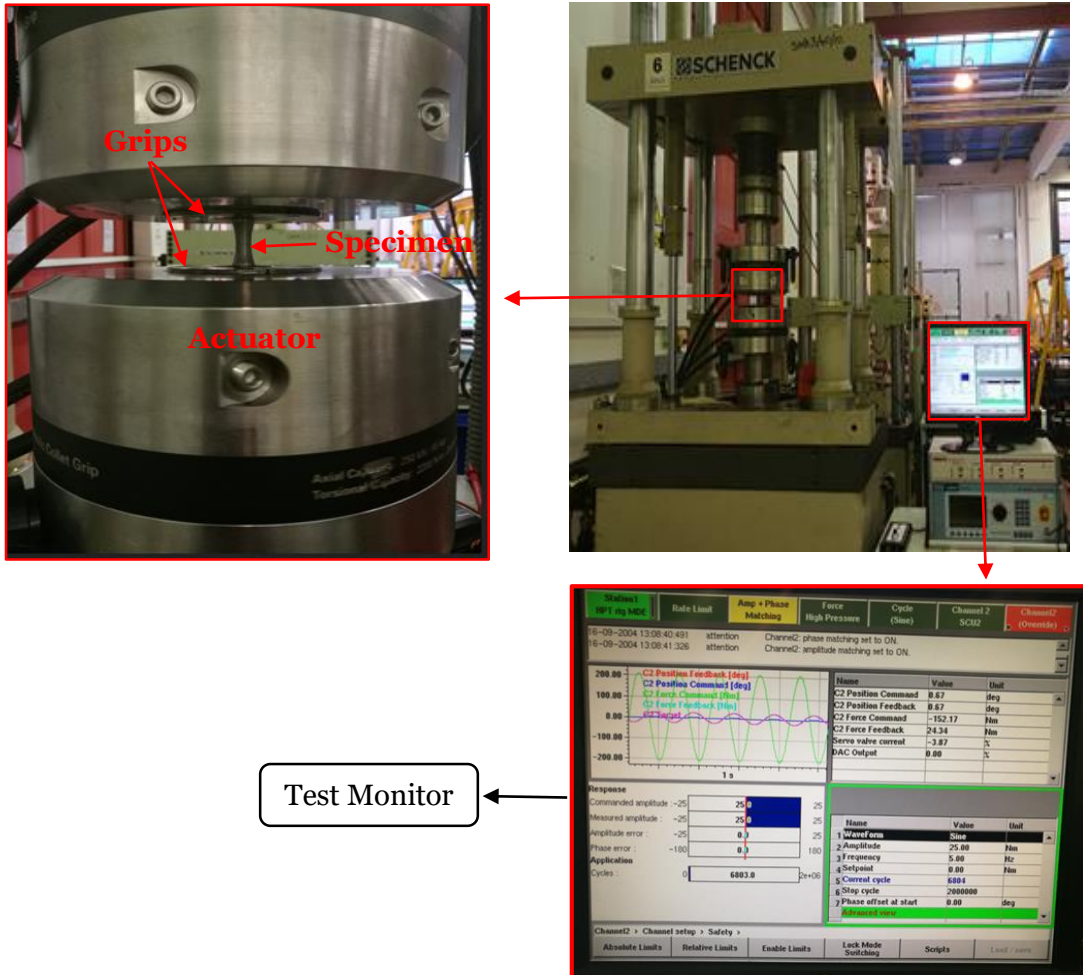


Figure 4-17 Fully-reversed torsion fatigue experiment rig.



Figure 4-18 Example of the specimen used for the torsion experiments.

The torsion fatigue tests consisted of clamping a round specimen (Figure 4-18) as shown in Figure 4-17. One end of the clamped specimen was fixed while the other was subjected to a sinusoidal constant amplitude torque load at a frequency of $5H_z$ with a load ratio $R = -1$. Before the start of each tests, the initial position of the specimen was set to zero degree. For both types of materials, all fatigue tests were carried out up to 2 million cycles unless a visible crack similar to the one in Figure 4-19 was noted. The machine was set up to record the number of cycles N_f , the applied torque feedback and the rotational position feedback in the course of each test. The recording frequency was $10H_z$.

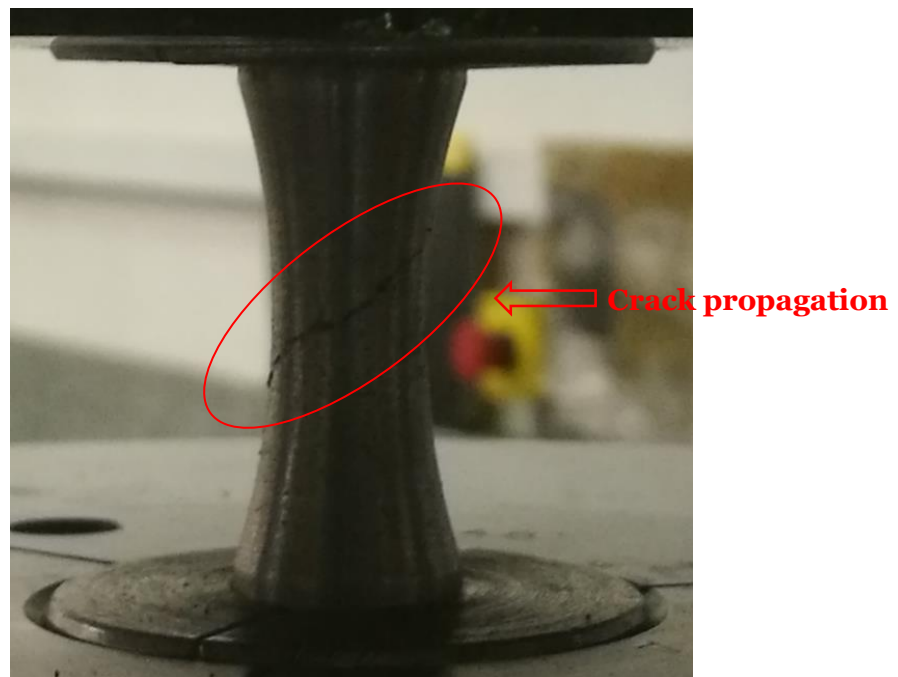


Figure 4-19 Crack propagation during the torsion test.

The specimens geometry of all the tested specimens are listed in Appendix D, while the inputs of all the experiments are summarised in Table 4-19 and Table 4-20.

Table 4-19 Fully-reversed torsion test input parameters for material 40054.

Specimens reference	Net section			Fatigue Test inputs		
	ϕ (mm)	L (mm)	I_p mm ⁴	R	τ_{amp} (MPa)	T_{amp} (N. m)
L1	9.83	33.93	914.81	-1	155.73	29
L1*	9.83	33.93	914.81	-1	214.80	40
L2	9.81	33.93	909.23	-1	159.84	30
L2**	9.82	33.93	911.09	-1	231.62	43
L3	9.82	33.93	911.09	-1	188.52	35
L4	9.81	33.93	909.23	-1	237.36	44
L5	9.91	33.93	944.97	-1	226.93	43
L6	9.92	33.93	950.71	-1	198.25	38
L7	9.92	33.93	950.71	-1	219.12	42
L8	9.91	33.93	944.97	-1	188.67	36
L9	9.91	33.93	946.88	-1	225.02	43

* Specimen L1 re-tested at 214.8 MPa after the run-out

** Specimen L2 re-tested at 231.6 MPa after the run-out

Table 4-20 Fully-reversed torsion test input parameters for material 40060

Specimens reference	Net section			Fatigue Test inputs		
	ϕ (mm)	L (mm)	I_p (mm ⁴)	R	τ_{amp} (MPa)	T_{amp} (N. m)
B1	9.86	31.25	926.03	-1	186.24	35
B2	9.88	31.25	933.57	-1	264.44	50
B3	9.83	31.25	914.81	-1	204.06	38
B4	9.88	31.25	935.47	-1	195.02	37
B5	9.86	31.25	926.03	-1	186.24	35
B6	9.88	31.25	935.47	-1	190.11	36
B7	9.88	31.25	933.57	-1	158.66	30
B8	9.90	31.25	943.06	-1	104.98	20
B9	9.89	31.25	937.36	-1	131.82	25
B10	9.86	31.25	927.91	-1	148.76	28

In Table 4-19 and Table 4-20, T_{amp} is the amplitude of the sinusoidal torque applied to the specimen, τ_{amp} is the corresponding shear stress amplitude, I_p is the polar second moment of area, L is the length of net section and ϕ the diameter. The mathematical relation linking T_{amp} to τ_{amp} is:

$$\tau_{amp} = \frac{(T_{amp}) \cdot r}{I_p} \quad 4-9$$

$$I_p = \frac{\pi \cdot r^4}{2} \quad 4-10$$

Where, r is the radius of net section of the specimen and I_p is the corresponding polar second moment of area.

4.4.2.2 Post-processing of the experimental results

The purpose of post processing is to determine the stiffness reduction of the material throughout the test. For any given cycle N_f , the corresponding stiffness, k is calculated using the equations:

$$k = \frac{\tau_{amp}}{\gamma} \quad 4-11$$

Where
$$\gamma = \frac{r\theta}{L} \quad 4-12$$

By substituting Eqs.(4-9) and (4-12) into Eq.(4-11), k takes on the following value:

$$k = \frac{2LT}{\pi\theta r^4} \quad 4-13$$

Where, T is the torque feedback and θ is the rotational position feedback at a given cycle. Having determined the k value associated to every cycles of a particular test, the stiffness behaviour of the specimen throughout the experiment is observed by plotting k vs N_f . The failure criteria of each specimen occurs when the stiffness reduces by 20%. The stiffness behaviour of specimens L6 and B6 are shown in Figure 4-20 and Figure 4-21 respectively. From the stiffness behaviour graphs, the number of cycles corresponding to 20% stiffness reduction are calculated.

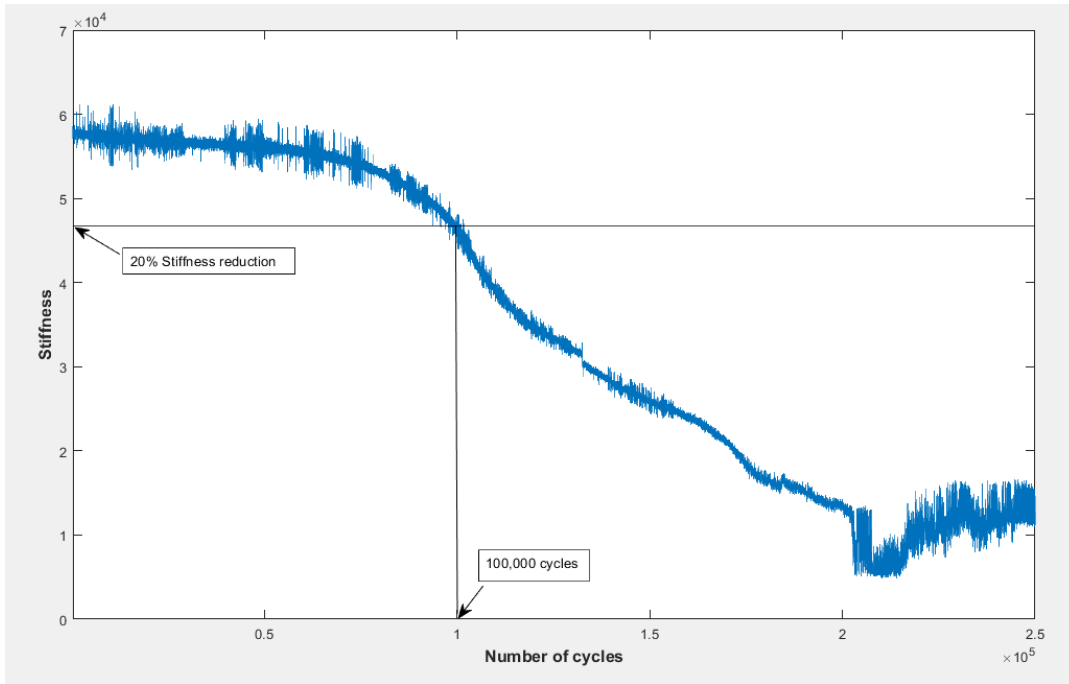


Figure 4-20 Stiffness behaviour of specimen L6 during the fully-reversed torsional fatigue experiment.

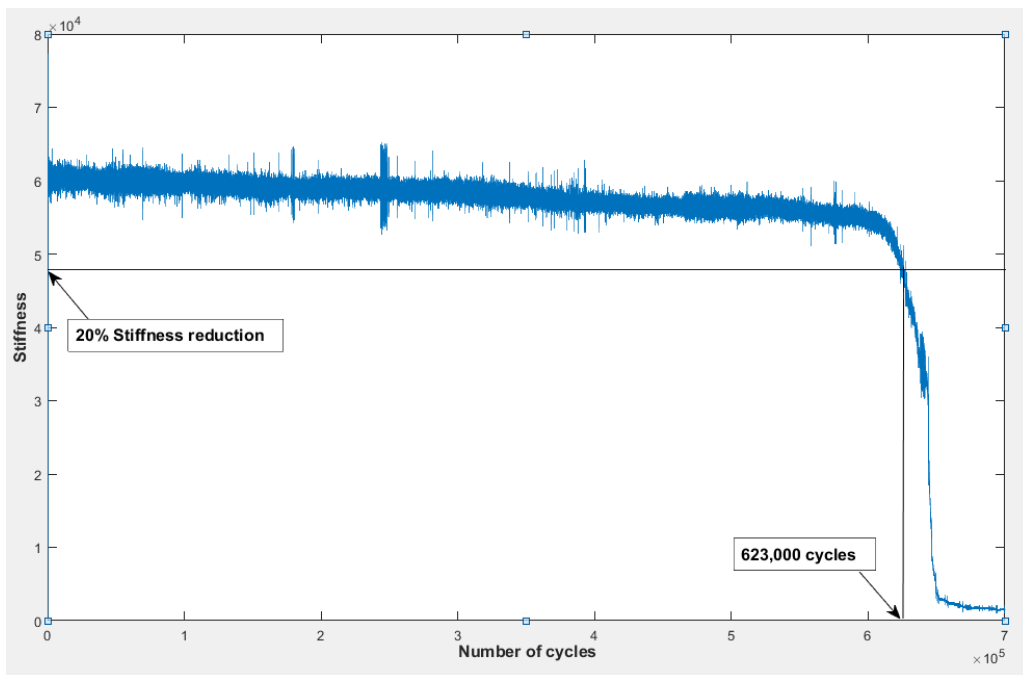


Figure 4-21 Stiffness behaviour of specimen B8 during the fully-reversed torsional fatigue experiment.

The stiffness behaviour during the torsional tests of the remaining specimens of both materials can be seen in Appendix E. Table 4-21 and Table 4-22 summarise the torsional fatigue test results for materials 40054 and 40060, respectively.

Table 4-21 Summary of the torsional fatigue test results generated by testing material 40054 under fully-reversed loading.

Specimens reference	Fatigue results		
	R	τ_A (MPa)	N_f (Cycles)
L1	-1	155.73	run out
L1*	-1	214.80	64,000
L2	-1	159.84	run out
L2*	-1	231.62	43,000
L3	-1	188.52	379,500
L4	-1	237.36	51,300
L5	-1	226.93	35,000
L6	-1	198.253	100,000
L7	-1	219.121	50,040
L8	-1	188.673	102,000
L9	-1	225.018	51,000

Table 4-22 Summary of the torsional fatigue test results generated by testing material 40060 under fully-reversed loading.

Specimens reference	Fatigue results		
	R	τ_A (MPa)	N_f (Cycles)
B1	-1	186.24	10,430
B2	-1	264.44	1,190
B3	-1	204.06	6,635
B4	-1	195.02	6,950
B5	-1	186.24	44,980
B6	-1	190.11	38,330
B7	-1	158.66	35,000
B8	-1	104.98	623,000
B9	-1	131.82	run out
B10	-1	148.76	run out

4.4.2.3 S-N curve, endurance limit and negative inverse slope under fully-reversed torsional loading

The S-N curves of the materials are generated by post-processing the fatigue results summarised in Table 4-21 and Table 4-22. The post-processing procedure used in this case is similar to the one used for the uniaxial fatigue results of material 40054

described in chapter 4.3.1.1. The generated S-N curves of materials 40054 and 40060 are shown in Figure 4-22 and Figure 4-23, respectively.

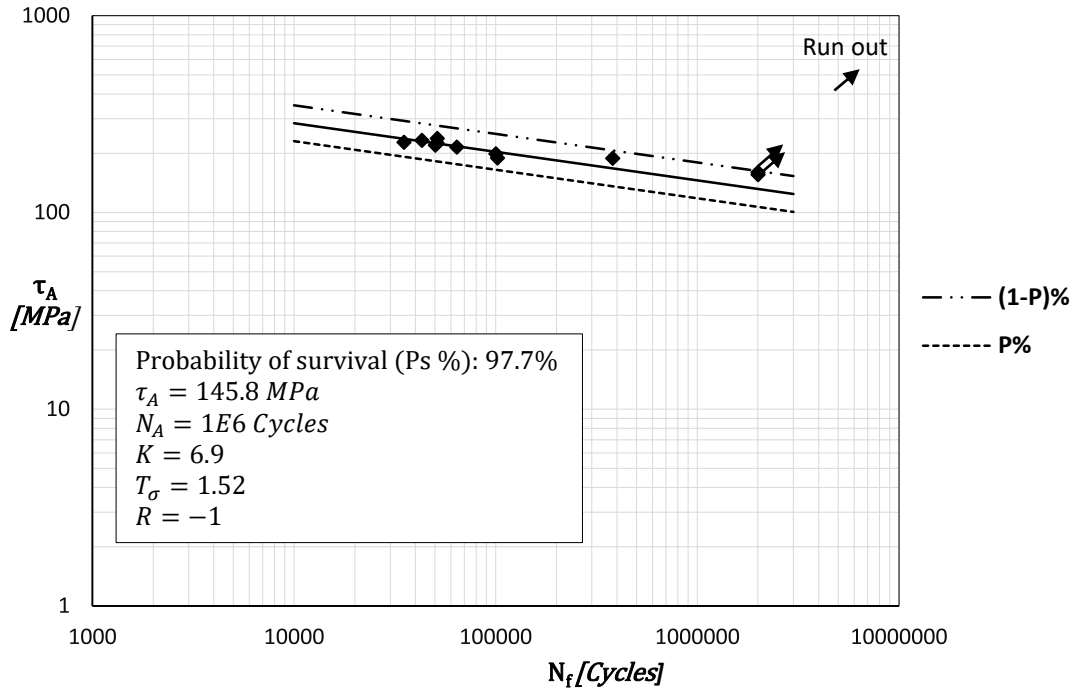


Figure 4-22 S-N Curve of material 40054 under fully-reversed torsional fatigue loading.

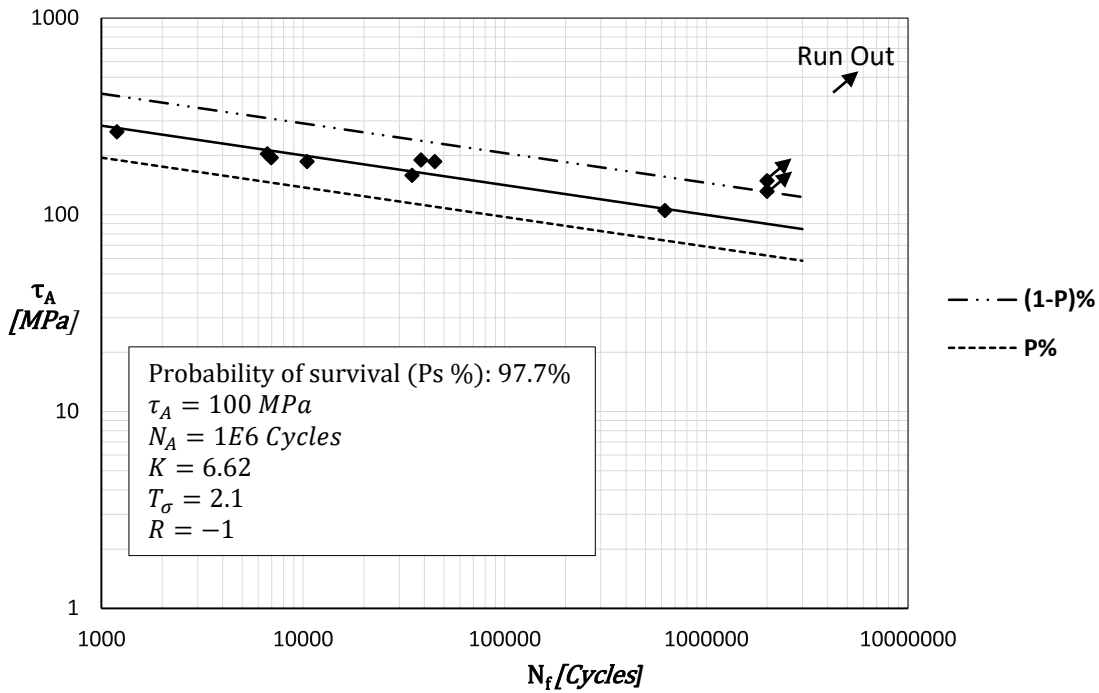


Figure 4-23 S-N Curve of material 40060 under fully-reversed torsional fatigue loading.

The endurance limit, τ_A , the inverse slope k_0 (extrapolated at 10^6 cycles) and the scattered band index, T_σ are summarised in Table 4-23.

Table 4-23 Torsion fatigue properties of materials 40054 and 40060.

Material	R	k_0	τ_A (MPa)	N_A (Cycles)	P %	T_σ
40054	-1	6.9	145.8	1E+06	97.7	1.52
40060	-1	6.6	100	1E+06	97.7	2.10

4.5 Calculation of the mean stress sensitivity index

The mean stress sensitivity index (MSSI) m , in Eq.(2-76) defines the portion of the mean stresses normal to the critical plane which effectively contributes to the opening of the micro cracks. In this section, the mean stress sensitivity index, m for both materials is calculated according to the experimental protocol detailed in chapter 2.4.8.

4.5.1 The endurance limit under fully reversed uniaxial fatigue loading

The endurance limit σ_A is required to calculate the mean stress sensitivity index m . The experimental procedures and results which enabled the calculation of σ_A for materials 40054 and 40060 have been described in chapters 4.3.1.1 and 4.3.2.1, respectively. The endurance limits of both materials are summarise in Table 4-18.

4.5.2 The endurance limit under fully reversed torsional fatigue loading

Another key parameter needed to estimate the mean stress sensitivity index m is the endurance limit, τ_A under fully reversed torsional fatigue loading. Similarly, the experimental procedures and results leading to the calculation of τ_A for both materials have been described in chapter 4.4.2. The endurance limits of both materials can be seen in Table 4-23.

4.5.3 The endurance limit under uniaxial fatigue loading with load ratio equal to 0.1

To calculate m according to the procedure summarised in chapter 2.4.8, the endurance limit, σ_a and the stress components relative to the critical plane under $R = 0.1$ are required. These values are obtained from the S-N curve of fatigue data generated by testing specimens 40054 and 40060 under uniaxial fatigue loading with $R = 0.1$. The Mayes 1 Moog Integrated servo-hydraulic (Figure 4-2) was used to carry out uniaxial fatigue tests according to the protocol described in chapter 4.3.1.1. The geometry of the tested specimens are similar to the one in Figure 4-1. The dimensions are details in Appendix B while the fatigue results are summarised in Table 4-24 and Table 4-25.

Table 4-24 Summary of the uniaxial fatigue results for plain material 40054 under $R = 0.1$.

Specimens reference	Fatigue Results							
	R	σ_a	σ_{max}	σ_m	F_{max}	F_{min}	F_m	N_f
		(MPa)	(MPa)	(MPa)	(KN)	(KN)	(KN)	(Cycles)
R(0.1)1	0.1	120	266.667	146.667	14.571	1.457	8.014	1,221
R(0.1)2	0.1	90	200.000	110.000	12.055	1.205	6.630	14,973
R(0.1)3	0.1	70	155.556	85.556	9.200	0.920	5.060	Run-out
R(0.1)3*	0.1	90	200.000	110.000	11.829	1.183	6.506	17,315
R(0.1)4	0.1	80	177.778	97.778	10.665	1.066	5.866	62,284
R(0.1)5	0.1	75	166.667	91.667	10.037	1.004	5.520	382,158
R(0.1)6	0.1	72	160.000	88.000	9.752	0.975	5.363	163,610
R(0.1)7	0.1	72	160.000	88.000	9.768	0.977	5.372	257,467
R(0.1)8	0.1	70	155.556	85.556	9.031	0.903	4.967	459,084
R(0.1)9	0.1	67	148.889	81.889	8.596	0.860	4.728	Run-out
R(0.1)9**	0.1	100	222.222	122.222	12.829	1.283	7.056	17,849
R(0.1)10	0.1	80	177.778	97.778	10.828	1.083	5.955	69,357

* Specimen R(0.1)3 re-tested at $\sigma_a = 90$ MPa after the run-out

** Specimen R(0.1)9 re-tested at $\sigma_a = 100$ MPa after the run-out

Table 4-25 Summary of the uniaxial fatigue results for plain material 40060 under $R=0.1$.

Specimens reference	Fatigue Results							
	R	σ_a	σ_{max}	σ_m	F_{max}	F_{min}	F_m	N_f
		(MPa)	(MPa)	(MPa)	(KN)	(KN)	(KN)	(Cycles)
B(Ro.1)1	0.1	60	133.333	73.333	8.116	0.812	4.464	290,273
B(Ro.1)2	0.1	80	177.778	97.778	10.831	1.083	5.957	6,835
B(Ro.1)3	0.1	70	155.556	85.556	9.429	0.943	5.186	37,247
B(Ro.1)4	0.1	50	111.111	61.111	6.738	0.674	3.706	run-out
B(Ro.1)4*	0.1	85	188.889	103.889	11.454	1.145	6.300	8,481
B(Ro.1)5	0.1	55	122.222	67.222	7.454	0.745	4.100	605,464
B(Ro.1)6	0.1	80	177.778	97.778	10.756	1.076	5.916	16,874
B(Ro.1)7	0.1	70	155.556	85.556	9.426	0.943	5.184	18,441
B(Ro.1)8	0.1	60	133.333	73.333	8.107	0.811	4.459	50,961
B(Ro.1)9	0.1	55	122.222	67.222	7.452	0.745	4.099	176,033
B(Ro.1)10	0.1	50	111.111	61.111	6.783	0.678	3.731	run-out
B(Ro.1)10**	0.1	85	188.889	103.889	11.532	1.153	6.342	4,029
B(Ro.1)11	0.1	60	133.333	73.333	8.116	0.812	4.464	272,701
B(Ro.1)12	0.1	55	122.222	67.222	7.388	0.739	4.063	run-out
B(Ro.1)12***	0.1	80	177.778	97.778	10.746	1.075	5.910	9,787

* Specimen B(0.1)4 re-tested at $\sigma_a = 85$ MPa after the run-out

** Specimen B(Ro.1)10 re-tested at $\sigma_a = 85$ MPa after the run-out

*** Specimen B(Ro.1)12 re-tested at $\sigma_a = 80$ MPa after the run-out

The S-N curves shown in Figure 4-24 and Figure 4-25 are generated by post-processing the uniaxial fatigue results of both materials according to the procedure detailed in chapter 4.3.1.1. The endurance limit σ_a , the inverse slope k and the scattered band, T_σ are summarised in Table 4-26.

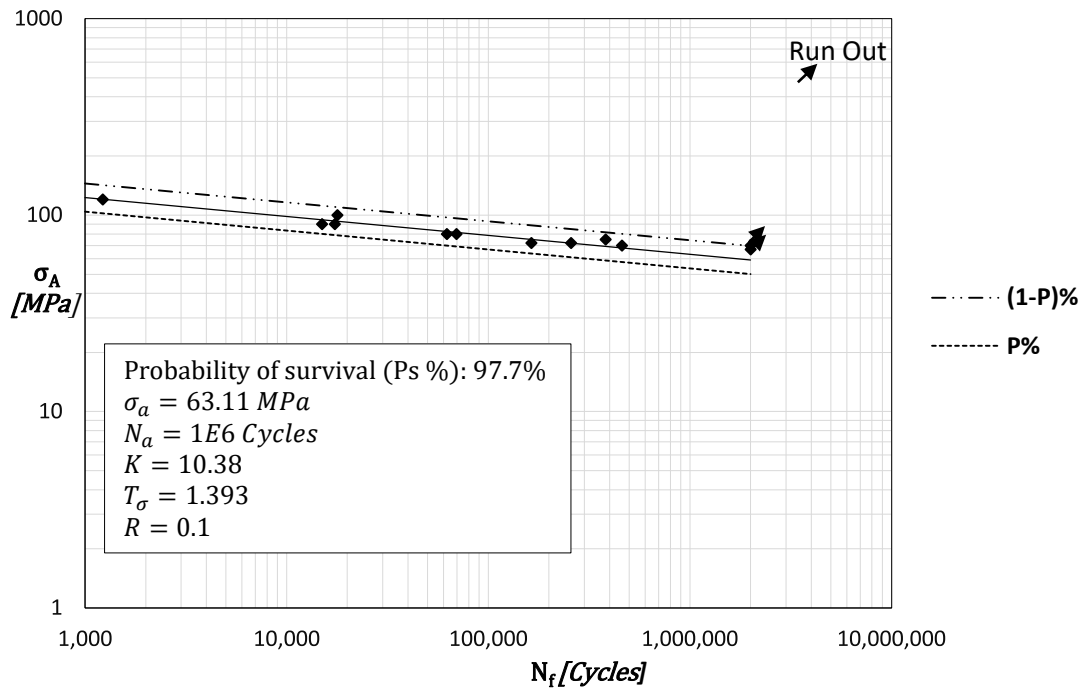


Figure 4-24 S-N curve of plain material 40054 under uniaxial fatigue loading with $R = 0.1$.

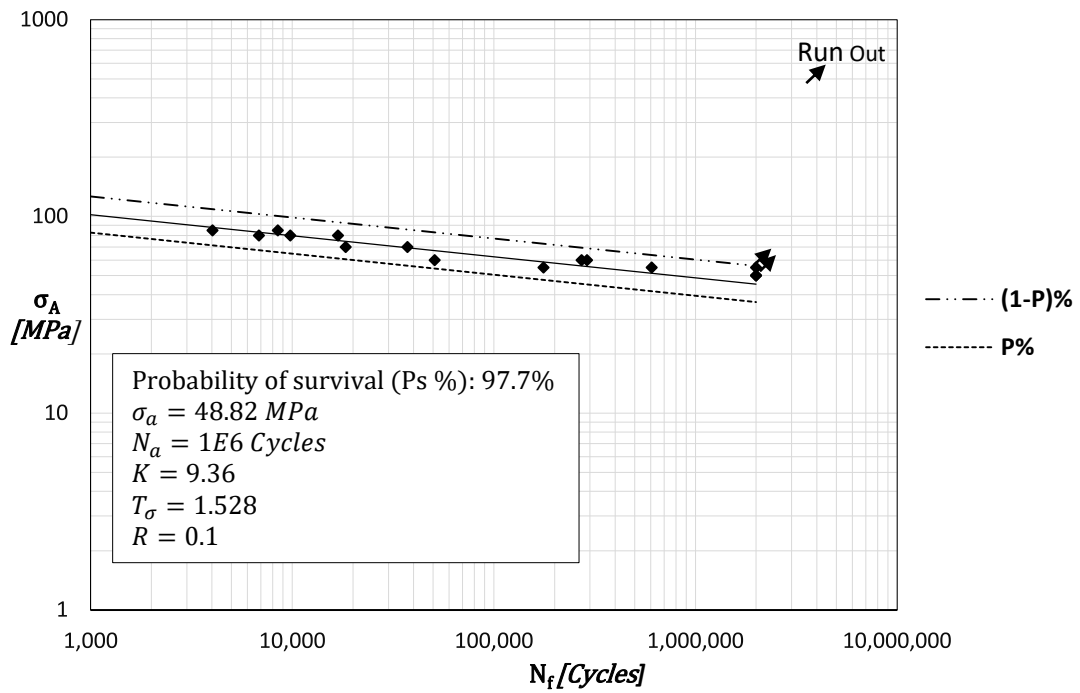


Figure 4-25 S-N curve of plain material 40060 under uniaxial loading with $R = 0.1$.

Table 4-26 Endurance limit under uniaxial fatigue loading with $R = 0.1$.

Material	R	σ_a (MPa)	k	N_A (Cycles)	P% (%)	P% (%)	T_σ
40054	0.1	63.11	10.38	1E+06	97.7	2.3	1.393
40060	0.1	48.82	9.36	1E+06	97.7	2.3	1.528

Having determined σ_a for both materials, the stress components τ_a^* , $\sigma_{n,a}^*$ and $\sigma_{n,m}^*$ relative to the critical plane are calculated directly according to Eqs. (2-84 to 2-88). Table 4-27 summarises the critical plane stress constants used in Eq. 2-83 .

Table 4-27 Critical plane stress components under $R = 0.1$.

Material	R	σ_a (MPa)	N_a (Cycles)	τ_a^* (MPa)	$\sigma_{n,a}^*$ (MPa)	$\sigma_{n,m}^*$ (MPa)
40054	0.1	63.11	1E+06	31.55	31.55	38.57
40060	0.1	48.82	1E+06	24.41	24.41	29.83

4.5.4 Calculation of the mean stress sensitivity index

As explained in chapter 2.4.8, the mean stress sensitivity index, m is calculated using the following expression:

$$m = \frac{\tau_a^*}{\sigma_{n,m}^*} \left(2 \frac{\tau_A - \tau_a^*}{2\tau_A - \sigma_A} - \frac{\sigma_{n,a}^*}{\tau_a^*} \right)$$

The values of the stress components τ_a^* , $\sigma_{n,a}^*$ and $\sigma_{n,m}^*$ for both materials are summarised in Table 4-27 while the endurance limits σ_A and τ_A are found in Table 4-18 and Table 4-23. This permit the determination of the mean stress sensitivity index and it is stated in Table 4-28.

Table 4-28 Mean stress sensitivity index values.

Material	m
40054	0.141
40060	0.146

4.6 Summary of the material properties used to calibrate the proposed design methodology

The properties of materials 40054 and 40060 which are required to calibrate the MWCM's functions (Eqs. 2-77 to 2-81) and the critical distance, L_M (Eq.2-75) have been summarised in this chapter. Table 4-29 outlines these material properties.

Table 4-29 Summary of the material properties to be used in the proposed design methodology.

Material	σ_A (MPa)	k	τ_A (MPa)	k_0	N_A (Cycles)	m	A	B
40054	96.63	7.7	145.8	6.9	10^6	0.141	1.218	-0.042
40060	71.68	6.8	100.0	6.6	10^6	0.146	1.672	-0.032

Chapter 5

Fretting fatigue experiments

This chapter aims to carry out the fretting fatigue experiments. This will be achieved in three stages. The first stage will consist of the calibration of the fretting fatigue machine. The second stage will involve the fretting fatigue experiments under constant amplitude loading. In the third stage, the fretting fatigue experiments under variable amplitude loading will be investigated.

5.1 Calibration of the fretting fatigue machine

Calibration of the machine means comparing the output from the machine with the input. This was achieved by comparing the load feedback signals from the actuators with the signals obtained from strain gages attached to the pads and specimen. Before comparison, the signals from the strain gauges were converted to load signals using Hooke's law. The schematic diagram of the fretting fatigue machine is shown in Figure 5-1 which is located in the structure laboratory of the university of Sheffield. The rig is equipped with a Moog controller and four actuators which are each fitted with a load cell of ± 100 KN and a maximum displacement limit of 25 mm.

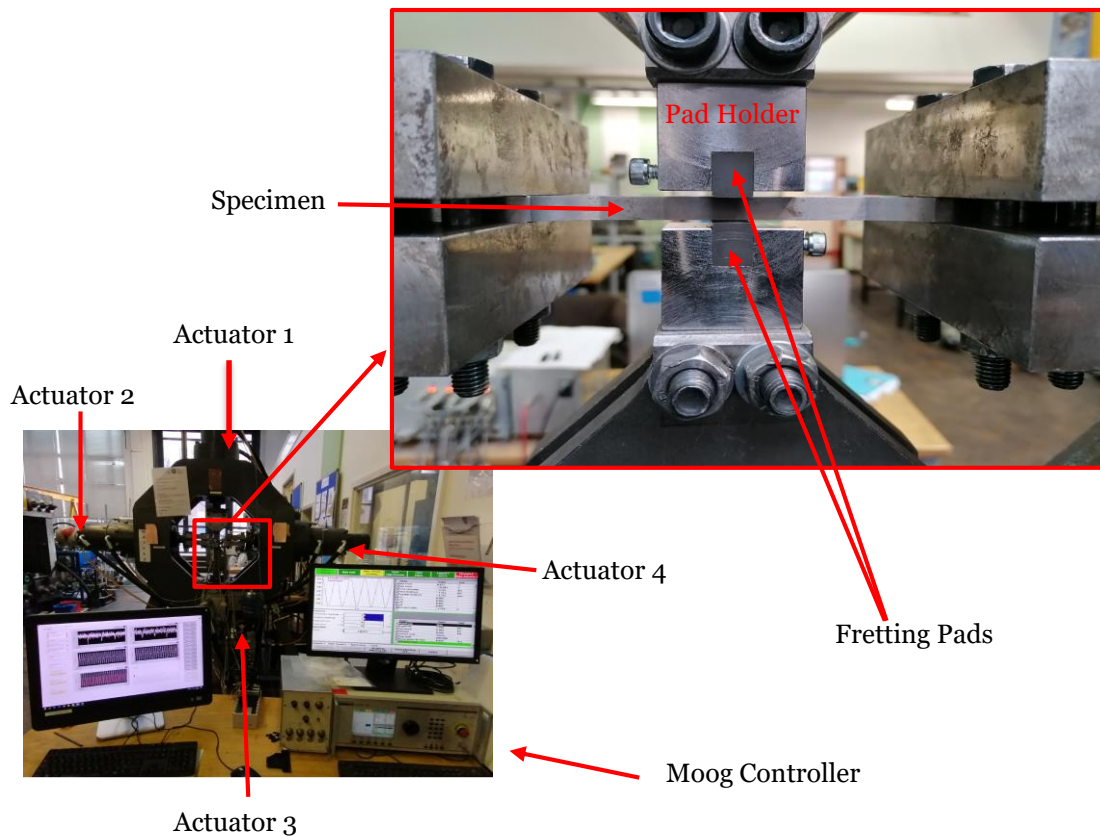


Figure 5-1 Hydraulic fretting fatigue test rig.

The calibration of the machine set-up is shown in Figure 5-2. In this arrangement, the fretting specimen is attached to actuators 2 and 4 and the pads to actuators 1 and 3. The materials used in the calibration process was made from steel. Several calibration tests were carried out and the loading steps used in each of the test are summarised as follows:

- Clamp the specimen between actuator 2 and 4.
- Apply a mean tension load to the specimen through actuator 4.
- Attached pads to actuator 1 and 3.
- Enable contact of the pads with the specimen under position control. The controller is capable of detecting variation in the contact arrangement between each pad and the surface of the specimen.
- Apply a normal load P to the pads through the actuator 1 under force control.
- Apply a fatigue load F to the specimen through actuator 4 which is in force control.

Strain gauges were attached to the specimen and the pads (in Figure 5-2) in order to measure the strain signals which were later converted to forces using Hook's Law.

Four different calibration set-up tests were carried out. During these tests, the contact load P , applied to the pads was either constant or cyclic. The fatigue load F , applied to the specimen was either variable cyclic or constant cyclic. A data acquisition system was used to record the signals from the strain gauges and load feedback of actuators 1 to 4. chapters 5.1.1 to 5.1.4 summarise all calibration set-up tests for different loading configurations while the post processing and the interpretation of the calibration results can be seen in chapter 5.1.5.

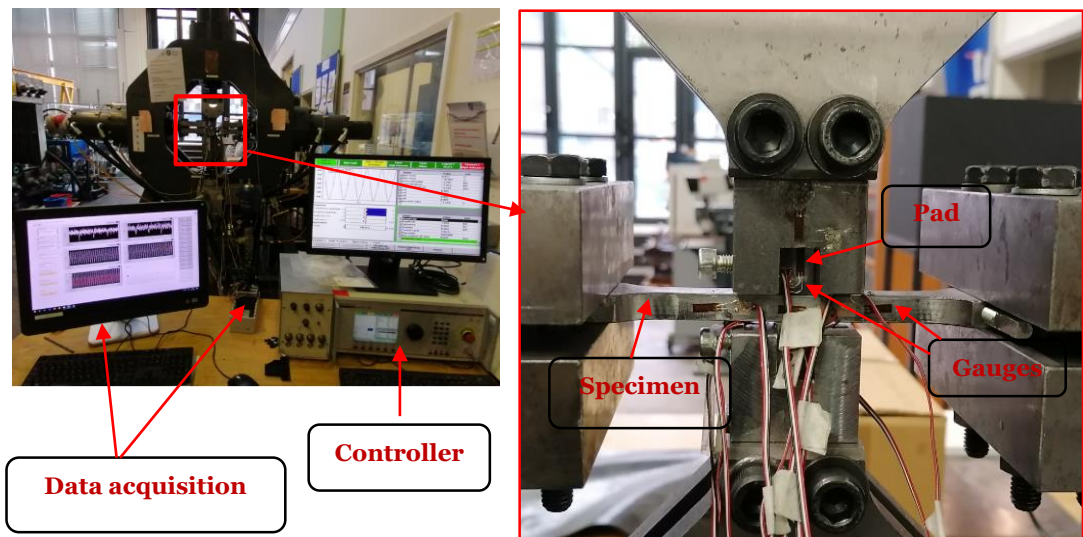


Figure 5-2 Calibration set-up test.

5.1.1 First calibration test (P CA-cyclic and F VA-cyclic)

Two tests were carried out during the first calibration set-up test. For both tests, a CA cyclic load P was applied to the pad through the actuator 1 at a frequency of $10H_z$ while a VA fatigue load F was applied to the specimen. The VA spectrum in Figure 5-3 was designed in order to apply different load levels to the specimen. Both the CA load P and VA cyclic load F were in phase and running at a frequency of $10H_z$. This is summarised in Table 5-1 Figure 5-3 and Table 5-2.

Table 5-1 First calibration test: Contact load.

Test N ^o	P _m (KN)	P _a (KN)
1	-2	1
2	-1.5	0.5

In Table 5-1, P_m is the contact mean normal load in compression and P_a is the amplitude of cyclic contact load.

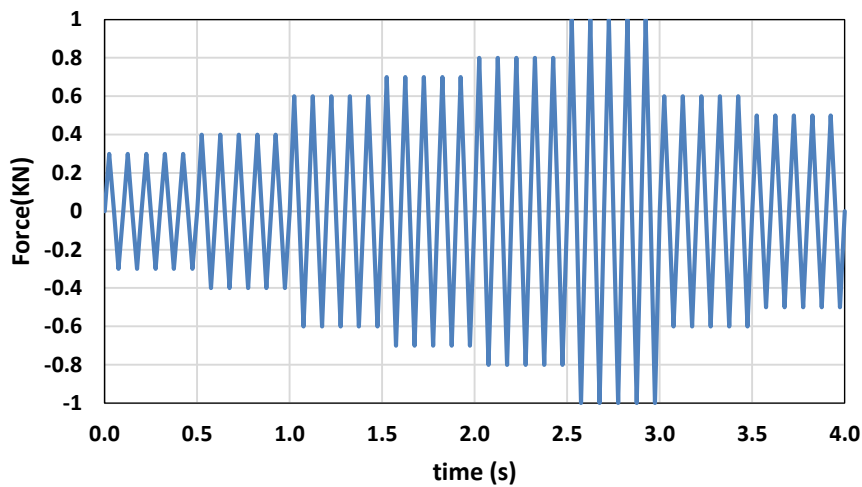


Figure 5-3 First calibration test: VA fatigue load spectrum.

Table 5-2 First calibration test: Maximum amplitude applied to the fatigue load spectrum.

Test N ^o	F _a (KN)
1	10
2	6

5.1.2 Second calibration test (P constant and F VA-cyclic)

In this calibration test, a constant compression load of 3KN was applied to the pads while a VA fatigue load spectrum shown in Figure 5-3 was applied to the specimen. The maximum amplitude of the fatigue load spectrum was 10KN.

5.1.3 Third calibration test (P CA-cyclic and F CA-cyclic)

In the third calibration test, the contact load P and the fatigue load F were both CA cyclic.

Table 5-3 and Table 5-4 summarised the load inputs of the two tests of this set-up.

Table 5-3 Third calibration test: Contact load inputs.

Test N ^o	P _m (KN)	P _a (KN)
1	-2.5	1
2	-2	0.5

Table 5-4 Third calibration test: Fatigue load inputs.

Test N ^o	F _m (KN)	F _a (KN)
1	0	9
2	0	7

5.1.4 Fourth calibration test (P constant and F CA-cyclic)

In the last calibration set-up, the contact load P was constant and the fatigue load was fully reversed CA cyclic at frequency of $10 H_z$. Two tests were carried out, one in which P was $3 KN$ and $2 KN$ in the second. The fatigue load inputs for both tests are summarised in Table 5-5.

Table 5-5 Fourth calibration test: Fatigue load inputs.

Test N ^o	F _m (KN)	F _a (KN)
1	0	10
2	0	8

5.1.5 Post-processing and interpretation of the calibration tests

A data acquisition system was used to record the fatigue load feedback signal, the contact load feedback signals and the signals from the strain gauges attached to both the specimen and pads. All the recorded signals were synchronised. The signals from the strain gauges were converted to force signals according to the following Hooke's law equation:

$$F = \varepsilon * A * E \quad 5-1$$

In the above equation, ε is the strain, E the Young's modulus and A is the cross section area in the vicinity of the gauges. Finally, the force signals obtained from the strain gauge attached to the specimen and pads were compared to the fatigue and the contact load feedback signals obtained from actuators.

The calibration results were interpreted by using the correlation coefficient theory of two random variables. In order to achieve this, consider two random variables A and B with standard deviations s_A and s_B respectively. The correlation coefficient of A and B, $\rho(A, B)$ is a measure of their linear dependence which is expressed using a correlation coefficient matrix, R [64]:

$$R = \begin{pmatrix} \rho(A, A) & \rho(A, B) \\ \rho(B, A) & \rho(B, B) \end{pmatrix} \quad 5-2$$

Where

$$\rho(A, B) = \frac{cov(A, B)}{s_A s_B} \quad 5-3$$

In definition 5-2, $\rho(A, A)$ and $\rho(B, B)$ are equal to 1 since A and B are always directly correlated to themselves. A qualitative comparison between the loads feedback from the actuators and the loads obtained from strain gauges are shown in the next four figures (first and third calibration test). The remaining calibration results are shown in Appendix F.

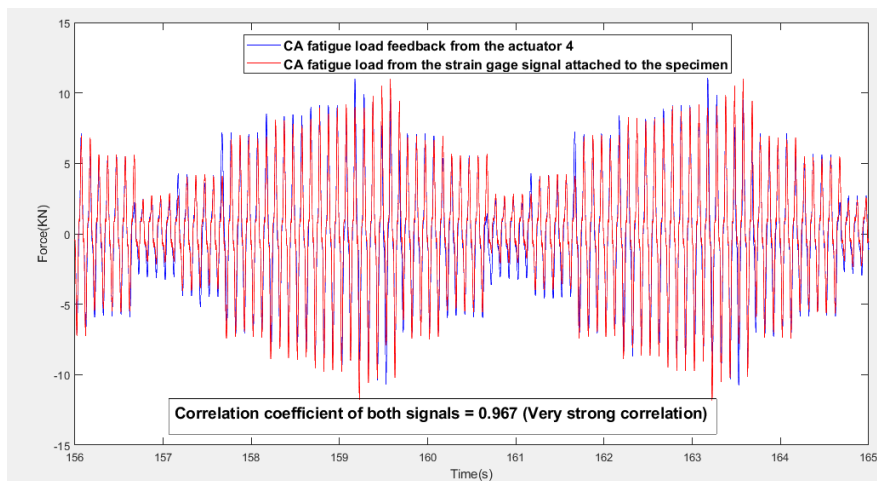


Figure 5-4 First calibration test (Test N° 1): Comparison between the load feedback from actuator 4 and the load obtained from the strain gauge signal attached to the specimen.

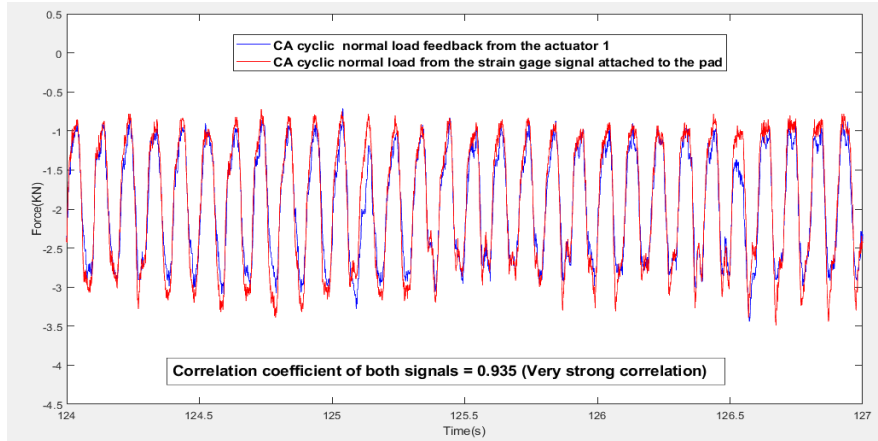


Figure 5-5 First calibration test (Test N° 1): Comparison between the load feedback from actuator 1 and the load obtained from the strain gauge attached to the pads.

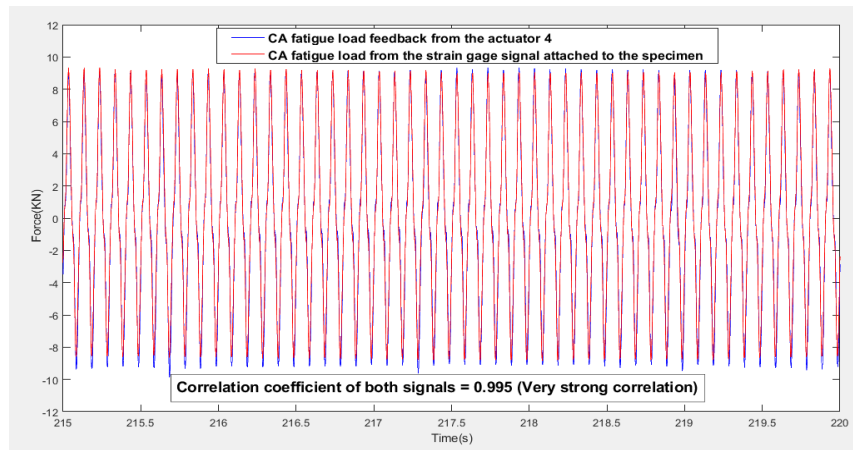


Figure 5-6 Third calibration test (Test N° 1): Comparison between the load feedback from actuator 4 and the load obtained from the strain gauge signal attached to the specimen.

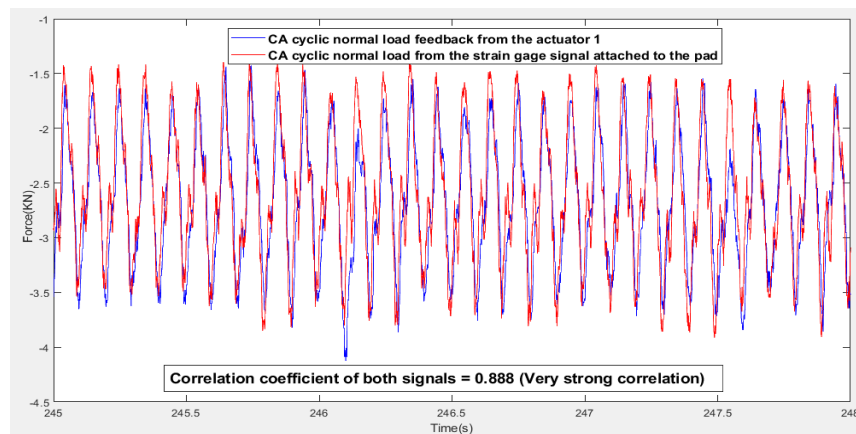
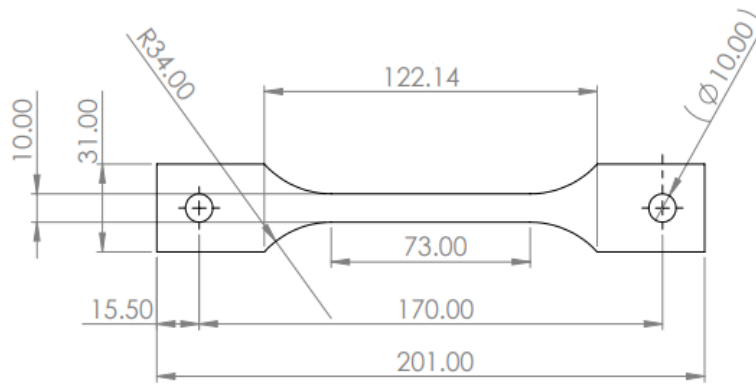


Figure 5-7 Third calibration test (Test N° 1): Comparison between the load feedback from actuator 1 and the load obtained from the strain gauge attached to the pad.

The calibration results summarised from Figure 5-4 to Figure 5-7 show that the correlation coefficients of the compared signals are in the range of 0.7 to 1 which is an indication of a very strong correlation from statistical perspective [69]. This results demonstrate that the load feedback from the machine is the accurate load that is subjected to the specimen. Therefore, the hydraulic biaxial rig can be confidentially used to run fretting fatigue experiments under CA and VA loading.

5.2 Fretting fatigue experiments under constant amplitude loading

The experimental set-up and load steps used to investigate the fretting fatigue damage of specimens made from materials 40054 and 40060 are summarised in chapter 5.1. The specimens geometry is detailed in Figure 5-8 and has a thickness of 9 mm. The pads used to clamped the specimen are made either from material 40054 or of steel coated with zinc phosphate. These pads were cylindrical with a thickness of 12 mm, a height of 15 mm and a contact radius R_p equal to 100 mm, 75 mm or 20 mm. The arrangement of the specimen and pads in the rig is shown in Figure 5-1. In this configuration, the pads are wider than the specimen in order to avoid the edge effect. Fretting fatigue experiments can be carry out using different loading configurations and load ratios. Due to limited number of materials, only three types of loading configurations were considered. In the first configuration, the contact load P applied to the pads was constant while a fully-reversed CA sinusoidal fatigue load F at the frequency of 10 H_z applied to the specimen. In the second load configuration, the contact load was constant while the fatigue load was CA with a load ratio $R = 0.1$ and a frequency of 10 H_z . In the third loading configuration, P and F were both CA sinusoidal load running in phase at frequency of 10 H_z . The loads used in all configurations, are summarised from Table 5-6 to Table 5-10. In these tables, P is the constant load applied to the pads, P_m is the contact mean normal load in compression, P_a is the amplitude of cyclic contact load, F_a is the amplitude of the CA fatigue load and R_p is the pad radius.



All dimensions in mm

Figure 5-8 Geometry of the specimens used to assess the fretting fatigue damage of materials 40054 and 40060.

Table 5-6 Fretting fatigue input loads used to test the material 40054. P is constant, F is CA and the pads are made from steel coated with zinc phosphate

Test N ^o	R _p (mm)	P (KN)	F _a (KN)	R
1	20	5.5	8.00	0.1
2	20	5.5	9.00	0.1
3	20	5.5	9.50	0.1
4	20	5.5	10.00	0.1
5	20	5.5	10.50	0.1
6	20	5.5	11.00	0.1
7	20	5.5	12.00	0.1
8	20	5.5	16.00	0.1
9	20	5.5	7.00	-1
10	20	5.5	6.50	-1
11	20	5.5	6.25	-1
12	20	5.5	6.00	-1
13	20	5.5	5.00	-1
14	100	5.5	7.00	-1
15	100	5.5	6.50	-1
16	100	5.5	6.25	-1
17	100	5.5	6.00	-1
18	100	5.5	5.50	-1
19	100	5.5	5.00	-1
20	100	5.5	4.75	-1

Table 5-7 Fretting fatigue input loads used to test material 40060. P is constant, F is CA and the pads are made from material 40054.

Test N ^o	R _p (mm)	P (KN)	F _a (KN)
1	75	5	8
2	75	5	7
3	75	5	6.5
4	75	4	9
5	75	3.5	6.25

Table 5-8 Fretting fatigue input loads used to test the material 40060. P is constant, F is CA and the pads are made from steel costed with zinc phosphate.

Test N ^o	R _p (mm)	P (KN)	F _a (KN)
1	75	4	3.5
2	75	4	4
3	75	4	4.75
4	75	4	5
5	75	4	5.5
6	75	4	6

Table 5-9 Fretting fatigue input loads to test the material 40060. P and F are CA and the pads made from material 40054.

Test N ^o	R _p (mm)	P _m (KN)	P _a (KN)	F _a (KN)
1	75	-4	0.5	5.5
2	75	-5	0.5	6.5
3	75	-5	0.5	6
4	75	-5	0.5	9.5
5	75	-5	0.5	7
6	75	-6	1	7.5

Table 5-10 Fretting fatigue input loads to test the material 40060. P and F are CA load and the pads are made from steel coated with zinc phosphate.

Test N ^o	R _p (mm)	P _m (KN)	P _a (KN)	F _a (KN)
1	75	-5	0.5	6
2	75	-5	0.5	5.5
3	75	-5	0.5	5
4	75	-5	0.5	4.5
5	75	-5	0.5	4
6	75	-5	0.5	4.25
7	75	-5	0.5	4.75

The tests were allowed to run up to 5,000,000 cycles unless failure occurred. The failure criterion adopted was the complete separation of the specimens. Figure 5-9 shows the damaged specimen of test N° 1 in Table 5-6 while the other damaged specimens can be seen in Appendix G and I. The results of the fretting fatigue tests are summarised in Table 5-11. It can be seen in Figure 5-9, Appendix G and I that crack initiated either at the trailing edge (side of the contact where the specimen was clamped) or leading edge (side of the contact where the fatigue load was applied to the specimen) of the contact. This can be justified through the action and reaction phenomena. In details, the fatigue load applied at the leading end of the specimen was equal to the fatigue load applied at the trailing end of the specimen.

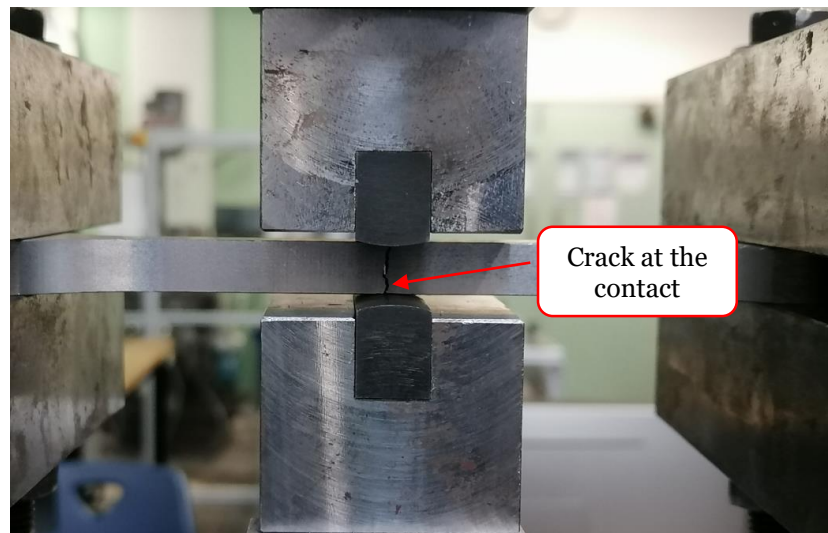


Figure 5-9 Damaged fretting specimen of test N°1 in Table 5-6.

Table 5-11 Summary of the fretting fatigue results of specimens 40054. P is constant, F is CA and the pads are made from steel coated with zinc phosphate

Test N°	R _p (mm)	P (KN)	F _a (KN)	R	N _f (cycles)	Status
1	20	5.5	8.00	0.1	970,764	Failure
2	20	5.5	9.00	0.1	1,107,093	Failure
3	20	5.5	9.50	0.1	347,554	Failure
4	20	5.5	10.00	0.1	328,400	Failure
5	20	5.5	10.50	0.1	368,132	Failure
6	20	5.5	11.00	0.1	193,466	Failure
7	20	5.5	12.00	0.1	166,731	Failure
8	20	5.5	16.00	0.1	86,731	Failure
9	20	5.5	7.00	-1	32,788	Failure
10	20	5.5	6.50	-1	86,847	Failure
11	20	5.5	6.25	-1	130,733	Failure
12	20	5.5	6.00	-1	547,361	Failure
13	20	5.5	5.00	-1	1,053,934	Failure
14	100	5.5	7.00	-1	21,619	Failure
15	100	5.5	6.50	-1	28,086	Failure
16	100	5.5	6.25	-1	44,523	Failure
17	100	5.5	6.00	-1	47,932	Failure
18	100	5.5	5.50	-1	111,079	Failure
19	100	5.5	5.00	-1	199,438	Failure
20	100	5.5	4.75	-1	138,909	Failure

Table 5-12 Summary of the fretting fatigue results of material 40060. P is constant, F is CA and pads are made of material 40054

Test N°	R _p (mm)	P (KN)	F _a (KN)	N _f (cycles)	Status
1	75	5	8	29,670	Failure
2	75	5	7	59,770	Failure
3	75	5	6.5	42,985	Failure
4	75	4	9	23,653	Failure
5	75	3.5	6.25	133,335	Failure

Table 5-13 Summary of the fretting fatigue results of material 40060. P is constant, F is CA and pads made from steel coated with zinc phosphate.

Test N°	R _p (mm)	P (KN)	F _a (KN)	N _f (cycles)	Status
1	75	4	3.5	1,703,890	Failure
2	75	4	4	1,218,640	Failure
3	75	4	4.75	283,325	Failure
4	75	4	5	351,381	Failure
5	75	4	5.5	173,542	Failure
6	75	4	6	53,257	Failure

Table 5-14 Summary of the fretting fatigue results of material 40060. P and F are both CA and pads made from material 40054.

Test N°	R _p (mm)	P _m (KN)	P _a (KN)	F _a (KN)	N _f (cycles)	Status
1	75	-4	0.5	5.5	208,500	Failure
2	75	-5	0.5	6.5	65,650	Failure
3	75	-5	0.5	6	124,504	Failure
4	75	-5	0.5	9.5	17,788	Failure
5	75	-5	0.5	7	52,773	Failure
6	75	-6	1	7.5	50,297	Failure

Table 5-15 Summary of the fretting fatigue results of material 40060. P and F are both CA and pads made from steel coated with zinc phosphate.

Test N°	R _p (mm)	P _m (KN)	P _a (KN)	F _a (KN)	N _f (cycles)	Status
1	75	-5	0.5	6	77,000	Failure
2	75	-5	0.5	5.5	135,000	Failure
3	75	-5	0.5	5	338,697	Failure
4	75	-5	0.5	4.5	397,873	Failure
5	75	-5	0.5	4	705,000	Failure
6	75	-5	0.5	4.25	561,658	Failure
7	75	-5	0.5	4.75	450,562	Failure

5.3 Fretting fatigue experiments under variable amplitude loading

The fretting fatigue experiments under variable amplitude loading were carried out using the testing protocol described in chapter 5.1. In these experiments, the pads were made either from material 40054 or steel coated with zinc phosphate. The assessed specimens whose geometry is shown in Figure 5-8 were made either from material 40054 or 40060. The pads were cylindrical with a contact radius R_p equal to 20mm, 75mm or 100 mm, a thickness equal to 12 mm, and a height equal to 15 mm. In order to carry the fretting fatigue tests, a constant normal load P was applied to the pads and a variable amplitude fatigue load F applied to the specimen. The variable amplitude spectrums designed to run the tests are shown in Figure 5-10, Figure 5-11 and Figure 5-12. In Figure 5-10 and Figure 5-12, the load ratio $R = -1$ whereas in Figure 5-11, $R \geq 0.1$. The frequency of each cycles within the load spectrums was maintained at 10 Hz. The main idea behind the design of the VA spectrums was to randomly apply different stress levels to the fretting specimen. The load ratios $R = -1$ and $R = 0.1$ were chosen because on the literature, they are the mostly used in carrying out fretting fatigue experiments. Because of materials constraint, it was not possible to explore other type of VA spectrums as well as load ratios.

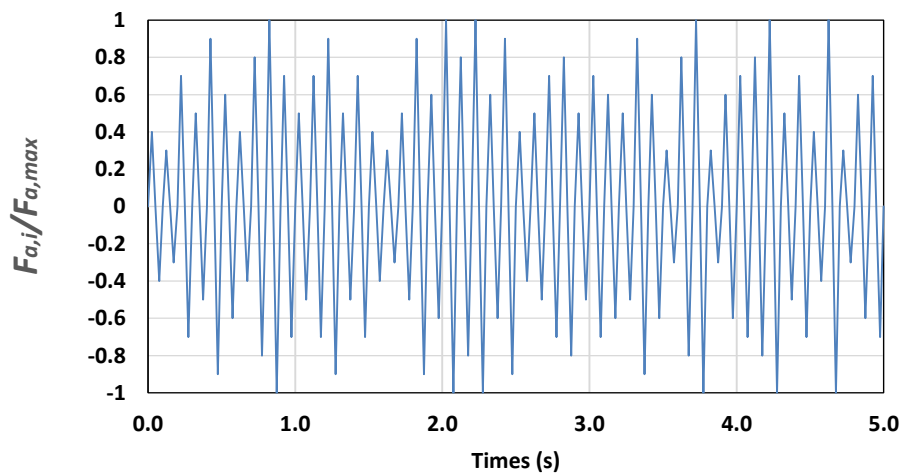


Figure 5-10 Variable amplitude fatigue load spectrum with a load ratio $R = -1$ used to assess material 40054 under fretting fatigue.

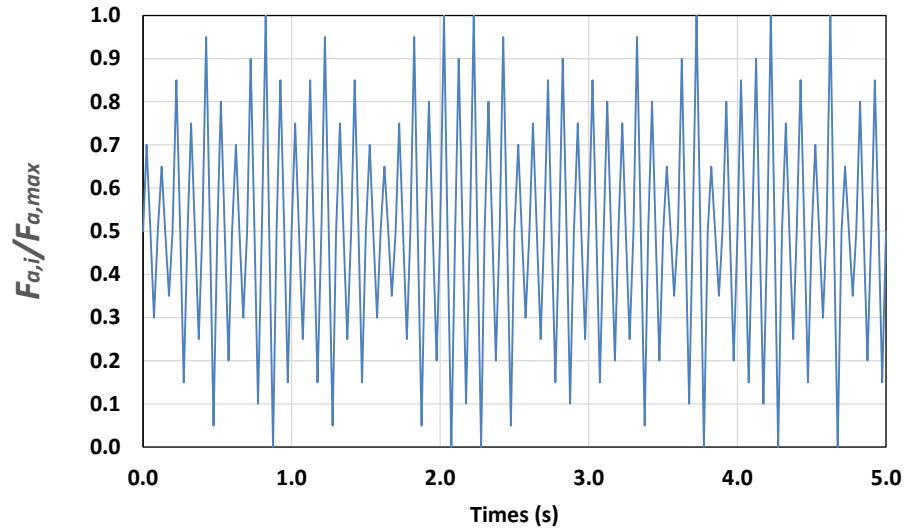


Figure 5-11 Variable amplitude fatigue load spectrum with a load ratio $R \geq 0$ used to assess the material 40054 under fretting fatigue.

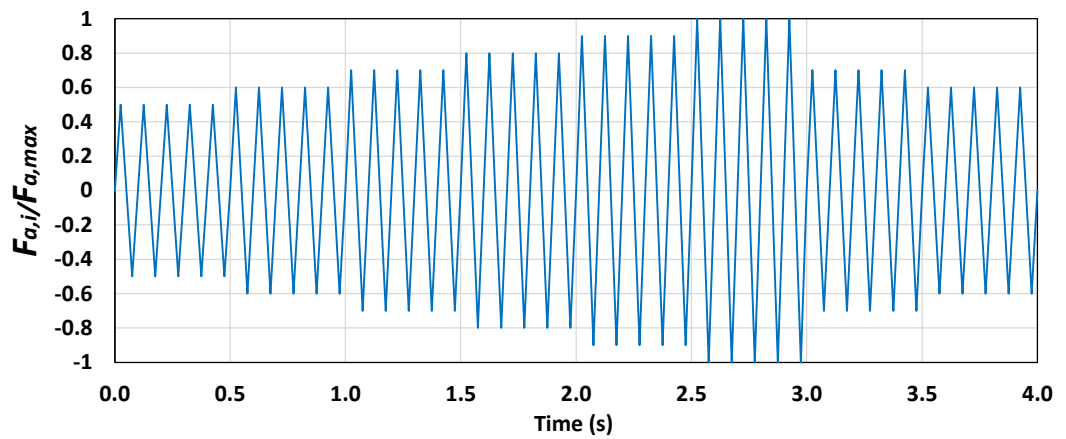


Figure 5-12 Variable amplitude load spectrum used to assess the cast iron 40060 under fretting fatigue

In the above figures, $F_{a,i}$ is the amplitude of the force associated with the i cycle while $F_{a,max}$ is the maximum value of the amplitude of the force in the load histories. The loads used to investigate the fretting fatigue damage of materials 40054 and 40060 are summarised from Table 5-16 to Table 5-18.

Table 5-16 Fretting fatigue input loads used to test material 40054. P is constant, F is VA and pads made from steel coated with zinc phosphate.

Test N ^o	R _p (mm)	P (KN)	F _{a,max} (KN)	Fatigue Load Spectrum
1	20	5.5	7.50	Figure 5-10
2	20	5.5	7.00	Figure 5-10
3	20	5.5	6.50	Figure 5-10
4	20	5.5	6.25	Figure 5-10
5	20	5.5	6.00	Figure 5-10
6	20	5.5	5.75	Figure 5-10
7	20	5.5	8.00	Figure 5-11
8	20	5.5	9.00	Figure 5-11
9	20	5.5	9.50	Figure 5-11
10	20	5.5	10.00	Figure 5-11
11	20	5.5	12.00	Figure 5-11
12	100	5.5	5.75	Figure 5-10
13	100	5.5	6.00	Figure 5-10
14	100	5.5	7.00	Figure 5-10
15	100	5.5	7.50	Figure 5-10
16	100	5.5	8.00	Figure 5-10
17	100	5.5	9.00	Figure 5-11
18	100	5.5	9.50	Figure 5-11
19	100	5.5	10.00	Figure 5-11
20	100	5.5	14.00	Figure 5-11
21	100	5.5	16.00	Figure 5-11

Table 5-17 Fretting fatigue input loads used to test material 40060. P is static, F is VA and the pads made from material 40054.

Test N ^o	R _p (mm)	P (KN)	F _{a,max} (KN)	Fatigue Load Spectrum
1	75	5	8	Figure 5-12
2	75	5	9	Figure 5-12
3	75	5	7	Figure 5-12
4	75	5	6	Figure 5-12
5	75	5	5.5	Figure 5-12
6	75	5	5.25	Figure 5-12
7	75	5	6.5	Figure 5-12
8	75	5	6.75	Figure 5-12

Table 5-18 Fretting fatigue input loads used to test material 40060. P is static, F is VA and the pads made from steel coated with zinc phosphate.

Test N ^o	R _p (mm)	P (KN)	F _{a,max} (KN)	Fatigue Load Spectrum
1	75	6	7	Figure 5-12
2	75	6	6.5	Figure 5-12
3	75	6	6	Figure 5-12
4	75	6	5.5	Figure 5-12
5	75	6	5	Figure 5-12
6	75	6	4.5	Figure 5-12
7	75	6	4	Figure 5-12

The fretting fatigue load inputs summarised in the above tables were used to carry out the tests up to 5,000,000 cycles before failure. The failure criterion adopted was the complete separation of the specimens. Figure 5-13 shows the failed specimen of test N^o12 in Table 5-16 while the other damaged specimens can be seen in Appendix H and J. It can be seen from Figure 5-13 that crack initiates and propagates either at the trailing edge or leading edge of the contact. This can be justified by the fact that the fatigue load applied at the leading end of the specimen is equal to the reaction load at the trailing end of the specimen. The number of cycles to failure N_f and the corresponding number of blocks to failure N_{block} recorded after each test are listed from Table 5-19 to Table 5-21.

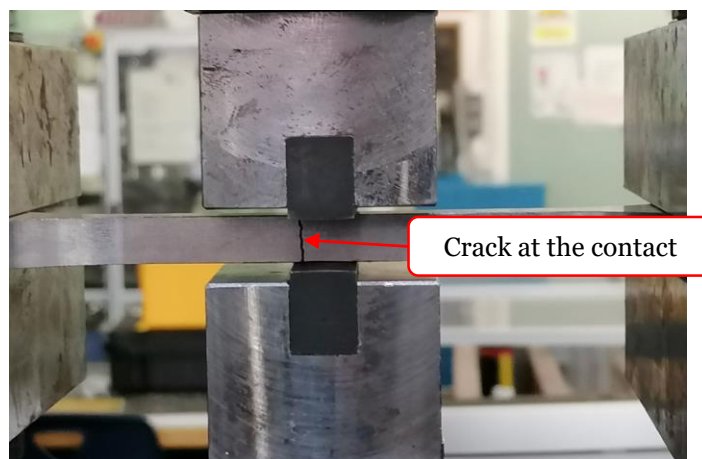


Figure 5-13 Damaged fretting specimen of test N^o 12 in Table 5-16.

Table 5-19 Summary of the fretting fatigue results of material 40054. P is constant, F is VA and pads made from steel coated with zinc phosphate.

Test N ^o	R _p (mm)	P (KN)	F _{a,max} (KN)	Fatigue Load Spectrum	N _{block} (Blocks)	N _f (Cycles)	Status
1	20	5.5	7.50	Figure 5-10	3,223	161,150	Failure
2	20	5.5	7.00	Figure 5-10	7,516	375,800	Failure
3	20	5.5	6.50	Figure 5-10	3,384	169,200	Failure
4	20	5.5	6.25	Figure 5-10	6480	324,000	Failure
5	20	5.5	6.00	Figure 5-10	9,525	476,250	Failure
6	20	5.5	5.75	Figure 5-10	23,659	1,182,950	Failure
7	20	5.5	8.00	Figure 5-11	85,924	4,296,200	Failure
8	20	5.5	9.00	Figure 5-11	20,449	1,022,450	Failure
9	20	5.5	9.50	Figure 5-11	26,998	1,349,900	Failure
10	20	5.5	10.00	Figure 5-11	9,180	459,000	Failure
11	20	5.5	12.00	Figure 5-11	5,784	289,200	Failure
12	100	5.5	5.75	Figure 5-10	12,503	625,150	Failure
13	100	5.5	6.00	Figure 5-10	7,223	361,150	Failure
14	100	5.5	7.00	Figure 5-10	3,699	184,950	Failure
15	100	5.5	7.50	Figure 5-10	1,712	85,600	Failure
16	100	5.5	8.00	Figure 5-10	1,060	53,000	Failure
17	100	5.5	9.00	Figure 5-11	45,281	2,264,050	Failure
18	100	5.5	9.50	Figure 5-11	23,415	1,170,750	Failure
19	100	5.5	10.00	Figure 5-11	39,964	1,998,200	Failure
20	100	5.5	14.00	Figure 5-11	11,361	568,050	Failure
21	100	5.5	16.00	Figure 5-11	5,360	268,000	Failure

Table 5-20 Summary of the fretting fatigue results of material 40060. P is static, F is VA fatigue and pads made of material 40054.

Test N ^o	R _p (mm)	P (KN)	F _{a,max} (KN)	N _{block} (blocks)	N _f (cycles)
1	75	5	8	3,050	122,000
2	75	5	9	2,480	99,200
3	75	5	7	2,921	116,840
4	75	5	6	13,000	520,000
5	75	5	5.5	29,465	1,178,600
6	75	5	5.25	33,039	1,321,560
7	75	5	6.5	8,981	359,240
8	75	5	6.75	5,867	234,680

Table 5-21 Summary of the fretting fatigue results of material 40060. P is static, F is VA fatigue and pads made from steel coated with zinc phosphate.

Test N ^o	R _p (mm)	P (KN)	F _{a,max} (KN)	N _{block} (blocks)	N _f (cycles)
1	75	6	7	2,548	101,920
2	75	6	6.5	3,658	146,320
3	75	6	6	3,643	145,720
4	75	6	5.5	18,279	731,160
5	75	6	5	25,897	1,035,880
6	75	6	4.5	44,481	1,779,240
7	75	6	4	125,000	5,000,000

Chapter 6

Validation of the design methodology

This chapter is seeking to validate the design methodology under constant amplitude (CA) fretting fatigue loading summarised in Figure 3-1 and the design methodology under variable amplitude (VA) fretting fatigue loading summarised in Figure 3-7. This will be achieved in three stages. In the first stage, the finite element (FE) analysis of the fretting fatigue experiments summarised in chapter 5 will be carried out. The second stage will involve the prediction of the experimental fretting fatigue lives. This will be achieved by post-processing the FE analysis results. In the third stage, the predicted fretting fatigue lives will be compared against the experimental fretting fatigue lives.

6.1 Finite element (FE) analysis of the fretting fatigue experiments

The FE analysis of the fretting fatigue experiments summarised in chapter 5 are carried out in order to calculate the stress components at the contact interface. This is achieved by modelling half of the experimental set-up as it is symmetrical along the axial centreline of the fretting specimen as shown in Figure 6-1.

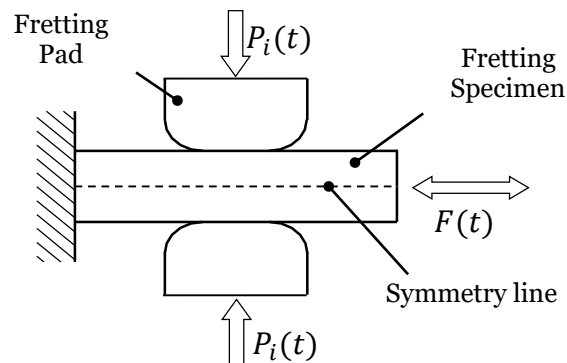


Figure 6-1 Schematic of the fretting fatigue experiment under constant and variable amplitude loading.

The diagrams in Figure 6-2, Figure 6-3 and Figure 6-4 represent a two-dimensional finite element model (FEM) of the fretting fatigue experiment summarised in chapter 5. The FEM was created in ANSYS Workbench. The contact radius of the pad is 100 mm in Figure 6-2, 20 mm in Figure 6-3 and 75 mm in Figure 6-4.

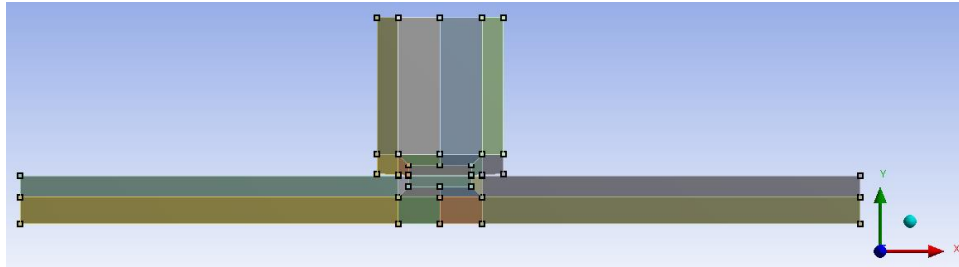


Figure 6-2 Model 1: Fretting fatigue experiment with a pad radius of 100 mm.

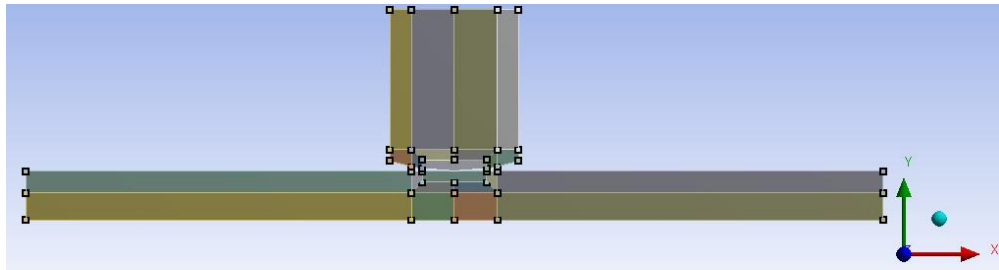


Figure 6-3 Model 2: Fretting fatigue experiment with a pad radius of 20 mm.

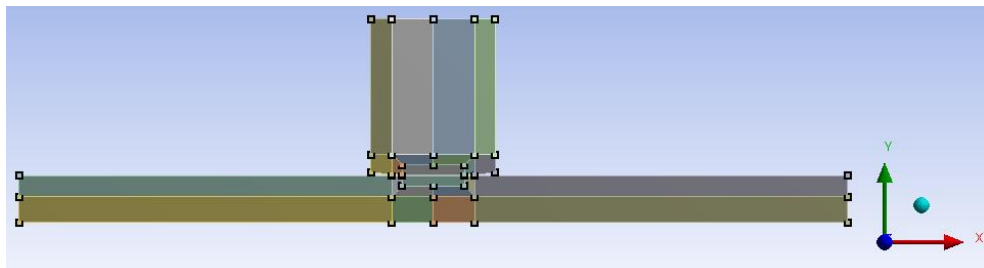


Figure 6-4 Model 3: Fretting fatigue experiment with a pad radius of 75 mm.

The aim of the FEM is to simulate the fretting fatigue experiment and obtain the stress tensor along the contact region. For model 1 and 2, the specimen is made from material 40054 and the pads are made from steel. The specimen in model 3 is made from material 40060 and the pads are made from material 40054. The Young's modulus and Poisson's

ratio of material 40054 are equal to 100 *GPa* and 0.26, for material 40060 108 *GPa* and 0.25 and for steel pads 200 *MPa* and 0.3. These material properties were provided by the industry partner Cummins Inc. In all models, the length of the fretting specimen is 80 mm and the width is equal to 4.5 mm. The pads have a width of 12 mm and height of 15 mm. The height of the pad is chosen in such a way that the boundary condition at the top of the pad does not affect the pressure distribution i.e., at least ten times the contact semi-width in accordance with [1]. The specimen is restricted to a horizontal displacement along the x axis. The specimen is fixed on the left side. Both sides of the pad are restricted so that they can only move in the vertical direction. Furthermore, when applying the boundary condition to the pad in the horizontal direction, the pad protrudes by 1.819 mm for model 1 with pad radius 100 mm, 1.079 mm for model 2 with pad radius 20 mm and 1.759 mm for model 3 with pad radius 75 mm. Figure 6-5 to Figure 6-7 show how the boundary conditions are assigned on the three models.

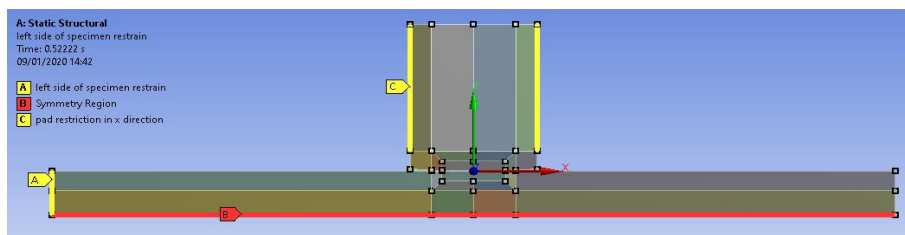


Figure 6-5 Boundary condition assigned to model 1.

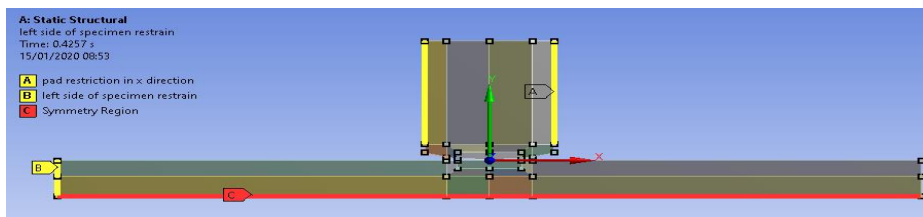


Figure 6-6 Boundary condition assigned to model 2.

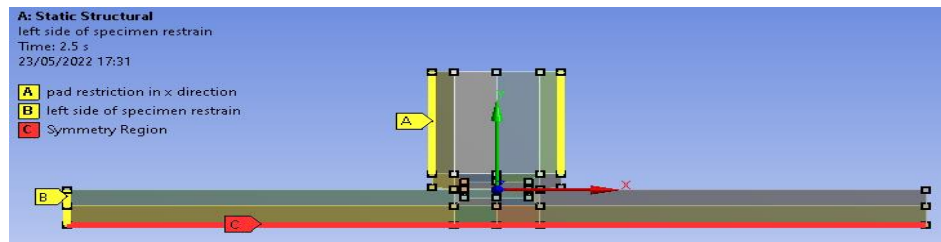


Figure 6-7 Boundary condition assigned to model 3

The contact region was modelled by defining the contact interface of both pad and specimen as frictional contact pair. The coefficient of friction 0.45 was used in model 1 and 2 and 0.4 in model 3 as advised by Cummins Inc. The contact between the fretting pad and the specimen was defined using the target-contact bodies algorithm in ANSYS workbench. The top surface of the specimen was defined as the target body while the circular surface of the pad defined as the contact body. In order to define the behaviour of the contact, the Augmented Lagrange algorithm was included in the frictional contact region.

Before the validation of the three models, a mesh convergence study was carried out to find the optimum mesh size to be used at the contact region. The load used for this purpose follows the same procedure used in the fretting fatigue experiments. The loading sequence was made up of three load steps. In the first step, the pad was moved downward by 0.0501 mm to establish the contact with the specimen. In the second load step, a normal pressure of about 16.667 MPa was applied at the surface of the pad of model 1 and 2 and 8.333 MPa at the surface of the pad of model 3. Finally, a fully-reversed CA sinusoidal load (amplitude of about 111 MPa) was applied at the right hand side of the specimen. Figure 6-8 to Figure 6-10 show how these loads were applied on the three models.

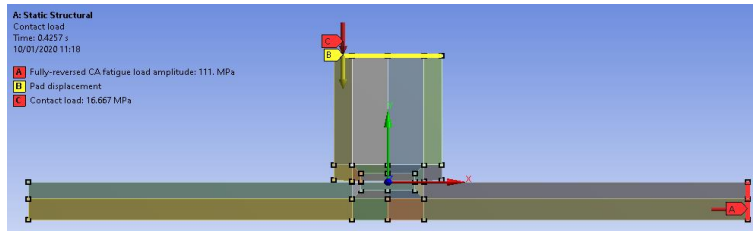


Figure 6-8 Loads applied on model 1.

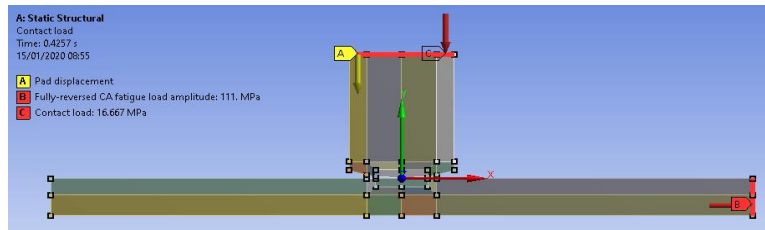


Figure 6-9 Loads applied on model 2.

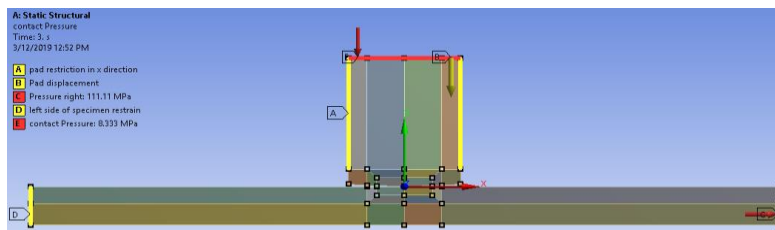


Figure 6-10 Loads applied on model 3.

The mesh convergence study was achieved by first assigning 5 elements along the contact half-width, a , and a coarse mesh away from the contact zone. According to Eq. 2-5, the contact half width of model 1 is equal to 0.60 mm, 0.27 mm for model 2 and 0.425 mm for model 3. A quadrilateral map mesh was assigned to the pad and specimen. At the end of the simulation, the stress components σ_{xx} , σ_{yy} and τ_{xy} was extracted along the contact surface of the specimen. The above strategy was repeated for 10, 15, 20, 25, 30, 35, 40, 45, 50, 55 and 60 elements. Figure 6-11 to Figure 6-19 summarise the mesh convergence study of the three models. They compared the stress components calculated with different number of elements along the contact half width.

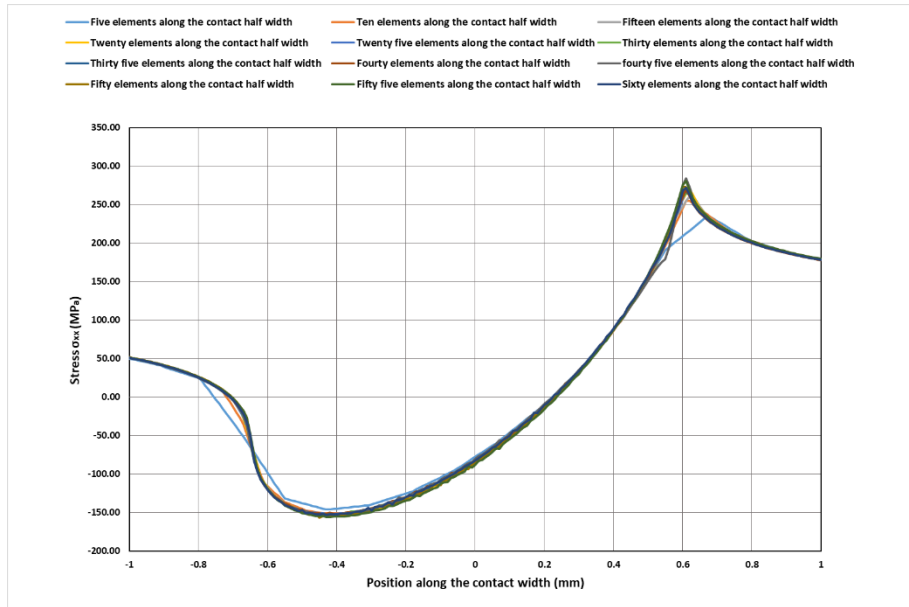


Figure 6-11 Stress σ_{xx} along the contact surface of model 1.

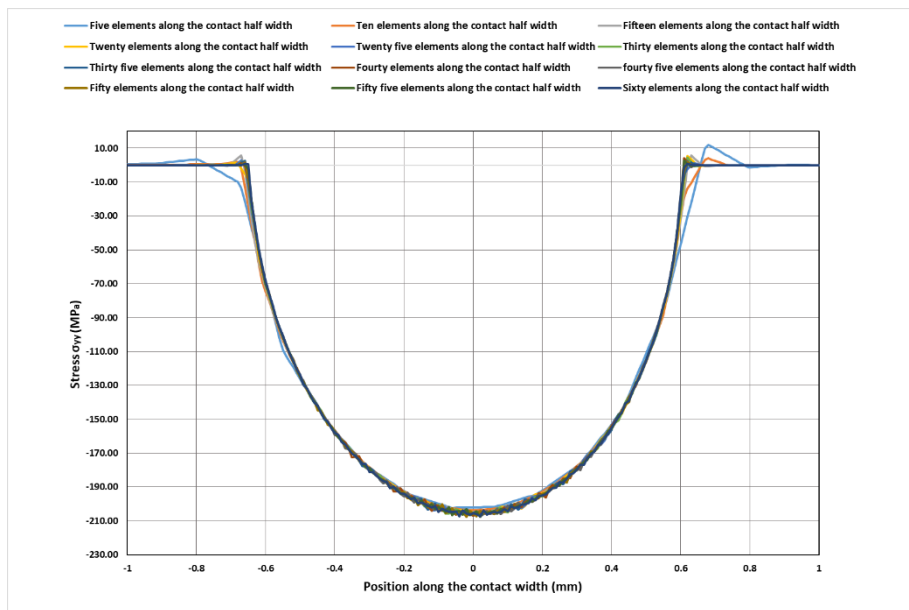


Figure 6-12 Stress σ_{yy} along the contact surface of model 1.

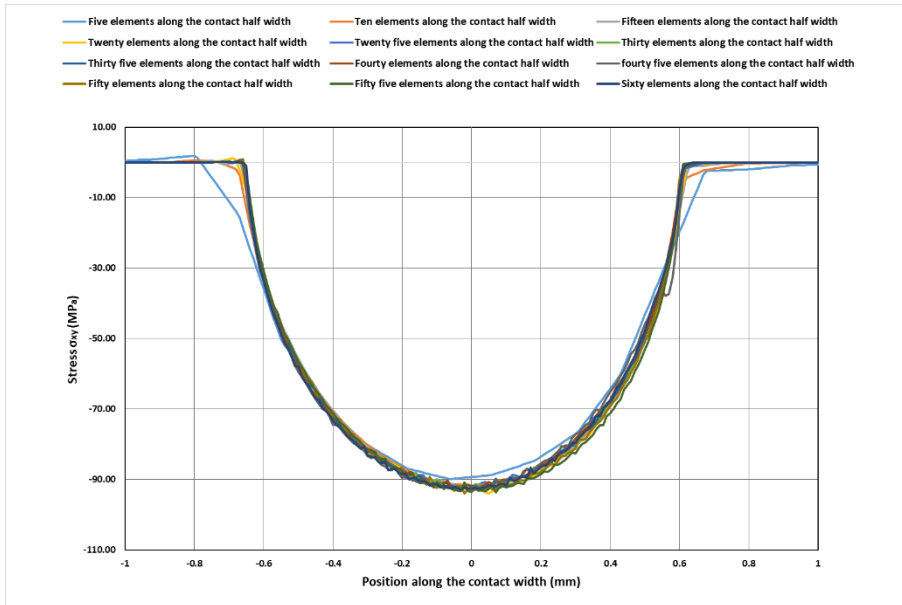


Figure 6-13 Shear stress τ_{xy} along the contact surface of model 1.

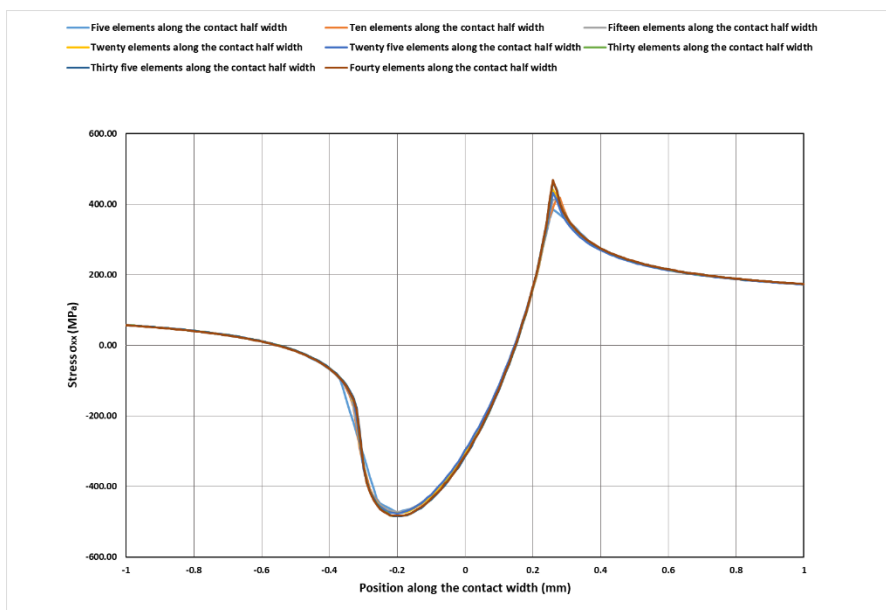


Figure 6-14 Stress σ_{xx} along the contact surface of model 2.

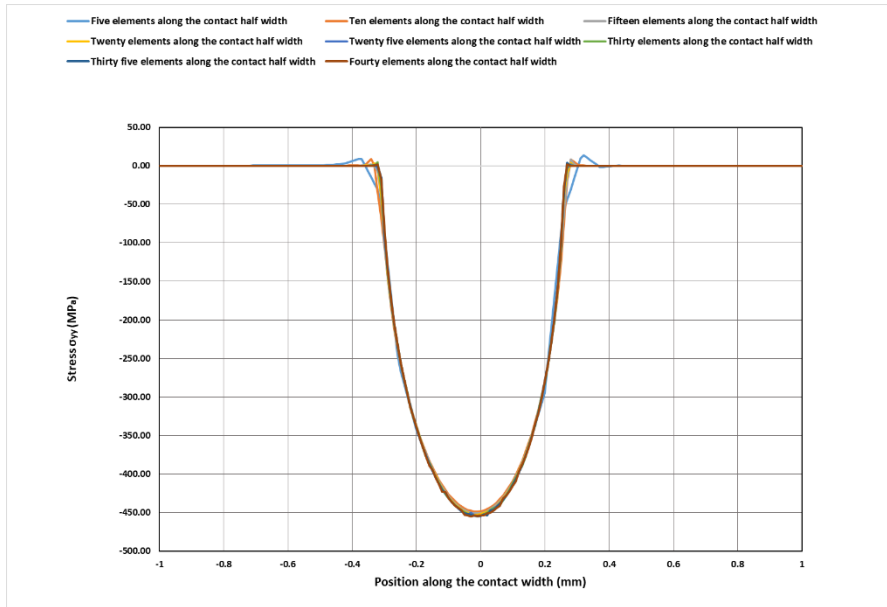


Figure 6-15 Stress σ_{yy} along the contact surface of model 2.

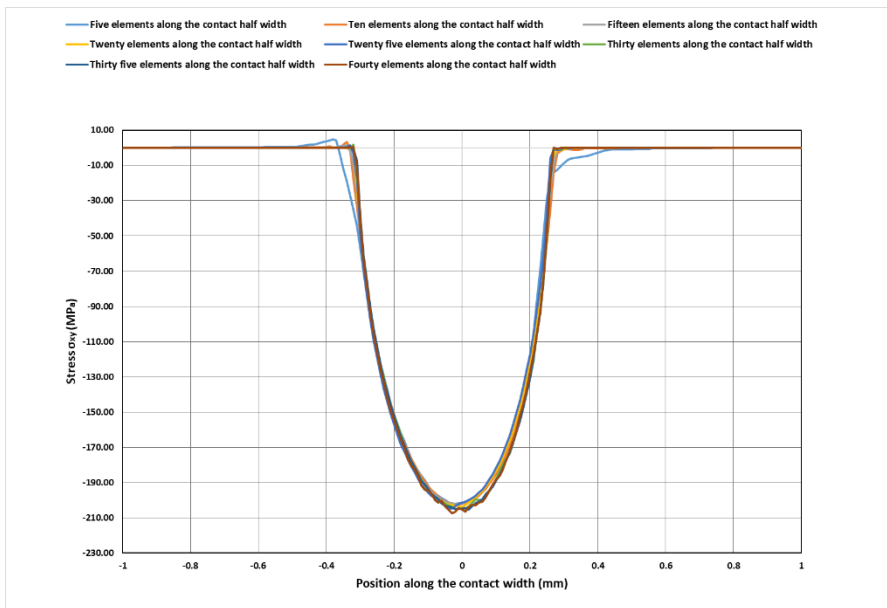


Figure 6-16 Shear stress τ_{xy} along the contact surface of model 2.

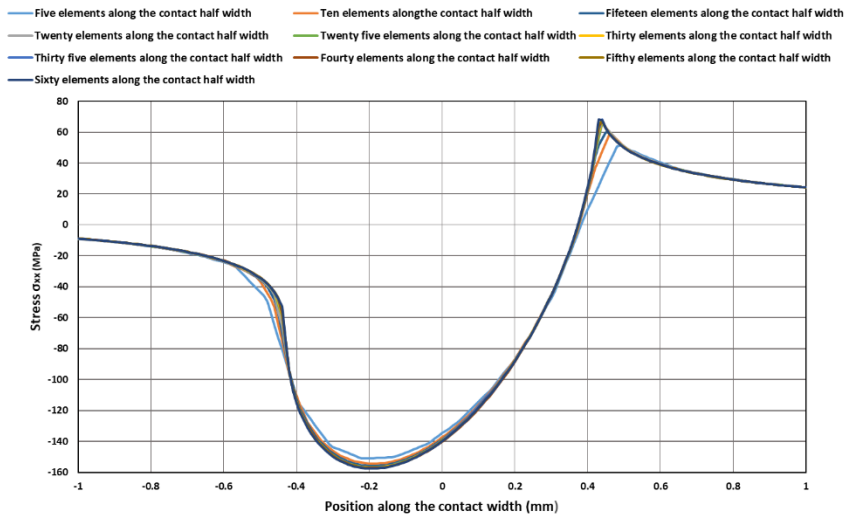


Figure 6-17 Stress σ_{xx} along the contact surface of model 3

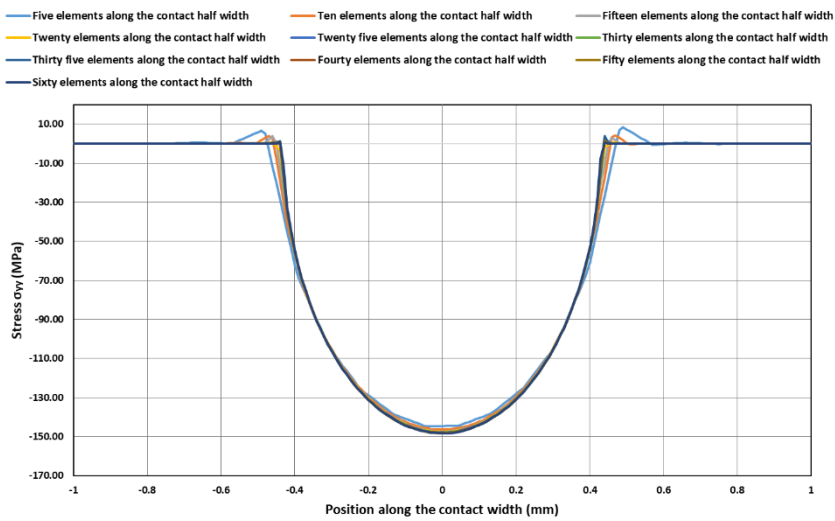


Figure 6-18 Stress σ_{yy} along the contact surface of model 3.

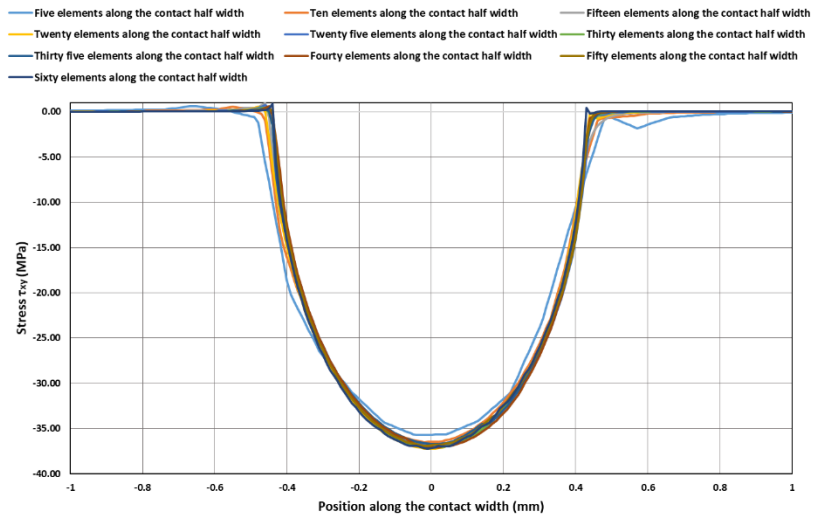


Figure 6-19 Stress τ_{xy} along the contact surface of model 3.

It can be seen from Figure 6-11 to Figure 6-19 that, for each stress component, the mesh convergence is reached when 15 elements are used along the contact half-width of model 2 and 20 elements along the contact half-width of model 1 and 3. Therefore, to analyse the fretting fatigue experiments, 20 elements will be used along the contact half-width of model 2 and 40 elements along the contact half-width of model 1 and 3. This corresponds to a mesh size of $15 \mu m \times 15 \mu m$ at the contact zone of model 1, $13.50 \mu m \times 13.50 \mu m$ at the contact zone of model 2 and $11 \mu m \times 11 \mu m$ at the contact zone of model 3 as shown from Figure 6-20 to Figure 6-22

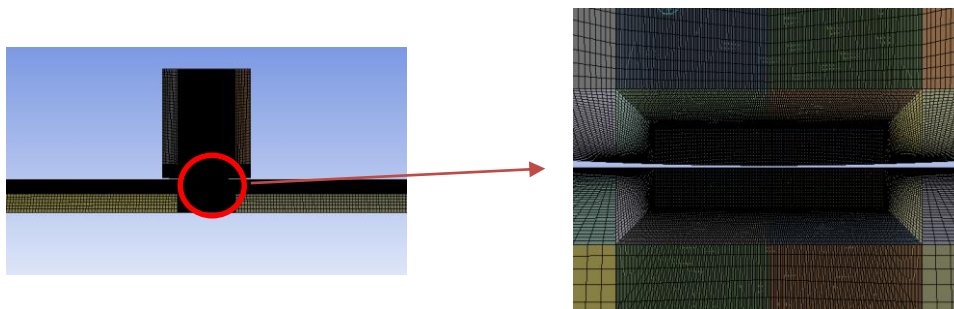


Figure 6-20 Mesh profile used in model 1.

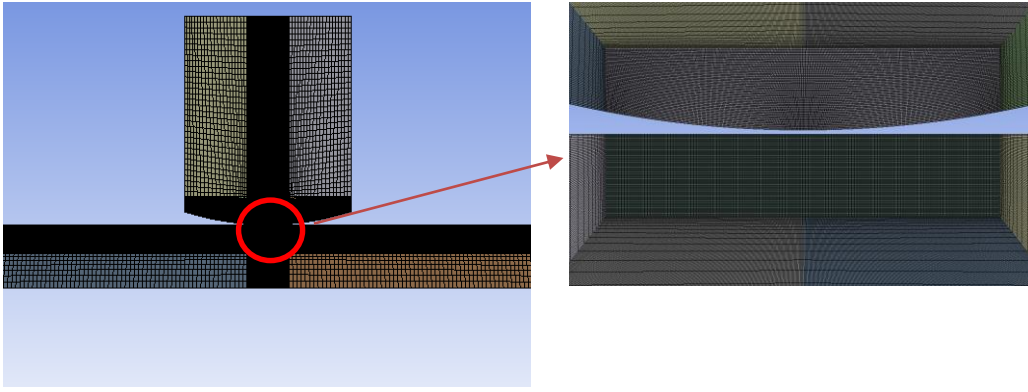


Figure 6-21 Mesh profile used in model 2.

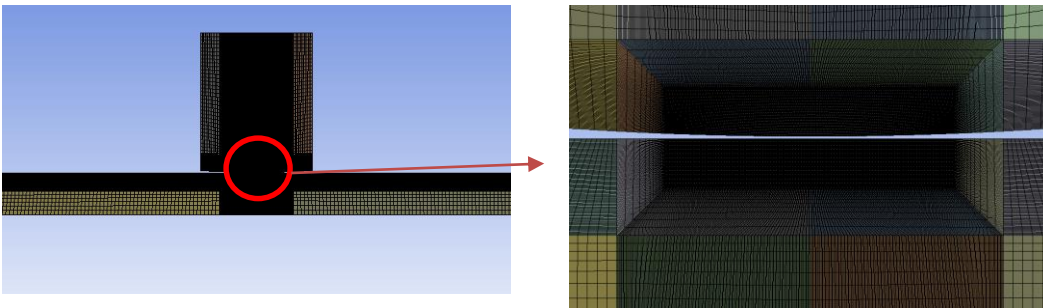


Figure 6-22 Mesh profile used in model 3.

The above finite element models were validated using the Hertzian analytical solution summarised in chapter 2.2.2. In the first part of the validation process, the contact half width obtained from the finite element analysis was compared with the contact half width calculated from Hertzian analytical solution. The contact half width of model 1, model 2 and model 3 obtained from the FE analysis are equal to 0.62 mm , 0.29 mm and 0.44 mm respectively. These values are very close to the results obtained from the Hertz solution (Eq. 2-5), 0.60 mm for model 1, 0.27 mm for model 2 and 0.425 mm for model 3. It can also be seen from the stress contours shown from Figure 6-23 to Figure 6-25 that, the contact stress (σ_{yy}) is maximum at the center and diminishes at the edge of the contact. This is in line with the Hertz solution (chapter 2.2.2). In the second part of validation, the contact pressure distribution, $P(x)$, along the contact surface of the specimen calculated using Hertzian solutions is compared with the numerical solution

as shown from Figure 6-26 to Figure 6-28. This qualitative comparison demonstrated that the Hertzian and the finite element solutions are similar. Therefore, the three models can be used to perform the stress analysis of the fretting fatigue experiments.

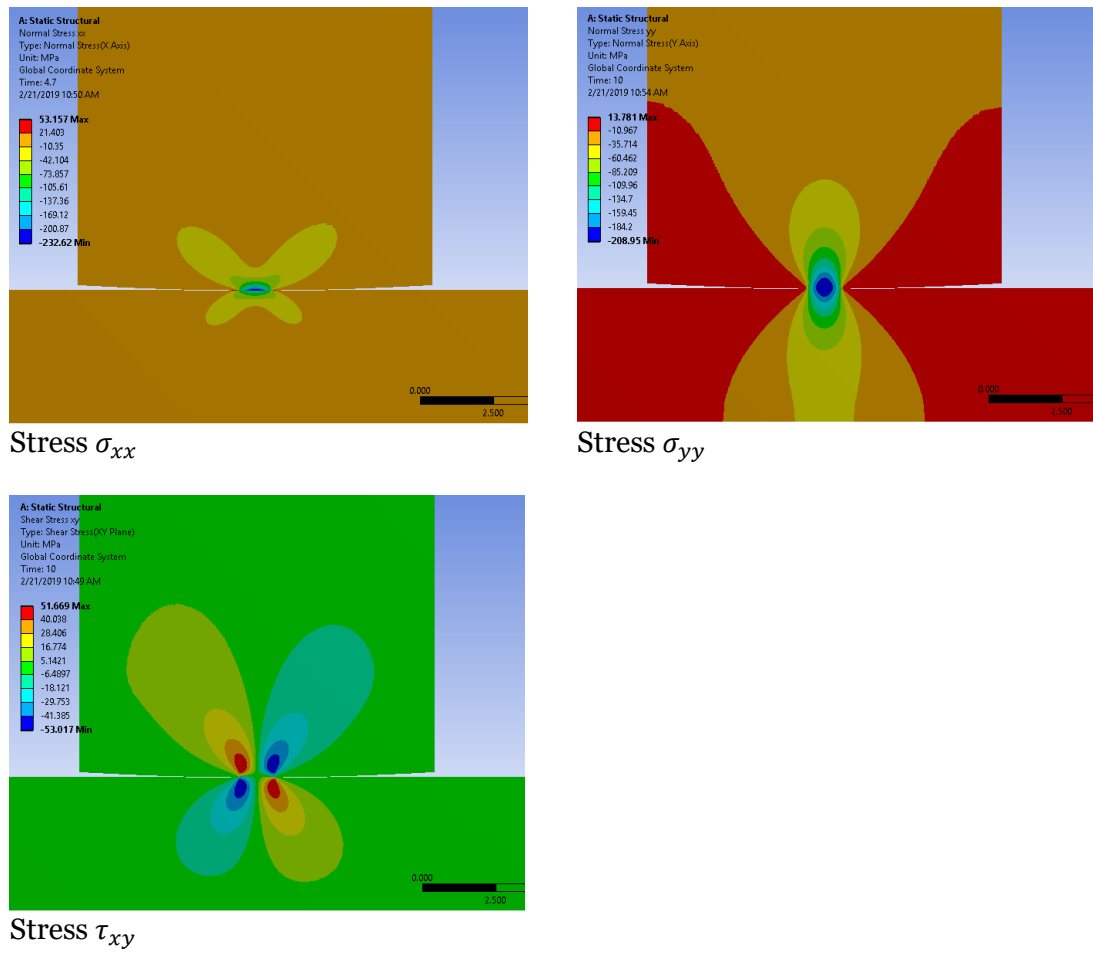
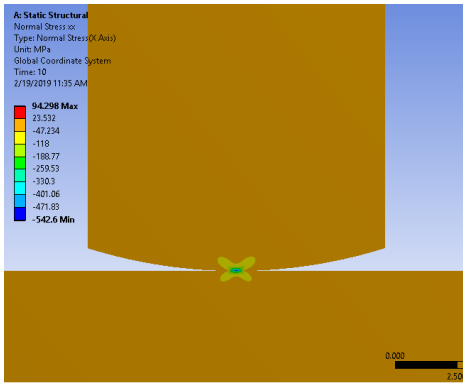
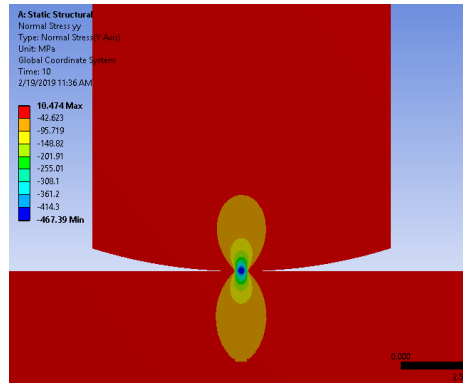


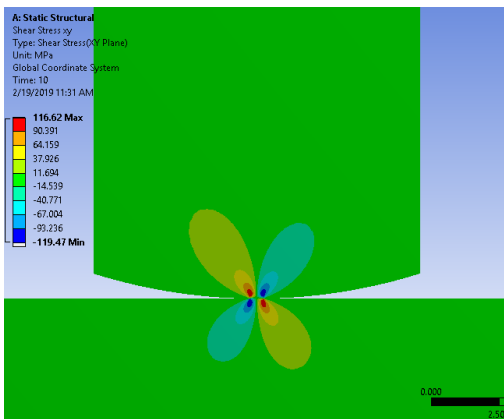
Figure 6-23 Stress contours at the contact zone of model 1.



Stress σ_{xx}

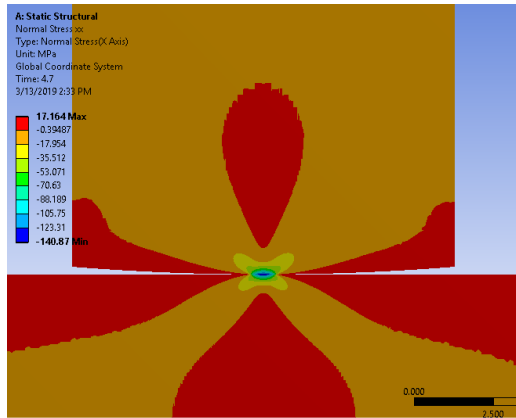


Stress σ_{yy}

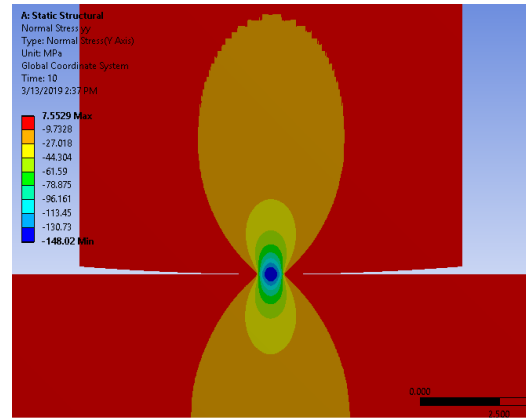


Stress τ_{xy}

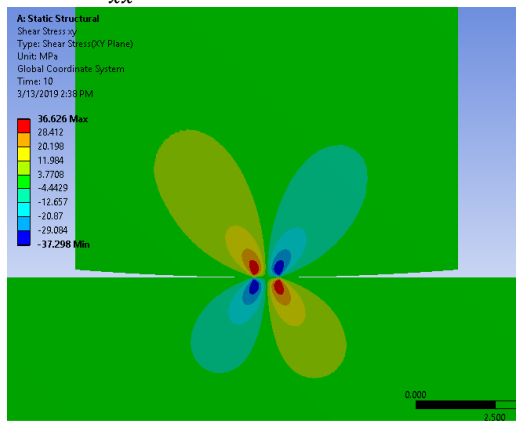
Figure 6-24 Stress contours at the contact zone of model 2.



Stress σ_{xx}



Stress σ_{yy}



Stress τ_{xy}

Figure 6-25 Stress contours at the contact zone of model 3.

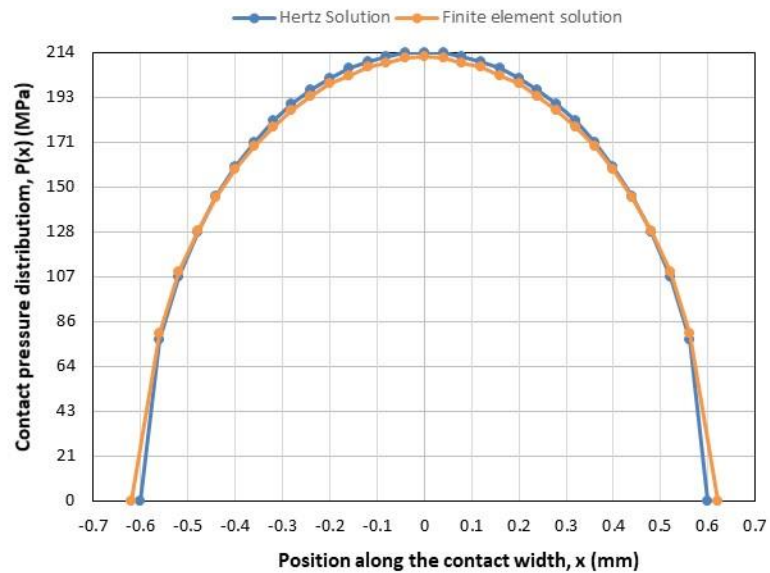


Figure 6-26 Comparison between the FEA and the Hertzian solution of model 1.

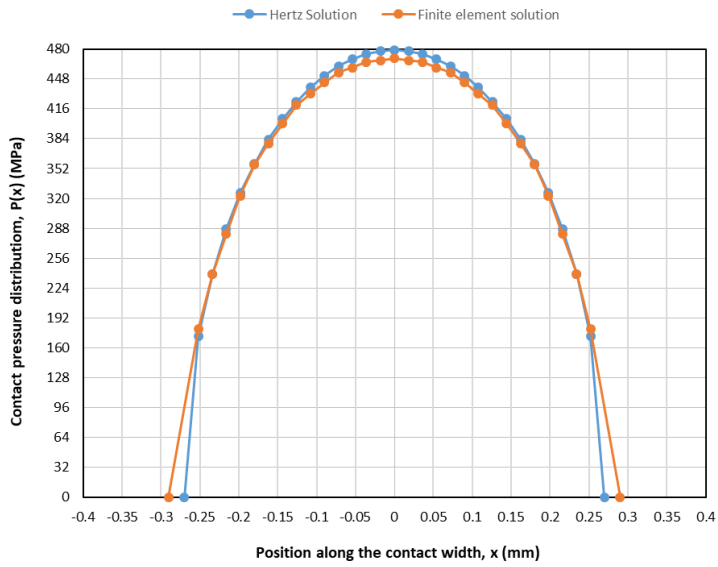


Figure 6-27 Comparison between the FEA and the Hertzian solution of model 2.

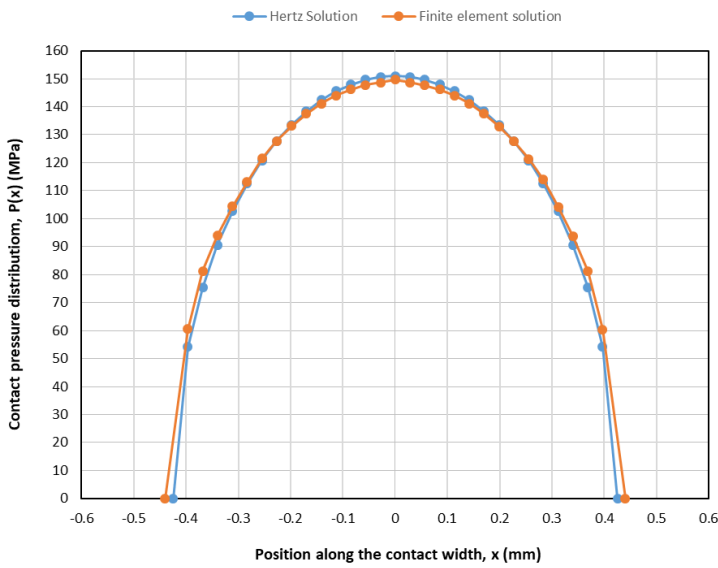


Figure 6-28 Comparison between the FEA and the Hertzian solution of model 3.

6.2 Prediction of the fretting fatigue lives

The prediction of the number of cycles to failure of the fretting fatigue experiments under CA and VA loading was achieved in two stages. In the first stage, the stress components at the contact interface of the specimen were obtained by performing the finite element analysis of the fretting fatigue experiments. The finite element model used for this purpose is detailed in chapter 6.1. The figures below show the stress components at the contact zone of test N°1 in Table 5-6.

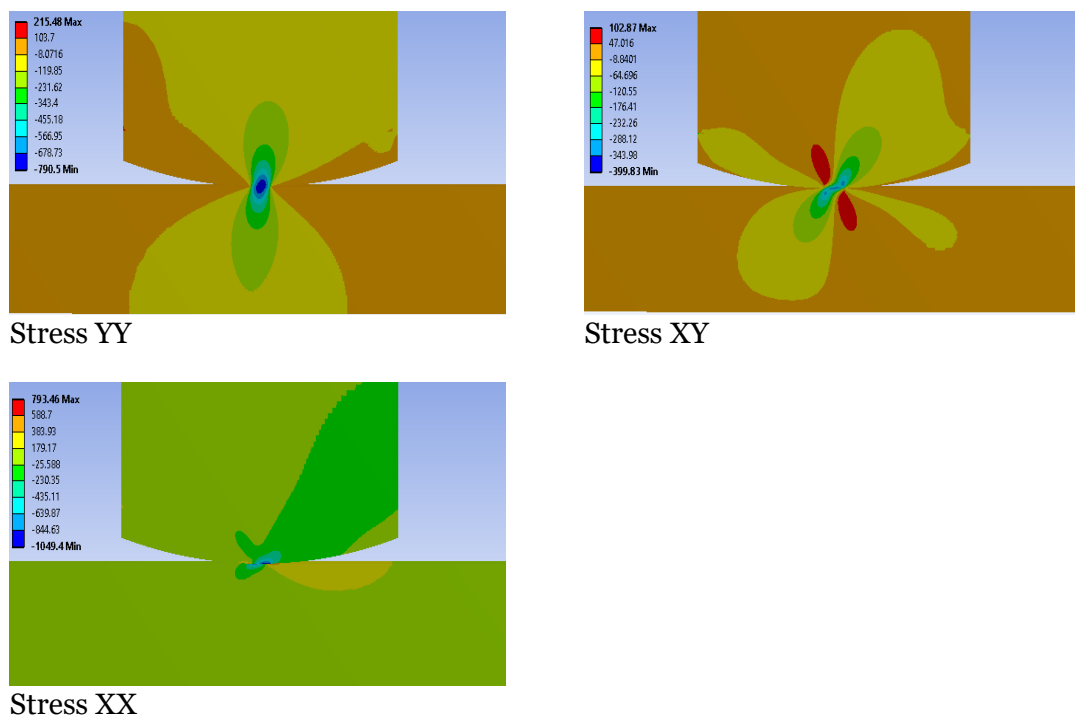


Figure 6-29 Stress components of test N°1 in Table 5-6.

In the second stage, the fretting fatigue lives were predicted. This was achieved by extracting from the FE model, the sub-surface distribution of the linear-elastic stress components along the focus path. According to Figure 3-1a and Figure 3-1b, the focus path was taken coincident with a straight line emanating from contact half width (leading edge of contact) and perpendicular to the contact surface. Finally, the extracted linear-elastic stress components were post-processed following the methodology detailed in chapter 3.2 for CA loading and the methodology detailed in chapter 3.3 for

VA loading. The predicted fretting fatigue lives $N_{f,e}$ of the experiments summarised in chapters 5.2 and 5.3 can be seen from Table 6-1 to Table 6-8.

Table 6-1 Prediction of the fretting fatigue lifetime of experiments summarised in Table 5-11. Specimens made from material 40054 and pads from steel, coated with zinc phosphate. P is constant and F is CA.

Test N°	R_p (mm)	P (KN)	$F_{a,max}$ (KN)	R	N_f (cycles)	$N_{f,e}$ (cycles)
1	20	5.5	8.00	0.1	970,764	732,203
2	20	5.5	9.00	0.1	1,107,093	640,589
3	20	5.5	9.50	0.1	347,554	496,413
4	20	5.5	10.00	0.1	328,400	417,807
5	20	5.5	10.50	0.1	368,132	351,556
6	20	5.5	11.00	0.1	193,466	320,865
7	20	5.5	12.00	0.1	166,731	231,089
8	20	5.5	16.00	0.1	86,731	83,872
9	20	5.5	7.00	-1	32,788	40,120
10	20	5.5	6.50	-1	86,847	100,650
11	20	5.5	6.25	-1	130,733	137,052
12	20	5.5	6.00	-1	547,361	312,929
13	20	5.5	5.00	-1	1,053,934	647,913
14	100	5.5	7.00	-1	21,619	22,515
15	100	5.5	6.50	-1	28,086	33,410
16	100	5.5	6.25	-1	44,523	43,687
17	100	5.5	6.00	-1	47,932	54,628
18	100	5.5	5.50	-1	111,079	93,714
19	100	5.5	5.00	-1	199,438	158,746
20	100	5.5	4.75	-1	138,909	223,149

Table 6-2 Prediction of the fretting fatigue lifetime of experiments summarised in Table 5-12. Specimens made from material 40060 and pads from material 40054. P is static and F is CA.

Test N°	R_p (mm)	P (KN)	F_a (KN)	N_f (cycles)	$N_{f,e}$ (cycles)
1	75	5	8	29,670	23,526
2	75	5	7	59,770	36,472
3	75	5	6.5	42,985	41,957
4	75	4	9	23,653	26,633
5	75	3.5	6.25	133,335	131,562

Table 6-3 Prediction of the fretting fatigue lifetime of experiments summarised in Table 5-13. Specimens made from material 40060 and pads from steel coated with zinc phosphate. P is static and F is CA.

Test N ^o	R _p (mm)	P (KN)	F _a (KN)	N _f (cycles)	N _{f,e} (cycles)
1	75	4	3.5	1,703,890	2,022,217
2	75	4	4	1,218,640	892,646
3	75	4	4.75	283,325	283,716
4	75	4	5	351,381	220,067
5	75	4	5.5	173,542	118,423
6	75	4	6	53,257	69,432

Table 6-4 Prediction of the fretting fatigue lifetime of experiments summarised in Table 5-14. Specimens made from material 40060 and pads from material 40054. P and F are CA.

Test N ^o	R _p (mm)	P _m (KN)	P _a (KN)	F _a (KN)	N _f (cycles)	N _{f,e} (cycles)
1	75	-4	0.5	5.5	208,500	208,859
2	75	-5	0.5	6.5	65,650	69,853
3	75	-5	0.5	6	124,504	133,076
4	75	-5	0.5	9.5	17,788	17,794
5	75	-5	0.5	7	52,773	53,579
6	75	-6	1	7.5	50,297	43,072

Table 6-5 Prediction of the fretting fatigue lifetime of experiments summarised in Table 5-15. Specimens made from material 40060 and pads made from steel coated with zinc phosphate. P and F are CA.

Test N ^o	R _p (mm)	P _m (KN)	P _a (KN)	F _a (KN)	N _f (cycles)	N _{f,e} (cycles)
1	75	-5	0.5	6	77,000	86,822
2	75	-5	0.5	5.5	135,000	121,882
3	75	-5	0.5	5	338,697	222,276
4	75	-5	0.5	4.5	397,873	393,692
5	75	-5	0.5	4	705,000	849,856
6	75	-5	0.5	4.25	561,658	570,860
7	75	-5	0.5	4.75	450,562	315,364

Table 6-6 Prediction of the fretting fatigue lifetime of experiments summarised in Table 5-19. Specimens made from material 40054 and pads from steel coated with zinc phosphate. P is constant and F is VA

Test N ^o	R _p (mm)	P (KN)	F _{a,max} (KN)	Fatigue Load Spectrum	N _{block} (Blocks)	N _{block,e} (Blocks)	N _f (cycles)	N _{f,e} (cycles)
1	20	5.5	7.50	Figure 5-10	3,223	2,356	161,150	117,815
2	20	5.5	7.00	Figure 5-10	7,516	3,510	375,800	175,501
3	20	5.5	6.50	Figure 5-10	3,384	5,645	169,200	282,250
4	20	5.5	6.25	Figure 5-10	6480	7611	324,000	380,535
5	20	5.5	6.00	Figure 5-10	9,525	10,324	476,250	516,210
6	20	5.5	5.75	Figure 5-10	23,659	15,126	1,182,950	756,285
7	20	5.5	8.00	Figure 5-11	85,924	44,152	4,296,200	2,207,593
8	20	5.5	9.00	Figure 5-11	20,449	23,910	1,022,450	1,195,503
9	20	5.5	9.50	Figure 5-11	26,998	22,099	1,349,900	1,104,947
10	20	5.5	10.00	Figure 5-11	9,180	18,703	459,000	935,161
11	20	5.5	12.00	Figure 5-11	5,784	10,792	289,200	539,601
12	100	5.5	5.75	Figure 5-10	12,503	8,481	625,150	424,054
13	100	5.5	6.00	Figure 5-10	7,223	6,512	361,150	325,614
14	100	5.5	7.00	Figure 5-10	3,699	2,294	184,950	114,682
15	100	5.5	7.50	Figure 5-10	1,712	1,474	85,600	73,680
16	100	5.5	8.00	Figure 5-10	1,060	1,171	53,000	58,569
17	100	5.5	9.00	Figure 5-11	45,281	49,997	2,264,050	2,499,853
18	100	5.5	9.50	Figure 5-11	23,415	42,704	1,170,750	2,135,212
19	100	5.5	10.00	Figure 5-11	39,964	36,396	1,998,200	1,819,788
20	100	5.5	14.00	Figure 5-11	11,361	12,330	568,050	616,497
21	100	5.5	16.00	Figure 5-11	5,360	7,143	268,000	357,162

Table 6-7 Prediction of the fretting fatigue lifetime of experiments summarised in Table 5-20. Specimens made from material 40060 and pads from material 40054. P is static and F is VA.

Test N ^o	R _p (mm)	P (KN)	F _{a,max} (KN)	N _{block}	N _{block,e}	N _f (cycles)	N _{f,e} (cycles)
1	75	5	8	3,050	3003	122,000	120,100
2	75	5	9	2,480	2026	99,200	81,046
3	75	5	7	2,921	3725	116,840	148,990
4	75	5	6	13,000	11396	520,000	455,856
5	75	5	5.5	29,465	20513	1,178,600	820,503
6	75	5	5.25	33,039	28131	1,321,560	1,125,254
7	75	5	6.5	8,981	6204	359,240	248,163
8	75	5	6.75	5,867	4944	234,680	197,758

Table 6-8 Prediction of the fretting fatigue lifetime of experiments summarised in Table 5-21. Specimens made from material 40060 and pads from steel coated with zinc phosphate. P is static and F is VA.

Test N ^o	R _p (mm)	P (KN)	F _{a,max} (KN)	N _{block} (blocks)	N _{block,e} (blocks)	N _f (cycles)	N _{f,e} (cycles)
1	75	6	7	2,548	2596	101,920	103,833
2	75	6	6.5	3,658	3921	146,320	156,859
3	75	6	6	3,643	6074	145,720	242,955
4	75	6	5.5	18,279	12875	731,160	515,009
5	75	6	5	25,897	24096	1,035,880	963,842
6	75	6	4.5	44,481	45971	1,779,240	1,838,829
7	75	6	4	125,000	102826	5,000,000	4,113,028

6.3 Results and discussion

The results summarised from Figure 6-30 to Figure 6-33 show the accuracy of the MWCM applied in conjunction with the PM and τ -MVM in estimating the lifetime of material 40054 and 40060 subjected to CA and VA fretting fatigue loading. These figures compare the predicted fretting fatigue lifetime calculated in chapter 6.2 against the experimental fretting fatigue lifetime summarised in chapters 5.2 and 5.3. In these figures, the horizontal axis represents the predicted fretting fatigue lifetimes while the vertical axis is the experimental fretting fatigue lifetime. The perfect correlation between N_f and $N_{f,e}$ is represented by a solid diagonal line while the two dash lines represent a scattered band with an error of 2. It can be seen that all the predicted fretting fatigue lives fall within the scattered band error. Therefore, the use of MWCM in conjunction with the PM and the τ -MVM give satisfying prediction of the finite lifetime of materials 40054 and 40060 subjected to CA and VA fretting fatigue loading.

Looking at the accuracy of the prediction under VA fretting fatigue loading summarised in Figure 6-32 and Figure 6-33, it can be observed that the fatigue damage sum, D_{cr} equal to one was used as advised by Palmgren-Miner rule summarised in chapter 2.4.9. Depending on the type of material, this value can vary in the range 0.002 – 5. Such a wide range suggests that the accurate way to estimate D_{cr} is to carry out appropriate

experiments [65]. Therefore, to design real components against VA fretting fatigue loading, one of the critical aspect is the correct estimation of the fatigue damage sum.

- Pads (R20 mm) steel, P constant and F CA (R=0.1) ● Pads (R20 mm) steel, P constant and F CA (R=-1)
- Pads (R100 mm) steel, P constant and F CA (R=-1)

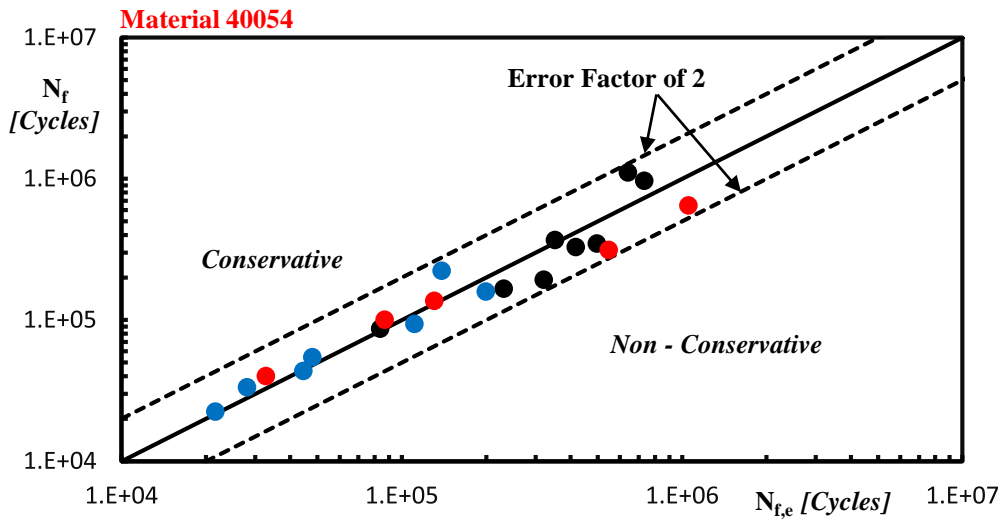


Figure 6-30 Accuracy of the MWCM applied in conjunction with the PM and τ -MVM in estimating the lifetime of material 40054 subjected to constant amplitude fretting fatigue loading.

- Pads (R75mm) cast iron 40054, P const and F CA ● Pads (R75mm) steel, P const and F CA
- Pads (R75mm) cast iron 40054, P CA and F CA ● Pads (R75mm) steel, P CA and F CA

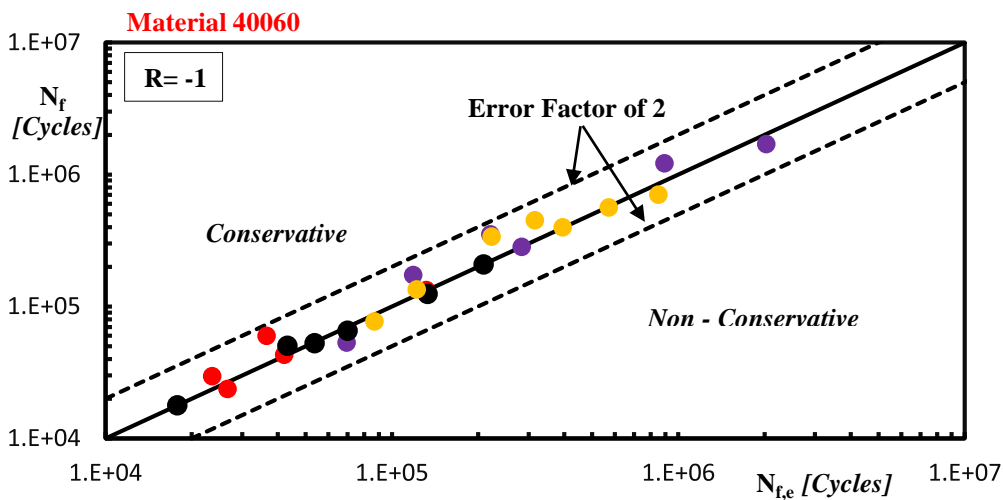


Figure 6-31 Accuracy of MWCM applied in conjunction TCD and τ -MVM in estimating the lifetime of the material 40060 subjected to constant amplitude fretting fatigue loading.

- Pads (R20 mm) steel, P constant and F VA (R=-1)
- Pads (R100 mm) steel, P constant and F VA (R=-1)
- Pads (R20 mm) steel, P constant and F VA (R≥0)
- Pads (100 mm) steel, P constant and F VA (R≥0)

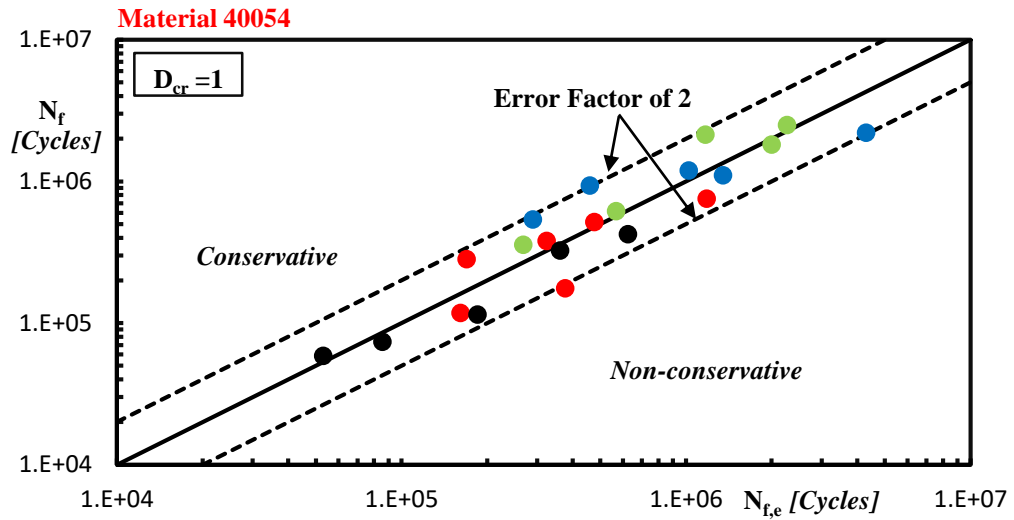


Figure 6-32 Accuracy of the MWCM applied in conjunction with the TCD and τ -MVM in estimating the lifetime of material 40054 subjected to variable amplitude fretting fatigue loading.

- Pads (R75mm) cast iron 40054, P const and F VA
- Pads (R75mm) steel, P const and F VA

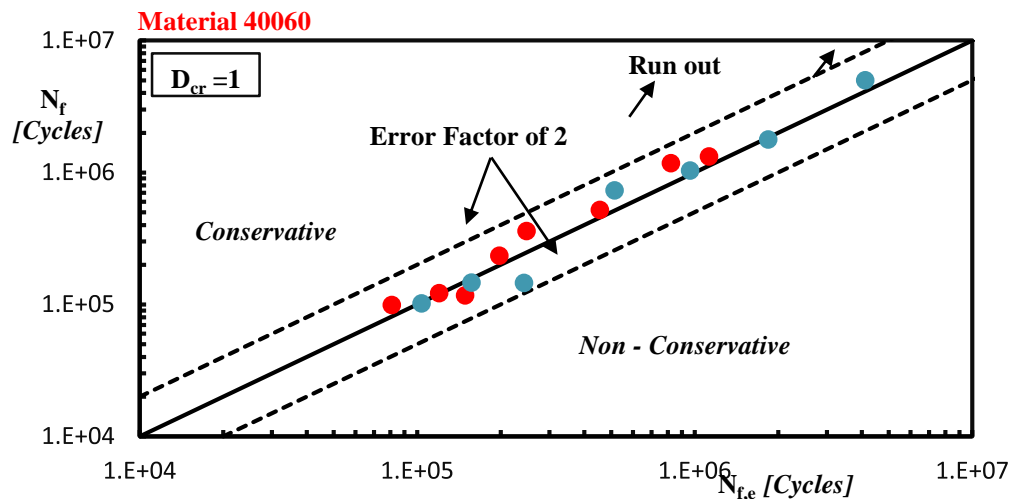


Figure 6-33 Accuracy of MWCM applied in conjunction TCD and τ -MVM in estimating the lifetime of the material 40060 subjected to variable amplitude fretting fatigue loading.

Chapter 7

Conclusion and recommendation for future work

7.1 Conclusion

The aim of this research was to formalise and validate a design methodology that can predict the lifetime of cast iron under constant and variable amplitude fretting fatigue loading. The proposed design methodology uses the MWCM applied in conjunction with the TCD and the τ -MVM. To achieve the aim of this work, uniaxial and torsional fatigue experiments were firstly carried out in order to estimate the fatigue properties of the assessed material. Then, the results obtained from the uniaxial and torsional tests were used to calibrate the MWCM's and the critical distance governing equations. Secondly, the assessed material was tested under constant and variable amplitude fretting fatigue loading. The results obtained from the fretting fatigue tests were then used to validate the proposed design methodology by comparing the experimental fretting fatigue lives against the predicted lives. This is shown in Figure 7-1 and Figure 7-2.

Based on all the results summarised in this write up, it can then be concluded that:

- The MWCM's governing equations and the critical distance L_M vs. N_f relationship were calibrated in chapter 3 by running uniaxial and torsional fatigue tests. The MWCM was capable of modelling not only the presence of a static load on the fretting specimen, but also the degree of multiaxiality and non-proportionality resulting from both the contact and fatigue load history.
- By comparing the experimental fretting fatigue lives against the predicted lives, the proposed design methodology is highly accurate in predicting finite lifetime under CA and VA fretting fatigue loading.

- To predict the fretting fatigue failure of real mechanical assemblies using the proposed design method, engineers only require to post-process the standard linear-elastic stresses from FE models.

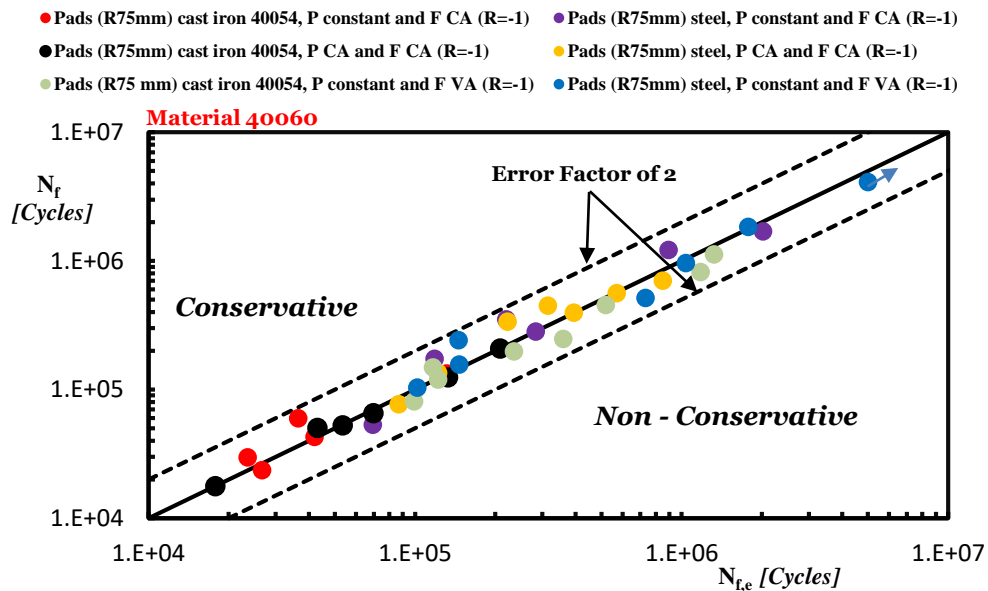


Figure 7-1 Summary of all the fretting fatigue results under CA and VA loading of material 40060.

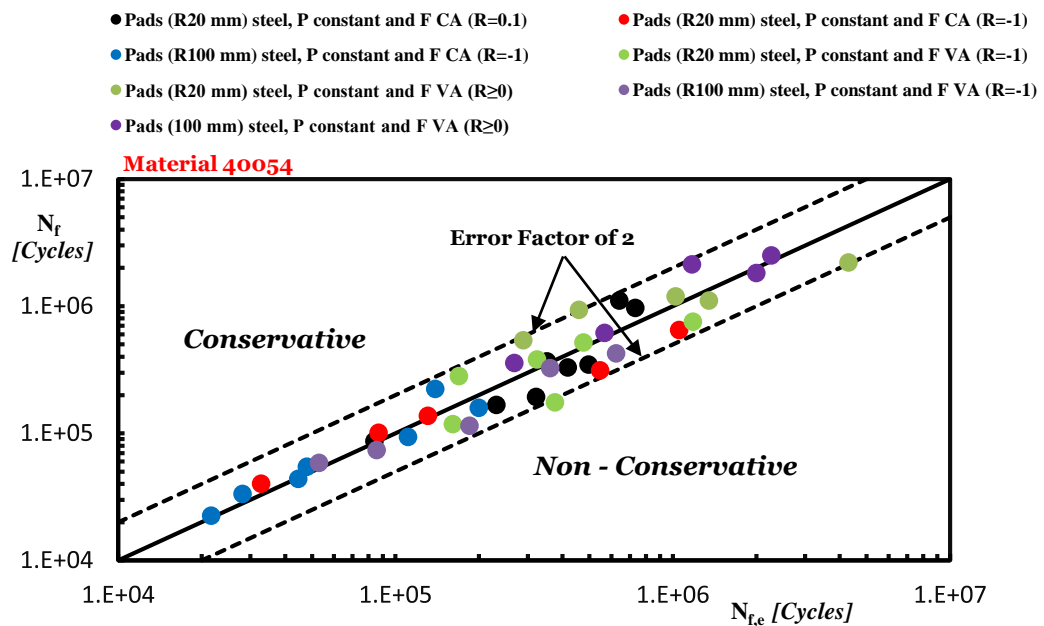


Figure 7-2 Summary of all the fretting fatigue results under CA and VA loading of cast iron 40054.

7.2 Recommendation for future work

The work carried out in this research demonstrates that fretting fatigue damage under CA and VA loading can be predicted accurately using MWCM applied in conjunction with the PM and τ -MVM. The main recommendations for future work could be summarised as follows:

- Recommendation 1: To further test the materials 40060 and 40060 in order to calculate the exact value of the critical fatigue damage sum D_{cr} . In this work D_{cr} was assumed to be equal to one.
- Recommendation 2: Use different design approach different from MWCM applied in conjunction with the PM and τ -MVM to predict the fretting fatigue lifetime.

Bibliography

- [1] Hills D, Nowell D. *Mechanics of Fretting Fatigue*. Kluwer Academic, Dordrecht, The Netherlands, 1994.
- [2] Giannakopoulos AE, Lindley TC, Suresh S. Similarities of stress concentrations in contact at round punches and fatigue at notches: implications to fretting fatigue crack initiation. *Fatigue Fract Eng Mat Struct* 2000; 23: 561-571.
- [3] Nowell D, Dini D, Dyson I. The use of notch and short crack approaches to fretting fatigue threshold prediction: Theory and experimental validation. *Tribology International* 2006; 39: 158-1165.
- [4] Waterhouse RB. Fretting fatigue. *Int Mater Rev* 1992; 77-98.
- [5] Jeung HK, Kwon JD, Lee CY. Crack initiation and propagation under fretting fatigue of inconel 600 alloy. *Journal Mechanical Science Technology* 2015; 29: 5241-5244.
- [6] Hojjati-Talemi R, Abdel Wahab M. Fretting fatigue crack initiation lifetime predictor tool: Using damage mechanics approach. *Tribology international* 2013; 60:176-186.
- [7] Hojjati-Talemi R, Abdel Wahab M. Numerical estimation of fretting fatigue lifetime using damage and fracture mechanics. *Tribology International* 2013; 52:11-25.
- [8] Smith K, Watson P, Topper T. Stress-strain function for fatigue of metals. *Journal Mater* 1970; 767-778.
- [9] Socie D. Multiaxial fatigue damage models. *Journal Engineering Mater Technology* 1987; 293-294.
- [10] Araujo J, Nowell D. The effect of rapidly varying contact stress fields on fretting fatigue. *International Journal of Fatigue* 2002; 24: 763-775.
- [11] Fatemi A, Socie DF. A critical plane approach to multiaxial fatigue damage including out-of-phase loading. *Fatigue Fracture Engineering Material Structure* 1988;11: 149-165.
- [12] Findley WN. A theory for the effect of mean stress on fatigue of metals under combined torsion and axial load or bending. *Engineering Materials Research Laboratory, Division of Engineering, Brown University* 1958.
- [13] Belloula A, Amrouche Abdelwaheb, M. Nait-Abdelaziz. Life Prediction of a Mono Contact Aluminum/Steel at Constant and Variable Amplitudes Loading in Fretting Fatigue Configuration. in *International Conference on New Trends in Fatigue and Fracture* 2018
- [14] Araújo J, Susmel L, Pires M, Castro F. A multiaxial stress-based critical distance methodology to estimate fretting fatigue life. *Tribology International* 2017; 108:2-6.
- [15] Araújo J, Susmel L, Taylor D, Ferro J, Mamiya E. on the use of the theory of critical distances and the Modified Wöhler curve method to estimate fretting fatigue strength of cylindrical contacts. *International journal of fatigue* 2007; 29:95-107.
- [16] Araújo J.A, Susmel L, Taylor D, Ferro J.C.T. On the prediction of High-Cycle Fretting Strength: Theory of Critical Distances vs. Hot spot Approach. *Engineering Fracture Mechanics*. *Eng Frac Mech* 2008; 75:1763-1778.
- [17] Susmel L, *multiaxial notch fatigue: from nominal to local stress-strain quantities*. Woodhead & CRC, Cambridge, UK, 2009.
- [18] Taylor D, *The Theory of Critical Distances. A New Perspective in Fracture Mechanics*. ELSEVIER, Oxford,UK, 2007.
- [19] Mamiya EN, Araújo JA. Fatigue limit under multiaxial loadings: on the definition of the equivalent shear stress. *Mech Res Commun* 2000; 29:141-151.

- [20] Araújo JA, Dantas AP, Castro AP, Mamiya EN, Ferreira JLA. On the characterization of the critical plane with a simple and fast alternative measure of the shear stress amplitude in multiaxial fatigue. *Int J Fatigue* 2011; 33:1092–1100.
- [21] Araújo JA, Carpinteri A, Ronchei C, Spagnoli A, Vantadori S. An alternative definition of the shear stress amplitude based on the maximum rectangular hull method and application to the C-S (Carpinteri-Spagnoli) criterion. *Fatigue Fract Engng Mater Struct* 2014; 37:764-771.
- [22] Carpinteri A, Ronchei C, Spagnoli A, Vantadori S. On the use of the Prismatic Hull method in a critical plane-based multiaxial fatigue criterion. *Int J Fatigue* 2014; 68:159-167.
- [23] Araújo J, Castro F, Matos I, Cardoso R. Life prediction in multiaxial high cycle fretting fatigue. *International Journal of Fatigue* 2020; 134-141.
- [24] Fouvry S, Liskiewicz T, Khapsa Ph, Hannel S, Sauger E. An energy description of wear mechanisms and its applications to oscillating sliding contacts. *Wear* 2003; 255:287-298.
- [25] Garcin S, Fouvry S, Heredia S. A FEM fretting map modeling: Effect of surface wear on crack nucleation. *Wear* 2015; 330:145-159.
- [26] Cardoso R, ferry B, Montebello C, Meriaux J, Araújo J. Study of size effects in fretting fatigue. *Tribology International* 2020; 143:106-117.
- [27] Gailliegue T, Doca T, Araújo J, Ferreira J. Fretting life of the Al7050-T7451 under out-of-phase loads: Numerical and experimental analysis. *Theoretical and Applied Fracture Mechanics* 2020; 102:492-498.
- [28] A.L. Pinto, R.A. Cardoso, R. Talemi, J.A. Araujo. Fretting fatigue under variable amplitude loading considering partial and gross slip regimes: numerical analysis. *Tribology International* 202; 146(93):106-199.
- [29] Dini D, Nowell D, Dyson IN. Experimental validation of a short crack approach for fretting fatigue threshold prediction. In 12th International conference on experimental mechanics, Bari, Italy, 29 August - 2 September 2004.
- [30] Taylor D. Geometrical effects in fatigue: a unifying theoretical model. *International Journal of Fatigue* 1999; 21:413-420.
- [31] Nowell D. An analysis of fretting fatigue. PhD Thesis, University of oxford, Oxford, UK, 1988.
- [32] Nowell D, Rajasekaran R. Fretting fatigue in dovetail blade roots: Experiment and analysis. *Tribology International* 2006; 39:1277-1285.
- [33] Nowell L, Araújo JA. Analysis of pad size effects in fretting fatigue using short crack arrest methodologies. *International Journal Fatigue* 1999; 21:947-956.
- [34] Araújo J, Susmel L, Taylor D, Ferro J, Mamiya E. On the use of the Theory of Critical Distances and the Modified Wohler Curve Method to estimate fretting fatigue strength of cylindrical contacts. *International Journal of fatigue* 2007; 29:95-107.
- [35] C. V. Teuchou Kouanga, J. D. Jones, I. Revill, A. Wormald, D. Nowell, R. S. Dwyer-Joyce, J. A. Araújo, L. Susmel. Finite Lifetime Estimation of Mechanical Assemblies Subjected to Fretting Fatigue Loading. In: Abdel Wahab M. (eds) *Proceedings of the 7th International Conference on Fracture Fatigue and Wear*, Singapore, Springer 2019; 345-358.
- [36] C.T. Kouanga, J.D. Jones, I. Revill, A. Wormald, D. Nowell, R.S. Dwyer-Joyce, J.A. Araújo, L. Susmel. On the estimation of finite lifetime under fretting fatigue loading. *International Journal of Fatigue* 2018; 112: 138-152.

- [37] Suresh S, *Fatigue of Materials*. Cambridge University Press 1998, Cambridge, UK.
- [38] Brown. A theory for fatigue under multiaxial stress–strain conditions. *Proceedings of the Institution of Mechanical Engineers* 1973; 187:745-755.
- [39] Socie D. Multiaxial fatigue damage models. *Trans ASME, J Eng Mater Technol* 1987; 109:293-298.
- [40] Susmel L. A simple and efficient numerical algorithm to determine the orientation of the critical plane in multiaxial fatigue problems. *International Journal of fatigue* 2010; 32:1875-1883.
- [41] Kaufman and Topper. *Biaxial and Multiaxial Fatigue and Fracture*. Elsevier andESIS 2003.
- [42] Wohler A. Versuche zur Ermittlung der auf die Eisenbahnwagennachsen einwirkenden Kräfte und die Widerstandsfähigkeit der Wagen-Achsen 1860; 583–616.
- [43] L. Lee, J. Pan, R. Hathaway, M. Barkey. *Fatigue testing and analysis*. Elsevier Butterworth-Heinemann 2005.
- [44] R. Hertzberg. *Deformation and Fracture Mechanics of Engineering Materials*. 4th Edition, Chichester, New York, USA, 1996.
- [45] Susmel L, Taylor D. A novel formulation of the theory of critical distances to estimate lifetime of notched components in medium-cycle fatigue regime. *Fatigue Fract Engng Mater Struct* 2007; 30:567-581.
- [46] Susmel L, Taylor D. The Modified Wöhler Curve Method applied along with the Theory of Critical Distances to estimate finite life of notched components subjected to complex multiaxial loading paths. *Fatigue Fract. Engng. Mater. Struct* 2008; 31:1047-1064.
- [47] Susmel L, Taylor D. A critical distance/plane method to estimate finite life of notched components under variable amplitude uniaxial/multiaxial fatigue loading. *International Journal of Fatigue* 2012; 38:7-24.
- [48] Peterson RE. Notch sensitivity. *Metal fatigue*, New York: Sines G, Waisman 1959; 293–306.
- [49] Neuber. *Theory of notch stresses: principles for exact calculation of strength with reference to structural form and material*. Springer Verlag II Edition, Berlin, Germany, 1958.
- [50] Susmel L. Four stress analysis strategies to use the Modified Wöhler Curve Method to perform the fatigue assessment of weldments subjected to constant and variable amplitude multiaxial fatigue loading. *International Journal of Fatigue* 2014; 67:38-54.
- [51] Susmel L, Tovo R, Benasciutti D. A novel engineering method based on the critical plane concept to estimate lifetime of weldments subjected to variable amplitude multiaxial fatigue loading. *Fatigue Fract Eng Mater Struct* 2009; 32:441-459.
- [52] Susmel L, Tovo R, Socie D. Estimating the orientation of Stage I cracks paths through the direction of maximum variance of the resolved shear stress. *International Journal of Fatigue* 2014; 58:94-101.
- [53] Susmel L, Taylor D. The Theory of Critical Distances to estimate lifetime of notched components subjected to variable amplitude uniaxial fatigue loading. *International Journal of Fatigue* 2011; 33:900-911.
- [54] Tanaka K. Engineering formulae for fatigue strength reduction due to crack-like notches. *International journal of Fracture* 1983; 22:39-45.
- [55] Taylor D. Predicting the fracture strength of ceramic materials using the theory of critical distances. *Engineering Fracture Mechanic* 2004; 71:2407-2416.

- [56] Susmel L Taylor D. A novel formulation of the theory of critical distances to estimate lifetime of notched components in the medium-cycle fatigue regime. *Fatigue Fract. Engng. Mater. Struct* 2007; 30:567-81.
- [57] Susmel L, Lazzarin P. A Bi-parametric modified wohler curve for high cycle multiaxial fatigue assessment. *Fatigue Fract Eng Mater Struct* 2002; 25:63-78.
- [58] kanazawa K, Miller K, Brown M. Low-cycle fatigue under out-of-phase loading conditions. *Trans ASME, J Eng Mater Technol* 1977; 222-228.
- [59] Susmel L. Multiaxial fatigue limits and material sensitivity to non-zero mean stresses normal to critical planes. *Fatigue Fract. Engng. Mater. Struct* 2008; 31:295-309.
- [60] Susmel L, Taylor D. A critical distance/plane method to estimate finite life of notched components under variable amplitude uniaxial/multiaxial fatigue loading. *International Journal of Fatigue* 2012; 38:7-24.
- [61] Susmel L, Tovo R. Estimating fatigue damage under variable amplitude multiaxial fatigue loading. *Fatigue Fract. Eng. Mater. Struct* 2011; 34:1053-1077.
- [62] Kaufman RP, Topper T. The influence of static mean stresses applied normal to the maximum shear planes in multiaxial fatigue. In *Biaxial and multiaxial fatigue and fracture*, Elsevier and ESIS, Oxford 2003; 123-143.
- [63] P. A. Die Lebensdauer von Kugellagern. *Verfahrenstechnik Berlin* 1924; 68:339-341.
- [64] M. MA. Cumulative damage in fatigue. *J Appl Mech* 1945; 67:59-64.
- [65] S. CM. Fatigue testing under variable amplitude loading. *International Journal of fatigue* 2007; 29:1080-1089.
- [66] Haibach. *Betriebsfestigkeit-verfahren und Daten zur Bauteilberechnung*. VDI-Verlag GmbH Dusseldorf, Germany, 1989.
- [67] S. D Downing, D. F Socie. Simple rainflow counting algorithms. *International Journal of Fatigue* 1982; 4:31-40.
- [68] C. Sonsino. Course of SN-curves especially in the high-cycle fatigue regime with regard to component design and safety. *International Journal of Fatigue* 2007
- [69] M. Kendall. *The Advanced Theory of Statistics*. 4th Edition, Macmillan, 1979.

Appendix A: Results of the ultimate tensile experiments

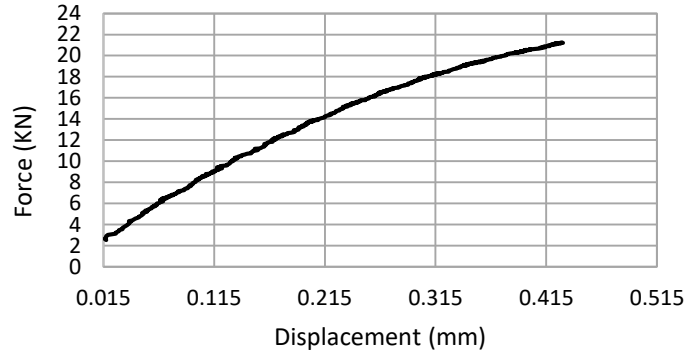


Figure A1 Ultimate tensile test of material 40054, Test N°1.

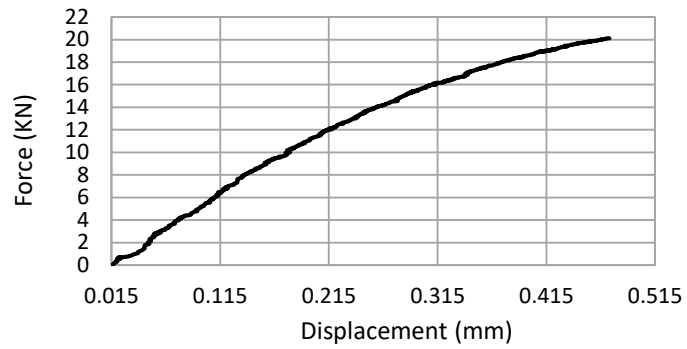


Figure A2 Ultimate tensile test of material 40054, Test N°2.

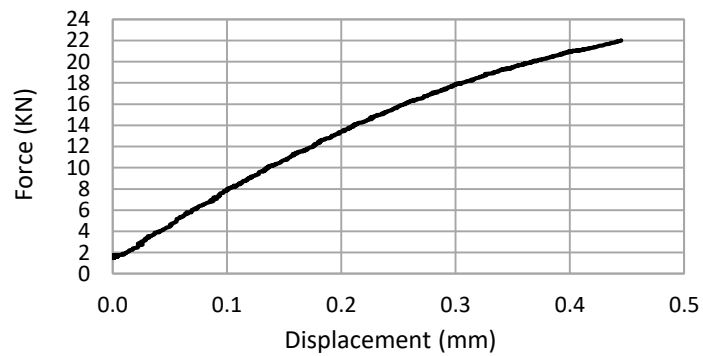


Figure A3 Ultimate tensile test of material 40054, Test N°3.

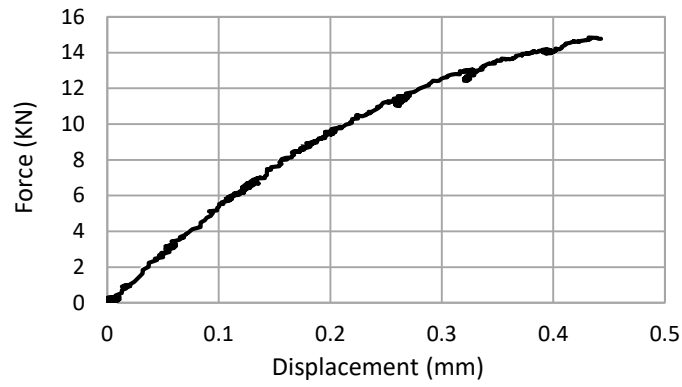


Figure A4 Ultimate tensile test of material 40060, Test N°1.

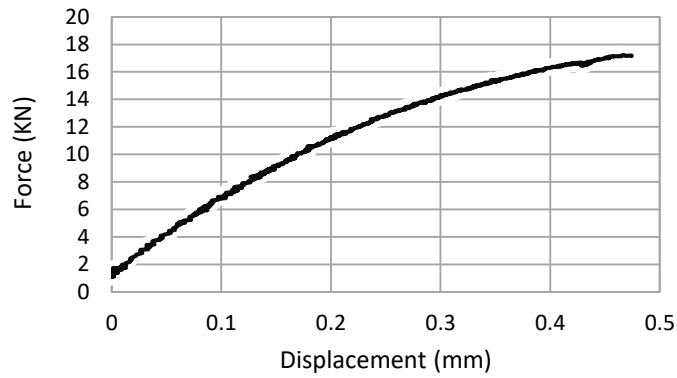


Figure A5 Ultimate tensile test of material 40060, Test N°2.

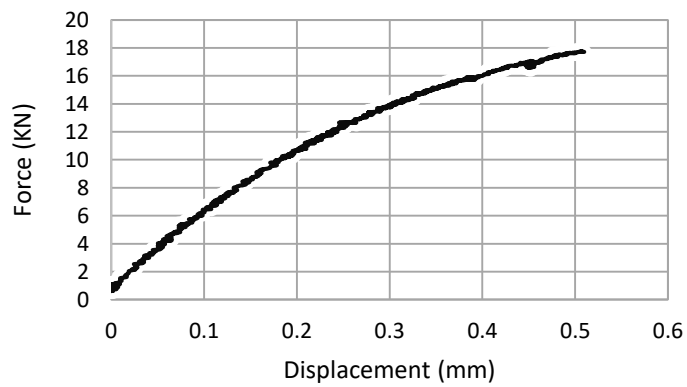


Figure A6 Ultimate tensile test of material 40060, Test N°3.

Appendix B: Uniaxial fatigue experiments and dimensions of all the tested specimens

Table B1 Uniaxial fatigue tests (R=-1), dimensions of all the tested plain specimens made of material 40054.

Specimens reference	Specimens	Gross section			Net section		
	Length (mm)	Width (mm)	Thickness (mm)	Section area (mm ²)	Width (mm)	Thickness (mm)	Section area (mm ²)
P(R1)U1	119.81	25.57	6.10	155.86	9.94	6.07	60.32
P(R1)U2	120.02	25.70	6.11	156.98	9.95	6.08	60.46
P(R1)U3	120.02	25.54	6.08	155.36	9.94	6.05	60.14
P(R1)U4	119.96	25.76	6.11	157.44	9.98	6.09	60.80
P(R1)U5	119.93	25.78	5.95	153.33	9.98	5.93	59.20
P(R1)U6	120.12	25.86	5.97	154.40	9.97	5.95	59.32
P(R1)U7	119.88	25.82	5.94	153.31	9.99	5.91	59.02
P(R1)U8	119.91	25.59	6.16	157.51	9.97	6.12	61.03
P(R1)U9	119.85	25.73	6.09	156.71	9.97	6.07	60.48
P(R1)U10	120.04	25.65	6.15	157.75	9.99	6.12	61.15

Table B2 Uniaxial fatigue tests (R=-1), dimensions of all the tested notched specimens made of material 40054.

Specimens reference	Sample	Gross section			Net section				
	Length (mm)	Width (mm)	Thickness (mm)	Section area (mm ²)	Width (mm)	Thickness (mm)	Section area (mm ²)	Root of the Notch (mm)	Opening angle of the notch (degree)
L1	101.13	25.64	5.94	152.25	9.74	5.94	57.83	0.23	29.79
L2	101.07	25.79	6.08	156.84	9.72	6.08	59.09	0.23	29.69
L3	101.04	25.82	5.75	148.53	9.77	5.75	56.17	0.22	29.94
L4	101.09	25.60	6.08	155.57	9.85	6.08	59.83	0.23	30.04
L5	101.04	25.76	5.89	151.76	9.72	5.89	57.25	0.21	29.91
L6	100.95	25.64	5.77	147.80	9.70	5.77	55.92	0.22	29.79
L7	101.02	25.59	5.92	151.56	9.74	5.92	57.69	0.23	30.10
L8	100.97	25.61	5.83	149.32	9.73	5.83	56.70	0.23	29.85
L9	100.72	25.60	5.89	150.71	9.69	5.89	57.05	0.21	29.86
L10	100.93	25.75	5.85	150.48	9.71	5.85	56.75	0.23	29.70

Table B3 Uniaxial fatigue tests (R=-1), dimensions of all the tested plain specimens made of material 40060.

Specimens reference	Specimens	Gross section			Net section		
	Length (mm)	Width (mm)	Thickness (mm)	Section area (mm ²)	Width (mm)	Thickness (mm)	Section area (mm ²)
B(R1)1	119.99	25.68	6.09	156.40	9.82	6.16	60.52
B(R1)2	119.92	25.64	6.21	159.21	9.82	6.18	60.74
B(R1)3	120.00	25.69	6.11	157.03	9.85	6.14	60.48
B(R1)4	119.97	25.64	6.14	157.35	9.85	6.14	60.47
B(R1)5	120.00	25.68	6.10	156.65	9.86	6.16	60.79
B(R1)6	119.98	25.72	6.07	156.12	9.85	6.12	60.27
B(R1)7	119.98	25.67	6.13	157.21	9.87	6.20	61.18
B(R1)8	119.99	25.68	6.02	154.53	9.87	6.15	60.72
B(R1)9	119.97	25.67	6.14	157.50	9.87	6.19	61.08
B(R1)10	120.01	25.70	6.20	159.24	9.88	6.18	61.07
B(R1)11	119.98	25.69	6.17	158.51	9.87	6.22	61.34
B(R1)12	120.00	25.70	6.13	157.38	9.86	6.21	61.25

Table B4 Uniaxial fatigue tests (R=-1), dimensions of all the tested notched specimens made of material 40060.

Specimens reference	Sample	Gross section			Net section				
	Length (mm)	Width (mm)	Thickness (mm)	Section area (mm ²)	Width (mm)	Thickness (mm)	Section area (mm ²)	Root of the Notch (mm)	Opening angle of the notch (degree)
B1	101.04	25.63	6.06	155.30	10.20	6.13	62.50	0.12	29.20
B2	100.95	25.49	6.10	155.59	10.38	6.14	63.73	0.15	30.12
B3	101.02	25.61	6.04	154.60	10.27	6.08	62.42	0.12	29.11
B4	101.09	25.51	6.08	155.16	10.17	6.15	62.56	0.12	29.04
B5	101.04	25.58	6.10	155.97	10.29	6.15	63.29	0.13	28.70
B6	100.72	25.63	6.05	155.05	10.20	6.13	62.50	0.13	28.62
B7	100.93	25.71	6.05	155.52	10.29	6.09	62.67	0.12	28.73
B8	101.13	25.59	6.04	154.55	10.27	6.06	62.22	0.12	28.31
B9	101.07	25.59	6.07	155.33	10.27	6.11	62.74	0.12	28.98
B10	101.04	25.51	5.97	152.28	10.22	6.03	61.63	0.13	28.88
B11	100.95	25.46	6.10	155.36	10.27	6.17	63.35	0.13	29.14
B12	101.02	25.52	6.11	155.98	10.34	6.17	63.79	0.12	29.42
B13	100.97	25.68	6.04	155.21	10.36	6.15	63.73	0.13	29.15

Table B5 Uniaxial fatigue tests (R=0.1), dimensions of all the tested plain specimens made of material 40054.

Specimens reference	Specimens	Gross section			Net section		
	Length (mm)	Width (mm)	Thickness (mm)	Section area (mm ²)	Width (mm)	Thickness (mm)	Section area (mm ²)
R(0.1)1	120.04	25.71	5.54	142.45	9.89	5.53	54.64
R(0.1)2	119.95	25.76	6.12	157.64	9.87	6.11	60.27
R(0.1)3	120.12	25.67	6.02	154.48	9.85	6.01	59.15
R(0.1)4	120.01	25.69	6.08	156.20	9.87	6.08	59.99
R(0.1)5	120.07	25.68	6.10	156.68	9.88	6.09	60.22
R(0.1)6	120.10	25.63	6.18	158.36	9.86	6.18	60.95
R(0.1)7	120.02	25.68	6.19	158.85	9.87	6.18	61.05
R(0.1)8	120.03	25.76	5.88	151.45	9.87	5.88	58.06
R(0.1)9	120.10	25.78	5.87	151.31	9.88	5.84	57.73
R(0.1)10	120.12	25.60	6.17	157.95	9.88	6.17	60.91

Test B6 Uniaxial fatigue tests (R=0.1), dimensions of all the tested plain specimens made of material 40060.

Specimens reference	Specimens	Gross section			Net section		
	Length (mm)	Width (mm)	Thickness (mm)	Section area (mm ²)	Width (mm)	Thickness (mm)	Section area (mm ²)
B(R0.1)1	120.04	25.66	6.17	158.37	9.88	6.16	60.87
B(R0.1)2	119.95	25.73	6.13	157.65	9.85	6.18	60.93
B(R0.1)3	120.12	25.57	6.09	155.80	9.84	6.16	60.61
B(R0.1)4	120.01	25.63	6.10	156.36	9.86	6.15	60.64
B(R0.1)5	120.07	25.65	6.12	156.88	9.86	6.18	60.99
B(R0.1)6	120.10	25.69	6.06	155.73	9.87	6.13	60.50
B(R0.1)7	120.02	25.57	6.11	156.18	9.85	6.15	60.60
B(R0.1)8	120.03	25.63	6.13	157.05	9.84	6.18	60.80
B(R0.1)9	120.10	25.67	6.15	157.74	9.88	6.17	60.97
B(R0.1)10	120.12	25.66	6.18	158.58	9.87	6.18	61.05
B(R0.1)11	119.97	25.66	6.04	154.99	9.89	6.16	60.87
B(R0.1)12	119.98	25.62	6.10	156.27	9.88	6.12	60.45

Appendix C: Use of the online tool e-fatigue to calculate the stress concentration factor



Figure C1 Calculation of the stress concentration factor at the notch tip of the material 40054.



Figure C2 Calculation of the stress concentration factor at the notch tip of the material 40060.

Appendix D: Torsional fatigue experiments and dimensions of all the tested specimens

Table D1 Torsional fatigue tests (R=-1), dimensions of all the tested specimens made of material 40054.

Specimens reference	Specimens	Gross section		Net section	
	Length (mm)	ϕ (mm)	Section area (mm ²)	ϕ (mm)	Section area (mm ²)
L1	132.00	14.85	173.11	9.83	75.78
L1*	132.00	14.85	173.11	9.83	75.78
L2	132.00	14.87	173.58	9.81	75.62
L2*	132.00	14.87	173.58	9.82	75.62
L3	132.00	14.82	172.47	9.82	75.62
L4	132.00	14.81	172.06	9.81	75.55
L5	132.00	14.86	173.29	9.91	77.02
L6	132.00	14.86	173.29	9.92	78.34
L7	132.00	14.88	173.81	9.92	77.64
L8	132.00	14.92	174.63	9.91	77.02
L9	132.00	14.83	172.53	9.91	77.09

* Specimen L1 re-tested at 214.8 MPa after run-out

** Specimen L2 re-tested at 231.6 MPa after run-out

Table D2 Torsional fatigue tests (R=-1), dimensions of all the tested specimens made of material 40060.

Specimens reference	Specimens	Gross section		Net section	
	Length (mm)	ϕ (mm)	Section area (mm ²)	ϕ (mm)	Section area (mm ²)
B1	101.54	14.91	174.48	9.86	76.28
B2	101.60	14.92	174.83	9.88	76.59
B3	101.61	14.85	173.26	9.83	75.81
B4	101.64	14.91	174.48	9.88	76.67
B5	101.75	14.89	174.02	9.86	76.28
B6	101.75	14.91	174.54	9.88	76.67
B7	101.40	14.92	174.83	9.88	76.59
B8	101.68	14.95	175.54	9.90	76.98
B9	101.55	14.92	174.83	9.89	76.74
B10	101.72	14.92	174.78	9.86	76.36

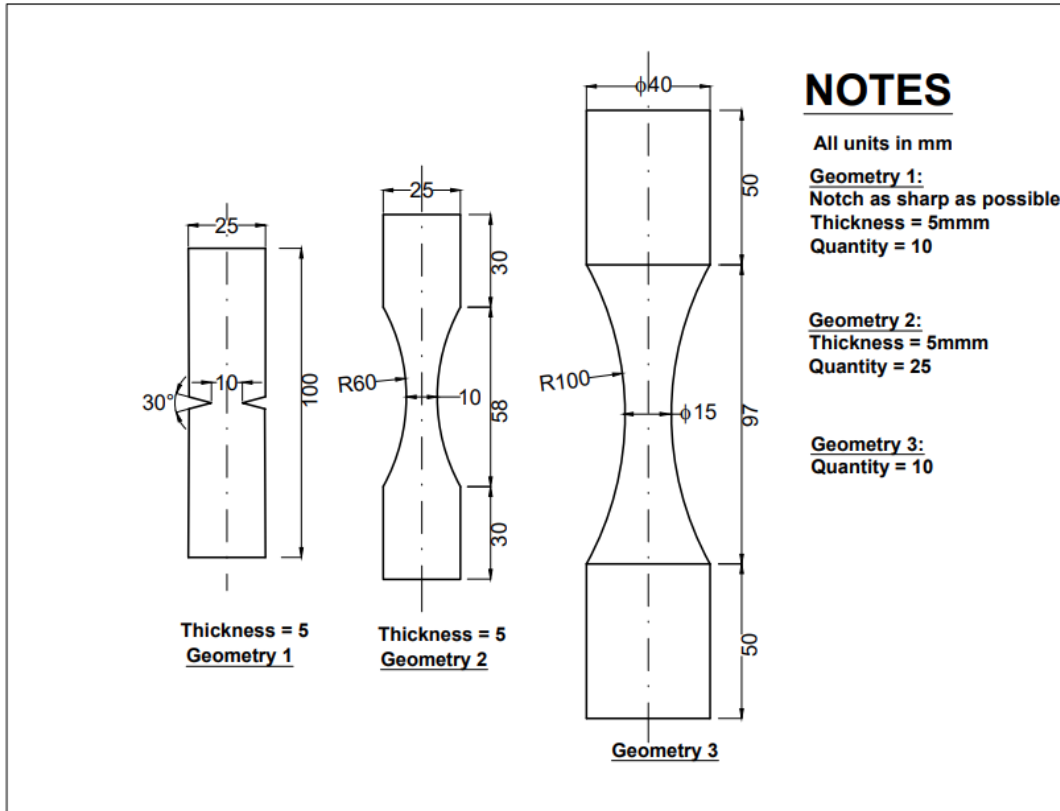


Figure B1 Geometry of the notched, plane and round specimen

Appendix E: Stiffness behaviour of specimens during the fatigue test under torsion

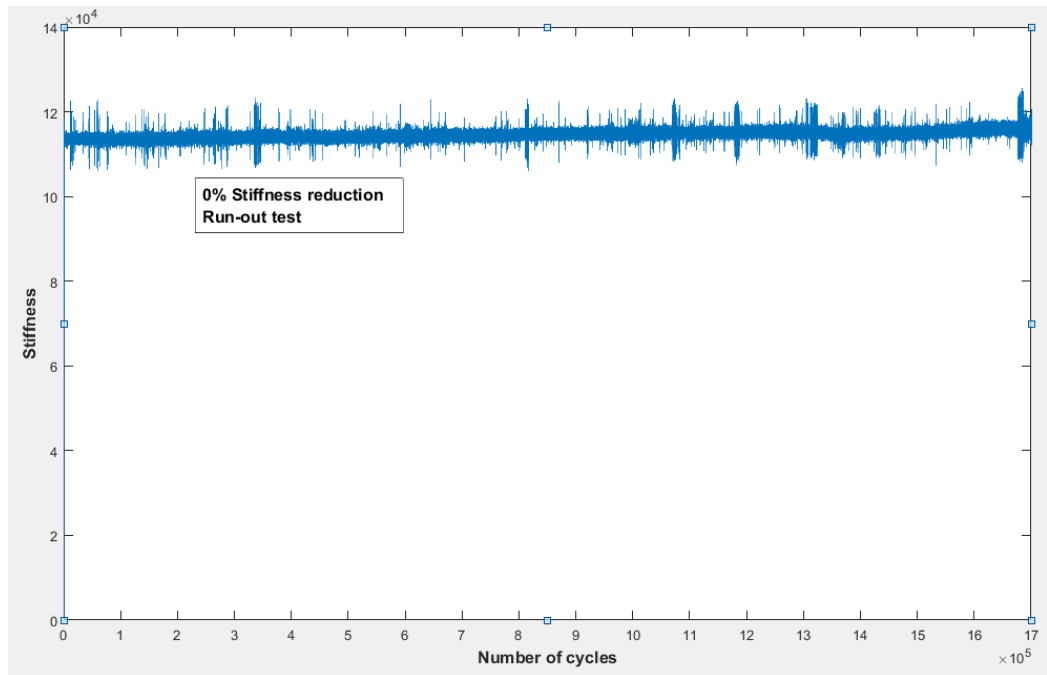


Figure E1 Stiffness behaviour of specimen L1 during the fully reversed torsional fatigue test.

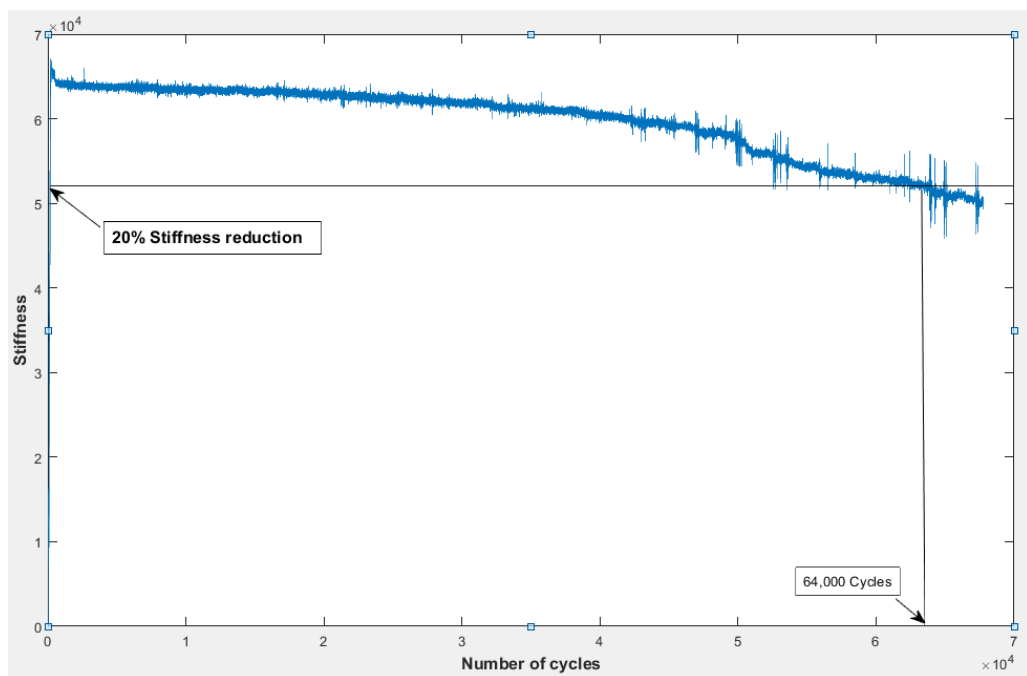


Figure E2 Stiffness behaviour of specimen L1* during the fully reversed torsional fatigue test.

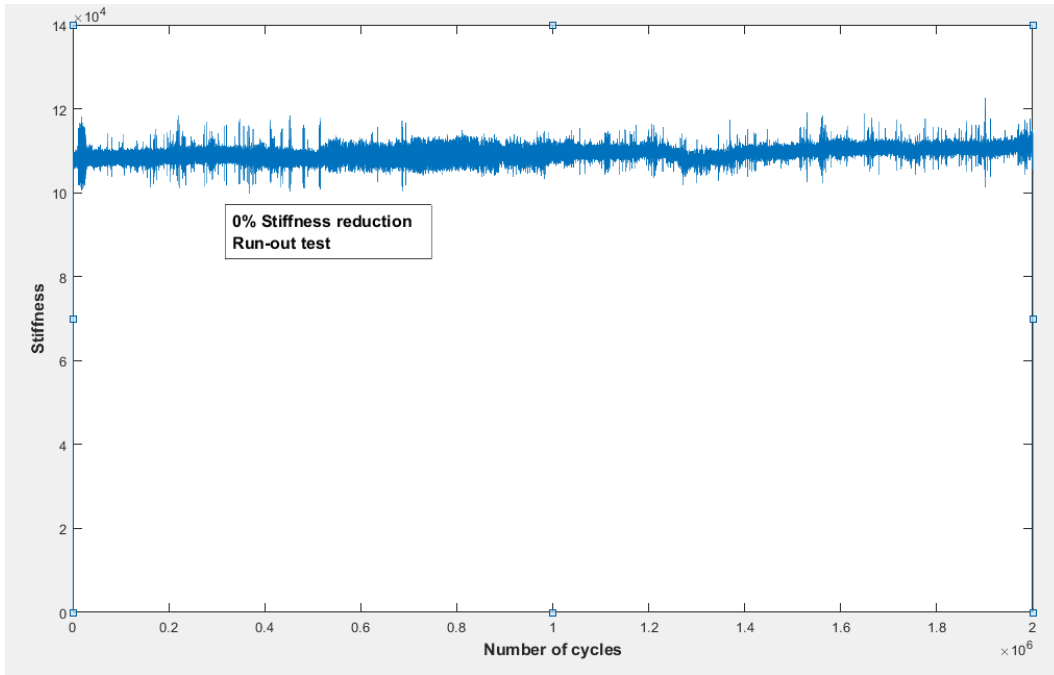


Figure E3 Stiffness behaviour of specimen L2 during the fully reversed torsional fatigue test.

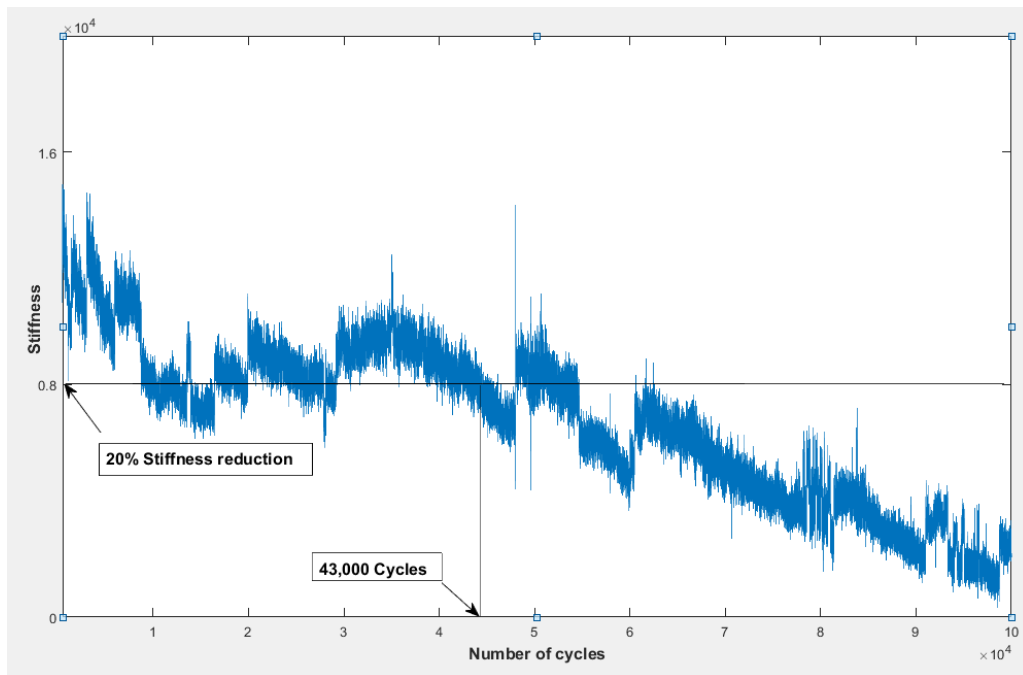


Figure E4 Stiffness behaviour of specimen L2* during the fully reversed torsional fatigue tests.

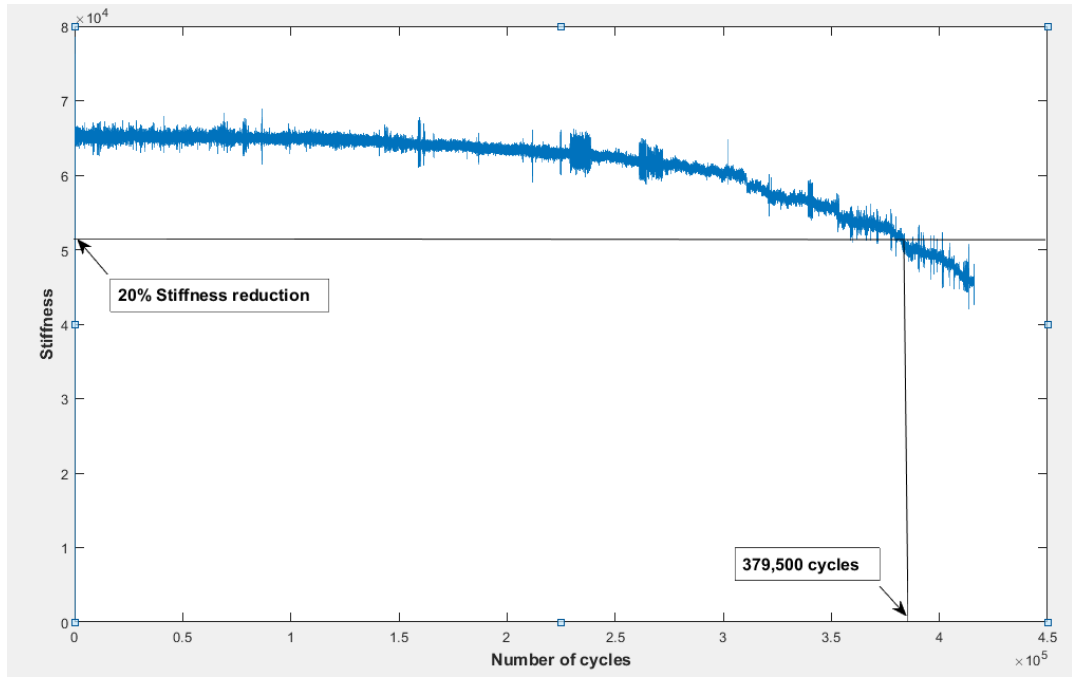


Figure E5 Stiffness behaviour of specimen L3 during the fully reversed torsional fatigue tests.

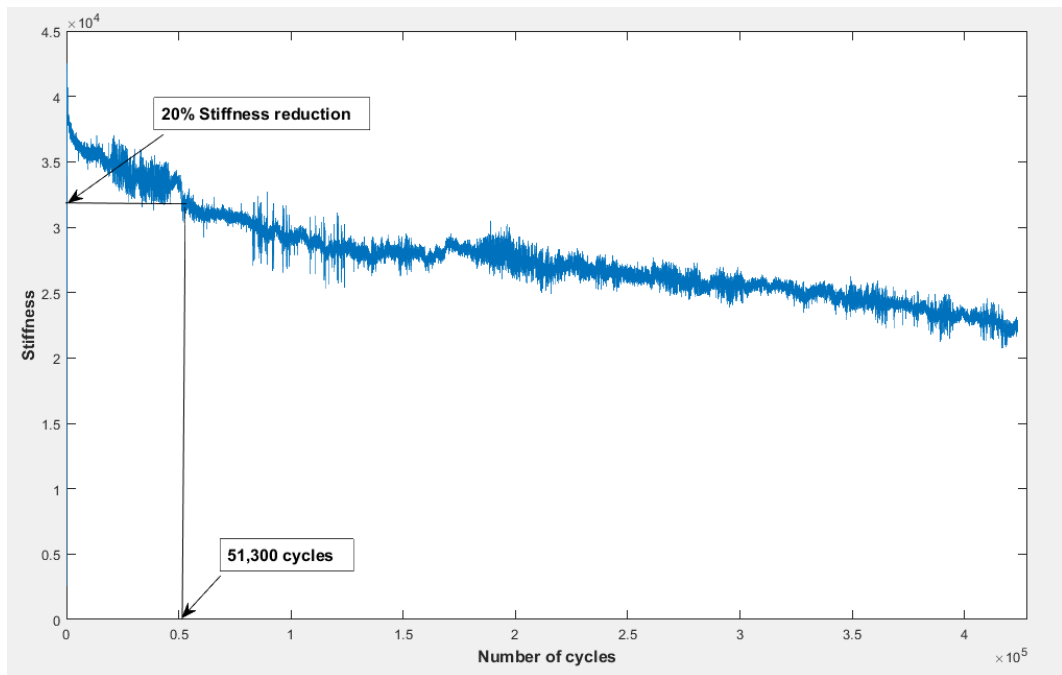


Figure E6 Stiffness behaviour of specimen L4 during the fully reversed torsional fatigue test.

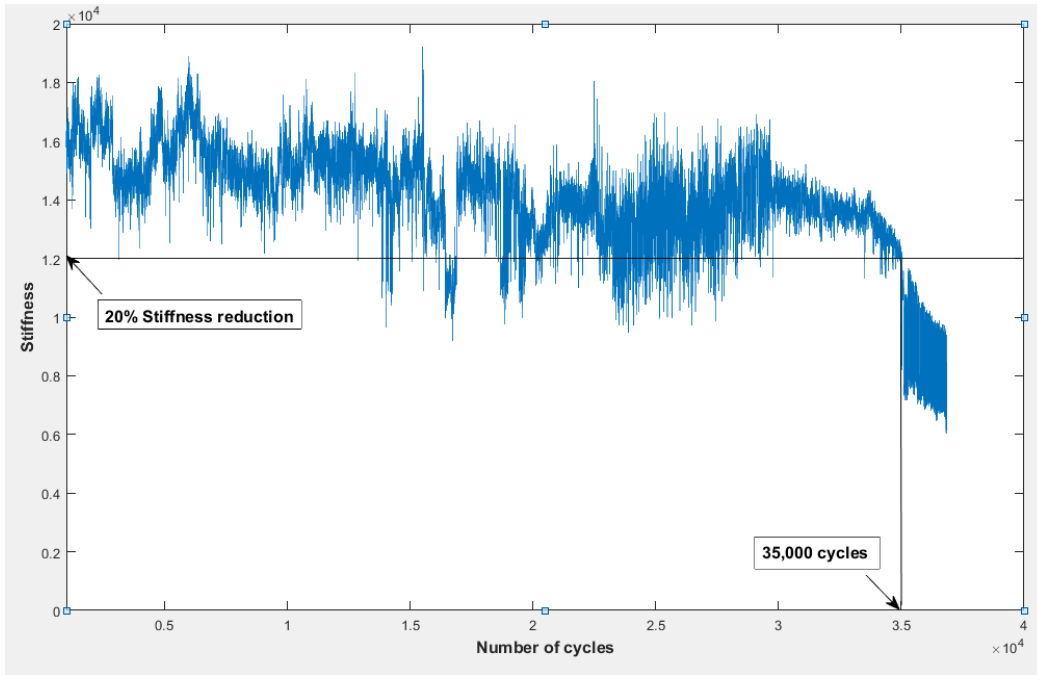


Figure E7 Stiffness behaviour of specimen L5 during the fully reversed torsional fatigue test.

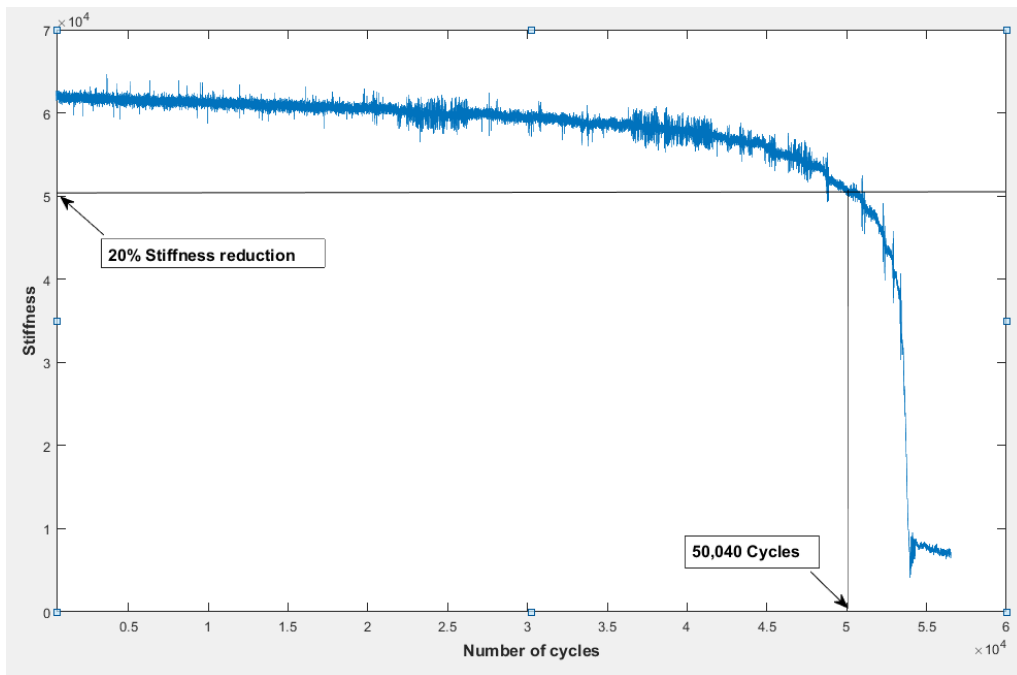


Figure E8 Stiffness behaviour of specimen L7 during the fully reversed torsional fatigue test.

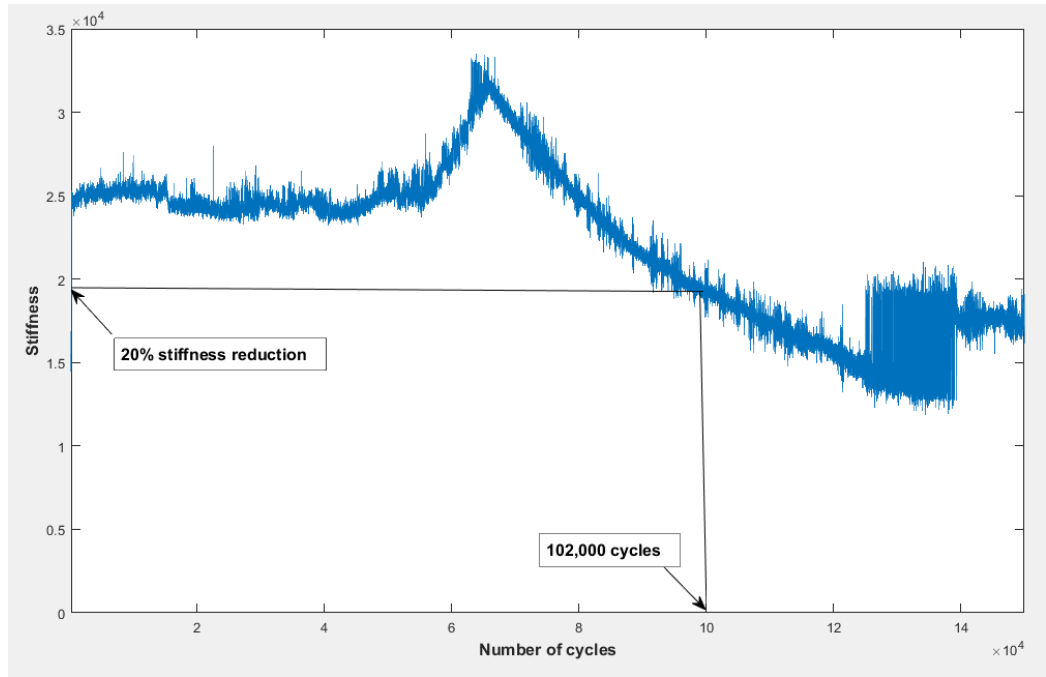


Figure E9 Stiffness behaviour of specimen L8 during the fully reversed torsional fatigue test.

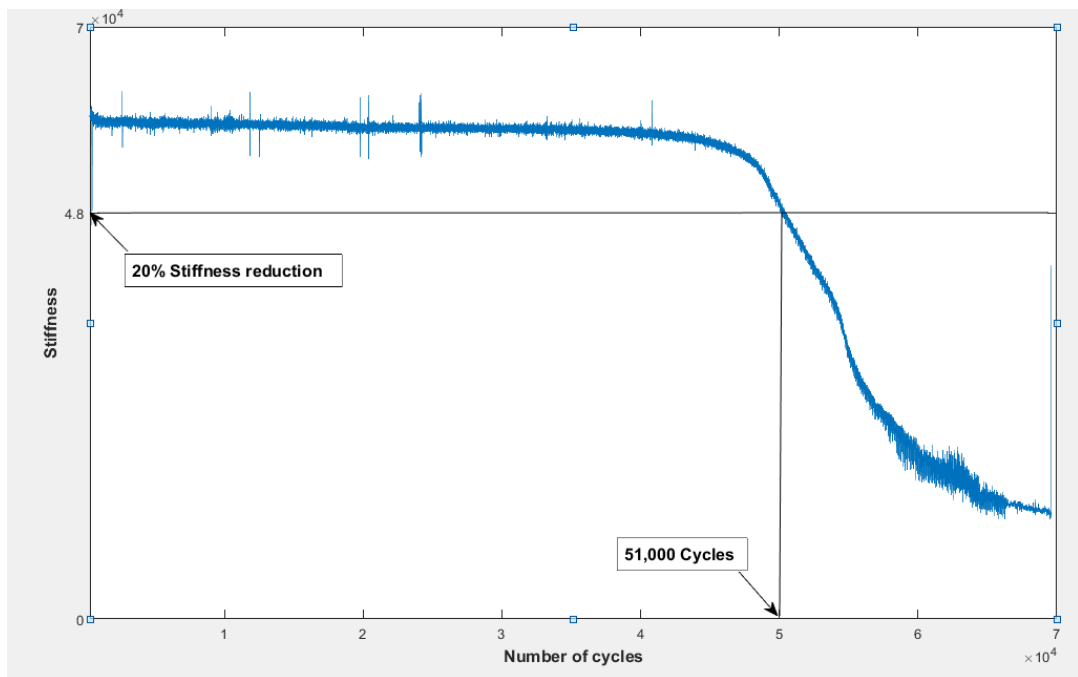


Figure E10 Stiffness behaviour of specimen L9 during the fully reversed torsional fatigue test.

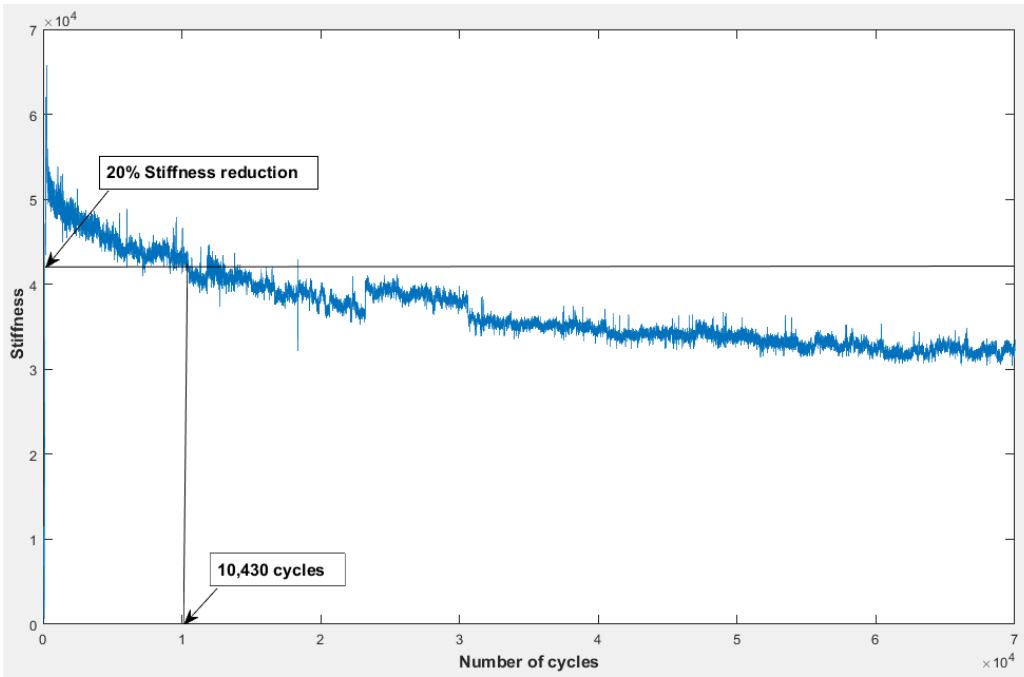


Figure E11 Stiffness behaviour of specimen B1 during the fully reversed torsional fatigue test.

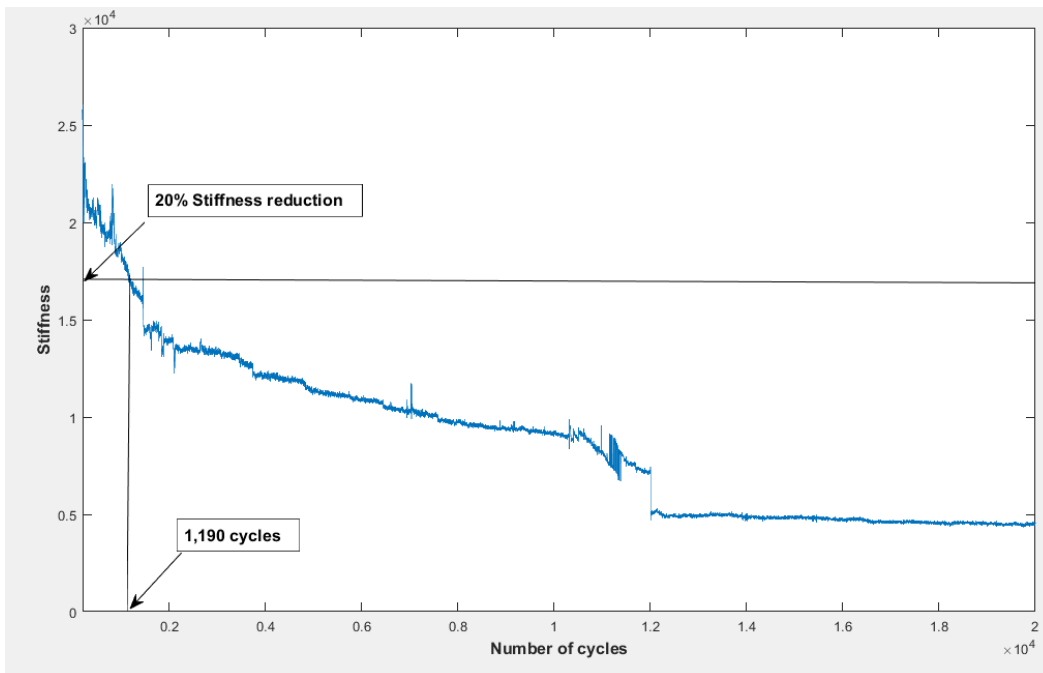


Figure E12 Stiffness behaviour of specimen B2 during the fully reversed torsional fatigue test.

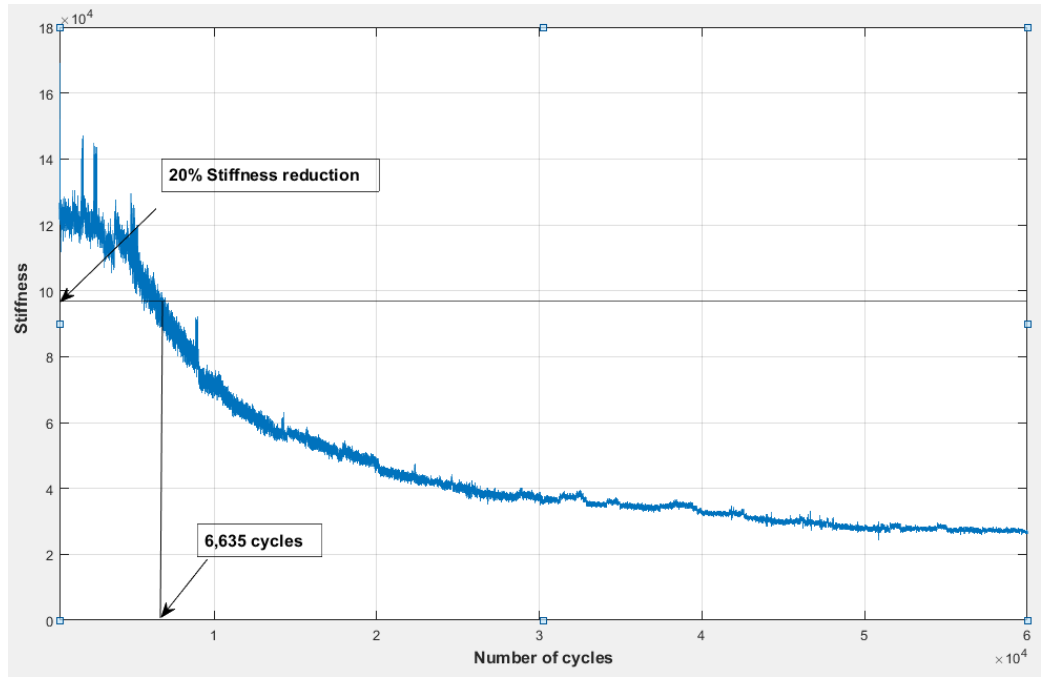


Figure E13 Stiffness behaviour of specimen B3 during the fully reversed torsional fatigue test.

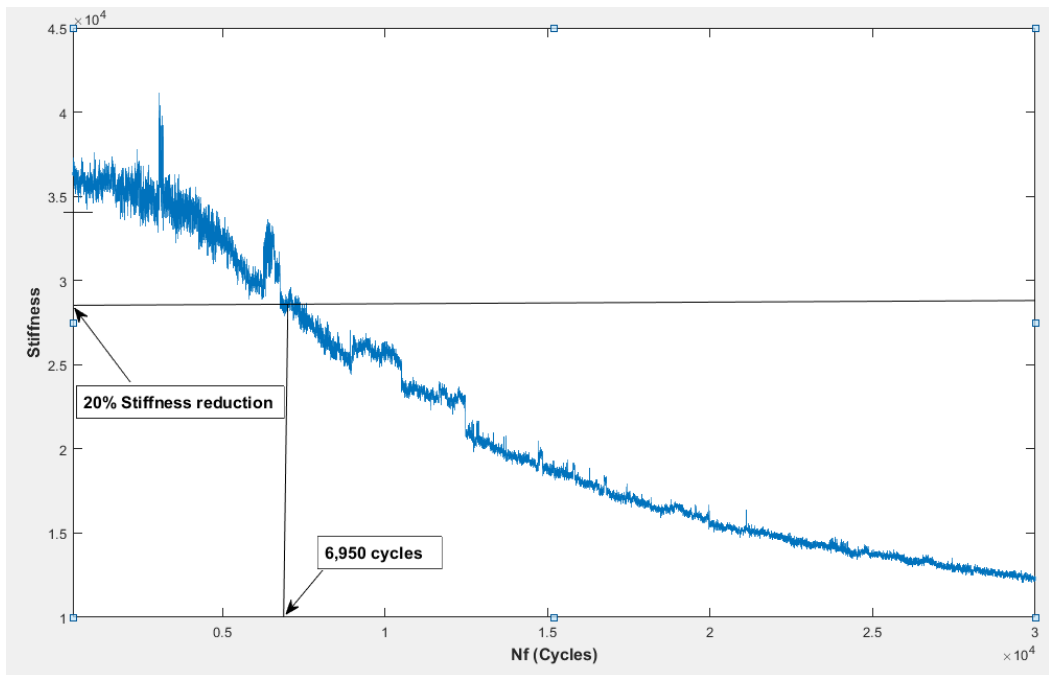


Figure E14 Stiffness behaviour of specimen B4 during the fully reversed torsional fatigue test.

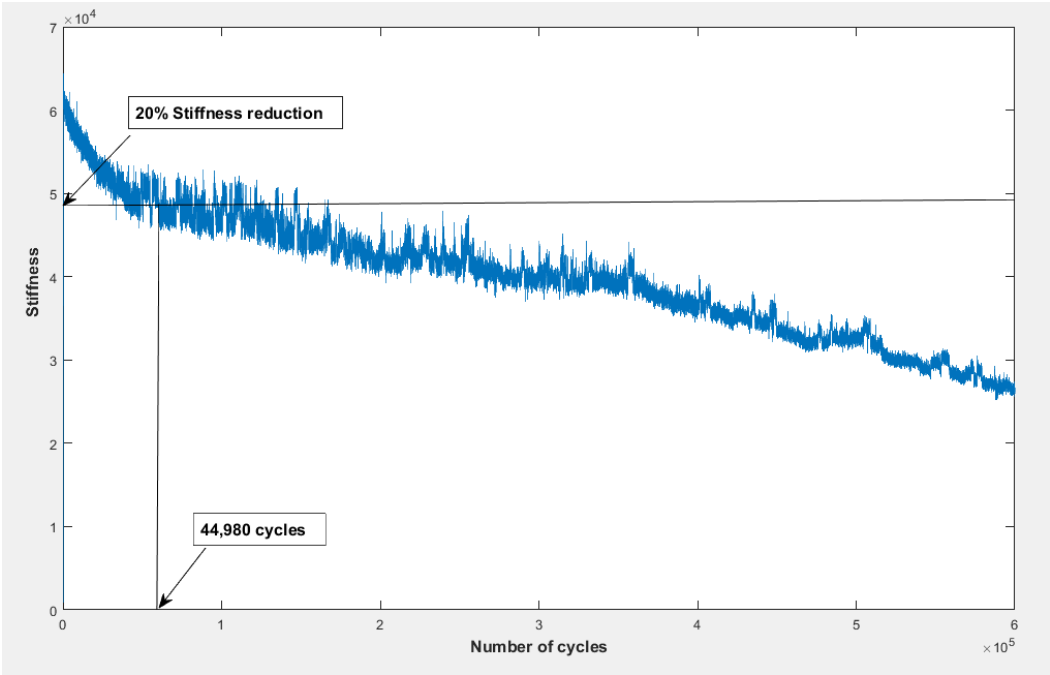


Figure E15 Stiffness behaviour of specimen B5 during the fully reversed torsional fatigue test.

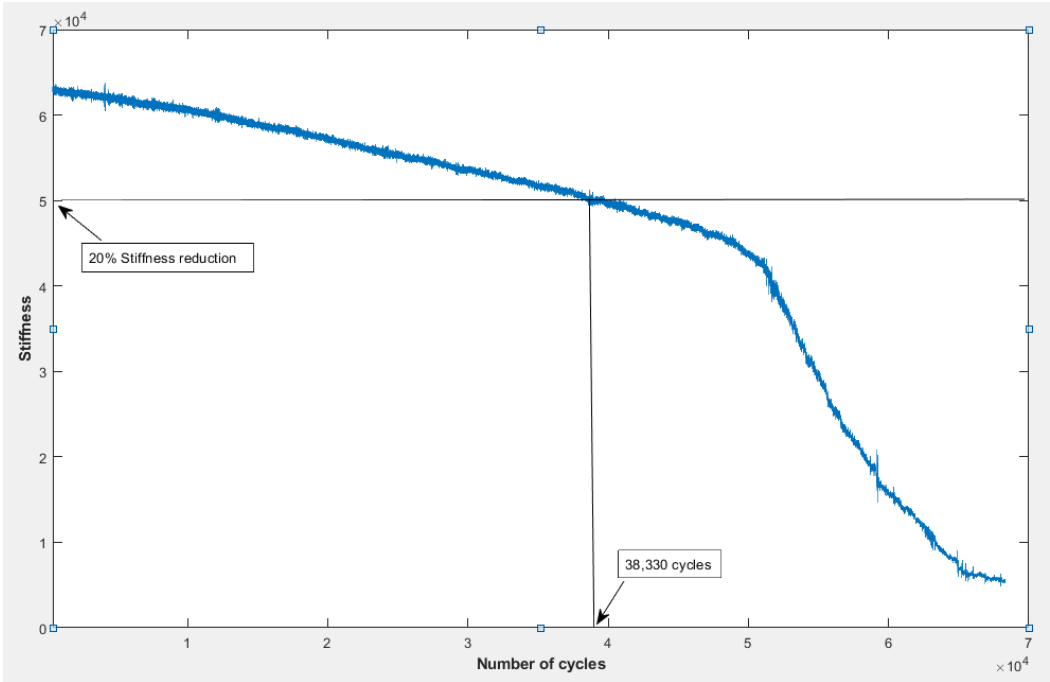


Figure E17 Stiffness behaviour of specimen B6 during the fully reversed torsional fatigue test.

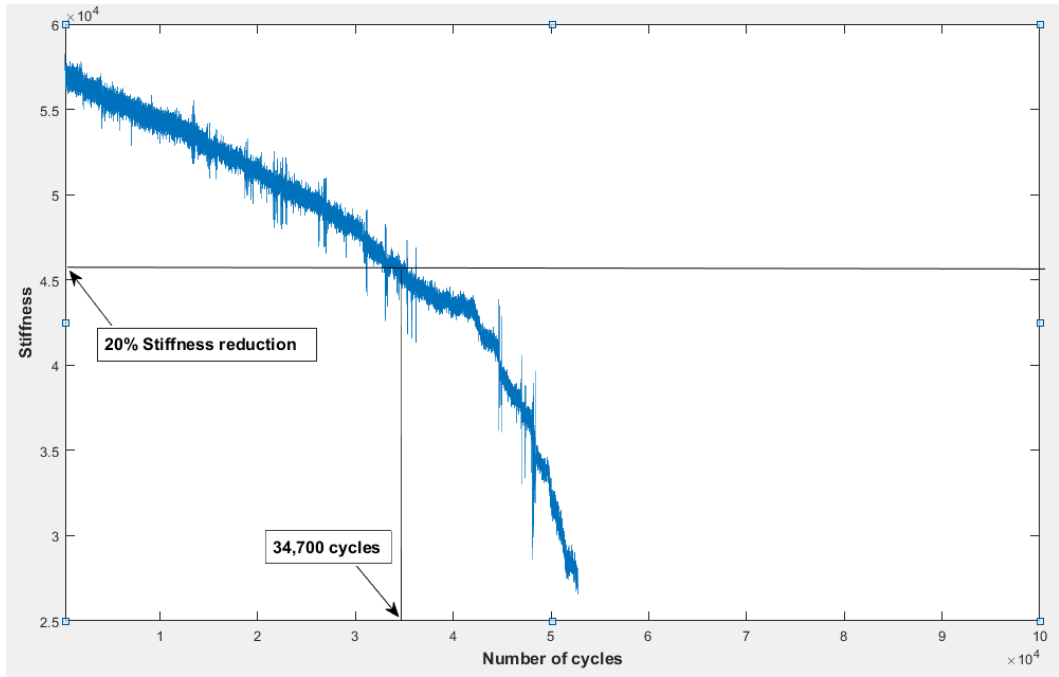


Figure E16 Stiffness behaviour of specimen B7 during the fully reversed torsional fatigue test.

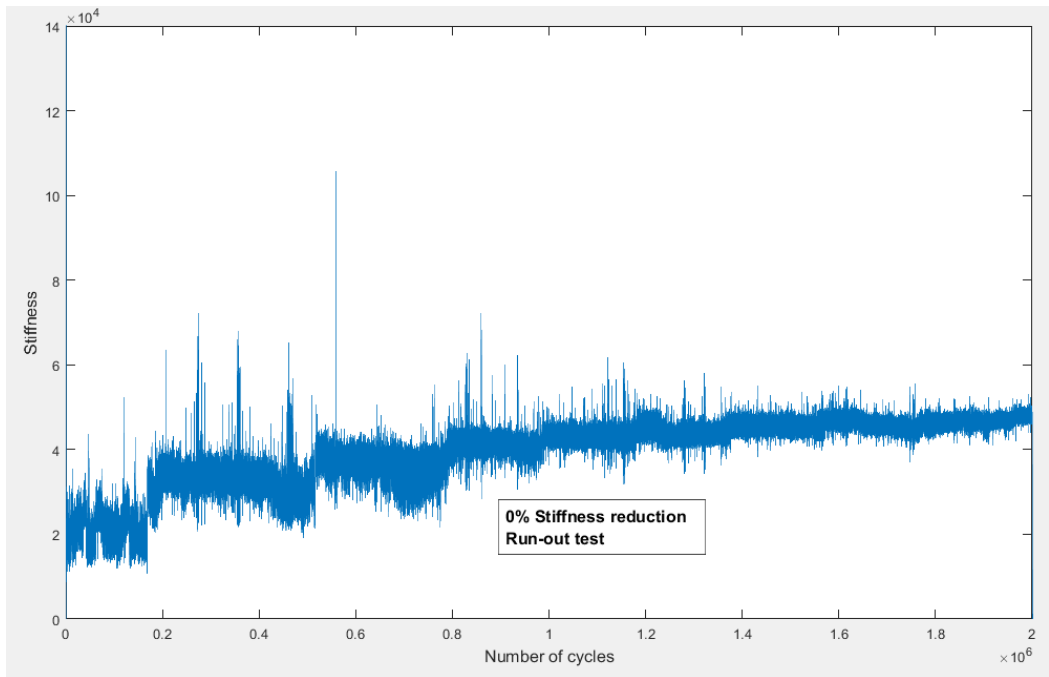


Figure E18 Stiffness behaviour of specimen B9 during the fully reversed torsional fatigue test.

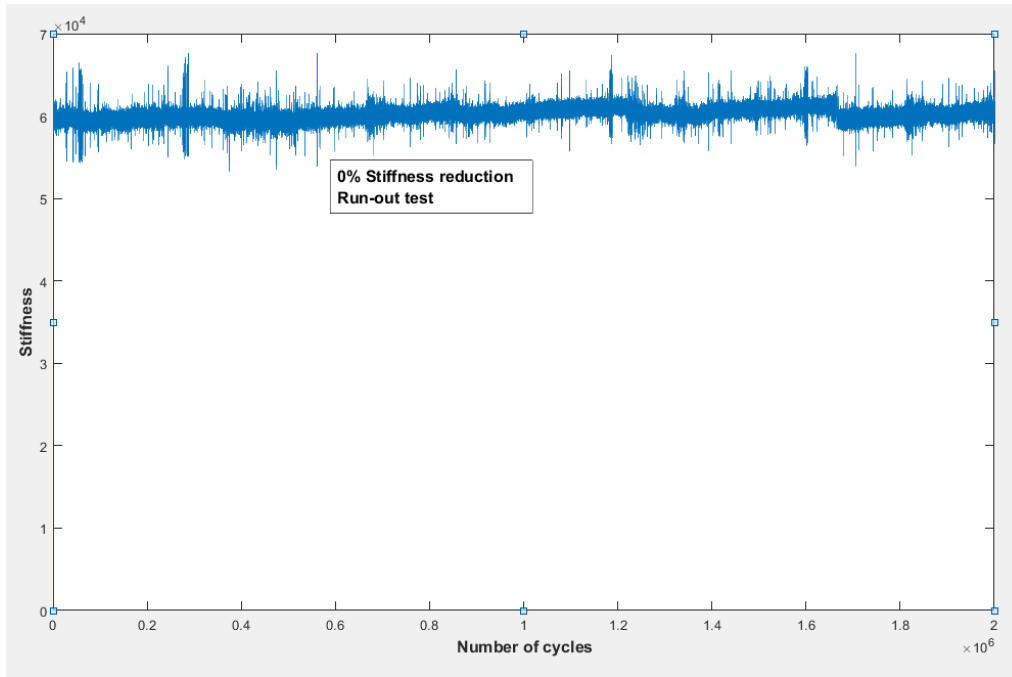


Figure E19 Stiffness behaviour of specimen B10 during the fully reversed torsional fatigue test.

Appendix F: Calibration results of the fretting fatigue machine

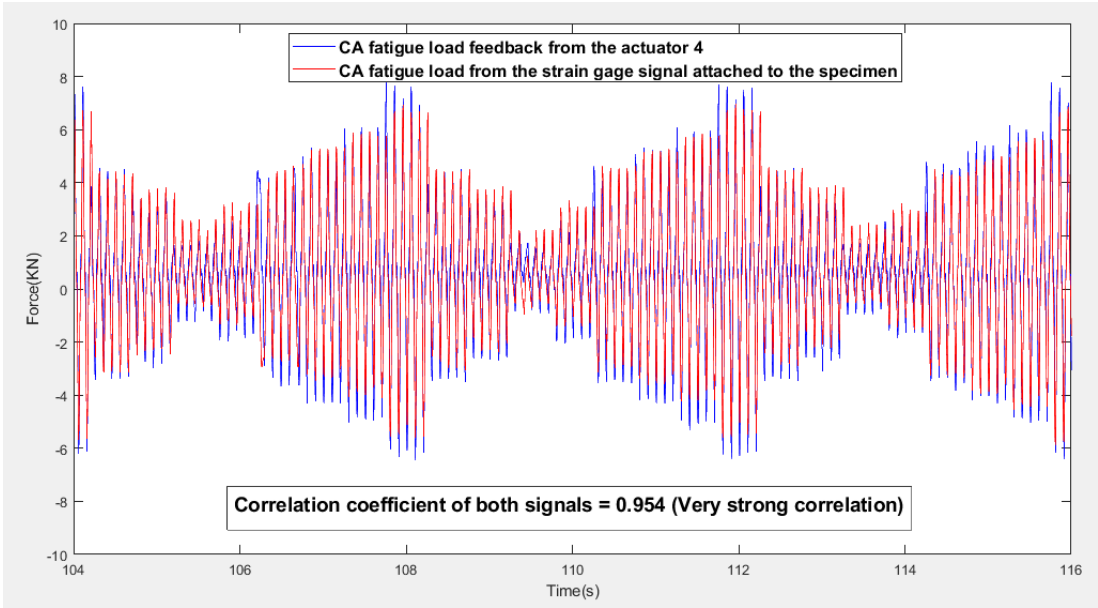


Figure F1 First calibration test (Test N°2): Comparison between the load feedback from actuator 4 and the load obtained from the strain gauge signal attached to the specimen.

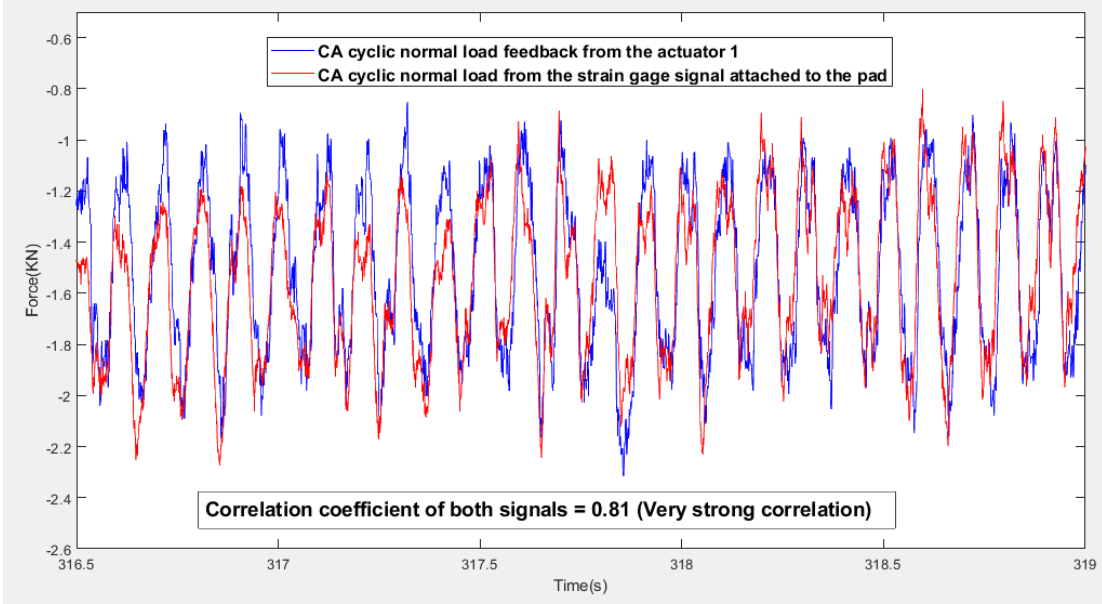


Figure F2 First calibration test (Test N°2): Comparison between the load feedback from actuator 1 and the load obtained from the strain gauge attached to the pad.

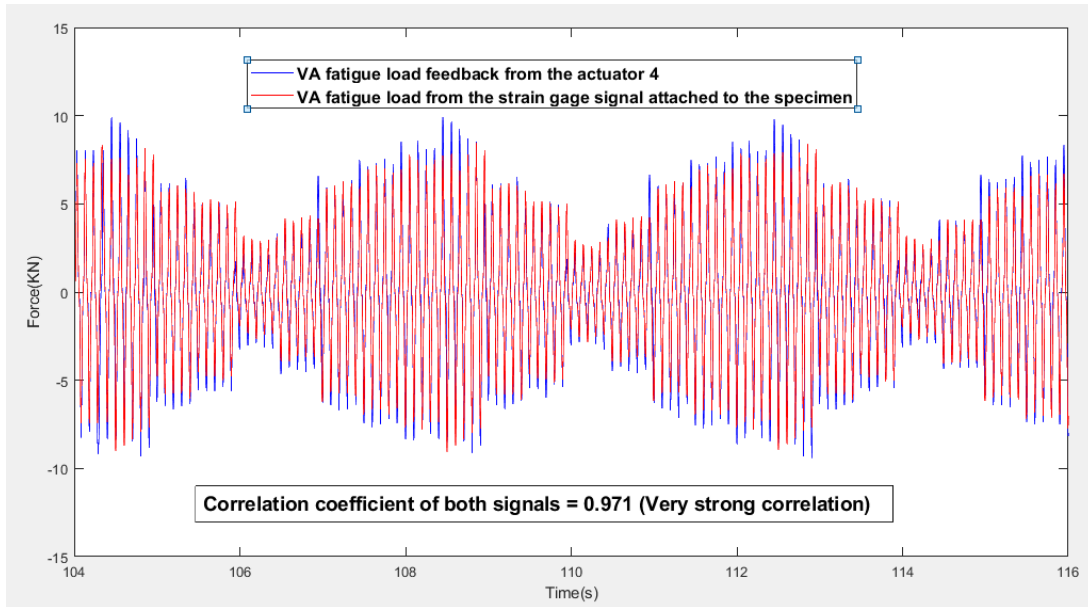


Figure F3 Second calibration test: Comparison between the load feedback from actuator 4 and the load obtained from the strain gauge signal attached to the specimen.

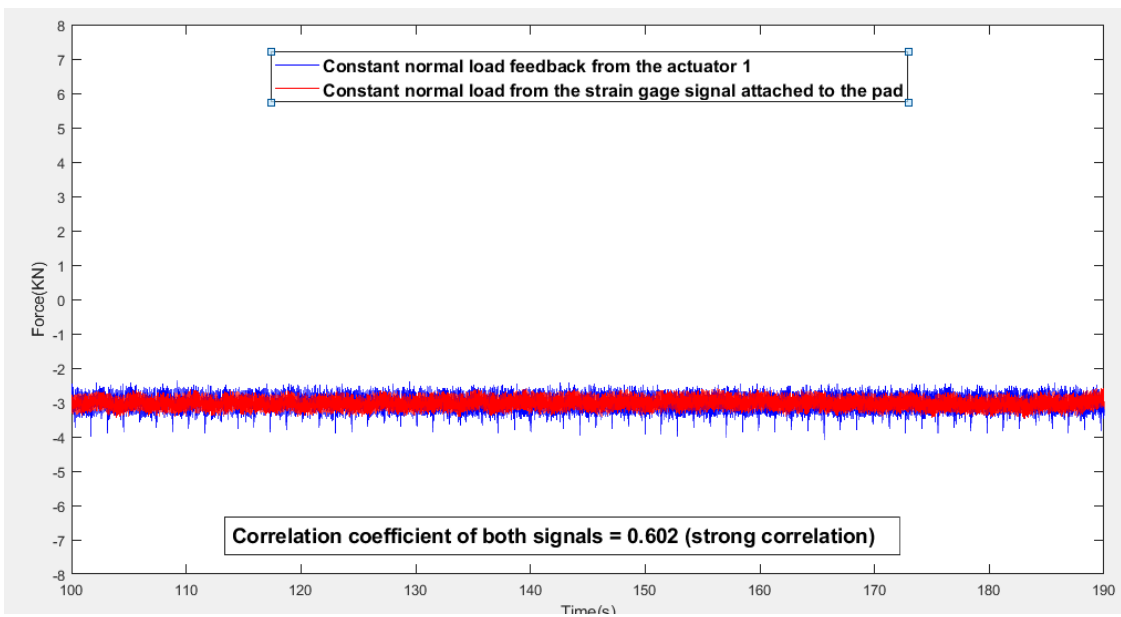


Figure F4 Second calibration test: Comparison between the load feedback from actuator 1 and the load obtained from the strain gauge attached to the pad.

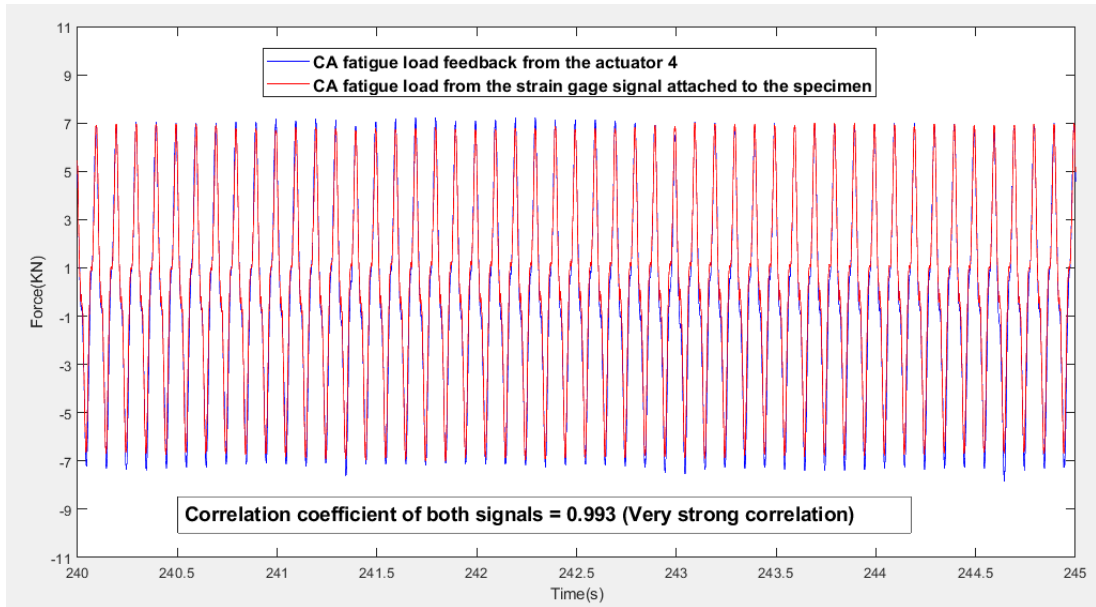


Figure F5 Third calibration test (Test N_o2): Comparison between the load feedback from actuator 4 and the load obtained from the strain gauge signal attached to the specimen.

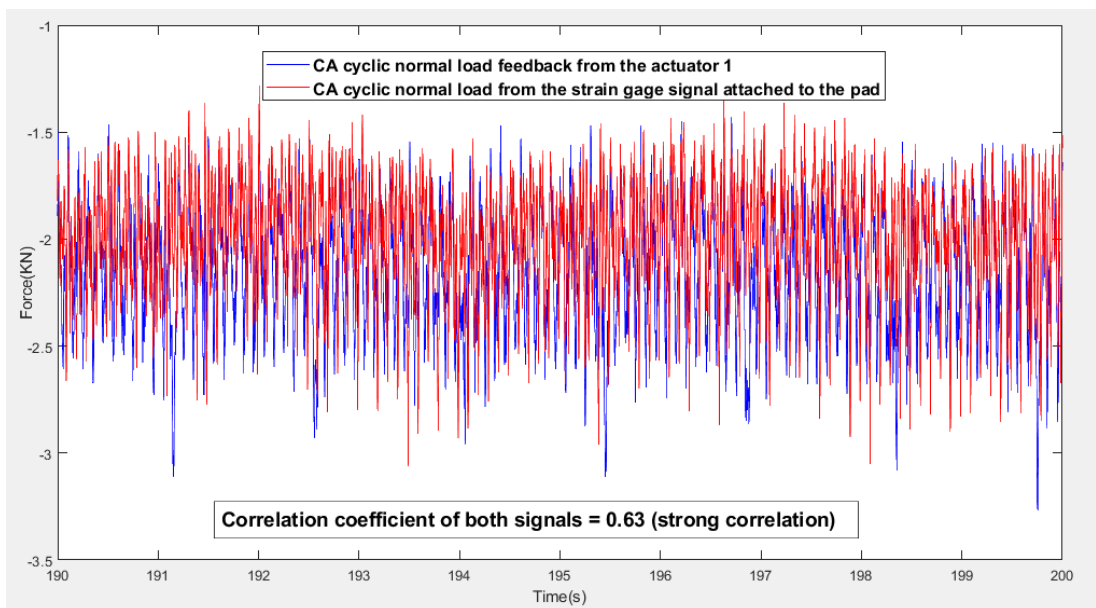


Figure F6 Third calibration test (Test N_o2): Comparison between the load feedback from actuator 1 and the load obtained from the strain gauge attached to the pad.

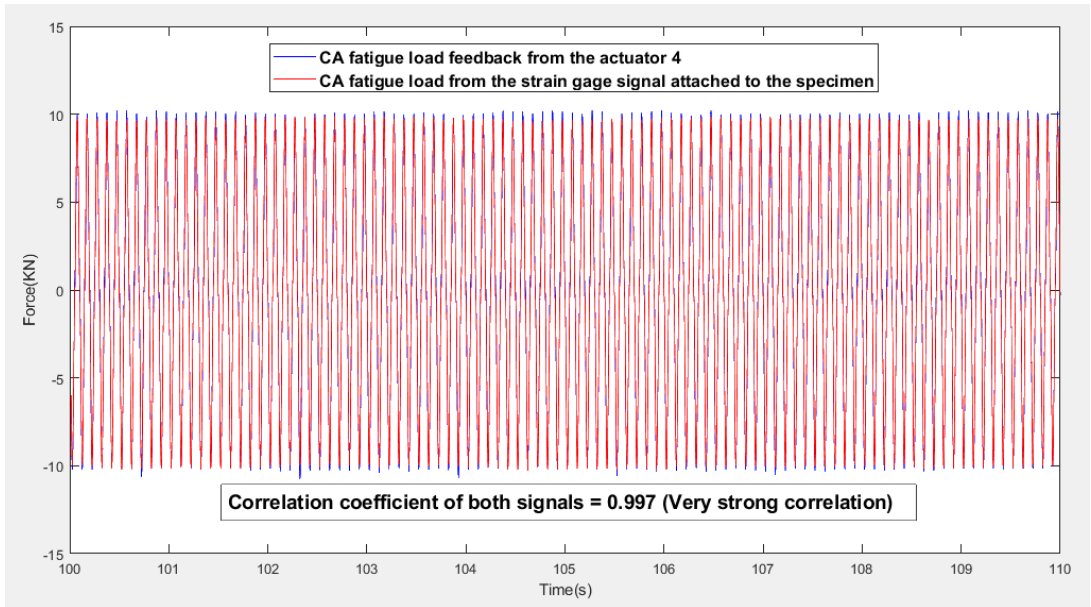


Figure F7 Fourth calibration test (Test N^o1): Comparison between the load feedback from actuator 4 and the load obtained from the strain gauge signal attached to the specimen.

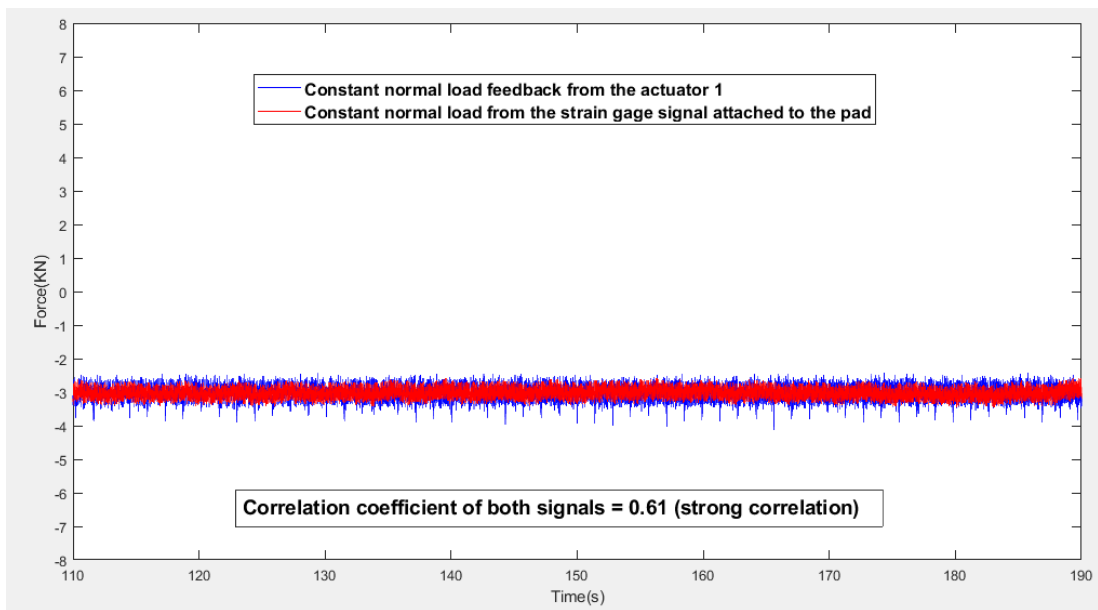


Figure F8 Fourth calibration test (Test N^o1): Comparison between the load feedback from actuator 1 and the load obtained from the strain gauge attached to the pad.

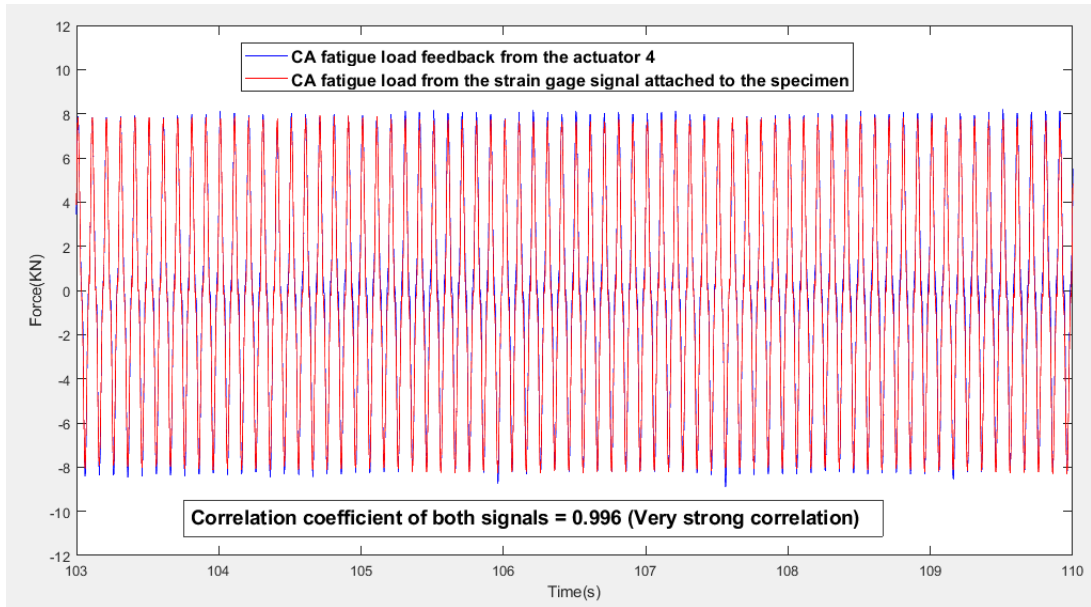


Figure F9 Fourth calibration test (Test N°2): Comparison between the load feedback from actuator 4 and the load from the strain gauge signal attached to the specimen.

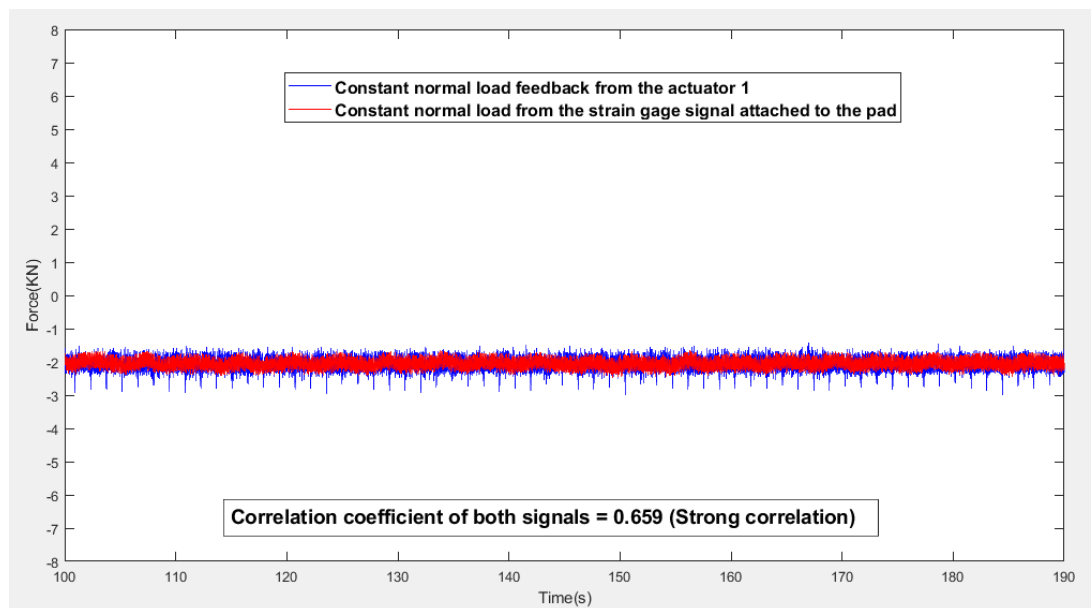
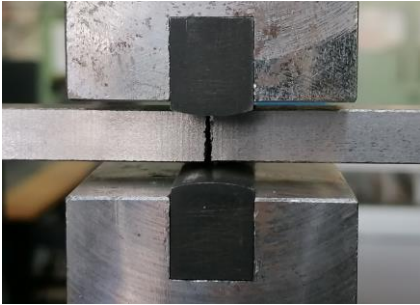
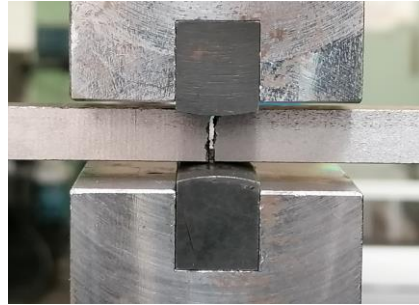


Figure F10 Fourth calibration test (Test N°2): Comparison between the load feedback from actuator 1 and the load obtained from the strain gauge attached to the pad.

Appendix G: Damaged material 40054 under constant amplitude fretting fatigue loading



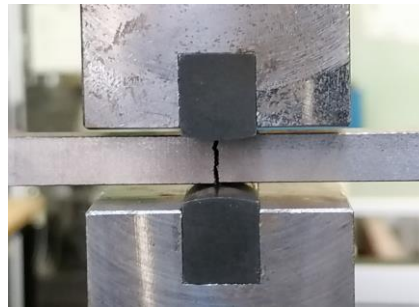
Test 1 summarised in Table 6-2
Specimen made from cast iron 40054
Pads (radius 20 mm) made from steel
Static contact load, $P=5.5\text{KN}$
CA cyclic fatigue load. $F_a=8\text{KN}$ and $R=0.1$
 $N_f=970,764$ cycles



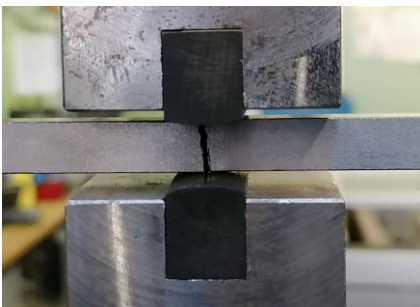
Test 2 summarised in Table 6-2
Specimen made from cast iron 40054
Pads (radius 20 mm) made from steel
Static contact load, $P=5.5\text{KN}$
CA cyclic fatigue load. $F_a=9\text{KN}$ and $R=0.1$
 $N_f=1,107,093$ cycles



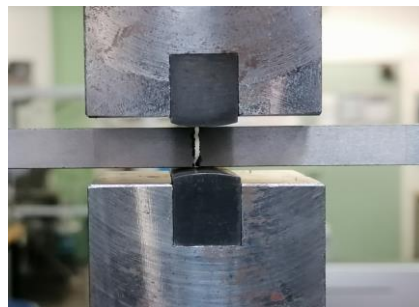
Test 3 summarised in Table 6-2
Specimen made from cast iron 40054
Pads (radius 20 mm) made from steel
Static contact load, $P=5.5\text{KN}$
CA cyclic fatigue load. $F_a=9.5\text{KN}$ and $R=0.1$
 $N_f=347,554$ cycles



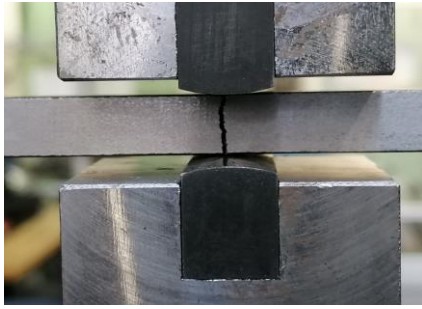
Test 4 summarised in Table 6-2
Specimen made from cast iron 40054
Pads (radius 20 mm) made from steel
Static contact load, $P=5.5\text{KN}$
CA cyclic fatigue load. $F_a=10\text{KN}$ and $R=0.1$
 $N_f=328,400$ cycles



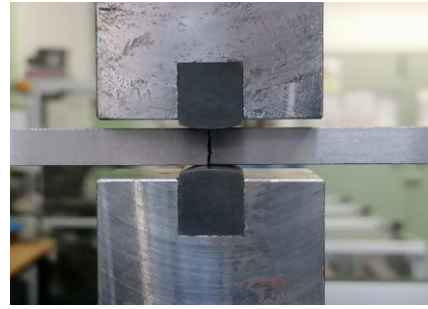
Test 5 summarised in Table 6-2
Specimen made from cast iron 40054
Pads (radius 20 mm) made from steel
Static contact load, $P=5.5\text{KN}$
CA cyclic fatigue load. $F_a=10.5\text{KN}$ and $R=0.1$
 $N_f=368,132$ cycles



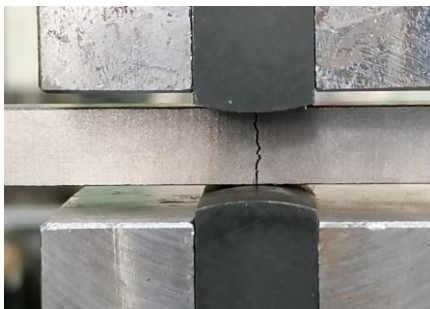
Test 6 summarised in Table 6-2
Specimen made from cast iron 40054
Pads (radius 20 mm) made from steel
Static contact load, $P=5.5\text{KN}$
CA cyclic fatigue load. $F_a=11\text{KN}$ and $R=0.1$
 $N_f=193,466$ cycles



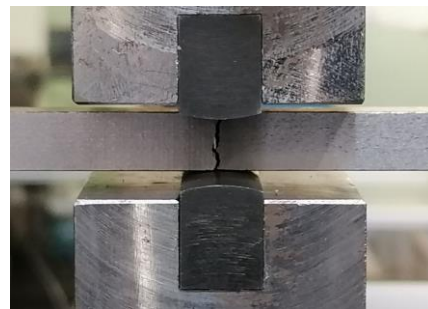
Test 7 summarised in Table 6-2
Specimen made from cast iron 40054
Pads (radius 20 mm) made from steel
Static contact load, $P=5.5\text{KN}$
CA cyclic fatigue load. $F_{max}=12\text{KN}$ and $R=0.1$
 $N_f=166,731$ cycles



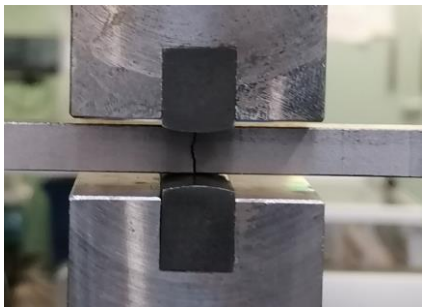
Test 8 summarised in Table 6-2
Specimen made from cast iron 40054
Pads (radius 20 mm) made from steel
Static contact load, $P=5.5\text{KN}$
CA cyclic fatigue load. $F_{max}=16\text{KN}$ and $R=0.1$
 $N_f=86,731$ cycles



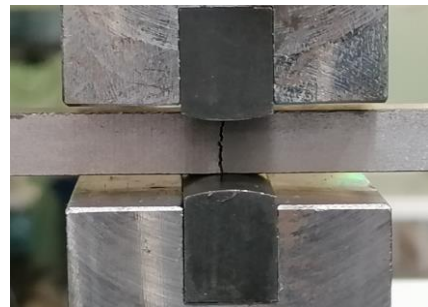
Test 9 summarised in Table 6-2
Specimen made from cast iron 40054
Pads (radius 20 mm) made from steel
Static contact load, $P=5.5\text{KN}$
CA cyclic fatigue load. $F_{max}=7\text{KN}$ and $R=-1$
 $N_f=32,788$ cycles



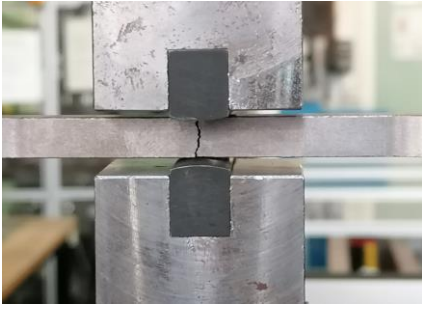
Test 10 summarised in Table 6-2
Specimen made from cast iron 40054
Pads (radius 20 mm) made from steel
Static contact load, $P=5.5\text{KN}$
CA cyclic fatigue load. $F_{max}=6.5\text{KN}$ and $R=-1$
 $N_f=86,847$ cycles



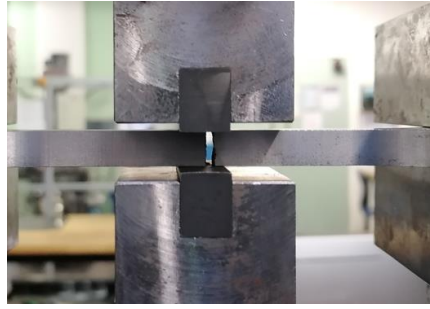
Test 11 summarised in Table 6-2
Specimen made from cast iron 40054
Pads (radius 20 mm) made from steel
Static contact load, $P=5.5\text{KN}$
CA cyclic fatigue load. $F_{max}=6.25\text{KN}$ and $R=-1$
 $N_f=130,733$ cycles



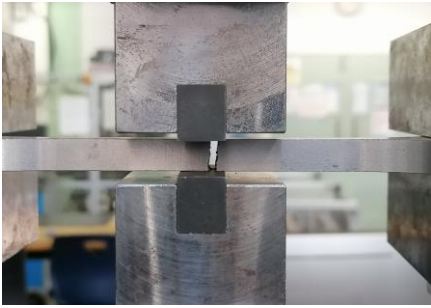
Test 12 summarised in Table 6-2
Specimen made from cast iron 40054
Pads (radius 20 mm) made from steel
Static contact load, $P=5.5\text{KN}$
CA cyclic fatigue load. $F_{max}=6\text{KN}$ and $R=-1$
 $N_f=547,361$ cycles



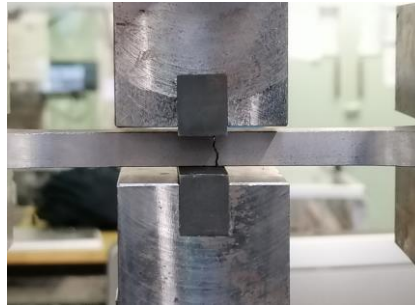
Test 13 summarised in Table 6-2
Specimen made from cast iron 40054
Pads (radius 20 mm) made from steel
Static contact load, $P=5.5\text{KN}$
CA cyclic fatigue load. $F_{max}=5\text{KN}$ and $R=-1$
 $N_f=1,053,934$ cycles



Test 14 summarised in Table 6-2
Specimen made from cast iron 40054
Pads (radius 100 mm) made from steel
Static contact load, $P=5.5\text{KN}$
CA cyclic fatigue load. $F_{max}=7\text{KN}$ and $R=-1$
 $N_f= 21,619$ cycles



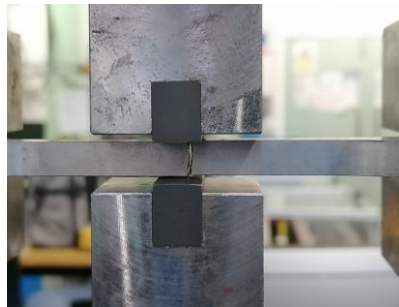
Test 15 summarised in Table 6-2
Specimen made from cast iron 40054
Pads (radius 100 mm) made from steel
Static contact load, $P=5.5\text{KN}$
CA cyclic fatigue load. $F_{max}=6.5\text{KN}$ and $R=-1$
 $N_f=28,086$ cycles



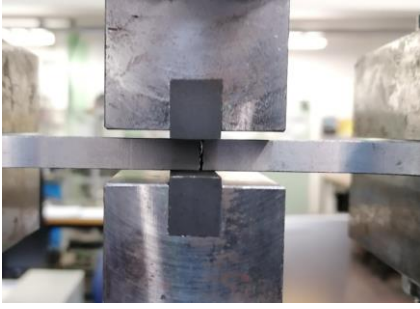
Test 16 summarised in Table 6-2
Specimen made from cast iron 40054
Pads (radius 100 mm) made from steel
Static contact load, $P=5.5\text{KN}$
CA cyclic fatigue load. $F_{max}=6.25\text{KN}$ and $R=-1$
 $N_f= 44,523$ cycles



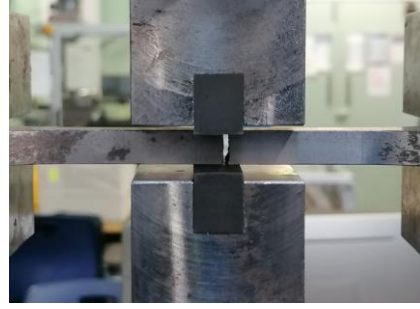
Test 17 summarised in Table 6-2
Specimen made from cast iron 40054
Pads (radius 100 mm) made from steel
Static contact load, $P=5.5\text{KN}$
CA cyclic fatigue load. $F_{max}=6\text{KN}$ and $R=-1$
 $N_f= 47,932$ cycles



Test 18 summarised in Table 6-2
Specimen made from cast iron 40054
Pads (radius 100 mm) made from steel
Static contact load, $P=5.5\text{KN}$
CA cyclic fatigue load. $F_{max}=5.5\text{KN}$ and $R=-1$
 $N_f= 111,079$ cycles



Test 19 summarised in Table 6-2
Specimen made from cast iron 40054
Pads (radius 100 mm) made from steel
Static contact load, $P=5.5\text{KN}$
CA cyclic fatigue load. $F_{max}=5\text{KN}$ and $R=-1$
 $N_f=199,438$ cycles

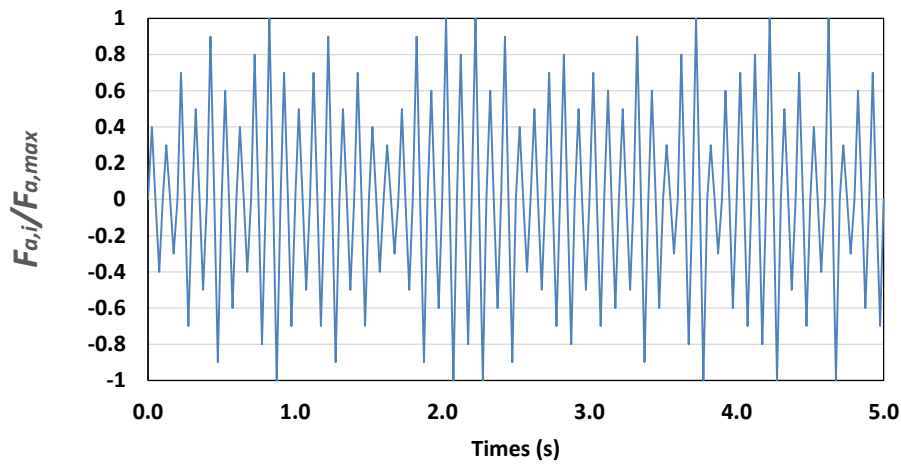


Test 20 summarised in Table 6-2
Specimen made from cast iron 40054
Pads (radius 100 mm) made from steel
Static contact load, $P=5.5\text{KN}$
CA cyclic fatigue load. $F_{max}=4.75\text{KN}$ and $R=-1$
 $N_f=138,909$ cycles

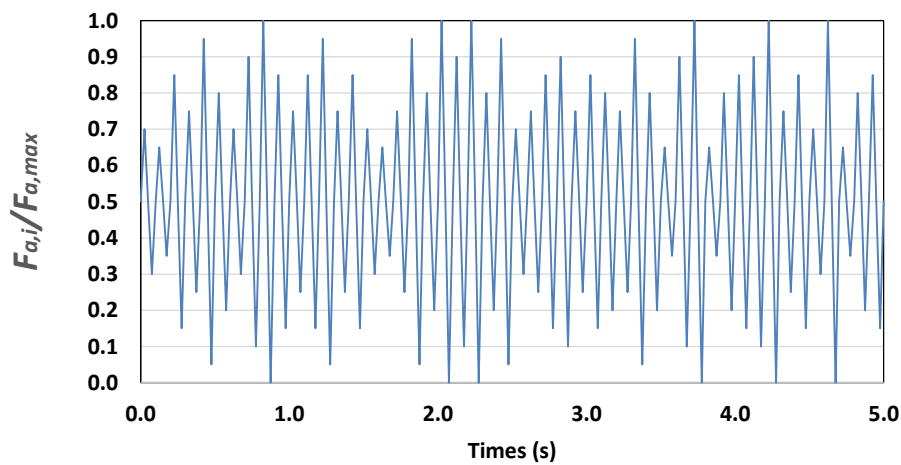
Appendix H: Damaged material 40054 under variable amplitude fretting Fatigue loading

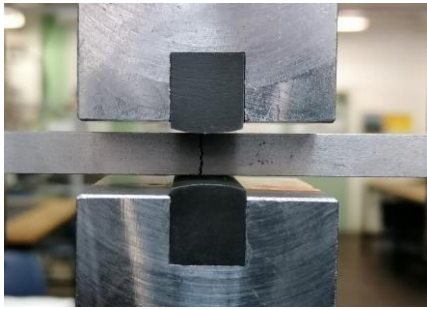
The figures below are the variable amplitude block loads used to assess material 40054 under VA fretting fatigue loading. A static contact load P was applied to the pads while a VA block load was applied on the specimen. Block 1 is characterized by a load ratio $R = -1$ while block 2 by a load ratio $R \geq 0$. In both figures, $F_{a,i}$ is the amplitude of the force associated with the i -th cycle. $F_{a,max}$ is the maximum value of the amplitude of the force in the load spectrum.

Block 1

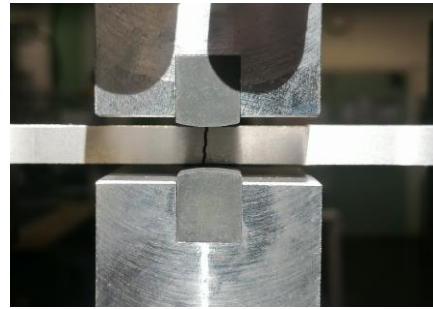


Block 2

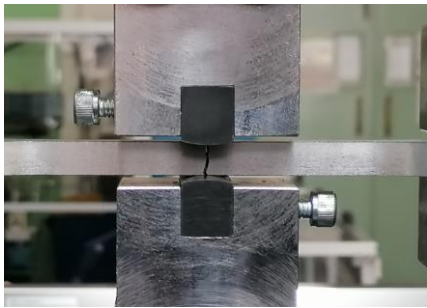




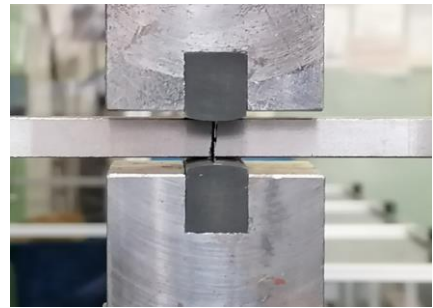
Test 1 summarised in Table 7-2
 Specimen made from cast iron 40054
 Pads (radius 20mm) made from steel
 Static contact load, $P=5.5\text{KN}$
 $F_{a,max}=7.5\text{KN}$ is multiplied by block 1 signal
 $N_f=161,150$ cycles and $N_{block}=3,223$ blocks



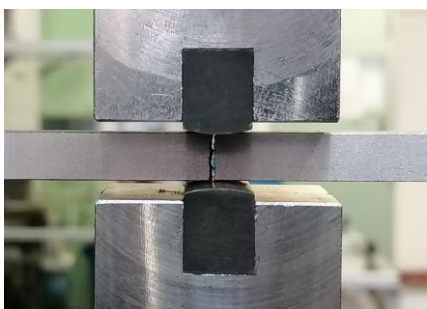
Test 2 summarised in Table 7-2
 Specimen made from cast iron 40054
 Pads (radius 20mm) made from steel
 Static contact load, $P=5.5\text{KN}$
 $F_{a,max}=7\text{KN}$ is multiplied by block 1 signal
 $N_f=375,800$ cycles and $N_{block}=7,516$ blocks



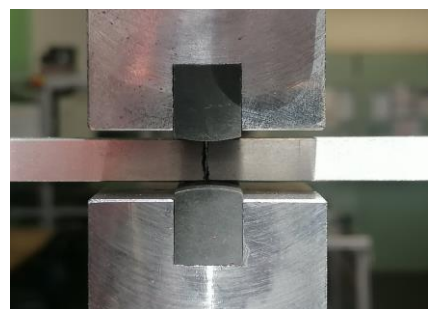
Test 3 summarised in Table 7-2
 Specimen made from cast iron 40054
 Pads (radius 20mm) made from steel
 Static contact load, $P=5.5\text{KN}$
 $F_{a,max}=6.5\text{KN}$ is multiplied by block 1 signal
 $N_f=169,200$ cycles and $N_{block}=3,384$ blocks



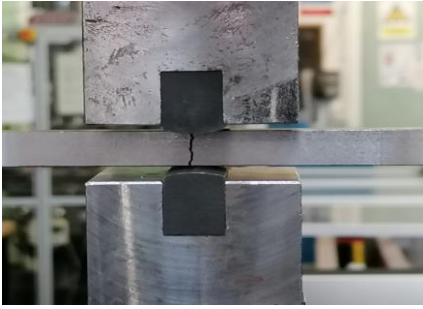
Test 4 summarised in Table 7-2
 Specimen made from cast iron 40054
 Pads (radius 20mm) made from steel
 Static contact load, $P=5.5\text{KN}$
 $F_{a,max}=6.25\text{KN}$ is multiplied by block 1 signal
 $N_f=324,000$ cycles and $N_{block}=6,480$ blocks



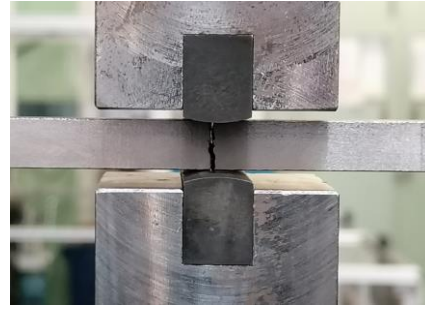
Test 5 summarised in Table 7-2
 Specimen made from cast iron 40054
 Pads (radius 20mm) made from steel
 Static contact load, $P=5.5\text{KN}$
 $F_{a,max}=6.0\text{KN}$ is multiplied by block 1 signal
 $N_f=476,250$ cycles and $N_{block}=9,525$ blocks



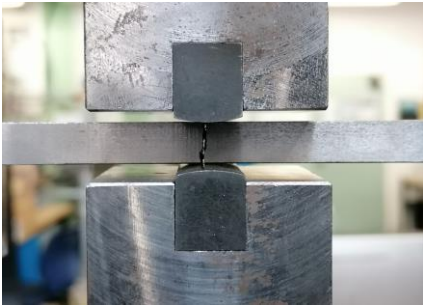
Test 6 summarised in Table 7-2
 Specimen made from cast iron 40054
 Pads (radius 20mm) made from steel
 Static contact load, $P=5.5\text{KN}$
 $F_{a,max}=5.75\text{KN}$ is multiplied by block 1 signal
 $N_f=1,182,950$ cycles and $N_{block}=23,659$ blocks



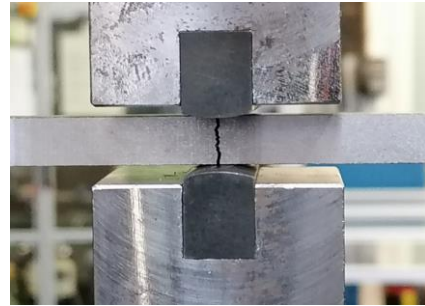
Test 7 summarised in Table 7-2
 Specimen made from cast iron 40054
 Pads (radius 20mm) made from steel
 Static contact load, $P=5.5\text{KN}$
 $F_{a,max}=8\text{KN}$ is multiplied by block 2 signal
 $N_f=4,296,200$ cycles and $N_{block}=85,924$ blocks



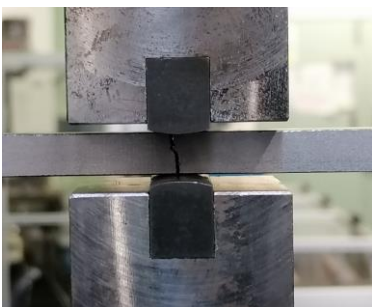
Test 8 summarised in Table 7-2
 Specimen made from cast iron 40054
 Pads (radius 20mm) made from steel
 Static contact load, $P=5.5\text{KN}$
 $F_{a,max}=9\text{KN}$ is multiplied by block 2 signal
 $N_f=1,022,450$ cycles and $N_{block}=20,449$ blocks



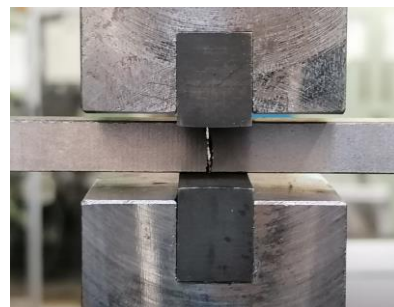
Test 9 summarised in Table 7-2
 Specimen made from cast iron 40054
 Pads (radius 20mm) made from steel
 Static contact load, $P=5.5\text{KN}$
 $F_{a,max}=9.5\text{KN}$ is multiplied by block 2 signal
 $N_f=1,349,900$ cycles and $N_{block}=26,998$ blocks



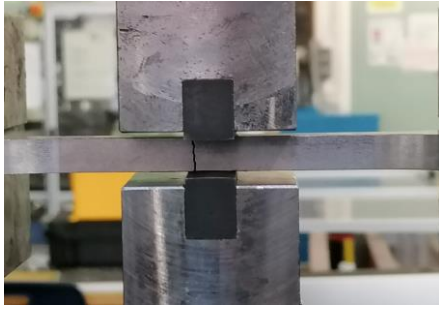
Test 10 summarised in Table 7-2
 Specimen made from cast iron 40054
 Pads (radius 20mm) made from steel
 Static contact load, $P=5.5\text{KN}$
 $F_{a,max}=10\text{KN}$ is multiplied by block 2 signal
 $N_f=459,000$ cycles and $N_{block}=9,180$ blocks



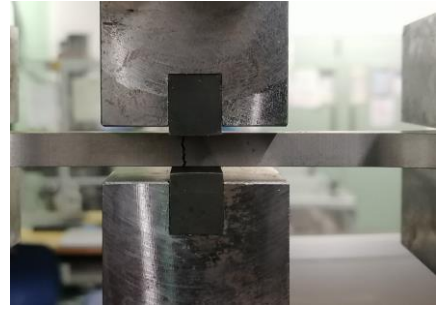
Test 11 summarised in Table 7-2
 Specimen made from cast iron 40054
 Pads (radius 20mm) made from steel
 Static contact load, $P=5.5\text{KN}$
 $F_{a,max}=12\text{KN}$ is multiplied by block 2 signal
 $N_f=289,200$ cycles and $N_{block}=5,784$ blocks



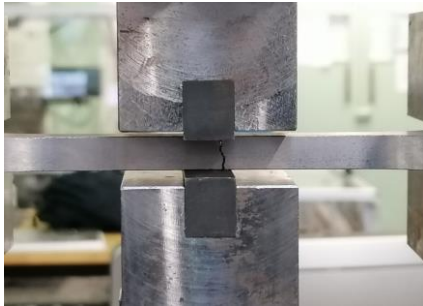
Test 12 summarised in Table 7-2
 Specimen made from cast iron 40054
 Pads (radius 100mm) made from steel
 Static contact load, $P=5.5\text{KN}$
 $F_{a,max}=5.75\text{KN}$ is multiplied by block 1 signal
 $N_f=625,150$ cycles and $N_{block}=12,503$ blocks



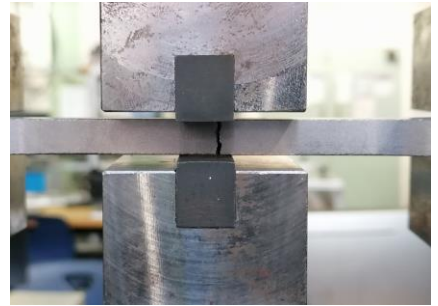
Test 13 summarised in Table 7-2
 Specimen made from cast iron 40054
 Pads (radius 100mm) made from steel
 Static contact load, P=5.5KN
 $F_{a,max}$ =6 KN is multiplied by block 1 signal
 N_f = 361,150 cycles and N_{block} = 7,223 blocks



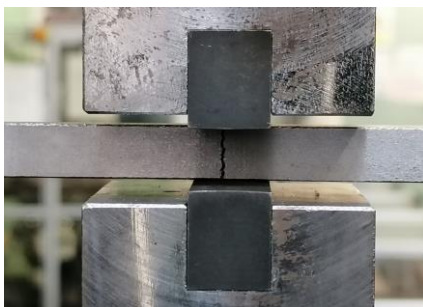
Test 14 summarised in Table 7-2
 Specimen made from cast iron 40054
 Pads (radius 100mm) made from steel
 Static contact load, P=5.5KN
 $F_{a,max}$ =7KN is multiplied by block 1 signal
 N_f =184,950 cycles and N_{block} = 3,699 blocks



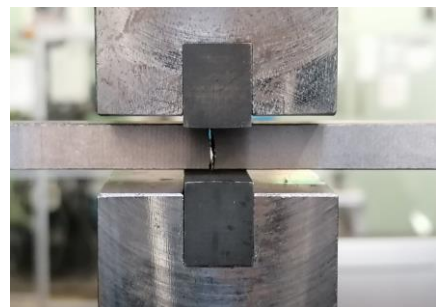
Test 15 summarised in Table 7-2
 Specimen made from cast iron 40054
 Pads (radius 100mm) made from steel
 Static contact load, P=5.5KN
 $F_{a,max}$ =7.5KN is multiplied by block 1 signal
 N_f =85,600 cycles and N_{block} = 1,712 blocks



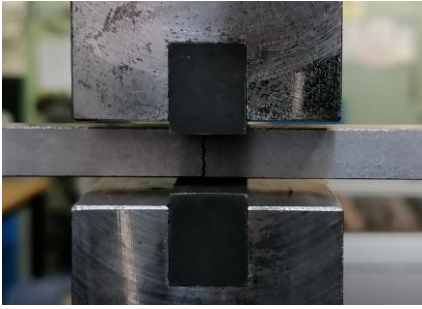
Test 16 summarised in Table 7-2
 Specimen made from cast iron 40054
 Pads (radius 100mm) made from steel
 Static contact load, P=5.5KN
 $F_{a,max}$ =8KN is multiplied by block 1 signal
 N_f =53,000 cycles and N_{block} =1,060 blocks



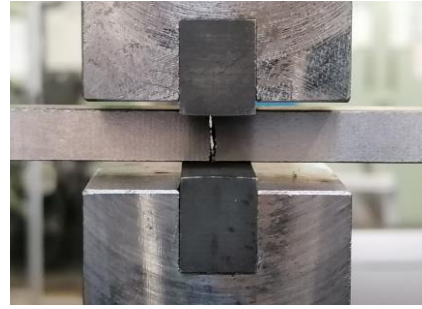
Test 17 summarised in Table 7-2
 Specimen made from cast iron 40054
 Pads (radius 100mm) made from steel
 Static contact load, P=5.5KN
 $F_{a,max}$ =9KN is multiplied by block 2 signal
 N_f =2,264,050cycles and N_{block} = 45,281 blocks



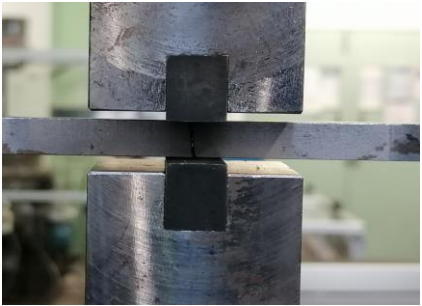
Test 18 summarised in Table 7-2
 Specimen made from cast iron 40054
 Pads (radius 100mm) made from steel
 Static contact load, P=5.5KN
 $F_{a,max}$ =9.5KN is multiplied by block 2 signal
 N_f =1,170,750 cycles and N_{block} = 23,415 blocks



Test 19 summarised in Table 7-2
Specimen made from cast iron 40054
Pads (radius 100mm) made from steel
Static contact load, $P=5.5\text{KN}$
 $F_{a,max}=10\text{ KN}$ is multiplied by block 2 signal
 $N_f=1,998,200$ cycles and $N_{block}=39,964$ blocks



Test 20 summarised in Table 7-2
Specimen made from cast iron 40054
Pads (radius 100mm) made from steel
Static contact load, $P=5.5\text{KN}$
 $F_{a,max}=14\text{ KN}$ is multiplied by block 2 signal
 $N_f=568,050$ cycles and $N_{block}=11,361$ blocks



Test 21 summarised in Table 7-2
Specimen made from cast iron 40054
Pads (radius 100mm) made from steel
Static contact load, $P=5.5\text{KN}$
 $F_{a,max}=16\text{ KN}$ is multiplied by block 2 signal
 $N_f=268,000$ cycles and $N_{block}=5,360$ blocks

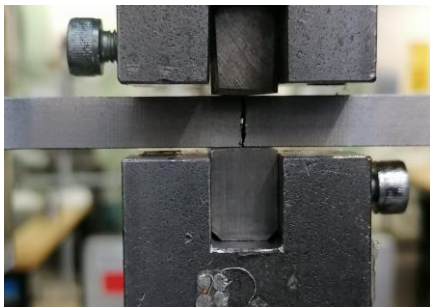
Appendix I: Damaged material 40060 under constant amplitude fretting Fatigue loading



Test 1 summarised in Table 6-8
Specimen made from cast iron 40060
Pads (radius 75mm) made from cast iron 40054
Static contact load, $P=5\text{KN}$
CA cyclic fatigue load. $F_a=8\text{KN}$ and $R=-1$
 $N_f=29,670$ cycles



Test 2 summarised in Table 6-8
Specimen made from cast iron 40060
Pads (radius 75mm) made from cast iron 40054
Static contact load, $P=5\text{KN}$
CA cyclic fatigue load. $F_a=7\text{KN}$ and $R=-1$
 $N_f=59,770$ cycles



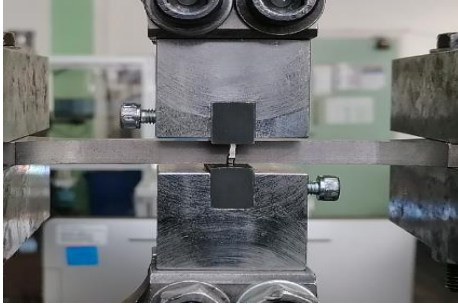
Test 3 summarised in Table 6-8
Specimen made from cast iron 40060
Pads (radius 75mm) made from cast iron 40054
Static contact load, $P=5\text{KN}$
CA cyclic fatigue load. $F_a=6.5\text{KN}$ and $R=-1$
 $N_f=42,985$ cycles



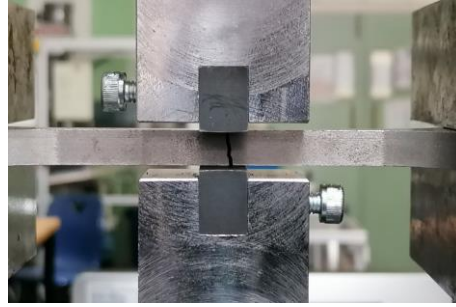
Test 4 summarised in Table 6-8
Specimen made from cast iron 40060
Pads (radius 75mm) made from cast iron 40054
Static contact load, $P=4\text{KN}$
CA cyclic fatigue load. $F_a=9\text{KN}$ and $R=-1$
 $N_f=23,653$ cycles



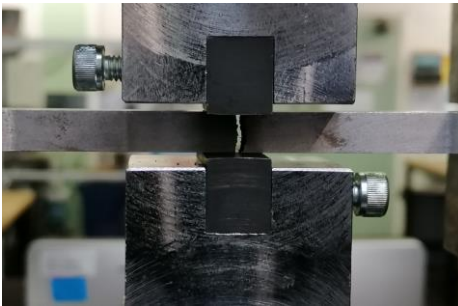
Test 5 summarised in Table 6-8
Specimen made from cast iron 40060
Pads (radius 75mm) made from cast iron 40054
Static contact load, $P=3.5\text{KN}$
CA cyclic fatigue load. $F_a=6.25\text{KN}$ and $R=-1$
 $N_f=133,335$ cycles



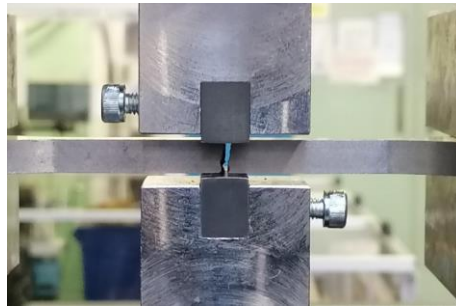
Test 1 summarised in Table 6-9
Specimen made from cast iron 40060
Pads (radius 75mm) made from steel
Static contact load, $P=4\text{KN}$
CA cyclic fatigue load. $F_a=3.5\text{KN}$ and $R=-1$
 $N_f=1,703,890$ cycles



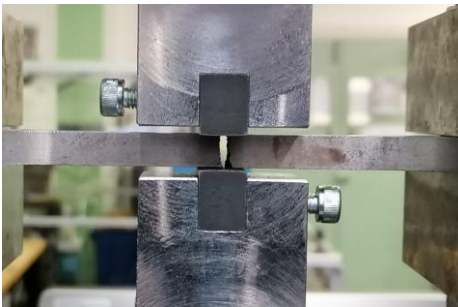
Test 2 summarised in Table 6-9
Specimen made from cast iron 40060
Pads (radius 75mm) made from steel
Static contact load, $P=4\text{KN}$
CA cyclic fatigue load. $F_a=4\text{KN}$ and $R=-1$
 $N_f=1,218,640$ cycles



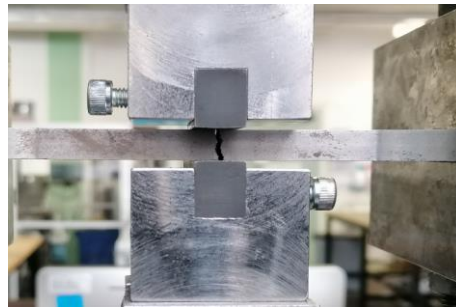
Test 3 summarised in Table 6-9
Specimen made from cast iron 40060
Pads (radius 75mm) made from steel
Static contact load, $P=4\text{KN}$
CA cyclic fatigue load. $F_a=4.75\text{KN}$ and $R=-1$
 $N_f=283,325$ cycles



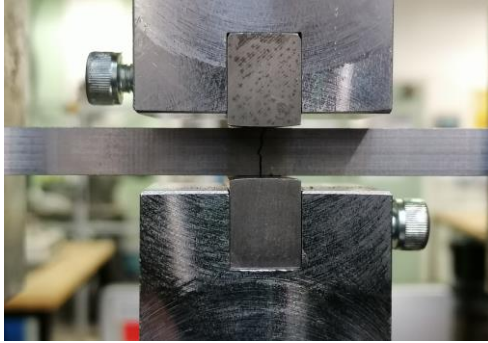
Test 4 summarised in Table 6-9
Specimen made from cast iron 40060
Pads (radius 75mm) made from steel
Static contact load, $P=4\text{KN}$
CA cyclic fatigue load. $F_a=5\text{KN}$ and $R=-1$
 $N_f=351,381$ cycles



Test 5 summarised in Table 6-9
Specimen made from cast iron 40060
Pads (radius 75mm) made from steel
Static contact load, $P=4\text{KN}$
CA cyclic fatigue load. $F_a=5.5\text{KN}$ and $R=-1$
 $N_f=173,542$ cycles



Test 6 summarised in Table 6-9
Specimen made from cast iron 40060
Pads (radius 75mm) made from steel
Static contact load, $P=4\text{KN}$
CA cyclic fatigue load. $F_a=6\text{KN}$ and $R=-1$
 $N_f=53,257$ cycles



Test 1 summarised in Table 6-10
 Specimen made from cast iron 40060
 Pads (radius 75mm) made from 40054
 CA cyclic contact load, $P_m = -4\text{KN}$ and $P_a = 0.5\text{KN}$
 CA cyclic fatigue load, $F_a = 5.5\text{KN}$ and $R = -1$
 $N_f = 208,500$ cycles



Test 2 summarised in Table 6-10
 Specimen made from cast iron 40060
 Pads (radius 75mm) made from 40054
 CA cyclic contact load, $P_m = -5\text{KN}$ and $P_a = 0.5\text{KN}$
 CA cyclic fatigue load, $F_a = 6.5\text{KN}$ and $R = -1$
 $N_f = 65,650$ cycles



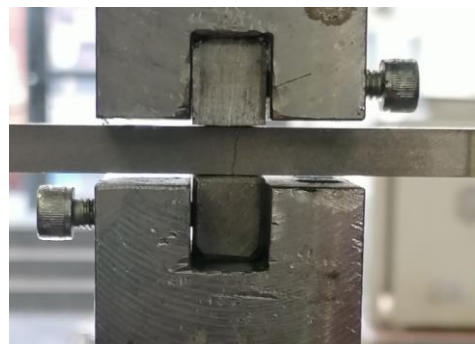
Test 3 summarised in Table 6-10
 Specimen made from cast iron 40060
 Pads (radius 75mm) made from 40054
 CA cyclic contact load, $P_m = -5\text{KN}$ and $P_a = 0.5\text{KN}$
 CA cyclic fatigue load, $F_a = 6\text{KN}$ and $R = -1$
 $N_f = 124,504$ cycles



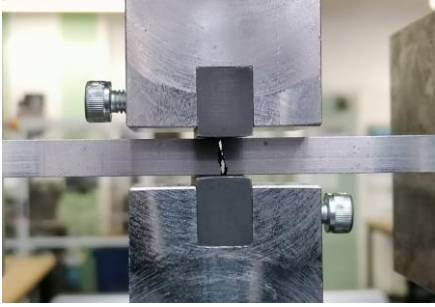
Test 4 summarised in Table 6-10
 Specimen made from cast iron 40060
 Pads (radius 75mm) made from 40054
 CA cyclic contact load, $P_m = -5\text{KN}$ and $P_a = 0.5\text{KN}$
 CA cyclic fatigue load, $F_a = 9.5\text{KN}$ and $R = -1$
 $N_f = 17,788$ cycles



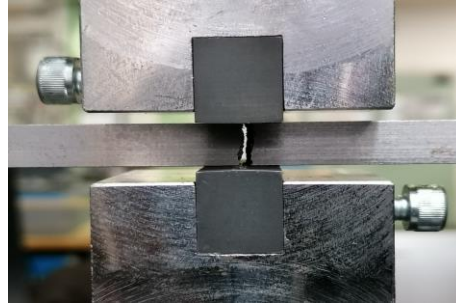
Test 5 summarised in Table 6-10
 Specimen made from cast iron 40060
 Pads (radius 75mm) made from 40054
 CA cyclic contact load, $P_m = -5\text{KN}$ and $P_a = 0.5\text{KN}$
 CA cyclic fatigue load, $F_a = 7\text{KN}$ and $R = -1$
 $N_f = 52,773$ cycles



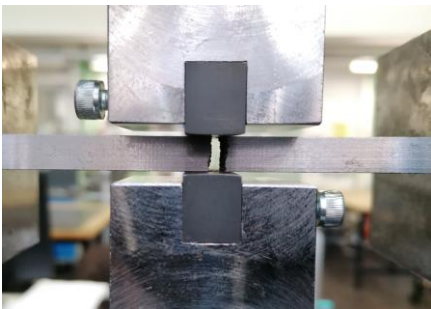
Test 6 summarised in Table 6-10
 Specimen made from cast iron 40060
 Pads (radius 75mm) made from 40054
 CA cyclic contact load, $P_m = -6\text{KN}$ and $P_a = 1\text{KN}$
 CA cyclic fatigue load, $F_a = 7.5\text{KN}$ and $R = -1$
 $N_f = 50,297$ cycles



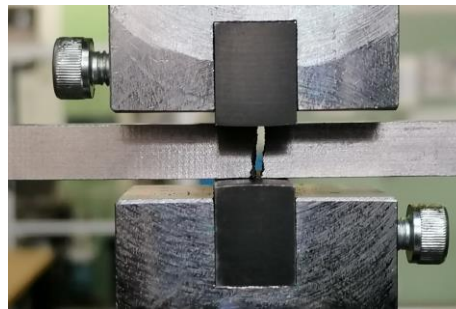
Test 1 summarised in Table 6-11
 Specimen made from cast iron 40060
 Pads (radius 75mm) made from steel
 CA cyclic contact load, $P_m = -5\text{KN}$ $P_a = 0.5\text{KN}$
 CA cyclic fatigue load. $F_a = 6\text{KN}$ and $R = -1$
 $N_f = 77,000$ cycles



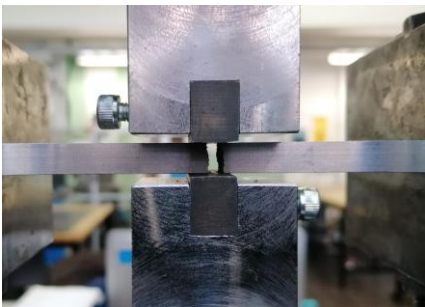
Test 2 summarised in Table 6-11
 Specimen made from cast iron 40060
 Pads (radius 75mm) made from steel
 CA cyclic contact load, $P_m = -5\text{KN}$ a $P_a = 0.5\text{KN}$
 CA cyclic fatigue load. $F_a = 5.5\text{KN}$ and $R = -1$
 $N_f = 135,000$ cycles



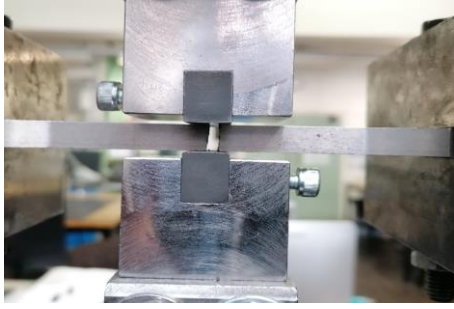
Test 3 summarised in Table 6-11
 Specimen made from cast iron 40060
 Pads (radius 75mm) made from steel
 CA cyclic contact load, $P_m = -5\text{KN}$, $P_a = 0.5\text{KN}$
 CA cyclic fatigue load. $F_a = 5\text{KN}$ and $R = -1$
 $N_f = 338,697$ cycles



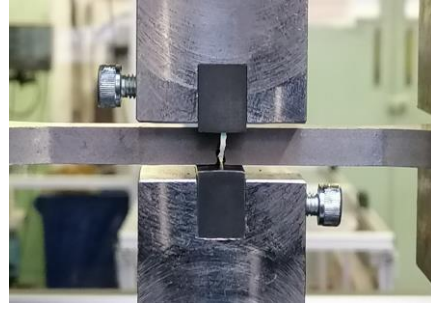
Test 4 summarised in Table 6-11
 Specimen made from cast iron 40060
 Pads (radius 75mm) made from steel
 CA cyclic contact load, $P_m = -5\text{KN}$, $P_a = 0.5\text{KN}$
 CA cyclic fatigue load. $F_a = 4.5\text{KN}$ and $R = -1$
 $N_f = 397,873$ cycles



Test 5 summarised in Table 6-11
 Specimen made from cast iron 40060
 Pads (radius 75mm) made from steel
 CA cyclic contact load, $P_m = -5\text{KN}$, $P_a = 0.5\text{KN}$
 CA cyclic fatigue load. $F_a = 4\text{KN}$ and $R = -1$
 $N_f = 705,000$ cycles



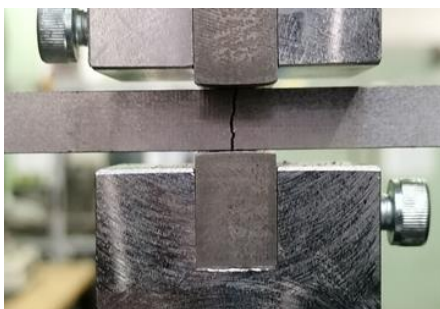
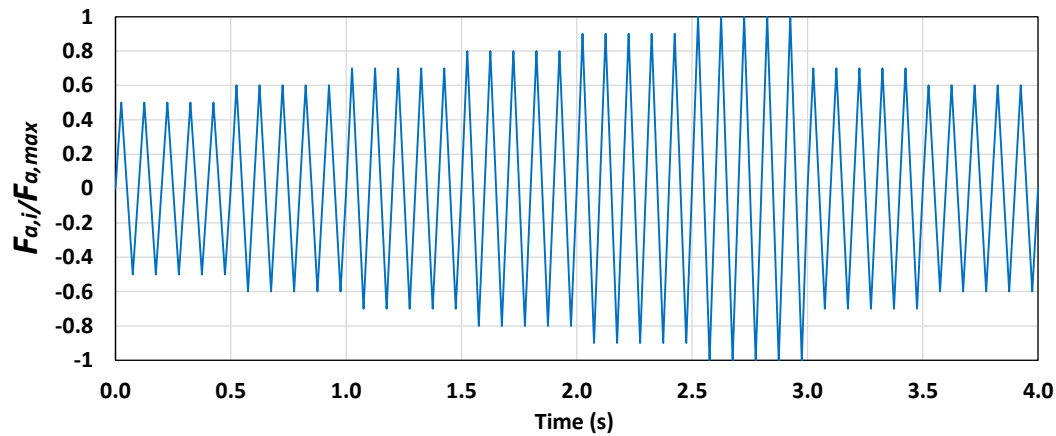
Test 6 summarised in Table 6-11
Specimen made from cast iron 40060
Pads (radius 75mm) made from steel
CA cyclic contact load, $P_m = -5\text{KN}$, $P_a = 0.5\text{KN}$
CA cyclic fatigue load. $F_a = 4.25\text{KN}$ and $R = -1$
 $N_f = 561,658$ cycles



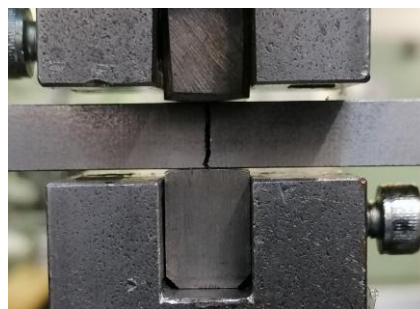
Test 7 summarised in Table 6-11
Specimen made from cast iron 40060
Pads (radius 75mm) made from steel
CA cyclic contact load, $P_m = -5\text{KN}$, $P_a = 0.5\text{KN}$
CA cyclic fatigue load. $F_a = 4.75\text{KN}$ and $R = -1$
 $N_f = 450,562$ cycles

Appendix J: Damaged material 40060 under variable amplitude fretting Fatigue loading

The graph below is the variable amplitude block signal used to assess the specimen 40060 under VA fretting fatigue loading. In all tests, the static contact load P was applied to the pads and the VA block load was applied on the specimen. In the figure below, $F_{a,i}$ is the amplitude of the force associated with the i -th cycle. $F_{a,max}$ is the maximum value of the amplitude of the force in the load spectrum.



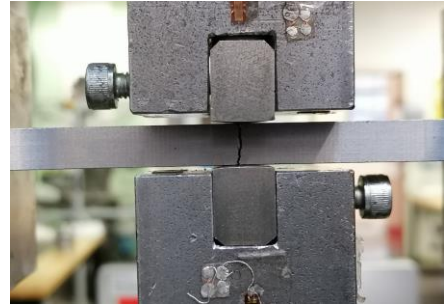
Test 1 summarised in Table 7-6
 Specimen made from cast iron 40060
 Pads (radius 75mm) made from 40054
 Static contact load, $P=5\text{KN}$
 $F_{a,max}=8\text{KN}$ is multiplied to VA fatigue block signal
 $N_f=122,000$ cycles and $N_{block}=3,050$ blocks



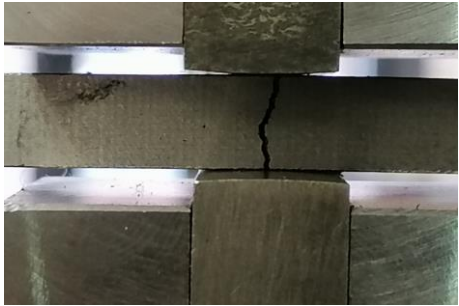
Test 2 summarised in Table 7-6
 Specimen made from cast iron 40060
 Pads (radius 75mm) made from 40054
 Static contact load, $P=5\text{KN}$
 $F_{a,max}=9\text{KN}$ is multiplied to VA fatigue block signal
 $N_f=99,200$ cycles and $N_{block}=2,480$ blocks



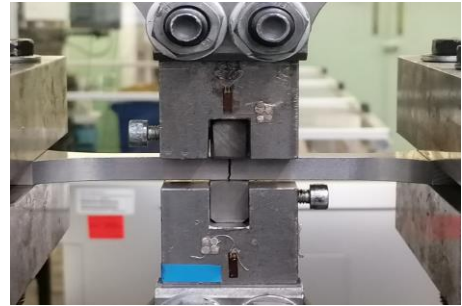
Test 3 summarised in Table 7-6
 Specimen made from cast iron 40060
 Pads (radius 75mm) made from 40054
 Static contact load, $P=5\text{KN}$
 $F_{a,max}=7\text{KN}$ is multiplied by block signal
 $N_f=116,840$ cycles and $N_{block}=2,921$ blocks



Test 4 summarised in Table 7-6
 Specimen made from cast iron 40060
 Pads (radius 75mm) made from 40054
 Static contact load, $P=5\text{KN}$
 $F_{a,max}=6\text{KN}$ is multiplied by block signal
 $N_f=520,000$ cycles and $N_{block}=13,000$ blocks



Test 5 summarised in Table 7-6
 Specimen made from cast iron 40060
 Pads (radius 75mm) made from 40054
 Static contact load, $P=5\text{KN}$
 $F_{a,max}=5.5\text{KN}$ is multiplied to VA fatigue block signal
 $N_f=1,178,600$ cycles and $N_{block}=29,465$ blocks



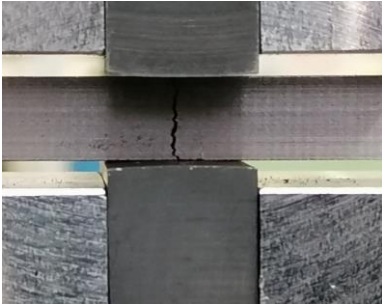
Test 6 summarised in Table 7-6
 Specimen made from cast iron 40060
 Pads (radius 75mm) made from cast iron 40054
 Static contact load, $P=5\text{KN}$
 $F_{a,max}=5.25\text{KN}$ is multiplied by block signal
 $N_f=1,321,560$ cycles and $N_{block}=33,039$ blocks



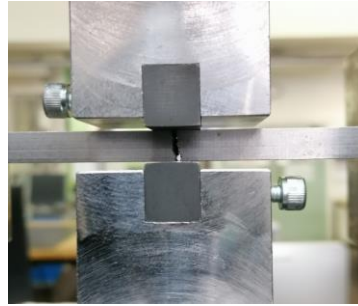
Test 7 summarised in Table 7-6
 Specimen made from cast iron 40060
 Pads (radius 75mm) made from cast iron 40054
 Static contact load, $P=5\text{KN}$
 $F_{a,max}=6.5\text{KN}$ is multiplied by block signal
 $N_f=359,240$ cycles and $N_{block}=8,981$ blocks



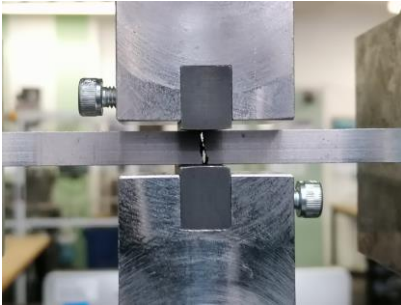
Test 8 summarised in Table 7-6
 Specimen made from cast iron 40060
 Pads (radius 75mm) made from cast iron 40054
 Static contact load, $P=5\text{KN}$
 $F_{a,max}=6.75\text{KN}$ is multiplied by block signal
 $N_f=234,680$ cycles and $N_{block}=5,867$ blocks



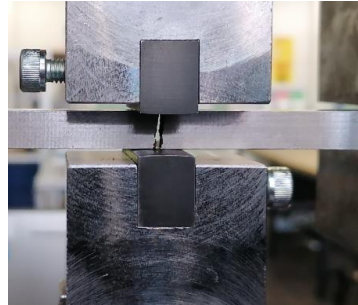
Test 1 summarised in Table 7-7
 Specimen made from cast iron 40060
 Pads (radius 75mm) made from steel
 Static contact load, P=6KN
 $F_{a,max}$ =7KN is multiplied by block signal
 N_f =101,920 cycles and N_{block} =2,548 blocks



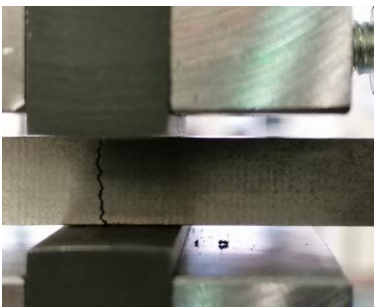
Test 2 summarised in Table 7-7
 Specimen made from cast iron 40060
 Pads (radius 75mm) made from steel
 Static contact load, P=6KN
 $F_{a,max}$ =6.5KN is multiplied by block signal
 N_f =146,320 cycles and N_{block} =3,658 blocks



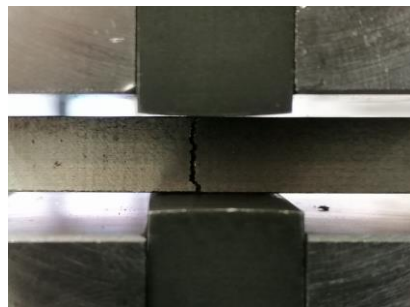
Test 3 summarised in Table 7-7
 Specimen made from cast iron 40060
 Pads (radius 75mm) made from steel
 Static contact load, P=6KN
 $F_{a,max}$ =6KN is multiplied by block signal
 N_f =145,720 cycles and N_{block} =3,643 blocks



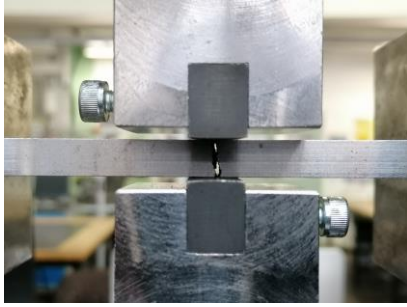
Test 4 summarised in Table 7-7
 Specimen made from cast iron 40060
 Pads (radius 75mm) made from steel
 Static contact load, P=6KN
 $F_{a,max}$ =5.5KN is multiplied by block signal
 N_f =731,160 cycles and N_{block} =18,279 blocks



Test 5 summarised in Table 7-7
 Specimen made from cast iron 40060
 Pads (radius 75mm) made from steel
 Static contact load, P=6KN
 $F_{a,max}$ =5KN is multiplied by block signal
 N_f =1,035,880 cycles and N_{block} =25,897 blocks



Test 6 summarised in Table 7-7
 Specimen made from cast iron 40060
 Pads (radius 75mm) made from steel
 Static contact load, P=6KN
 $F_{a,max}$ =4.5KN is multiplied by block signal
 N_f =1,779,240 cycles and N_{block} =44,481 blocks



Test 7 summarised in Table 7-7
Specimen made from cast iron 40060
Pads (radius 75mm) made from steel
Static contact load, $P=6\text{KN}$
 $F_{a,max}=4\text{KN}$ is multiplied by block signal
 $N_f=5,000,000$ cycles and $N_{block}=125,000$ blocks